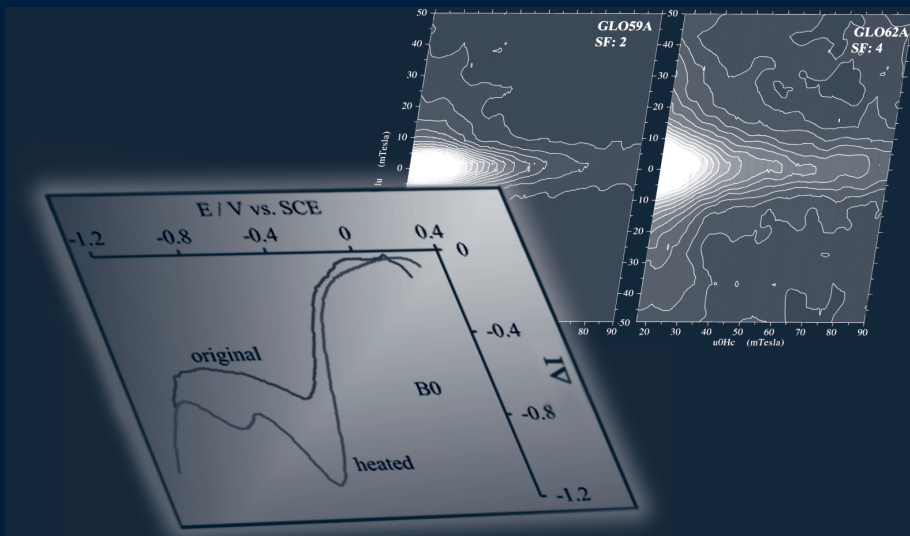


Chemical distinction between lithogenic and pedogenic iron oxides in environmental magnetism

A search for the perfect solution



GEOLOGICA ULTRAIECTINA

Mededelingen van de
Faculteit Aardwetenschappen
Universiteit Utrecht

No. 208

**Chemical distinction between lithogenic
and pedogenic iron oxides in
environmental magnetism**

A search for the perfect solution

Ingeborg H.M. van Oorschot

Chemical distinction between lithogenic and pedogenic iron oxides in environmental magnetism

A search for the perfect solution

Chemisch onderscheid tussen lithogene en pedogene ijzeroxides in milieu-magnetisme

‘Op zoek naar de beste oplossing’

(met een samenvatting in het Nederlands)

PROEFSCHRIFT

TER VERKRIJGING VAN DE GRAAD VAN DOCTOR AAN DE UNIVERSITEIT UTRECHT, OP GEZAG VAN DE RECTOR MAGNIFICUS, PROF. DR. W.H. GISPEN, INGEVOLGE HET BESLUIT VAN HET COLLEGE VOOR PROMOTIES IN HET OPENBAAR TE VERDEDIGEN OP MAANDAG 17 SEPTEMBER 2001 DES NAMIDDAGS TE 16.15 UUR

DOOR

Ingeborg Herma Maria van Oorschot

geboren op 18 mei 1973, te Heesch

Promotor: Prof. Dr. C.G. Langereis

Co-promotor: Dr. M.J. Dekkers

Dissertation committee:

Prof. Dr. P. van Cappellen Geochemie, Faculteit Aardwetenschappen, Universiteit Utrecht

Prof. Dr. F. Heller Instituut für Geophysik, ETH Zürich, Switzerland

Dr.Ir. J.P.G. Loch Geochemie, Faculteit Aardwetenschappen, Universiteit Utrecht

Prof. Dr. B. Maher Centre for Environmental Magnetism and Palaeomagnetism,
Department of Geography, Lancaster University, U.K.

Dr. E. Petrovský Department of Geomagnetism, Geophysical Institute, Czech
Academy of Science, Czech Republic

The research for this thesis was carried out at:

Palaeomagnetic laboratory 'Fort Hoofddijk', Faculty of Earth Sciences, Utrecht University, Budapestlaan 17, 3584 CD Utrecht, the Netherlands.

Part of this work was conducted under the programme of the Vening Meinesz Research School of Geodynamics. This study was supported by the Netherlands Organisation for Scientific Research (NWO).

ISBN nummer: 90-5744-065-2

The most exciting phrase to hear in science, the one that heralds new discoveries, is not "Eureka!" but "That's funny...."

Isaac Asimov, American author and biochemist (1920-1992)

Voor mijn ouders

Contents

Prologue and summary	9
Part 1: Synthetic samples	21
Chapter 1: Extraction methods in environmental magnetism: dissolution principles	23
Chapter 2: Dissolution behaviour of magnetite and maghemite in the citrate-bicarbonate-dithionite extraction method	41
Chapter 3: Selective dissolution of magnetic iron oxides in the acid-ammonium-oxalate/ferrous-iron extraction method; I. Synthetic samples	55
Part 2: Natural samples	71
Chapter 4: Environmental magnetism - Applications in natural loess-palaeosol sequences	73
Chapter 5: Dissolution of iron oxides from a loess-palaeosol sequence with the citrate-bicarbonate-dithionite extraction method	91
Chapter 6: Selective dissolution of magnetic iron oxides in the acid-ammonium-oxalate/ferrous-iron extraction method; II. Natural loess and palaeosol samples	105
Part 3: Voltammetry of Microparticles	125
Chapter 7: An introduction to electrochemistry	127
Chapter 8: Detection of low concentrations of fine-grained iron oxides in soils and sediments by voltammetry of microparticles	137
Chapter 9: Voltammetric identification of pedogenic iron oxides in palaeosol and loess	151
Epilogue	161
References	165
Samenvatting in het Nederlands (summary in Dutch)	177
Dankwoord	191
Create your own compass / Maak zelf een kompas	193
Curriculum Vitae	195
Publications	197

Prologue and Summary

Magnetism & Climate

Environmental magnetism studies among others the link between climate change and the characteristics of magnetic particles in rocks, soils and sediments. Rock-magnetic analyses sometimes are non-unique, which hinders an unambiguous identification of the magnetic particles that carry the climatic information. In this thesis, several complementary methods from chemistry and soil science are examined to explore whether they could assist in improving the determination of mineral-magnetic climate proxies. In this prologue, the reader is first introduced to the history of magnetic research, after which some important rock-magnetic discoveries will be touched upon. The historical overviews are followed by a brief introduction to the link between global climate change and magnetic minerals. Finally, a summary is given of the aims and results of this thesis.

History of the discovery of magnets and the Earth's magnetic field

Since the discovery of the magnet, people have been fascinated by its 'magic' behaviour. In the ancient Greek and Chinese cultures, the attractive force of lodestone was generally recognised. Lodestone is an iron ore rich in (oxidised) magnetite (Fe_3O_4), a very common magnetic mineral. However, usually magnetite ores will not display such strong magnetic behaviour as lodestones do. These stones owe their magnetic 'power' to two factors: 1. the configuration and concentration of the magnetite crystals 2. the ore has been struck by lightning during which a strong transient magnetic field magnetised the ore. A rich source of lodestone was the ancient Greek city of Magnesia (in Asia Minor or modern Turkey). Reputedly, around 900 BC a Greek shepherd named Magnus walked across a field of black stones which pulled the iron nails out of his sandals and the iron tip from his shepherd's staff. But the unique property of this 'lapus vivas' (live stone) to point to the magnetic north was not recognised by the Greeks.

This was not the case in China, where the first compass was invented by Luan Te (around 83 AD). He had a board game in which one of the pieces was a spoon made of *ci shi* or 'loving stone' (lodestone). When he dropped the other metal pieces near the board, the spoon would spin around until the handle was pointing south. From this moment, the Chinese started developing the compass and studying lodestones to understand their power. They realised that as long as a lodestone can rotate freely, it will always point north. Around 600 AD they discovered that lodestone can be used to magnetise small iron needles, but these needles lost their magnetism with time. Their greatest discovery therefore, was that they could permanently magnetise iron by heating it to red-hot and subsequently cooling it rapidly in a north-south orientation. With this knowledge they were able to improve the latest version of the compass, which consisted of a fish-shaped lodestone floating freely in a bowl of water. They replaced the lodestone fish with an iron needle, and thus was born the modern day compass: a magnetised iron needle rotating freely in a liquid. The first written reference to such compasses dates back to the 'Essays from the

torrent of dreams’ by Shen Kua in 1086 AD, and shortly after that it is also mentioned in European literature. The knowledge of the compass was possibly transported to the western world by Marco Polo via the old ‘Silk Road’. However, there is no direct evidence to support this idea and other theories exist, such as: transport by sea and via the Arabic countries, or by the Vikings.

In Europe, magnets were generally recognised as magical or containing special powers. The first explicit reference is found in the ‘Roman d’Enéas’ (1155-1160 AD). This novel was written by an anonymous Norman poet, and in it he says: “the walls of Dido’s Carthage are studded with magnets so that an armed man, approaching too closely, would be pulled to the wall and held tightly”. He refers to lodestone as ‘adamant’ or lovestone (from which the French word for magnet ‘aimant’ is derived). In those days, people believed that if you gave your loved one a piece of ‘adamant’ he or she would always return to you.

The first western reference to the use of compasses for navigation dates from 1190-1199 AD, just a century after the Chinese compass was perfected. It is found in a book by Alexander Neckam, an Augustinian abbot. In his book ‘De naturis rerum’ (Of all things natural) he writes about a device that was used to navigate the seas in clouded weather. With the introduction of the compass, lodestone starts to fascinate European scholars, and in 1269 Pierre de Maricourt (also known as Petrus Peregrinus) publishes a study of compasses and magnets which would serve as a reference book for several centuries to come. In his ‘Epistola de Magnete’ he writes letters to his friend Sygerus of Foucaucourt, in which he describes how he discovered that a sphere of lodestone behaved as a dipole; opposite poles attract one another while similar poles repel each other (figure 1). His book is the first truly scientific study known to us: the researcher does (careful) experiments, and uses only his observations to postulate a theory.

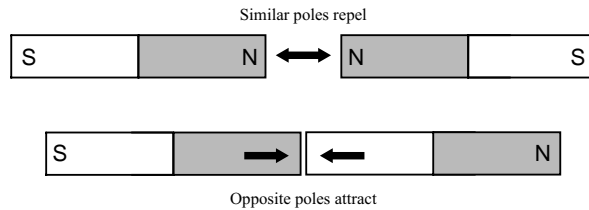


Figure 1: Similar poles of a dipole magnet repel each other, while the opposite poles attract each other.

For centuries, scientists have wondered about the origin of this magnetic power of lodestone, and most assumed a celestial origin. They believed it must originate in the only star that never changes its position in the sky: the North Star or polestar. But in 1600 this all changes. In that year William Gilbert (who is soon to be the court physician of Queen Elisabeth I) publishes the outcome of his 18 years of research on magnets: ‘De Magnete, Magneticisque Corporibus, et de Magno Magnete Tellure – Physiologia Nova, Plurimis et Argumentis et Experimentis Demonstrata’¹. He is the first to realise that the Earth itself is like a giant lodestone with north and south poles, and that the compass needle aligns to the magnetic field generated by the Earth (figure 2). In this way, he was the first to attribute a physical property to the Earth as a body. Furthermore, the origin of the magnetic field was redirected from a celestial location (pole star) to one inside

¹On the Magnet, Magnetic Bodies, and the Great Magnet the Earth – A New Physiology, Demonstrated by Many Arguments and Experiments

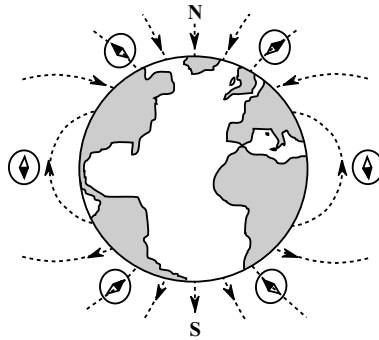


Figure 2: Dipole representation of the earth's magnetic field, field lines as represented by dashed lines. The dip of a compass needle depends on the geographical location, as shown in the examples given for high and low latitudes.

the Earth. He also showed that the magnetic poles of the Earth do not coincide with the geographic poles. With his scientific approach he was able to dismiss several superstitions about magnets, for instance he disproved the widely held belief that the magnetism of a lodestone can be removed by rubbing it with garlic. Still, it would take more than a hundred years before it ceased to be an offence punishable by flogging, for a British naval helmsman to have garlic on his breath for fear of demagnetising the ship's compass.

The work of Gilbert has served as a guideline for other important discoveries. Edmond Halley (of the comet) was looking for an explanation for the origin of the Earth's magnetic field. In 1692, he postulated that the interior of the Earth consisted of layers (spheres within spheres). Each sphere was independently magnetised, and each rotated slowly with respect to the others. Although this was not correct mechanism generating the Earth's magnetic field, he was the first to postulate that the Earth consists of several layers. This was proven to be true by geophysical research approximately two centuries later.

Hans Christian Oersted (1777-1851) also studied magnetism, and he discovered that a magnetic needle orientates itself perpendicular to the current flowing through a wire. His idea was picked up by André-Marie Ampère (1775-1836), who showed that when a current runs trough a coil of wire it produces a magnetic field similar to that of a dipole. These observations were crucial for developing theories on the origin of the Earth's magnetic field, which we now know originates from its fluid outer core (through a

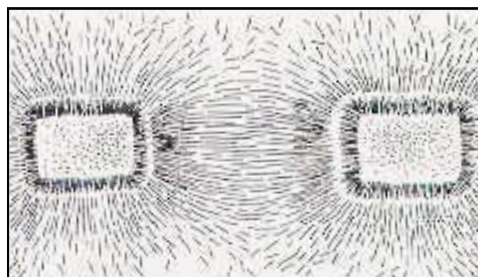


Figure 3: The magnetic field lines can be made visible by placing one or more magnets on a piece of paper covered with magnetic filings. The filings will orientate themselves to the magnetic field lines as generated by the magnets, just as the compass needle orientates itself to the fieldlines generated by the earth's magnetic field.

dynamo process). Because of the high temperatures in the Earth's core, any type of magnet would lose its magnetic powers, thus there must be a different mechanism. This is – simply put – the circulation of electrically conductive fluids in the Earth's liquid outer core, a process similar to the circular electric currents in Ampère's experiments. Around the same time (in 1838) Carl Friedrich Gauss, a German mathematician, developed a mathematical description of the geomagnetic field that is still used today.

Michael Faraday was the first to make a visual presentation (field lines) of the magnetic forces of a magnet (figure 3). His contemporary James Clerk Maxwell devised a mathematical model in 1855 that described all that was known about electrical and magnetic fields. To this day, the Maxwell laws form one of the cornerstones in physics; they explain phenomena such as radiowaves, X-rays and microwaves.

After the realisation that the Earth itself produced a magnetic field, it was not until the 20th century that the most characteristic property of this field was discovered: its ability to reverse polarity. The French physicist Bruhnes (1906) discovered that the direction of remanent magnetisation in a lava flow and its adjacent baked clay was exactly opposite to that of the present-day field (figure 4). He suggested that the

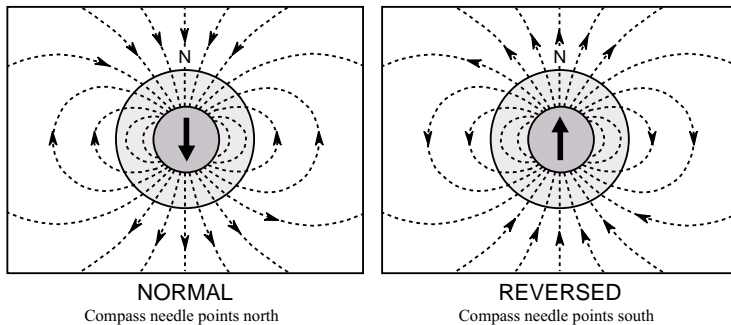


Figure 4: The most important characteristic of the earth's magnetic field is its ability to reverse. The left panel shows the 'normal' or current direction of the magnetic field, while the right panel shows the reversed magnetic field (adapted from Langereis & Krijgsman (in press)).

Earth's magnetic field must have been reversed at the time of extrusion of this lava flow: the magnetic north must have become the magnetic south and vice versa. Later studies by Mercanton (1926) and Matuyama (1929) confirmed his observations. They found reversed magnetic directions in rocks from all over the world, and Matuyama noted that the reversed directions were consistently found in older rocks. Subsequently, more reversals were detected, and in 1955 the Dutch scientist Hospers proposed that the pattern of reversals could be used to correlate and date stratigraphic records from all over the world (hence was born the discipline of magnetostratigraphy).

With the advent of reliable dating methods for rocks in the 1960's the geological age of the magnetic reversals could be determined (Cox et al., 1963). This has led to the development of the geomagnetic polarity time scale (GPTS); a time scale based on the distinctive pattern of reversals of the direction of the magnetic field. By that time, researchers had studied patterns of magnetic directions recorded in rocks from all over the world. They found that the ancient magnetic field direction and the corresponding positions of the magnetic poles not only varied through time but also geographically. This could only mean two things: either the magnetic pole had moved (true polar wander) or the continents had moved (continental drift or

apparent polar wander). In the following years there was much scientific debate, but no clear evidence to support either theory, until finally palaeomagnetism was able to prove the hypothesis of continental drift as proposed earlier by Alfred Wegener (1912). The mechanism that generated continental drift however, was still unclear. During the 1950's, ocean-going research vessels discovered that the magnetic signal of the ocean floor was aligned in long strips (figure 5), parallel to the mid-Atlantic ridge, which is part of an Earth-

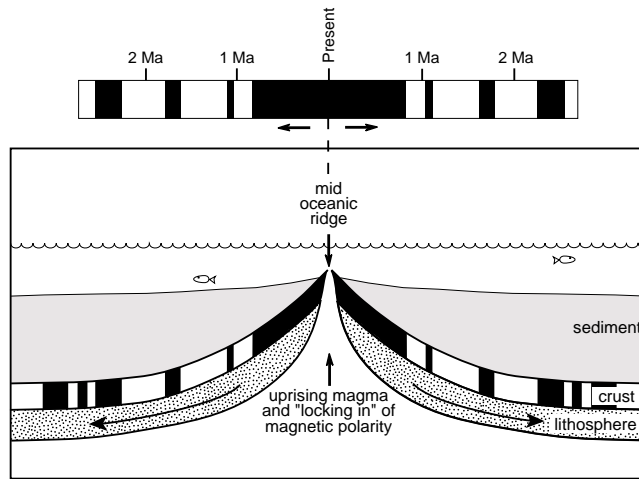


Figure 5: A schematic picture of the mid-oceanic ridge (MOR) system (lower panel). As magma rises up in the centre of the ridge, it pushes apart the two oceanic plates causing 'continental drift'. While new oceanic plates are formed along the MOR, the magnetic domains in these new rocks will orientate themselves to the ambient magnetic field. This results in a pattern of normal and reversed magnetic signals (similar to a bar code on a supermarket product) parallel to the MOR and symmetrical on both sides of the MOR (as shown in the upper panel) (adapted from Langereis & Krijgsman (in press)).

encircling system of ridges. The structure and distribution of the seafloor magnetic signal seemed remarkably symmetric on both sides of the ridge. Following the hypothesis of sea-floor spreading by Hess (1962), Fred Vine and Drummond Matthews (1963) put both observations together, and argued that the sea floor was in constant motion, pulling away from the central ridge. They had found the mechanism responsible for continental drift. We call it plate tectonics: the foundation of modern Earth Sciences.

The founders of rock magnetism

Much of the early research was focussed on describing the Earth's magnetic field, but in the late 18th century researchers started investigating how this signal is recorded in rocks and minerals. Around this time researchers had already observed that some rocks possess extremely strong remanent magnetisations, but these effects had been attributed to lightning strikes by Alexander von Humboldt in 1797. The first observations that certain rocks were magnetised parallel to the Earth's magnetic field were made by Delesse in 1849 and Melloni in 1853. Pierre Curie (who married Marie Curie in 1895) was also fascinated by magnetism before he and his wife started working on radiation studies. He discovered that magnets lose their magnetism above a certain temperature (now known as the Curie temperature).

In France, Paul Langévin published his work on the atomic theory of paramagnetism in 1905. He suggested that the alignment of molecular moments in a paramagnetic substance would be random in the absence of an externally applied magnetic field, but would be non-random in its presence. The higher the temperature, however, the larger the thermal motion of the molecules and thus the greater the disturbance to their alignment by the magnetic field. His contemporary, Pierre Ernst Weiss, worked on magnetism as well. In 1907 he published his molecular field theory in which he proposes a mechanism for the origin of magnetic moments in minerals. He postulated that magnetic minerals contain internal magnetic fields (domains). In the absence of an external field, these domains cancel each other out, while in the presence of even a small applied field, the domains will either rotate, or enlarge at the expense of others. He had found an explanation for the magnetic behaviour of ferromagnets (figure 6). The experiments of Heinrich Georg Barkhausen (1919) confirmed the existence of magnetic domains and the movement of the domain walls. He demonstrated that the movement of a ferromagnetic material in a coil produces a change in the position of the domain walls (now known as Barkhausen jumps) which can be heard as sharp clicks when an amplifier is hooked up to the coil.

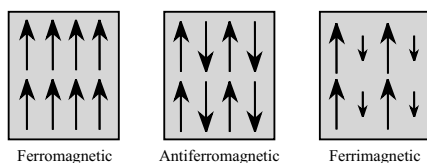


Figure 6: Different forms of coupling of spin moments result in different magnetic behaviour. In ferromagnetic materials, the moments are all parallel, which results in a net magnetic moment in the direction of the individual moments. Metallic iron is an example of a ferromagnetic substance. For antiferromagnetic minerals, the moments of the individual sublattices are of equal strength, but the directions of the moments are antiparrallel and thus they oppose each other. This results in a net magnetic moment equal to zero. Usually, antiferromagnetic materials have imperfect moments with directions that are not exactly opposite, this is called canted antiferromagnetism. In such cases the net magnetic moment is not equal to zero. Hematite is an example of a mineral with a canted antiferromagnetic moment. In ferrimagnetic materials, the opposing sublattice moments are of different strength, resulting in a magnetic moment pointing in the direction of the dominant sublattice. Magnetite and maghemite are examples of ferrimagnetic minerals (adapted from Langereis & Krijgsman (in press)).

The studies of magnetism in minerals and of the Earth's magnetic field had developed separately, until the late 1930's, when the two were brought together by people like Koenigsberger, Thellier, Nagata and Néel. These scientists studied the processes responsible for the magnetisation of rocks from a physical viewpoint, and tried to reproduce it in the laboratory. This type of research was given the name rock magnetism by Nagata (1953), and it has become the foundation of palaeomagnetic research. They discovered that they could induce a magnetisation in a rock sample by exposing it to heat and then cooling the sample in a (laboratory induced) magnetic field. Indeed, very similar to the way the ancient Chinese made compass needles. Néel then showed (1949) that this thermoremanent magnetisation (TRM) was locked into the sample during cooling at a specific temperature determined by the size and shape of a particular magnetic grain (later named the Néel temperature for antiferromagnetic minerals, which has similarities to the Curie temperature for ferromagnetic minerals) (Néel, 1949). Despite Landau and Lifshitz's prediction (1935) that ferromagnetism was the only possible magnetism in nature, Néel used the theories of Weiss to show that

magnetic minerals do not all have similar distributions of magnetic domains, and his theory for single-domain minerals is still valid. He also discovered a phenomenon known as viscous magnetisation: the gradual change of magnetisation with time at constant temperature. Furthermore, he distinguished ferrimagnetic and antiferromagnetic minerals and described the difference in magnetic sublattice exchange coupling in these minerals (Néel, 1955). In 1970 he received a Nobel Prize for his work.

Relationship between climate and magnetic minerals

The climate of the Earth varies both locally as well as globally, and we know that in the past major glaciations have occurred. In the 1920's, Milutin Milankovitch explained the occurrence of such drastic changes in global climate by calculating the variation in the Earth's orbit with time: the orbital or Milankovitch cycles. He discovered that there are three important orbital cycles that determine the distribution of solar heat received by the Earth: eccentricity, obliquity and precession (figure 7). The eccentricity cycle determines the shape of the orbit of the Earth around the Sun; it changes from circular (low eccentricity) to elliptical (high eccentricity) in ~ 100.000 and ~ 400.000 year cycles. In periods of circular orbits, the seasonal contrast between northern and southern hemisphere is small. It will be larger in periods of maximum eccentricity, and the length of the respective seasons will be different.

The obliquity cycle determines the change in tilt angle of the Earth's rotation axis with respect to the orbital plane. The tilt angle varies between 22° and 24.6°, with a period of ~ 41.000 years, and has a stronger effect at high latitudes than at the equator. The smaller the tilt, the less seasonal contrast; meaning mild winters and cool summers during small tilt, and cold winters and hot summers during maximum tilt.

The climatic precession cycle takes ~ 21.700 years and describes the position of the Earth's axis of rotation with respect to the Sun. The 'wobble' of the axis will affect the position of the equinoxes (the time when the Sun is positioned directly over the equator). This means that, at some moments in the precession cycle, the (northern hemisphere) summer solstice is closest to the Sun, while at that same moment the winter solstice is farthest from the Sun (see figure 7). Then ~ 11.000 years later they will be in the opposite position. The effect on the global climate is that in the first situation (for the northern hemisphere) the winter is cold because the winter solstice is farthest from the Sun, while the summer is hot because the summer solstice is closest to the Sun. In the second situation, the winter will be mild and the summer cool, which is the present-day situation.

From the combined effect of these three cycles the insolation curve can be calculated which gives a representation of the amount of energy the Earth receives from the Sun at any given latitude. This varies

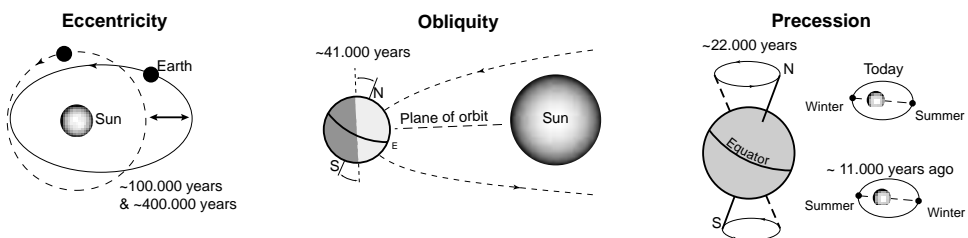


Figure 7: The three Milankovitch cycles: eccentricity, obliquity and precession. The combined cycles influence global climate (adapted from Langereis & Krijgsman (in press)).

with time because the three cycles all have different periods and thus they can both enhance or reduce each others effect. The most favourable conditions for the growth of ice caps are cold summers. Hence, orbital forcing is one of the major causes for the cyclic thickening and shrinking of the polar ice caps. An ice age is most likely to occur in a situation where the obliquity is at its minimum, the eccentricity is at its maximum and the Earth is furthest away from the Sun during the summer solstice. Although at present we are in a warm (interglacial) period, the current trend of the orbital cycles suggests that we are heading for a new ice age in the northern hemisphere. However, exactly when this new ice age will start is unknown, particularly because it is still unknown to what extent the recent increase in anthropogenic greenhouse gasses can counterbalance the effects of orbital forcing, and prevent the cooling of the global climate.

The theory of Milankovitch provides a mechanism for periodic climate changes that have occurred in the past. The changes in the distribution of energy received from the Sun has had an important effect on climate and environment, and thus on environmental factors such as precipitation, wind direction and intensity, vegetation, etcetera. These environmental factors, in turn, have influenced the weathering rate of rocks, the amount of aeolian dust, the build-up and retreat of glaciers, growth of carbonate reefs in the sea, and many other phenomena that are recorded in the geological archive of the Earth. Thus, the past pattern of climatic changes is recorded in rocks and sediments that we see today. One of the markers for the record of the Earth's climate in the sediments is the variation in concentration of stable isotopes of oxygen (^{18}O and ^{16}O). Ocean sediments represent an almost continuous record of the geological past, and they contain many fossils of planktonic foraminifera (tiny sea creatures with a calcareous shell). These 'forams' take up oxygen from the ocean water to make their carbonate shells, and the ratio ($\delta^{18}\text{O}$) of their heavy oxygen (^{18}O) and light oxygen (^{16}O) isotopes reflects the amount of ice at the poles. This is because the lighter ^{16}O evaporates more easily from the oceans (especially at low ocean surface temperatures), and is preferentially stored in the ice sheets at the poles. This implies that an increase of heavy ^{18}O oxygen in the oceans, and therefore an increase in the $\delta^{18}\text{O}$ value in foram shells indicates more ice and hence a colder climate (figure 8).

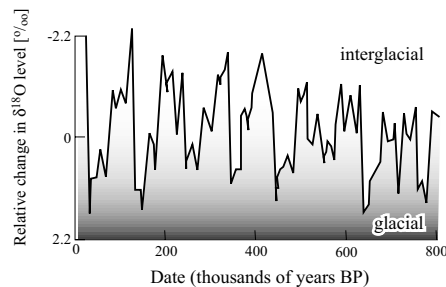


Figure 8: The oxygen isotope record for the past 800.000 years. An increase in $\delta^{18}\text{O}$ ratio indicates a glacial period, while a decrease in this ratio is caused by an interglacial climate.

The observation that the variation in the oxygen isotope ratio in oceanic sediments also shows a corresponding variation in magnetic properties, stimulated considerably more palaeomagnetic research. This discovery had to imply that the magnetic signal recorded in rocks and sediments not only records the

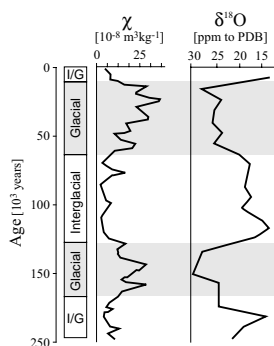


Figure 9: Example of the correlation between magnetic susceptibility and oxygen isotope ratio in a deep-sea sediment. Glacial periods are indicated in grey and have high oxygen isotope ratios, while the interglacial periods have low oxygen isotope ratios. The magnetic susceptibility in this deep-sea sediment section is enhanced in horizons correlated to glacials, and low in horizons correlated to interglacials (after Thompson & Olfield 1986, fig. 12.7).

Earth's magnetic field (direction and intensity), but also global climate. It became clear that (often) the changes in magnetic signal of the ocean sediments reflect the pattern of climate changes (figure 9). One explanation is that during glacial times the input of foraminifera (as oceanic carbonate) would be limited due to the cold climate, thus the detrital and aeolian input of material is seemingly enhanced. During interglacials, this input would be diluted by the increased input of carbonate from the foraminifera, and the magnetic signal in the sediments would be weaker than in glacial times. An alternative explanation is that during glacial times there is less vegetation, or there are changes in the wind directions that cause an increased and/or changed input of lithogenic particles. Both mechanisms would enhance the magnetic signal in ocean sediments during glacial periods.

The fluctuations of the oxygen isotope ratio as well as magnetic parameters in the deep-sea sediments thus reflect global climate. It was difficult, however, to find a similarly long and continuous continental record of global climate. This changed when in the 1980's continental loess deposits in China were dated with magnetostratigraphy. These Quaternary Chinese deposits consist of sequences of loess deposits of high sedimentation rate intercalated by palaeosols. Subsequently, it was shown that the magnetic signal in these deposits behaved similarly to the marine oxygen isotope record (e.g. Heller and Liu, 1984). The magnetic susceptibility of these deposits varies with lithology; it is low in the loess horizons and high in the palaeosols. The loess was deposited in glacial periods, while during interglacial stages the precipitation and temperature increased and thus encouraged pedogenesis and neoformation of strongly magnetic minerals in the palaeosols (figure 10).

This thesis

An important tool to derive and understand mineral-magnetic properties and their origin, is rock magnetism. It studies not only the fundamental magnetic properties of natural and synthetic minerals, but also the relationship between magnetism and mineralogy, grain size, shape, crystallinity, chemical composition, and temperature is used to understand the magnetism of minerals and rocks. Furthermore, these parameters can be used to determine the concentration and composition of the magnetic particles in

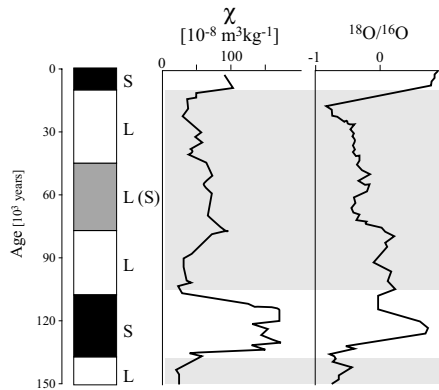


Figure 10: Example of the correlation between enhanced magnetic susceptibility (increase concentration of fine-grained magnetic iron oxides) and oxygen isotope record. The left column shows the lithology of a loess-palaeosol section with the palaeosols indicated in black and loess in white. A weathered loess is present in the middle of the section and shows a slightly increased susceptibility, which is not related to the oxygen isotope record. For the majority of the section, the susceptibility record correlates well to the oxygen isotope curve, and is high during interglacial stages (low oxygen isotope ratio) and low during glacial stages (high oxygen isotope ratio, grey areas in the figure) (after Liu et al., 1995).

natural samples. Rock magnetism therefore appears ideal for the identification of pedogenic magnetic particles. However, the signal of ferrimagnetic particles often swamps that of other, weakly-magnetic particles and this prevents an accurate identification by rock-magnetic techniques alone. Other techniques are required to help identify the exact composition of the pedogenic material. For this purpose, extraction methods were introduced because it was argued that they selectively dissolve certain minerals or grain sizes. The results of several studies, however, showed there are some controversial issues about the exact minerals that would be selectively removed by these methods.

The Chinese loess sequences were the first continuous continental records of climate change that were recognised as such, and soon similar patterns were found in loess sequences from other areas of the world. In these sequences, the changes in magnetic signal could also be correlated to the global climate (as in the deep-sea sediments). In certain areas such as Alaska and Siberia, however, the pattern of magnetic enhancement is exactly opposite to that of the Chinese sequences; with higher susceptibilities in the loess (glacial stages) and lower in the palaeosols (interglacial stages). The mechanism that is responsible for the magnetic enhancement must thus have varied geographically. Still, the magnetic signal of these sediments is an excellent indicator of global climate, even if the regional recording mechanisms can strongly vary. To understand the origin of these differences, it was important to better understand the processes that lead to opposite observations of the same (climatic) mechanism. For instance, about why and how magnetic minerals were formed during pedogenesis, and which were remains of the parent material. Because the formation of new minerals (and the alteration of lithogenic minerals) depends on factors such as climate, soil pH and moisture, it is important to be able to derive the composition and concentration of pedogenic magnetic minerals, because they will better reveal the climatic history of the site.

The primary aim of this thesis is to get a better understanding of how chemical extraction methods work, to improve their role in identifying magnetic climate proxies. For this reason, the emphasis was directed to

the discrimination of spinel-type ferrimagnetic oxides, i.e. magnetite and maghemite. Besides investigating the effectiveness of the chemical methods already used in environmental magnetism studies it was important to establish whether there were techniques in other disciplines (such as soils science or chemistry) that might be suitable for the identification and characterisation of magnetic minerals. A search of other disciplines led us to the field of electrochemistry and the possibilities for selective identification of iron oxides by voltammetry of microparticles (VMP). This thesis is divided in three parts; the first part discusses the results of a study of the protocol of two extraction methods, the second part discusses the results of a study on the effect of these methods on natural loess and palaeosol samples, and the third part introduces a new electrochemical analytical tool for environmental magnetism.

In **Part I**, we start with an introduction to the principles of chemical extraction (**Chapter 1**). The two methods used in this thesis are introduced as well: the citrate-bicarbonate-dithionite method (CBD), and the acid-ammonium-oxalate/ferrous iron method (AAO-Fe²⁺). For both methods, we investigated whether the method preferentially dissolved fine-grained or coarse-grained minerals, and whether it had a preference for dissolving either magnetite or maghemite. To achieve this, we used samples with accurately known composition, grain size and concentration of the magnetic mineral assemblage. These synthetic samples were prepared with a quartz or calcium carbonate matrix, into which magnetic minerals were mixed.

Chapter 2 discusses the results of CBD extraction of these synthetic samples. The conditions of the CBD procedures used in previous studies varied in temperature, sample amount and concentration, extraction time, and amount of dithionite. Along with a study of the effectiveness of this extraction method for selective dissolution of spinel-type iron oxides, we investigated the effects of changing experimental conditions on the dissolution behaviour of the magnetic minerals. The results show that the CBD method is sensitive to changes in extraction temperature and concentration of iron oxides. An increase in temperature enhanced the dissolution of all iron oxides, while an increase in iron oxide concentration led to a decrease in dissolution rate. The results showed that little distinction could be made between the dissolution of fine-grained magnetite and maghemite. Further testing with coarse-grained minerals showed that the method is sensitive to grain size rather than to mineralogy. The fine-grained oxides were removed much faster than the coarse grained oxides.

The synthetic samples were also used to investigate the selectivity of the AAO-Fe²⁺ method (**Chapter 3**). During the extractions, we discovered that the calcium carbonate matrix of the synthetic samples buffered the extraction solution and severely affected the dissolution behaviour. By using a quartz matrix, this effect could be prevented. The results show that this method is less aggressive in its attack on iron oxides than the CBD method. The main distinction for this method was in grain size: like the CBD method it dissolved the fine-grained oxides much faster than the coarse-grained oxides. With the aid of extensive rock-magnetic analysis we furthermore showed that the method indeed provides some mineralogical distinction when dealing with mixtures of minerals.

The results of the extractions with synthetic samples improved our understanding of the selectivity of the methods, and showed that the AAO-Fe²⁺ might be more promising for selective dissolution of specific magnetic minerals. This was tested on natural samples (**Part II**). A loess-palaeosol sequence from the Czech Republic was selected, because of the clear relationship of the cycles of loess deposition and soil formation with glacial and interglacial climate. **Chapter 4** provides the reader with the basic principles of

environmental magnetism and, more specifically, with the relationship between loess-palaeosol sequences and climate change. **Chapter 5** discusses the results of extractions with the CBD method. Because this method is rather aggressive, the effect on silicate minerals was studied with ICP-OES to see whether any iron was released from these minerals. The results show that the method preferentially dissolved the fine-grained (pedogenic) minerals (magnetite as well as Al substituted goethite and hematite) and it also attacks the oxidised rims of the coarse-grained (lithogenic) magnetite particles. Furthermore, with each extraction step part of the silicate minerals was dissolved as well, indicating that the CBD method also removes iron from those minerals.

Samples from the same site were also extracted with the AAO-Fe²⁺ method (**Chapter 6**). In both Chapters 5 and 6, the rock-magnetic parameters of the samples were investigated, and several new mineral-magnetic techniques were used for the identification of the magnetic composition of the samples: first-order-reversal-curve (FORC) analysis and improved isothermal remanent magnetisation (IRM) component analysis. The AAO-Fe²⁺ method appears to be sensitive to the fine-grained pedogenic magnetite and only removed part of the (pedogenic) hematite and goethite, while it did attack the oxidised rims of the coarse-grained (lithogenic) magnetite.

In **Part III** we discuss the results of a pilot study for magnetic mineral identification with a new electrochemical technique: voltammetry of microparticles (VMP). It was developed for the purpose of studying mineralogy, crystallinity, reactivity, and other characteristics of solid species. **Chapter 7** introduces the reader to the field of electrochemistry and explains the theory and practice of voltammetry of microparticles.

In **Chapters 8 and 9**, the VMP method is discussed in more detail and results of magnetic mineral identification on natural samples from two different geological sites are presented. Besides mineralogical identification, a semi-quantitative method is proposed to evaluate the contributions of each mineral to the total magnetic mineral phase. The VMP method enabled us to make estimates of the contributions of goethite and hematite in each sample and to derive an interpretation of the pedogenic environments responsible for the magnetic mineral composition of the sections.

The VMP results were combined and compared with the results of rock-magnetic analysis. The method was not suitable for the determination of the content of magnetite, because the concentration in our loess and palaeosol samples fell below the detection limit. However, it did provide detailed information about the crystallinity and reactivity of the hard magnetic particles (hematite and goethite) in the samples. Since the magnetic signal of these minerals is usually swamped by that of magnetite, the VMP method provides a very useful instrument to discriminate the weak magnetic signal of hematite and goethite.

In the **Epilogue**, we combine the results of part I and II to draw an overall conclusion about the significance and use of chemical extraction methods in environmental magnetism. The results of the natural samples show that both methods extract part of the pedogenic minerals from the samples, although in a varying degree. Although neither method was able to remove only the newly formed pedogenic particles, they both gave new information about the composition of the samples, which could not be retrieved from the rock-magnetic data alone. The CBD and AAO-Fe²⁺ methods are therefore suitable tools in helping identify the composition of both lithogenic and pedogenic magnetic fractions in natural samples, but they must be applied with caution because the protocol can influence the outcome of the extractions. Finally, the future potential of VMP for environmental magnetism is discussed.

Part I

Synthetic samples

Extraction Methods in Environmental Magnetism: Dissolution Principles

In this chapter the use of sequential extraction methods in environmental magnetism is discussed. We start with a brief introduction to extraction methods and a discussion of the benefits of integration of these methods into environmental magnetism, followed by an explanation of dissolution principles. The kinetics of dissolution mechanisms are considered and rate laws and dissolution models are introduced as tools in identifying the reaction mechanism of iron oxide dissolution. The two extraction methods investigated in the present thesis, the citrate-bicarbonate-dithionite (CBD) and the acid-ammonium-oxalate (AAO) extractions, are discussed in the final sections of this chapter. Both methods have been incorporated into environmental magnetism, however, extraction protocols have been varied. Therefore, the parameters that influence the dissolution kinetics as well as the dissolution mechanisms are considered.

I. Introduction

Environmental processes including for example weathering, precipitation, and pedogenesis, influence the transport, deposition and transformation of magnetic particles. Thus, we can use magnetic properties for provenance analysis of sedimentary basins and for pollution assessment. Furthermore, the grain-size and type of magnetic minerals are related to climate factors such as precipitation and temperature, enabling the use of the magnetic characteristics of soils and sediments as climate proxies (Mullins, 1977; Thompson et al., 1980; Oldfield and Robinson, 1985; Thompson and Oldfield, 1986; Verosub and Roberts, 1995; Dekkers, 1997).

Selective dissolution of magnetic minerals can be used to further constrain palaeoclimate proxies as determined by rock-magnetic measurements. A sample is treated in steps with increasingly stronger reagents to selectively dissolve certain phases. Theoretically, samples can be mineralogically partitioned into specific phases using the appropriate reagents. Thus, when focussing on reagents targeting the dissolution of iron(oxy)(hydr)oxides, it is possible to obtain additional information about the geochemical and biological processes that have affected the magnetic signal (Martin et al., 1987; Fine et al., 1995; Hunt et al., 1995; Sun et al., 1995; Verosub and Roberts, 1995). Comparison of magnetic and chemical data before and after selective dissolution assists in the reconstruction of the environmental setting of the sample. Sequential extraction procedures have been developed predominantly in geochemistry and soil science.

Commonly, such a sequential extraction procedure involves the use of five different extraction reagents to monitor the stepwise dissolution of metals from five different soil-phases or soil-fractions: exchangeable/amorphous, carbonate/easily reducible, iron and manganese hydroxides, organic & sulphide, and the 'residual' phase (Bradshaw et al., 1974; Tessier et al., 1979; Förstner et al., 1981; Hilton et al., 1986;

Martin et al., 1987; Shannon and White, 1991; Raiswell et al., 1994). Sequential extractions can also be performed by repetition of the same extraction method. Here, one specific phase is dissolved by a single method applied in several steps, and the results are used to evaluate the presence and stability of the phase in question (Deb, 1950; Ryan and Gschwend, 1991; Erel et al., 1997). This technique can be used to investigate grain-size or concentration variations. Thus, the partitioning of iron over different phases is generally studied by using a range of extraction methods, while the specific concentration of one particular iron phase is assessed by applying a single extraction method several times.

Originally, selective dissolution was developed for various purposes in soil science such as optimising sample preparation and/or dispersion prior to further soil analysis. Subsequently, many of these methods have been used as well for specific dissolution of minerals and/or soil-phases from the samples. In environmental magnetism, the extraction methods aim at mineral-specific dissolution. They are, however, more commonly used to distinguish different magnetic minerals in the sample and their origin (Hilton et al., 1986; Fine et al., 1993b; Verosub et al., 1993; Fine et al., 1995; Hunt et al., 1995c; Singer et al., 1995; Sun et al., 1995; Verosub and Roberts, 1995; Cornell and Schwertmann, 1996). Magnetic-mineral phases of interest to environmental magnetism are lithogenic vs. non-lithogenic forms, residual vs. non-residual phases, a distinction of non-residual phases, and crystalline vs. non-crystalline phases (Goldberg and Arrhenius, 1958; Chester and Hughes, 1967; Agemian and Chau, 1977; Martin et al., 1987; Stucki et al., 1988). In soils, the most common magnetic minerals are magnetite (Fe_3O_4), maghemite ($\gamma\text{-Fe}_2\text{O}_3$), hematite ($\alpha\text{-Fe}_2\text{O}_3$), goethite ($\alpha\text{-FeOOH}$) and ferrihydrite. Usually the spinel phases (magnetite and maghemite) occur in trace amounts, but are readily detected by magnetic methods due to their strong magnetic signal. In lake and marine sediments, trace amounts of iron sulphides may be common in addition to the magnetic minerals previously mentioned.

The citrate-bicarbonate-dithionite (CBD) method is the most frequently used extraction method in environmental magnetism. The acid-ammonium-oxalate (AAO) method is used as well although less often. In most cases, the CBD method is used to determine the total free iron in the samples, while the AAO method is used to determine non-crystalline iron (Schwertmann, 1959; Mehra and Jackson, 1960; Schwertmann, 1964).

Application of sequential extractions is based on the surmise that different phases have different dissolution mechanisms and react specifically during the experiment. To understand which methods are most suitable for environmental magnetism, information on the dissolution mechanism(s) of the magnetic minerals is of interest. In the next section, the basic principles of dissolution theory and the application to iron oxides are evaluated.

2. Dissolution Principles

2.1. Introduction

Dissolution is the decomposition of a solid resulting in the release of its components into solution. The dissolving solid is called the substrate, the compound responsible for the dissolution of the substrate is the solutant, and the solution carrying both the solutant and the products of the dissolution is the solvent. Solutants can be divided into reductants, oxidants, ligands, complex-formers and chelators. This

classification is based on the adsorption mechanism of the solutant and/or the type of reaction between solutant and substrate prior to dissolution. The corresponding mechanisms will be discussed in sections 2.2 and 2.3.

The dissolution of a mineral is a sum of chemical and physical reaction steps (Hering and Stumm, 1990). The first step of a dissolution reaction is the diffusion of the solutant through the solvent to the substrate. The second step is the reaction by which the solutant is adsorbed to the substrate surface. The migration of the combined solutant and surface ion over the substrate surface is the third step. The final step involves the release of the solutant with the attached substrate-ion into the solvent. Dissolution is not achieved unless all steps in the dissolution process are completed in this order (Morel and Hering, 1993; Cornell and Schwertmann, 1996).

Ligands and complexes

Ligands and complexation are important concepts in a discussion of dissolution processes. Ligands are compounds that can replace water on hydrated solid surfaces; they can share one or more free pairs of electrons with the surface atoms of the substrate and can therefore easily replace adsorbed water (Atkins, 1989; Morel and Hering, 1993). Ligands can either be single ions or larger molecules (charged as well as neutral). The attachment of the ligand to the substrate surface is called complexation, the combination of the ligand with the surface atom is called a surface complex. Complexation results in formation of π -bonds by the sharing of excess electron pairs between the ligand and the surface atom. During complexation, the ligand will either act as an electron pair donor or as an electron pair acceptor. In complexes with electron donor ligands, there is increased electron density at the surface atom, whereas with electron acceptor ligands the electron density at the surface atom is decreased (Atkins, 1989; Morel and Hering, 1993).

Ligands can have one or more functional groups that share electron pairs with a surface atom. They are classified according to the number of functional groups that react with one or more surface atoms. Figure 1 shows examples of the different ligand complexes that can form.

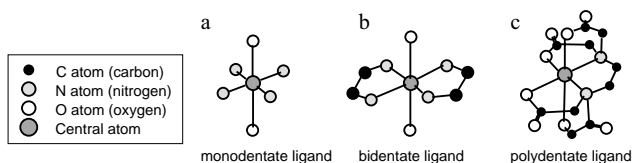


Figure 1: Examples of ligand classification. The central atom is a metal in solution, the hydrogen atoms are not indicated in the figures. Panel (a) shows the combination of four monodentate ligands (NH_3) with one central atom. Panel (b) is a complex formed by two bidentate ligands ($\text{C}_2\text{N}_2\text{H}_6$) and panel (c) shows a complex polydentate ligand complex (after: Morel & Hering, 1993).

Monodentate ligands have only one electron pair to share, they form only one bond with the surface atom. Bidentate and polydentate ligands have two or more reactive functional groups and can form more than one bond with the surface atom. When several of the functional groups of a polydentate ligand react with one central surface atom the complex is called a chelate (Atkins, 1989; Sposito, 1989; Sulzberger et al., 1989; Morel and Hering, 1993). From figure 1c it is clear that a chelating ligand encloses the central surface atom like a claw.

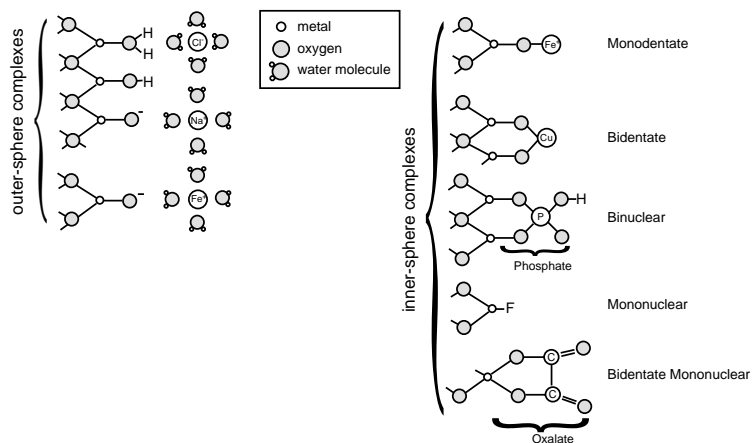


Figure 2: Examples of various forms of complexes, the left panel shows examples of outer-sphere complexes (i.e. watermolecules between ligand and surface site, and only electrostatic bonding). The right panel shows examples of inner-sphere complexes (i.e. no watermolecules between ligand and surface site, and ionic as well as covalent bonding). In binuclear complexes one ligand combines with two surface sites, while in mononuclear complexes, the ligand combines with only one surface site. Monodentate ligands have only one bond with the surface site, while multidentate ligands have more than one bond with one surface site (after: B. Sulzberger et al., 1989).

Complexation is often classified according to the way the ligands are attached to the substrate. Figure 2 is a schematic representation of the inner-sphere and outer-sphere complexation (Sposito, 1989; Sulzberger et al., 1989). When no water molecule is situated between the ligand and the surface atom, the complex is inner-sphere. These complexes can be formed with one or two atoms in the solid surface, leading to mononuclear and binuclear complexes respectively. In an outer-sphere complex at least one water molecule is present between the ligand and the surface atom. Due to these water molecules, the outer-sphere surface complexes cannot easily form ionic or covalent bonds between the ligand and the surface atom. Outer-sphere complexes usually have electrostatic bonds, while inner-sphere complexes can form both ionic as well as covalent bonds. Therefore, inner-sphere complexes usually are much more stable than outer-sphere complexes (Sposito, 1989).

2.2. Classification of dissolution mechanisms

Dissolution mechanisms can be distinguished according to the most important step in the dissolution process. This usually is the slowest step in the entire process: the rate-limiting step. Classification according to the rate-limiting step yields two mechanisms: diffusion-controlled dissolution and surface-controlled dissolution (Segal and Sellers, 1984; Stumm and Sulzberger, 1992; Morel and Hering, 1993; Cornell and Schwertmann, 1996).

Diffusion-controlled dissolution. When a solid phase comes into contact with water, the charged ions in the surface attract or repel water molecules. The attracted water molecules are bound to the surface ions in a solvation complex. When the bonds between the surface ion and its neighbouring ions in the solid are weak, the solvation complex can detach from the solid. This type of dissolution is common and depends on the transport of water molecules to the substrate surface (Sposito, 1989).

In *surface-controlled dissolution* mechanisms the first step (diffusion of the solutant to the substrate) is rapid while the detachment of the solvation complex is rate limiting (Morel and Hering, 1993). For example, the detachment rate of exchangeable ions that are adsorbed to the mineral surface is different from that of atoms that form an integral part of the mineral. Exchangeable ions are easily released from the solid surface, while the release of atoms from within the crystal structure requires a more powerful solvation complex.

Dissolution mechanisms can also be classified according to the solutant type and the reaction that takes place prior to dissolution. Then, three dissolution mechanisms are distinguished: protonation, complexation, and reduction (Figure 3) (Sulzberger et al., 1989; Hering and Stumm, 1990; Stumm and Sulzberger, 1992; Morel and Hering, 1993). Figure 3a shows an example of dissolution by protonation; it is the mechanism by which protons (H^+) bind with an OH-group on the hydrated substrate surface. In iron (hydr)oxides the reaction weakens the Fe-O bond, and slow detachment of the surface Fe(III) species into solution occurs (Segal and Sellers, 1984; Spósito, 1989).

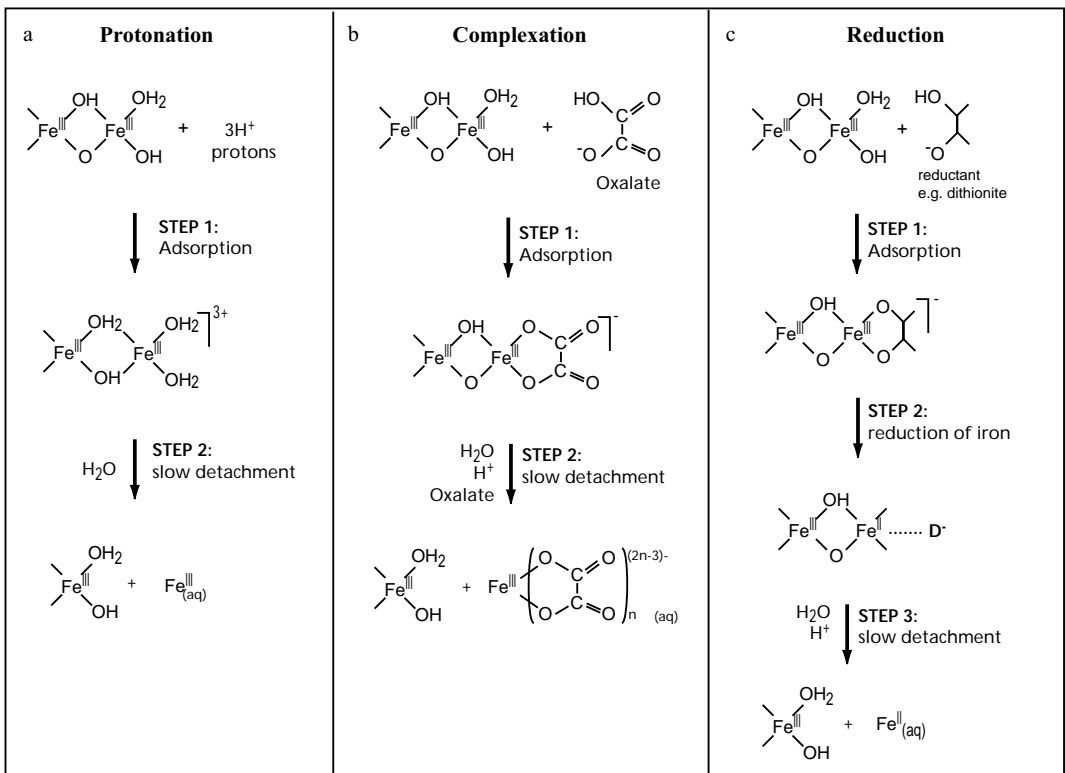


Figure 3 a-c: Several dissolution mechanisms: (a) protonation, (b) complexation, and (c) reduction of iron in iron oxides (after: Hering & Stumm, 1990, in Hochella and White, Reviews in Mineralogy).

Figure 3b illustrates an example of dissolution by complexation. This mechanism involves the attachment of a compound (other than H^+) onto the crystal surface; sometimes protonation is required prior to complexation. A strongly complexing ligand in the solution can exchange for a protonated OH-group

bound to the substrate. The surface ion-ligand complex ultimately detaches into the aqueous phase (Sposito, 1989). In iron(hydr)oxides, the high polarity of the surface complex will lead to a decrease in bond strength between the surface iron and its neighbouring atoms, which facilitates iron dissolution.

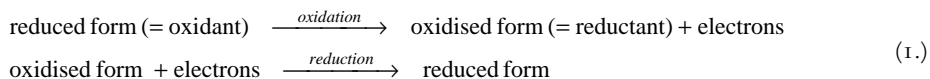
Many extraction methods used in soil science are based on ligand-promoted dissolution, and the mechanism has been studied at length (Olson and Ellis, 1982; Stucki et al., 1988; Cornell and Schwertmann, 1996). The polarising effect of the ligand distorts and weakens the bonds of the surface atom with its neighbouring atoms. The destabilised surface atom can then more easily be released from the surface (Atkins, 1989; Sposito, 1989; Morel and Hering, 1993). Polydentate ligands are more efficient in promoting dissolution than monodentate ligands because they can form surface chelates that have an even stronger polarising effect (Furrer and Stumm, 1986; Hering and Stumm, 1990; Cornell and Schwertmann, 1996).

Ligands can also inhibit dissolution. Some ligands bind to more than one surface atom (known as bi- or trinuclear complexation), the resulting complexes usually hinder dissolution (Stumm and Sulzberger, 1992). Sometimes, ligand-promoted dissolution is restrained by limited ligand adsorption due to unfavourable physical properties of the system (e.g. pH, temperature, available surface sites). For example, dissolved oxalate is protonated at low pH and this prevents its adsorption to mineral surfaces. A strong decrease in pH during extraction can thus interfere with the dissolution process (see also section 3.3).

Figure 3c gives an example of dissolution by reduction, which involves electron transfer between two compounds. For iron oxides this implies that the Fe(III) sites on the substrate surface gain an electron from the adsorbed solutant and reduce to Fe(II). The newly formed Fe(II) at the mineral surface has a less stable bond with oxygen than its predecessor Fe(III), thus the reduced metal is more easily detached from the surface than the originally present oxidised metal. Extraction methods using reductive dissolution will be discussed extensively in sections 2.3 and 4.

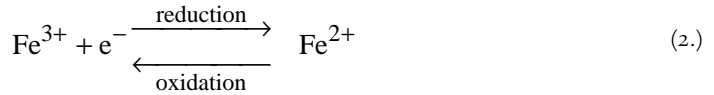
2.3. Redox reactions

In redox reactions, electron transfer takes place between two reacting compounds. The compound losing electrons is called the reductant, the compound gaining electrons is the oxidant. Redox reactions are a combination of two reactions: an oxidised form receives electrons during reduction while a reduced compound releases electrons to be oxidised (Atkins, 1989; Sposito, 1989; Atkins, 1990; Morel and Hering, 1993). The electron-transfer reactions are as follows:



A compound cannot release electrons unless another compound receives them; thus, reduction cannot occur separately from oxidation. Therefore the process of electron transfer is called redox.

Redox reactions are important in iron(hydr)oxide dissolution (Hering and Stumm, 1990; Stumm and Sulzberger, 1992). Iron occurs in different oxidation states. Ferrous iron (Fe^{2+}) has the electron configuration $1s^1 2s^2 2p^6 3s^2 3p^6 4s^2 3d^6$. Ferric iron (Fe^{3+}) contains one less electron in the outer d-shell ($1s^1 2s^2 2p^6 3s^2 3p^6 4s^2 3d^5$) and is the oxidised form of iron (Atkins, 1989). The generalised redox reaction for iron is:



Magnetite contains both ferrous and ferric iron, while maghemite is the oxidised form of magnetite and contains only ferric iron (Cornell and Schwertmann, 1996; De Boer, 1999). The oxidation state of iron in the mineral can influence the dissolution rate, because the bond length between oxygen and ferric iron is shorter than that between oxygen and ferrous iron (Borggaard, 1990; Hering and Stumm, 1990; Stumm and Sulzberger, 1992). A longer bond means a weaker bond, thus ferrous iron can be released from the crystal surface of iron oxides more easily than ferric iron.

Ferrous iron is several orders of magnitude more soluble in aqueous environments than ferric iron. Therefore, reductive dissolution is one of the most important dissolution mechanisms in natural environments. A reductant in the soil solution can adsorb to the minerals and reduce ferric iron to ferrous iron, which subsequently detaches from the crystal surface (Hering and Stumm, 1990; Morel and Hering, 1993; Cornell and Schwertmann, 1996).

Reductive dissolution takes place via three different mechanisms as shown in figure 3c and 4 (Segal and Sellers, 1984). One mechanism involves the direct attachment of the reductant to the ferric iron at the oxide surface (cf. figure 3c). This mechanism is applicable to reductants that form inner-sphere complexes, an example being the reduction of iron oxides by dithionite (see also section 4.1.2 and Chapter 2). Sometimes the reductant cannot bind directly with the ferric iron and a complex-former is required (figure 4a). This complex-former (usually a ligand) acts as a bridge for the electron transfer between reductant and ferric iron. An example of this kind of reductive dissolution is the reduction of ferric iron by dissolved ferrous iron, where oxalate is used as a bridging ligand (see also section 4.2.2 and Chapter 3). Finally, reduction can occur by photochemical reaction of a ligand attached to the oxide surface (Atkins, 1990; Morel and Hering, 1993). Some ligands, for example oxalate (Tamm, 1932; De Endredy, 1963; Schwertmann, 1964; Sulzberger et al., 1989; Sulzberger, 1990; Cornell and Schwertmann, 1996), can achieve a higher energy state in the presence of light of a specific wavelength. In this state, electron transfer can occur between the photoexcited ligand and the oxide surface, and reduction of ferric iron can take place (figure 4b). This mechanism will be further discussed in section 4.2.2.

3. Principles of dissolution kinetics

3.1 Introduction

The rate of a chemical reaction depends on the physical and chemical characteristics of the system, such as concentration of the reactants, temperature, and pH (Atkins, 1989). The rate of changes in concentration of reactants in a chemical reaction is called the kinetics (Atkins, 1989; Morel and Hering, 1993). Some reactions are slow under ambient conditions because one particular step, the rate-limiting step, in the reaction pathway has a high activation energy. The activation energy can be decreased by changing the reaction conditions, or an alternative reaction pathway (with lower activation energy) can be provided by adding a catalyst. This is a substance that increases the reaction-rate without being consumed in that

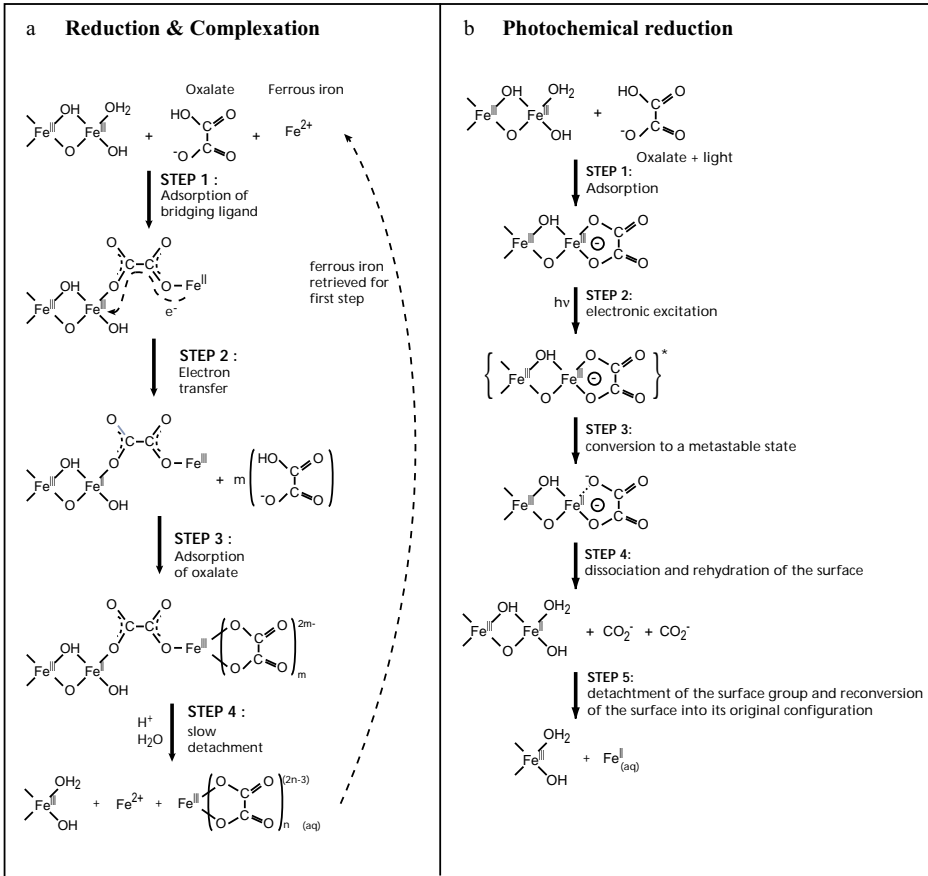


Figure 4: Several dissolution mechanisms involving oxalate: (d) reduction and complexation, and (e) photochemical reduction of iron in iron oxides (after:Hering & Stumm, 1990, in Hochella and White , Reviews in Mineralogy).

reaction; it does not change the reaction conditions (Atkins, 1989; Atkins, 1990; Morel and Hering, 1993). Dissolution of iron oxides often is a slow process, because the bond between iron and oxygen is strong. Catalysts are therefore commonly applied in iron oxide dissolution experiments. Here, the importance of reaction rates in determining reaction mechanisms is considered. We will discuss the parameters that can affect the reaction rate, and the models that are used in determining dissolution mechanisms. These models are based on rate laws, which describe the kinetic properties of the reaction, and are employed to infer the dissolution mechanism.

3.2 Rate laws

The reaction mechanism and all parameters affecting the dissolution rate are described by a rate law (Furrer and Stumm, 1986; Atkins, 1989; Atkins, 1990; Hering and Stumm, 1990; Stumm and Sulzberger, 1992; Morel and Hering, 1993), an empirically derived equation for the dissolution process containing the

rate constant and concentrations of reactants. The rate constant (k) is a parameter that depends on the reaction type and the temperature. It is, however, independent of the concentration of the reactants. The rate law for dissolution reactions describes the rate at which a compound is removed from the system. Since the rate constant depends on the type of reaction, there are separate rate laws for *diffusion-controlled* and *surface-controlled* dissolution.

Diffusion-controlled dissolution

Diffusion-controlled dissolution is common in natural systems of weathering where the water movement is slow and the phase being dissolved is static (Cornell and Schwertmann, 1996). In laboratory experiments, this type of dissolution is usually prevented by stirring the extraction solution.

The simplest rate law for diffusion-controlled dissolution depends on the concentration of the reactant and on the rate constant. For example, the rate law for dissolution of calcite can be described as:

$$\text{Rate} = k \cdot [\text{CaCO}_3] \quad (3.)$$

This is called a first-order rate law, which can be applied when the rate is proportional to the concentration of the reactant. In some reactions, the rate is proportional to the square of reactant-concentration, and it is then called a second-order rate law:

$$\text{Rate} = k \cdot [\text{reactant}]^2 \quad (4.)$$

The rate may depend on the concentration of more than one reactant, then, the order of the reaction is the sum of the individual orders of the reactants. For example, the order of the following rate law is (a+b):

$$\text{Rate} = k \cdot [\text{reactant A}]^a \cdot [\text{reactant B}]^b \quad (5.)$$

When the rate is independent of the reactant-concentration, it is proportional to the rate constant and the reaction is zero-order (Rate = k).

When dissolution is diffusion-controlled, it means that the concentration of dissolved species directly adjacent to the mineral surface corresponds to the equilibrium solubility of that species. In this case, the diffusion rate as well as the extraction time will determine the concentration of dissolved species. The concentration will increase with the square root of time (t):

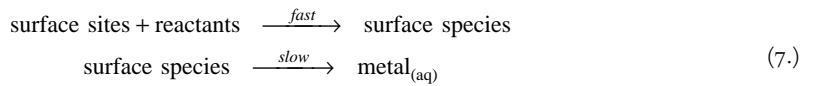
$$c(t) = c_e + 2kt^{1/2} \quad (6.)$$

Here, $c(t)$ represents the concentration of dissolved species at time t , c_e is the equilibrium solubility of the solid phase, and k is the rate constant.

Surface-controlled dissolution

The dissolution rates of many minerals have been shown to be surface-controlled (Sulzberger et al., 1989; Hering and Stumm, 1990; Cornell and Schwertmann, 1996). Rate laws for surface-controlled

dissolution are based on the proviso that the sorption of reactants to surface sites is fast, but the subsequent detachment of the metal species from the surface of the crystalline lattice into the solution is slow and thus rate limiting (Hering and Stumm, 1990). The dissolution mechanism is in those cases described by the surface complexation model (Furrer and Stumm, 1986; Zinder et al., 1986; Stumm and Furrer, 1987; Sulzberger et al., 1989; Hering and Stumm, 1990; Morel and Hering, 1993). This model describes surface adsorption reactions as consisting both of chemical bonding of solutes to surface atoms, and of electrostatic interaction between ions and a charged surface. According to this model, the dissolution reaction may be represented schematically by two steps. Step 1 involves the sorption of a reactant to the surface of the solid, a step that is assumed to be fast. Step 2 involves the detachment of the adsorption complex from the surface, this step is inferred to be slow and thus rate-limiting (Hering and Stumm, 1990).



The surface complexation model predicts a steady-state dissolution rate for reactions under conditions far from equilibrium and for which the concentrations of the reactants in solution are not depleted during the course of the reaction (Hering and Stumm, 1990). When this is the case, the rate law for dissolution is dependent on the concentration of the surface species (Hering and Stumm, 1990). It will be proportional to the surface area (A) of the solid (Cornell and Schwertmann, 1996), i.e.:

$$\text{Rate} = \frac{dc}{dt} = k \cdot A \quad (8.)$$

This means that the reaction rate shows a first-order dependence on the remaining surface area. The rate law is (with α denoting the proportion of solid dissolved at time t):

$$(1 - \alpha) = e^{-kt} \quad (9.)$$

Since the surface area of a particle is related to its shape, size and crystalline properties (defects, substitutions, and number of reactive sites), it is difficult to develop a generally applicable model that takes all factors into account. When considering specific particle types, surface-controlled dissolution can be successfully modelled. Commonly applied models are given in Table 1 (from: Cornell and Schwertmann,

Equation	physical meaning
$(1 - \frac{2}{3} \alpha) - (1 - \alpha)^{2/3} = kt$	three dimensional diffusion (Ginstling-Brounstein, deceleratory)
$[-\ln(1 - \alpha)]^{1/3} = kt$	random nucleation 3D (Avrami-Erofejev, sigmoidal)
$1 - (1 - \alpha)^{1/3} = kt$	phase boundary controlled for a contracting sphere (cube root, geometric)
$\alpha^{1/n} = kt$	acceleratory

Table 1: examples of rate laws (after Cornell & Schwertmann 1996, table 12.2).

1996), their suitability for application being related to the behaviour of the dissolved species with time or to changes in the geometry of the solid during dissolution. For isotropic dissolution, i.e. the particle shape is maintained during dissolution, the cube root law is the best approximation for the kinetics:

$$1 - (1 - \alpha)^{1/3} = k \cdot t \quad (10.)$$

This model is most suitable for spherical and cubic particles, but has been successfully applied to the dissolution of goethite and lepidocrocite as well (these minerals are commonly acicular or platy (Cornell and Schwertmann, 1996)). When the dissolution curves have a sigmoidal shape, the kinetics can best be described by the Avrami-Erofejev law:

$$(-\ln(1 - \alpha))^{1/3} = k \cdot t \quad (11.)$$

In this model the rate-limiting step is the process of random nucleation in a two-dimensional plane. Another suitable rate law is the Kabai law, which is a modified first-order rate law:

$$(1 - \alpha) = e^{(-kt)^a} \quad (12.)$$

Here, the constant a represents a material constant. For $a > 1$ the curve is sigmoidal in shape, for $a < 1$ the curve is deceleratory. Postma (1993) provided a very useful equation incorporating many of the factors influencing surface-controlled dissolution. In this model, the dissolution rate is a function of changing crystal size, morphology and site density:

$$\left(\frac{J}{m_0}\right) = k \cdot \left(\frac{m_t}{m_0}\right)^\gamma \quad (13.)$$

The left hand side represents a normalised rate (J) per initial mass of dissolving species (m_0), m_t represents the mass of dissolved species at time t , and γ is a material constant covering the change in properties (volume, surface area, reactive site density and relative size distribution) during dissolution. For spheres and cubes $\gamma = 2/3$, derived from the relationship between volume and surface area. This model describes the dissolution for particles of specific grain size and morphology. For mixtures of particles, the model has to be expanded:

$$\left(\frac{J}{m_0}\right) = \left(\frac{v}{a}\right) \cdot \left(\frac{m}{m_0}\right)^{1+(1/v)} \quad (14.)$$

Here, v and a are free parameters representing morphological characteristics of the sample (comparable to γ), with v/a representing the apparent rate constant for the mixture while the power $(1+1/v)$ is characteristic for the reactivity of the dissolving species (after: Boudreau and Ruddick, 1991). Postma's models have been successfully applied in dissolution studies of ferrihydrite, iron sulphides and oxides, and pure as well as substituted goethite (Postma, 1993; Grygar, 1996a; Grygar, 1997).

3.3 Rate-determining factors in dissolution experiments

Dissolution is influenced by the ambient conditions of the experiment, the composition of the solution, and the properties of the solid. The temperature and presence of light are two properties of the overall system, which influence the extraction results of the two methods used in the present thesis. In the citrate-bicarbonate-dithionite (CBD) method, the temperature is a very important parameter for the reaction rate (see also Chapter 2). With increasing temperature (between 60 and 80°C) the reaction progresses faster, but at high temperatures (~ 90°C) the dithionite decomposes, which evidently will inhibit further dissolution. The acid-ammonium-oxalate (AAO) method is distinctly affected by the presence of light. Photochemical excitation of the Fe(III)-oxalate complex at the solid surface causes reduction of the complex to Fe(II)-oxalate. The oxalate is subsequently dissociated and the ferrous iron can dissolve. This reduction mechanism is faster than the uncatalysed mechanism of AAO in the dark, and can dissolve amorphous as well as crystalline iron oxides (Cornell and Schwertmann, 1996) (see also section 4.2.2).

The composition of the solution is another important factor in dissolution experiments. Parameters such as pH, concentration of acids, and presence of reductants and complexing agents are of key importance in determining the reaction mechanism and kinetics. In the CBD and AAO methods, pH is critical. In the CBD method, the increase in oxidation potential of the system with increasing pH is counteracted by the strong decrease in solubility of Fe_2O_3 with increasing pH. At a pH of ~ 7.3 these parameters are optimal, and the bicarbonate buffer ensures that all experiments are carried out at this pH (Mehra and Jackson, 1960) (see also Chapter 2). The AAO- Fe^{2+} method can only be performed in the pH range of 2-4, outside this range the Fe-oxalate complex is not active and dissolution slows down considerably (see also Chapter 3).

Finally, the properties of the solid (such as stoichiometry of the particles, crystal shape, and isomorphous substitutions) influence dissolution behaviour. In iron oxides, an increased number of vacancies in the crystal structure, decreases the number of active sites with which the reactant can form a complex. Hence, defects decrease the dissolution rate of the mineral (Hering & Stumm in: White et al., 1994). The same holds for Al-for-Fe substitutions. For example, the decrease in dissolution rate of goethite is correlated to an increase in Al-for-Fe substitution (Norrish and Taylor, 1961; Torrent et al., 1987; Cornell and Schwertmann, 1996; Grygar, 1997). The exact mechanism behind this decrease in dissolution rate has not yet been discovered, but it is believed that it is related to an increase in bond strength which makes the Fe-O bonds more resistant to protonation (Cornell and Schwertmann, 1996). Furthermore, it has been shown that some minerals show preference for dissolution from one particular crystal plane or along faults in the surface (Segal and Sellers, 1984; Grygar et al., 1995). In a study by Grygar, longitudinally intergrown needle-shaped goethite particles showed predominating dissolution from the (010) and (110) planes (Grygar et al., 1995).

3.4 Detection of the dissolution mechanism

The simplest way to study dissolution mechanisms is by performing an experiment in which the concentration of dissolved solid is monitored with time. This can be done in two ways; by batch experiments or by continuous monitoring. In a batch experiment, a known amount of solid is placed in a specified volume of solution and the extraction is performed for a specific amount of time. Subsequently the solid is separated from the solution and the concentration of dissolved species in the solution is determined. The whole procedure is repeated with a fresh solution until no more dissolved species can be detected and equilibrium has been reached.

In continuous monitoring, the solid is added to an excess volume of solution and at specific time intervals an aliquot is taken from the solution and the amount of dissolved species is analysed. When the concentration of dissolved species has become constant, the reaction has reached equilibrium.

The concentration of dissolved species is plotted against time and a relationship can be inferred from the resulting curve. For diffusion-controlled dissolution, the concentration of dissolved species increases with the square root of time (section 3.2). In surface-controlled dissolution, there is no unique way in which the concentration will vary with time. Here, the resulting relationship has to be compared to known rate laws (section 3.2).

4. Extraction methods in environmental magnetism

The identification of a soil is based on its chemical and physical characteristics as well as on topography and local climate (Press and Siever, 1986). Iron oxides and hydroxides are important chemical phases in soils for two main reasons. Firstly, iron is one of the major components in all rocks and their weathering products. Secondly, iron(hydr)oxide formation is strongly dependent on climatic factors such as rainfall and temperature. In soil classification as well as in environmental magnetism it is imperative to differentiate between oxides formed as products of (recent) weathering and those originating from the parent material. Mineralogical identification of the iron compounds in soils is therefore an important topic of investigation. In this section we will discuss two methods that are frequently applied in soil science, sometimes in environmental magnetism as well, and that formed the starting point of this thesis. The first method is the citrate-bicarbonate-dithionite (CBD) method, the second is the acid ammonium oxalate (AAO) method.

4.1 CBD method

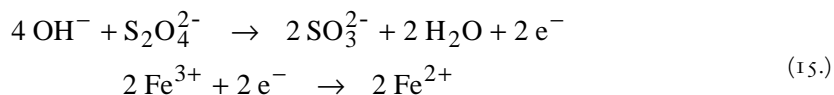
4.1.1 History of the CBD method

From the start, the primary goal for using dithionite for iron oxide extraction was to improve soil classification by getting more quantitative information on iron oxides. Another important purpose was to facilitate the identification of soil and clay minerals by X-ray diffraction analysis. As early as 1934, Galabutskaya and Govorova (1934) proposed an extraction method using sodium dithionite ($\text{Na}_2\text{S}_2\text{O}_4$) to dissolve coatings as well as crystals of iron oxides. In 1950, Deb (1950) incorporated the use of sodium tartrate and sodium acetate solutions into the method with the purpose of removing free iron oxides without affecting the clay minerals of the sample. Others found that, during extraction, the dissolved iron precipitated with dissolved sulphide from the dithionite as FeS (Aguilera and Jackson, 1953; Jackson, 1956). Aguilera and Jackson (1953) proposed an extraction method that used sodium dithionite combined with sodium citrate ($\text{Na}_3\text{C}_6\text{H}_5\text{O}_7 \cdot 2\text{H}_2\text{O}$). The addition of citrate prevented precipitation of the ferrous iron after dissolution. The disadvantage of using citrate-dithionite, however, was that the pH had to be kept constant, implying that pH adjustments had to be made during the extraction. Mehra and Jackson (1960) studied several buffers and proposed to adapt the method to include sodium bicarbonate (NaHCO_3). This resulted in a constant pH of 7.3 throughout the experiments. This is the optimum pH value for iron oxide dissolution because both the solubility of iron as well as the oxidising potential of dithionite in this system are close to maximum. The CBD method of Mehra and Jackson has since become a standard tool in soil science for extraction of free iron oxides.

Since magnetic iron oxides have compositions that vary in ferrous and ferric iron content, we may expect a varying dissolution behaviour in the CBD method. For example, (endmember) maghemite contains only ferric iron, while magnetite contains both ferric and ferrous iron. Depending on the detachment rate of the ferrous iron from the crystal structure and on the reduction rate of ferric iron in the oxide, one of these minerals will be dissolved more rapidly than the other. This is of interest to environmental magnetism, where different magnetic minerals may imply a different environmental signal.

4.1.2 CBD mechanism

The CBD extraction method is based on the principle of reductive dissolution (Figure 3c). The dithionite in the extraction solution adsorbs to the iron atoms in the mineral surface. Within the newly formed inner-sphere complex, electrons are transferred from the adsorbed dithionite to the ferric iron at the mineral surface. Thereby, the ferric iron is reduced and the dithionite is oxidised to sulphite (Loveland, 1988). The consumption of hydroxide ions that is required for the redox reaction is buffered by sodium bicarbonate. The redox reactions are:



The ferrous iron dissolves into the solution where it is chelated by citrate. Temperature, pH and redox-potential of the system influence the reaction mechanism. At high temperature ($T > 90^\circ\text{C}$) dithionite decomposes (Loveland, 1988). At increased pH ($\text{pH} > 9-10$) dithionite cannot reduce the ferric iron, while at lower pH ($\text{pH} < 6-6.5$) the dissolved iron may precipitate as iron sulphide. In addition, at low pH a second dissolution mechanism becomes active: the Fe(II)-citrate complex can dissolve ferric iron from the mineral surface (Borggaard, 1990). Solubility of iron oxides increases with decreasing pH, but the redox-potential of the CBD system counteracts this effect because it decreases with pH. The optimal pH value of the CBD method lies at 7.3 (Mehra and Jackson, 1960).

4.1.3 CBD procedure

The primary purpose of our study is to determine whether and how spinel-type magnetic iron oxides can be differentiated with this method. Furthermore, the influence of physical parameters (such as temperature and iron oxide concentration) on the extraction mechanism was investigated to optimise the extraction conditions. We used a procedure that is based on the original procedure by Mehra & Jackson (1960) and adaptations made by Hunt et al. (1995c). An overview of the procedures is given in table 2.

In our method, a smaller amount of sodium dithionite was used in each extraction step, and the extraction temperature as well as the concentration of iron oxides in the synthetic samples was varied (for details see Chapter 2). By reducing the amount of dithionite and lowering the extraction temperature the CBD method is less aggressive and subtle differences in dissolution behaviour may possibly be traced.

After each extraction step the bulk susceptibility as well as hysteresis parameters of the samples were measured. The bulk susceptibility was used as an indicator for iron oxide concentration, the hysteresis parameters were used to obtain information on changes in the grain-size range of the iron oxides. The extraction is repeated three times. The same procedure was used to extract iron oxides from natural samples of a loess-palaeosol transect in South Moravia (Chapter 5).

Author	Mehra & Jackson ('60)	Hunt et al. ('95c)	van Oorschoot & Dekkers ('99)
Temperature	80 °C	70-75 °C	60, 70 and 80 °C
amount of dithionite	1 gr	2 x 1 gr	1 gr
extraction time per step	15 minutes	15 minutes	15 minutes
number of steps	2 - 3 steps	2 steps	4 steps
sample mass	4 gr soil or 1 gr clay	4 gr commercial iron oxide	4 gr synthetic sample containing 0.1, 1 or 5 wt% iron oxides

Table 2: CBD procedures used by Mehra & Jackson ('60), Hunt et al. ('95c) and van Oorschoot & Dekkers ('99).

4.2 Acid ammonium oxalate (AAO) method

4.2.1 History of the AAO method

The acid ammonium oxalate (AAO) extraction method uses a mixture of oxalic acid and ammonium oxalate, and was introduced by Tamm (1922; 1932) for the purpose of dissolving an 'inorganic gel phase' from soils, better known as the amorphous iron oxides. Schofield (1949) and Deb (1950) discovered that the method, when performed in daylight, dissolved the same phases as dithionite (free iron oxides), but in lower quantities. In UV light, the dissolution of free iron oxides was more extensive, and was caused by photocatalytic dissolution of iron oxides with oxalate (De Endredy, 1963). Others modified the AAO method (Schwertmann, 1959; Schwertmann, 1964) and demonstrated that it dissolved only the amorphous iron oxides when performed in the dark. Several studies (McKeague and Day, 1965; McKeague et al., 1971) confirmed this result.

The 'dark' AAO method as modified by Schwertmann has been frequently applied in soil science as well as in some environmental magnetism studies to determine the amorphous or poorly crystalline iron oxide content of soils (Torrent et al., 1980; Olson and Ellis, 1982; Schwertmann et al., 1982; Schwertmann et al., 1985; Phillips and Lovley, 1987; Fine and Singer, 1989; Borggaard, 1990; Canfield et al., 1992; Golden et al., 1994; Pinheiro-Dick and Schwertmann, 1996; Rozan et al., 1997). Several studies have shown, however, that crystalline iron oxides can be dissolved as well with the AAO method (McKeague et al., 1971; Schwertmann, 1973; Walker, 1983; Borggaard, 1988; Fine and Singer, 1989; Borggaard, 1990). According to others (Chao and Zhou, 1983; Golden et al., 1994) the method is suited to dissolve specific minerals, such as magnetite, and differentiation on the basis of mineralogy should be possible. These results contrast with the original observations that the AAO-method only dissolves amorphous iron oxides.

In the method proposed by Schwertmann (1964) the dissolution rate changes with time. As shown in figure 5, the dissolution rate increases considerably after an initial period of slow dissolution (Fischer, 1972; Borggaard, 1990; Hering and Stumm, 1990). This change in dissolution rate was related to the increased concentration of ferrous iron in solution which has a catalytic effect on the dissolution mechanism (Borggaard, 1981). By adding a small amount of ferrous iron to the extraction solution at the start of the experiment, the initial slow dissolution rate disappears (Fischer, 1972; Baumgartner et al., 1983; Cornell and Schindler, 1987; Suter et al., 1988; Sulzberger et al., 1989; Borggaard, 1990; Hering and Stumm, 1990;

Stumm and Sulzberger, 1992) and a constant rate is established throughout the complete experiment (Fig. 5). A constant dissolution rate removes potential ambiguities as a consequence of changing extraction mechanisms, furthermore, it facilitates kinetic studies, and ensures similar extraction conditions for different experiments. In the following sections we will refer to this adapted method, with ferrous iron as a catalyst, as the AAO-Fe²⁺ method. In the next section we discuss the mechanism responsible for the slow initial dissolution as well as the catalytic properties of ferrous iron.

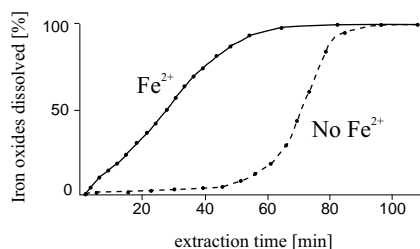


Figure 5: example of difference in dissolution rate of iron oxides in the presence of ferrous iron (solid line) and when ferrous iron is absent (dashed line).

4.2.2 AAO-Fe²⁺ mechanism

The original acid ammonium oxalate extraction is a ligand-promoted dissolution. As shown in figure 3b, the oxalate adsorbs to a ferric iron site at the crystal surface. The high polarity of the oxalate induces a weakening of the bonds between the ferric iron and other atoms at the surface, which results in the slow release of the iron-oxalate complex into the solution. Here, pH is an important factor: protons facilitate the dissolution process by protonating the OH groups on the mineral surface, thereby contributing to a weakening of the Fe-O bond. Thus, a decrease in pH will increase the dissolution rate. However, with decreasing pH the protonation of ligands in solution increases, while the adsorption of the ligands to the mineral surface decreases. As a result of these opposing processes, the AAO method has an optimum pH (~3) where dissolution is at its maximum (Cornell and Schwertmann, 1996).

The photo-sensitivity of the AAO method indicates that it may involve a radical mechanism (Borggaard, 1988). When oxalate is photochemically activated, it can reductively dissolve iron oxides (Cornell and Schwertmann, 1996) (see figure 4b); this can only occur when the surface complex is inner-sphere (Sulzberger et al., 1989). When the AAO extraction method is performed in light, the general reaction is similar to that described for the extraction in the dark. In the presence of light, however, photochemical excitation of the Fe(III)-oxalate complex at the crystal surface causes reduction of the complex to Fe(II)-oxalate. The oxalate complex is subsequently detached and the ferrous iron is released. This reduction mechanism is faster than the uncatalysed mechanism of AAO in the dark.

In the AAO-Fe²⁺ variant, the addition of ferrous iron to the extraction solution promotes iron oxide dissolution because the Fe²⁺-oxalate complex is a strong reductant. At low pH, both dissolved ferrous iron and the iron oxide surface are positively charged and repel each other. The charge reversal of ferrous iron caused by its complexation with oxalate enables adsorption of the complex to the solid (Figure 4a). The first step in the dissolution mechanism of the AAO-Fe²⁺ extraction method is the formation of a complex

between Fe^{2+} and oxalate in solution. This complex adsorbs to a Fe(III) site on the mineral surface. The newly formed inner-sphere complex shifts the electron density towards the Fe(III) on the mineral surface and facilitates electron transfer with oxalate as the bridging ligand between the two iron atoms (Baumgartner et al., 1983; Cornell and Schindler, 1987; Stumm and Sulzberger, 1992). The reduced iron complex at the mineral surface can then be detached.

The AAO- Fe^{2+} method is strongly influenced by pH, similar to the AAO method. The optimum pH varies between 2 and 4. In addition, when pH is increased above 4, the buffer capacity of the system and the amount of oxalate-extractable iron are decreased (McKeague and Day, 1965; Borggaard, 1988). This is partly related to the decrease in solubility of Fe^{2+} at $\text{pH} > 4$ as well as the increased oxidation of Fe^{2+} to Fe^{3+} (Fischer, 1972).

4.2.3 AAO- Fe^{2+} procedure

The procedure we use is partly based on the modifications made by Schwertmann (1964), and the method described by Grygar (1997). These are given in table 3 for comparison with our method, and a detailed description of the procedure can be found in Chapter 3.

Author	Schwertmann ('64)	Grygar ('97)	van Oorschot & Dekkers ('01)
purging gas	none	nitrogen	argon
pH	3	2.7	3
concentration Ferrous Iron	none	2 mM	2 mM
concentration Acid Ammonium Oxalate	200 mM	20 mM	20 mM
volume of solution	100 mL	-	50 mL
extraction time	2 hours	-	30 minutes (per step)
sample mass	1-5 gr soil	5 mg iron oxide	1 gr synthetic sample 1 wt% iron oxides

Table 3: AAO procedures as proposed by Schwertmann ('64), Grygar('97) and van Oorschot & Dekkers ('01)

We added a fraction of ferrous iron to the extraction solution to ensure a constant dissolution rate and to have a similar dissolution mechanism throughout the experiments. Furthermore, the extraction solution

was protected from sunlight and purged with Argon gas to prevent the precipitation of the added ferrous iron as iron(hydr)oxides. Finally, we used a smaller amount of oxalate in our extraction solution to have equilibrium reached within the short extraction time. In this way, the amount of steps required to remove a certain type of iron oxides, could be used as an indication of the concentration differences between samples or of differences in solubility between different oxides.

4.3 Purpose of the present investigation

CBD. This study was undertaken to remove the ambiguity concerning the type of minerals that are affected by the CBD method. We tried to determine whether the method was mineral-specific and/or grain-size specific. For this purpose, we studied synthetic samples of known composition as well as natural samples to verify the results obtained in synthetic systems. Furthermore the ambient conditions of the extractions were varied to establish whether and how these parameters affect the outcome of the experiments.

AAO-Fe²⁺. The primary purpose of our investigation is to determine whether or not the method dissolves crystalline iron oxides. Furthermore, we are interested in the possibility of using the method for mineral-specific extraction. As with the CBD method, we studied the dissolution behaviour of both synthetic as well as natural samples in the AAO-Fe²⁺ method.

Chapters 2 and 3 discuss the results of the dissolution behaviour of synthetic samples of known magnetic mineral composition extracted with the CBD and the AAO-Fe²⁺ method respectively. In Chapters 5 and 6 results obtained for natural samples are discussed.

Dissolution Behaviour of Magnetite and Maghemite in the Citrate-Bicarbonate-Dithionite Extraction Method

Mineral magnetic properties of soils and sediments are increasingly used as proxy parameters for environmental and palaeoclimate analysis. To investigate which magnetic minerals contribute to the environmental signal in the samples, chemical methods such as the Citrate-Bicarbonate-Dithionite (CBD) extraction have been introduced. This method is assumed to distinguish the lithogenic (magnetite) from the pedogenic (maghemite) mineral content in soils and sediments. Unfortunately, the interpretation of the CBD extractions is not straightforward because the procedure sometimes seems more suitable for distinction between grain size than for distinction between minerals.

The procedure of the CBD extraction method was investigated to determine the influence of extraction temperature, iron oxide concentration and grain size on the dissolution behaviour of the samples. Synthetic samples were extracted at three different temperatures (60°, 70° and 80°C) with similar iron oxide concentration (5 wt%), and for three different concentrations (0.1 wt%, 1 wt% and 5 wt%) at the same temperature (60°C). Furthermore, iron oxides of different grain size (< 0.5 or < 5 µm) were extracted at the same extraction temperature (60°C) and iron oxide concentration (1 wt%). Our results show that a lower extraction temperature reduces the dissolution rate for all samples, while decrease in iron oxide concentration as well as grain size increases the dissolution rate. Thus, the parameters in the CBD procedure have a major influence on the dissolution behaviour of the samples. In practice this means that when natural samples with varying iron oxide concentration or grain size are extracted with this method, the results of the extractions cannot be compared. Therefore, the outcome of this type of extraction experiment can only be accurately interpreted when the effect of the procedure on the dissolution behaviour is taken into account.

1. Introduction

Magnetic minerals can record the past geomagnetic field. The physical properties of these minerals vary as a function of mineral type, grain size and shape, crystallinity, and other factors. Palaeomagnetic studies are supported by analysis of these properties. The variations in magnetic properties can also reflect variations in (palaeo)environmental processes and palaeoclimate conditions. In environmental magnetism the mineral-magnetic parameters are applied as proxies for environmental and climate processes. One of the parameters that is often studied in environmental magnetism is the low-field magnetic susceptibility. Le Borgne (1955) demonstrated that magnetic enhancement of the topsoil in a soil profile was caused by formation of maghemite in the topsoil, which in turn was related to climatic factors such as soil humidity. Many others followed his example by studying magnetic susceptibility (e.g. Mullins, 1977; Fine et al., 1989; Fine et al.,

1992), or other magnetic parameters of soils and sediments (e.g. Maher, 1986; Thompson and Oldfield, 1986; Bloemendal et al., 1992; Weeks et al., 1995; Dearing et al., 1997).

Unfortunately, the interpretation of environmental magnetism data is not always unambiguous. Therefore, other methods must be incorporated into environmental studies to improve the interpretation of the magnetic data. Chemical extraction methods are frequently used for this purpose, particularly in soil studies (e.g. Fine et al., 1989; Fine et al., 1993a; Hunt et al., 1995c; Singer et al., 1995; Schwartz et al., 1997). A popular extraction method is the Citrate-Bicarbonate-Dithionite (CBD) method of Mehra and Jackson (1960). It is based on reductive iron dissolution with dithionite as reductant and citrate as a chelating agent to bind the dissolved iron. Bicarbonate is used to buffer the OH^- loss during the reaction.

Results of reported CBD extraction studies vary considerably. For example, in some cases the CBD method was reported to dissolve only the pedogenic maghemite (Fine et al., 1989; Singer and Fine, 1989; Singer et al., 1995), while in other cases the fine-grained magnetite was dissolved as well (Hunt et al., 1995c). However, the results of these studies are difficult to compare, because the extraction procedure of each study is not always clearly specified. Factors such as amount of sample, type of sample, amount of dithionite and extraction temperature may vary with each study. The reductive dissolution of iron oxides is a kinetic process and factors such as pH, crystallinity and temperature have a major effect on the dissolution rate (e.g. Zinder et al., 1986; Postma, 1993; Grygar, 1995). This was already shown by the results of Mehra and Jackson (1960) who examined the influence of buffer type, pH and oxidation potential of dithionite on iron dissolution. Therefore, results of extraction studies with differences in extraction procedures will not necessarily reflect the same dissolution behaviour.

In addition to difficulties resulting from the variation of the CBD extraction method, also the sample material itself has proved difficult to control. Preferably, natural samples are used in all experiments because they represent the natural conditions, but the concentration and physical parameters of the magnetic material are not precisely known. In synthetic samples, these conditions can be controlled. Synthetic samples, however, usually contain aggregates of very fine-grained magnetic material formed during sample preparation. Thus, the outcome of extraction experiments using synthetic samples will not necessarily reflect the natural circumstances. This complicates the interpretation of results for either type of samples.

The differences in the results of the various CBD extraction studies, could well be related to an incomplete control of the experimental parameters. The purpose of this study is to investigate how the outcome of CBD extractions is affected by changing parameters (extraction temperature, grain size and concentration of the iron oxides) in the extraction method. By having a more complete understanding of the extraction mechanism we hope to devise a procedure which is most effective for chemical maghemite-magnetite distinction. To control the variables in the extraction method more closely, synthetic samples were used. Samples were prepared to mimic natural samples as best as possible by minimising formation of magnetic aggregates during mixing.

2. Materials and methods

2.1 CBD method

Many of the adaptations of the CBD method in environmental magnetism have involved changes in extraction temperature, concentration of the magnetic minerals in the sample, or in the amount of dithionite used in the extraction step. The present study will therefore focus on two of these variables as

well as on the grain size of the iron oxides, to determine to which extent they influence the results of the extraction. Extractions with constant magnetic mineral concentration (5 wt%) were performed at three different temperatures; 60°C, 70°C and 80°C respectively. Further, extractions with a constant temperature of 60°C were performed with varying iron oxide concentrations of 5 wt%, 1 wt% or 0.1 wt%. Finally, the grain size of the iron oxides was varied between $< 0.5 \mu\text{m}$ and $< 5 \mu\text{m}$, with constant extraction temperature (60°C) and concentrations of 1 wt%. Table 1 gives an overview of all extraction experiments performed and characteristics of the iron oxides used in the experiments.

Experiment	Concentration magnetic mineral [wt%]	grain size [μm]	Extraction temperature [$^{\circ}\text{C}$]	Magnetic mineral used	Curie Temperature [$^{\circ}\text{C}$]	Cell edge [\AA]
1	5	< 0.5	80	Magnetite (batch 1)	580	8.37
2	5	< 0.5	80	Maghemite (batch 1)	645	8.35
3	5	< 0.5	70	Magnetite (batch 1)	580	8.37
4	5	< 0.5	70	Maghemite (batch 1)	645	8.35
5	5	< 0.5	60	Magnetite (batch 2)	580	8.37
6	5	< 0.5	60	Maghemite (batch 2)	645	8.33
7	1	< 0.5	60	Magnetite (batch 2)	580	8.37
8	1	< 0.5	60	Maghemite (batch 2)	645	8.33
9	1	< 5	60	Magnetite (Hartstra, 1982b)	~ 400	8.40
10	1	< 5	60	Titano-maghemite (Hartstra, 1982b)	~ 550	8.36
11	0.1	< 0.5	60	Magnetite (batch 2)	580	8.37
12	0.1	< 0.5	60	Maghemite (batch 2)	645	8.33

Table 1: The experimental parameters of the CBD procedure and some characteristics of the magnetic minerals used in the experiments.

2.2 The magnetic minerals

The very fine-grained magnetite and maghemite were prepared according to the procedures described by Schwertmann and Cornell (1991). The magnetite was formed by heating a de-oxygenated solution of ferrous sulphate and adding an oxygen-free solution of potassium nitrate and potassium hydroxide. The maghemite was formed by heating a batch of magnetite in air at 250°C for 2 hours. Approximately 20 g of material is formed.

Two batches of magnetite were prepared, one of these batches was subsequently transformed to maghemite (batch 1 magnetite and batch 1 maghemite). These batches were used to make the samples for the 70°C and 80°C experiments. For the 60°C experiments, which were carried out in a later stage, fresh batches of magnetite and maghemite were prepared (batch 2 magnetite and batch 2 maghemite) in a similar way as the batch 1 minerals.

Minerals of batch 1 were dried in air and stored in a desiccator with silica gel for several weeks prior to the mineralogical and magnetic analyses. Part of the minerals of batch 2 was stored in acetone (propanon) immediately after synthesis (batch 2A) and another part (batch 2B) was dried and stored to determine whether and how the dry storage affected the physical properties of the samples.

The coarse-grained iron oxides were taken from storage, they had been previously used in a study by Hartstra (1982b). These minerals had a grain size of $< 5 \mu\text{m}$, and the maghemite was partially substituted with titanium.

Preparation of synthetic samples

The magnetic material in natural samples is usually distributed homogeneously as separate particles in a paramagnetic matrix. We mimicked natural samples by dispersing the iron oxides in calcite powder in concentrations of 0.1 wt%, 1 wt% and 5 wt%. A common method for mixing synthetic samples is manual stirring in a slurry (e.g. Dankers, 1978; Kapicka, 1992; Borradaile, 1996). When using very fine-grained strongly magnetic particles, this method often results in heterogeneously dispersed samples containing aggregates of closely-spaced magnetic particles (e.g. Parry, 1980; Cisowski, 1981; Dunlop, 1986; Maher, 1988). The aggregates will exhibit magnetic interaction and may show differences in dissolution behaviour compared to natural samples, caused by a decrease in particle surface. To minimise formation of magnetic aggregates during stirring, the force exerted on the grains during mixing was increased. A combined method of manual and ultrasonic stirring (the 'ultrasonic stirring technique') was developed to prevent formation of aggregates of magnetic material in the matrix as much as possible.

An amount of calcium carbonate (4.00 g CaCO_3 , analytical grade) was transferred to a mould, placed in an ultrasonic bath (Stopler, Bransonic 12). Approximately 5 mL of acetone was added. After ~ 30 seconds of manual stirring of the matrix and the acetone in the ultrasonic bath, a specified amount of iron oxides was added. Subsequently the sample was stirred for at least another minute with the ultrasonic bath still switched on. After mixing, the sample was dried in air in an oven at 40°C overnight. Samples of 4.00 g calcite and 0.20 g (5 wt%) of either magnetite or maghemite were prepared. All samples were weighed in a semi-microbalance (Sartorius, MC1). Samples for the 0.1 wt% and 1 wt% experiments were prepared with respectively 0.004 g and 0.04 g iron oxides instead of 0.20 g. Blank samples (made of 4.00 g calcite only) underwent the same handling as the magnetic samples.

Magnetic analyses

A modified horizontal Curie balance (Mullender et al., 1993) was used for thermomagnetic analysis. Susceptibility changes with temperature were measured in an argon atmosphere, on a susceptibility bridge equipped with a heating unit (AGICO, KLY-2/CS-3). Isothermal remanent magnetisation (IRM) acquisition and back-field demagnetisation fields were induced with a PM4 pulse magnetiser, and measured with a JR5A spinner magnetometer (AGICO) to determine IRM and coercivity of the material. Stationary three-axis alternating field (AF) demagnetisation was performed in a laboratory-built coil (peak field 300 mT), the maximum field used for demagnetisation was 250 mT. All measurements were performed with samples containing 1 wt% or 5 wt% of magnetic mineral. Measurements were performed with samples that were either stirred ultrasonically or mixed manually, to determine whether there were differences in magnetic properties related to the stirring technique. The acquisition and demagnetisation data were used to plot Cisowski and Henkel diagrams (Henkel, 1964; Cisowski, 1981) to study variations in the magnetic interaction in the samples. Magnetic measurements of the samples for the extraction method were performed after each extraction step.

2.5 CBD extraction procedure

The procedure of Hunt et al. (1995c), essentially an adapted version of the original method by Mehra & Jackson (1960), formed the basis for our extraction procedure, which is detailed in figure 1. In each experiment 12 samples and 4 to 6 blanks were extracted.

1. Place sample in a 100 mL centrifuge tube
2. Measure bulk susceptibility of the sample
Weigh the sample
3. Add 40 mL 0.3 M citrate solution
Add 5 mL 1 M bicarbonate solution
4. Heat the sample to either 60°, 70° or 80°C
5. Add 1.00 g dithionite
6. Keep the sample at constant temperature
Stir the sample thoroughly every 5 minutes
7. Centrifuge at 3500 g (~4417 rpm) for 10 minutes
Decant the liquid
8. Rinse the sample with 50 mL demineralised water
Centrifuge the sample again at 3500 g for 10 minutes
9. Dry the sample at 40°C overnight

Figure 1: CBD protocol used in this study

Prior to the start of the extraction experiment the samples were transferred to 100 mL glass centrifuge tubes after which bulk susceptibility and mass of the samples were measured. The samples were kept in the centrifuge tubes during the entire course of the experiment. After each extraction step the samples were dried in air in an oven at 40°C for ~ 24 hours, bulk susceptibility and mass of the samples were measured before each new step.

The procedure of the CBD extraction is as follows (figure 1). A solution of 40 mL 0.3 M sodium citrate ($\text{Na}_3\text{C}_6\text{H}_5\text{O}_7 \cdot 2\text{H}_2\text{O}$, analytical grade) and 5 mL 1M sodium bicarbonate (NaHCO_3 , analytical grade) was added to the dry samples. The tubes were placed in a water bath (GFL 1003) at a temperature of either 60°, 70° or 80°C (temperature variation $\pm 0.1^\circ\text{C}$). When the mixture reached the required temperature, 1.00 g sodium dithionite ($\text{Na}_2\text{S}_2\text{O}_4$, analytical grade) was added and the samples were stirred thoroughly for approximately 10-15 seconds with a glass stirring rod. The samples were kept at constant temperature for another 15 minutes, and were stirred thoroughly every 5 minutes.

After 15 minutes the samples were slightly cooled in air and the liquid was separated from the sample by centrifuging for 10 minutes at 3500 g (~ 4417 rpm). The liquid was decanted and the samples were rinsed with ~ 50 mL of demineralised water and centrifuged again at the same settings to separate the solid from the rinsing liquid. The liquid was decanted and the samples were placed in an oven to dry. The bulk susceptibility of the dry samples was measured, mass of the samples was determined and the extraction was repeated three times to give a total of four extraction steps. Of every step one of the samples was kept for magnetic measurements.

3. Results and discussion

3.1 Synthetic iron oxide characterisation

3.1.1 Non-magnetic analysis

The synthetic magnetite grains are equidimensional, with an average diameter of $< 0.5 \mu\text{m}$ (SEM, XL30 lab 6) and a cubic crystal structure (XRD, Philips PW1700, see figure 2) The synthetic maghemite has a tetragonal crystal superstructure and a morphology equivalent to that of the original magnetite (XRD and SEM observations, see figure 2). The diffractograms of the maghemite correspond well with those published by Özdemir (1990) and Özdemir and Banerjee (1984) for a synthetic maghemite.

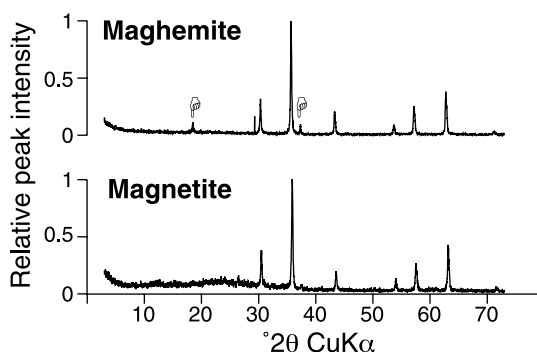


Figure 2: XRD diagrams of the synthetic iron oxides used in the experiment. XRD analysis was performed with a diffractometer using Cu-K α radiation, 0.02 $^{\circ}$ steps and a counting time of one second per step. The diagram of the maghemite shows some of the tetragonal superstructure peaks (indicated by pointing hands). The relative peak intensities were calculated by normalising the intensities with the highest value of the peak intensity measured in the sample.

SEM studies indicated that the synthetic minerals formed aggregates with a diameter of 5 to 50 μm . The SEM resolution was insufficient to discern separate particles. However, particle size can be estimated at $< 0.5 \mu\text{m}$, because that was the size of the smallest particles detectable by the SEM (see figure 3A). This size corresponds well with the results of Schwertmann & Cornell (1991) who found grain sizes in the range of 0.02-0.5 μm for minerals prepared in a similar way.

Effects of the stirring technique on the dispersion of the magnetic particles in the sample were studied with the SEM. Aggregates were present in all samples regardless of the mixing technique used. However, the average size of the aggregates was ~ 5 -10 μm smaller in the case of ultrasonic stirring of the samples.

3.1.2 Magnetic analysis of synthetic magnetite samples

IRM acquisition experiments indicate that the magnetite samples were saturated after application of a field of approximately 100 ± 5 mT. The remanent coercive force (B_{cr}) was 25 ± 2 mT. This compares well with published data (Maher, 1988; Dunlop and Özdemir, 1997) for randomly oriented single domain magnetite.

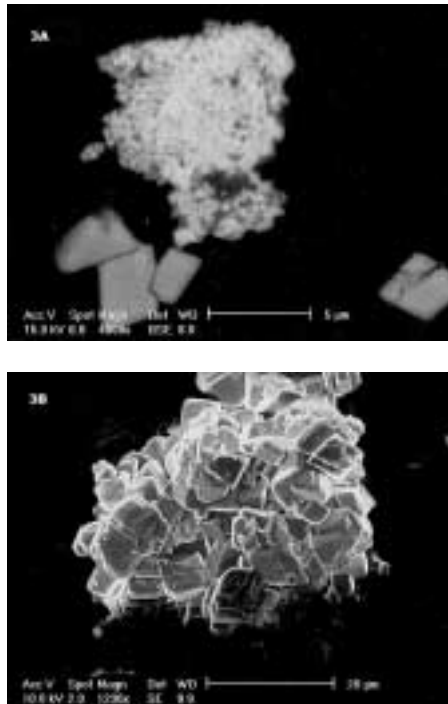


Figure 3: SEM pictures of the synthetic samples: (3A) shows an example of aggregated magnetic minerals (in this case maghemite in an ultrasonically stirred sample) adjacent to separate calcite grains, (3B) shows a cluster of calcite grains of various sizes.

Figure 4 gives thermomagnetic runs for the synthetic magnetite of batch 1 and batch 2B. For batch 2, there was no difference in thermomagnetic behaviour related to storage; samples stored in air and those stored in acetone gave similar results. The thermomagnetic behaviour of the magnetite of both batches was very similar except in the 500°–700°C temperature interval. The initial magnetisation varied between 75 and 80 $\text{Am}^2\text{kg}^{-1}$. After heating to 700°C, the remaining magnetisation at room temperature was approximately 1–5 $\text{Am}^2\text{kg}^{-1}$ (figure 4). In the temperature interval of ~ 200° to ~ 300°C there was an increase in decay of the magnetisation. The decrease in magnetisation was irreversible, as becomes apparent from the stepwise run of batch 2 (figure 4B). This indicates transformation of magnetite to maghemite. The temperature interval compares reasonably well with published data for conversion temperatures of magnetite to maghemite (e.g. 150°–250°C, Stacey and Banerjee, 1974).

The thermomagnetic behaviour of the magnetite batches differed in the value of the Curie temperature. The magnetite of batch 1 gave a T_C of ~ 570°C, but shows a tailing of the curve toward 640°C (figure 4A), indicating an alteration reaction. The magnetite in batch 2 gave a T_C of 640°C (figure 4B), implying complete conversion to maghemite. The maghemite formed from the magnetite during heating in the Curie balance in turn transforms to hematite upon further heating. For batch 1 this transformation starts at ~ 540°C and for batch 2 at ~ 630°C. These results are comparable to temperatures published for

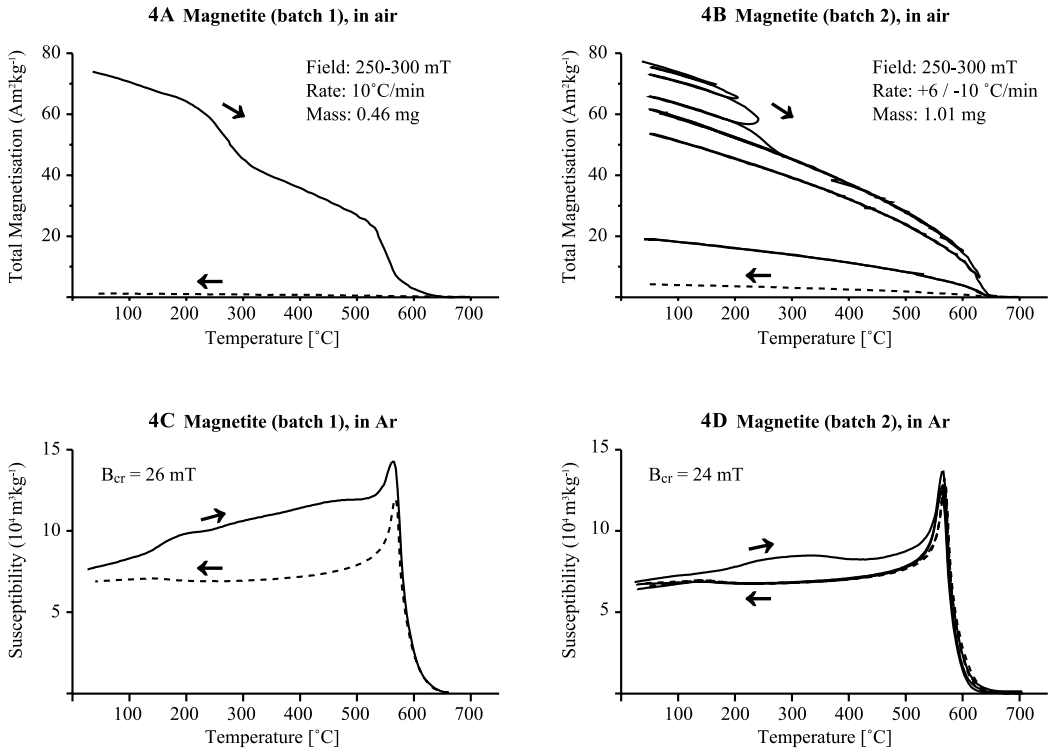


Figure 4: (4A) shows thermomagnetic data (in air) for the synthetic magnetite of the first batch. In (4B) the run was divided into several steps to study the loss of magnetisation of the synthetic magnetite of the second batch. The steps were: step 1: 20-60-50°C, step 2: 50-200-50°C, step 3: 50-240-50°C, step 4: 50-280-50°C, step 5: 50-600-50°C, step 6: 50-630-50°C, step 7: 50-660-50°C, step 8: 50-700-30°C. The sample mass as well as heating and cooling rate and field used for analysis are given in the graphs. (4C) and (4D) show the behaviour of low-field susceptibility versus temperature for the magnetite used in this study. Sample mass - 0.5 g. Analyses were performed in inert atmosphere.

maghemite-hematite transition (e.g. > 350°C Stacey and Banerjee, 1974, and more recently: 550°C or 700°C, Dunlop and Özdemir, 1997). The final room temperature magnetisation is close to zero, and the conversion is irreversible.

Magnetite of batch 1 transformed to maghemite and eventually hematite at lower temperatures than the magnetite of batch 2, therefore batch 2 is more stable upon heating than batch 1. These results indicate that although synthesis of both mineral batches occurred under seemingly identical circumstances, differences in magnetic behaviour can still occur (most likely caused by small differences in mineral structure).

The behaviour of low-field susceptibility (χ_{in}) as a function of temperature was studied as well, oxidation of magnetite was prevented by measuring in argon atmosphere. Batch 1 samples show irreversible behaviour indicating some structural rearrangement on annealing (figure 4C), while batch 2 shows virtually reversible behaviour with a distinct Hopkinson peak (figure 4D). Repeated runs on batch 2 magnetite show perfectly reversible behaviour. As concluded from the thermomagnetic runs, the second magnetite batch appears to be more thermally stable than the first. Curie temperatures are ~ 580°C, typical of magnetite.

3.1.3 Magnetic analysis of synthetic maghemite samples

IRM acquisition shows that the maghemite samples were saturated after application of a field of 80 ± 10 mT, lower than the saturation field of the magnetite samples. B_{cr} was 22 ± 1 mT, slightly lower than that of magnetite but comparable to literature values (e.g. natural maghemite ~ 23 mT, de Boer and Dekkers, 1996).

The thermomagnetic behaviour of the synthetic maghemite resembled the behaviour of ‘model’ ferrimagnetic minerals, and was similar for both batches (figure 5). The initial magnetisation was approximately $60 \text{ Am}^2\text{kg}^{-1}$, comparable to values found in literature for a natural maghemite (e.g. $64 \text{ Am}^2\text{kg}^{-1}$, de Boer and Dekkers, 1996). After heating to 700°C , the remaining magnetisation at room temperature was approximately $1\text{--}3 \text{ Am}^2\text{kg}^{-1}$.

Batch 2 maghemite (figure 5B) indicated a T_C of $\sim 640^\circ\text{C}$, typical of maghemite. Similar to the magnetite samples, the storage method did not affect the thermomagnetic behaviour of the maghemite samples. Samples of the first batch started transforming to hematite at a temperature lower than the T_C of maghemite. The observed, apparent T_C ($\sim 580^\circ\text{C}$) represents the rapid loss in magnetisation caused by

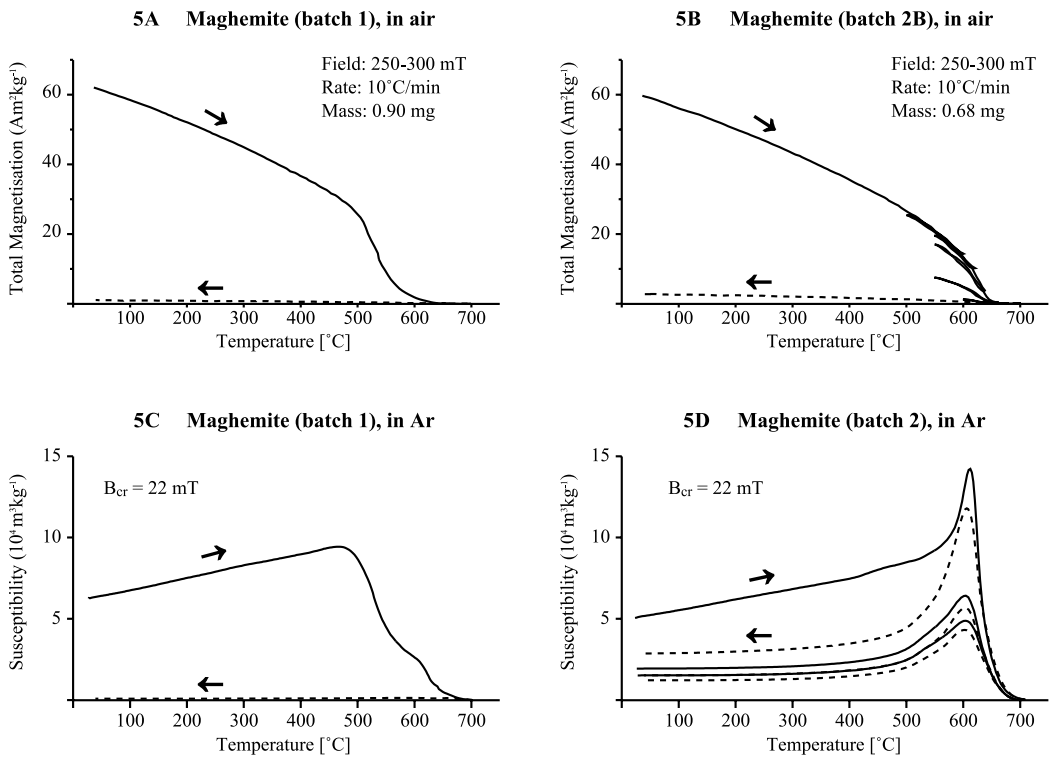


Figure 5: (5A) and (5B) show thermomagnetic data of synthetic maghemite of respectively the first batch and the second batch. The steps of the heating run in 5B were; step 1: $20\text{--}600\text{--}500^\circ\text{C}$, step 2: $500\text{--}620\text{--}550^\circ\text{C}$, step 3: $550\text{--}640\text{--}550^\circ\text{C}$, step 4: $550\text{--}660\text{--}550^\circ\text{C}$, step 5: $550\text{--}680\text{--}600^\circ\text{C}$, step 6: $600\text{--}700\text{--}30^\circ\text{C}$. The sample mass as well as heating and cooling rate and field used for analysis are given in the graphs. (5C) and (5D) show the behaviour of low-field susceptibility versus temperature for the maghemite used in this study. Sample mass ~ 0.5 g. Analyses were performed in inert atmosphere.

transformation to hematite, rather than the true Curie point of the sample. The early onset of conversion to hematite indicates that the maghemite of batch 1 was less stable than that of batch 2. For the maghemite of batch 2 the decrease in magnetisation in the temperature interval of $\sim 640^{\circ}\text{C}$ – 700°C was irreversible (figure 5B) and indicates transformation of maghemite to hematite. Comparable temperature ranges have been reported in the literature (e.g. 510°C – 660°C , Özdemir and Banerjee, 1984, and $\sim 650^{\circ}\text{C}$, de Boer and Dekkers, 1996). The results indicate – as in the case of magnetite – that the seemingly similar conditions under which the two batches were synthesised do not rule out the possibility of differences in magnetic or structural characteristics of the samples. They show that the maghemite of batch 1 was thermally less stable than that of batch 2. This is consistent with the results of the magnetite batches.

Thermal behaviour of χ_{in} in argon atmosphere for the two maghemite batches is shown in figure 5C and 5D. The results for the two batches differ. Maghemite of batch 1 shows a slow increase in susceptibility during heating. When the temperature rises above 500°C the susceptibility starts to decrease to a value of approximately zero at 700°C . Upon cooling it is evident that the decrease in susceptibility is irreversible and therefore caused by transformation to hematite. The onset of the transformation to hematite has been reported to occur around 300°C (e.g. 300°C – 450°C Sun et al., 1995), which is low compared to the 500°C found for our synthetic samples of batch 1. Thermal conversion of maghemite to hematite, however, is reported to start within a wide temperature range (e.g. 250 – 900°C) depending on factors such as method of preparation and morphology of the particles (Özdemir, 1990).

The second batch shows nearly ideal χ_{in} behaviour for maghemite, with a distinct Hopkinson peak at $\sim 600^{\circ}\text{C}$ and a T_{C} of $\sim 645^{\circ}\text{C}$. The cooling path of the previous run is similar to the heating path of the following run during the entire experiment. After heating to 700°C part of the susceptibility is lost due to conversion of maghemite to hematite. However, susceptibility loss progresses very slowly, and the conversion to hematite is still incomplete after four consecutive runs (figure 5D). This indicates that the second maghemite batch is thermally more stable than the first batch, as was concluded from the Curie balance results.

3.2 Results of ultrasonic stirring

The most notable difference between the manually stirred samples and those that were stirred ultrasonically was a more distinctive colour for all of the latter samples. The manually stirred samples were light in colour and showed visible aggregates of magnetic material, while the ultrasonically stirred samples had a much more homogeneous appearance. Figure 6 is an example of the difference in colour of samples of similar magnetite concentration, but stirred differently.

SEM observations show that the matrix material, calcite, occurred as aggregates of up to 20 or $30\ \mu\text{m}$ in diameter or as separate grains (figure 3). The calcite particles varied in size between 2 and $10\ \mu\text{m}$. In all samples aggregates of magnetic minerals were ubiquitous. The size of the magnetic aggregates varied from $5\ \mu\text{m}$ to a maximum of approximately $50\ \mu\text{m}$ in the ultrasonically stirred samples and also in the manually stirred samples. The average diameter of the aggregates is approximately 5 to $10\ \mu\text{m}$ smaller in the ultrasonically stirred samples compared to the manually stirred samples.

Henkel plots (Henkel, 1964, not shown) of back field demagnetisation versus IRM acquisition all showed positive interaction between the magnetic particles. Cisowski plots (Cisowski, 1981, not shown) of normalised AF demagnetisation and IRM acquisition versus field strength all showed an intersection

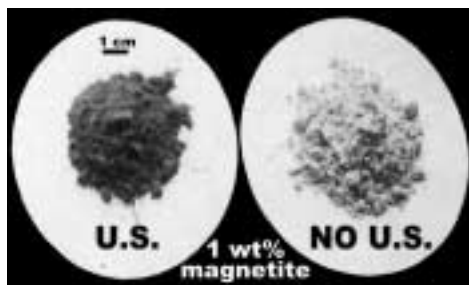


Figure 6: Photograph of the difference in colour between samples containing 1 wt% magnetite that were stirred ultrasonically (left) or manually (right).

point (the R-ratio) of less than 0.5 for both ultrasonically and manually stirred samples. The R-ratio of the two curves is $\sim 0.32 \pm 0.02$ for maghemite samples and $\sim 0.34 \pm 0.03$ for the magnetite samples. This value compares well with data for synthetic magnetite samples (Maher, 1988; Dunlop and Özdemir, 1997). The results show that, even with ultrasonic stirring, interaction between the magnetic particles is still present. Fabian and von Döbenek (1997) have found that the R-ratio is not very specific in differentiating grain sizes and intraparticle forces. Therefore, the ultrasonic method does improve dispersion of very fine-grained magnetic minerals in synthetic samples as was indicated by the change in colour and average magnetic aggregate diameter. The improvement, however, cannot be expressed in magnetic terms because the methods cannot sufficiently distinguish between magnetic interactions caused by varying sizes of aggregates. We have opted to use ultrasonically stirred samples in our extraction experiments.

3.3 Extraction results

In figure 7 the results of each extraction experiment are given (averages of 12 samples). CBD extractions at various temperatures and concentrations resulted in the extraction of magnetite as well as maghemite.

3.3.1 Effects of temperature variation

The first three left-hand panels in figure 7 (chart A and B) show the results of the extractions at different temperatures for samples containing 5 wt% magnetic minerals. The temperatures of 70° and 80°C were used, because these are the most commonly used extraction temperatures in previous studies. The reaction is expected to slow down at lower temperatures, which might make it possible to distinguish between magnetite and maghemite dissolution, therefore a third extraction temperature of 60°C was used.

The bulk low-field susceptibility of all samples decreases more quickly at higher extraction temperatures. The increased dissolution rate at higher temperature has resulted in an increased susceptibility loss. Magnetite dissolution is most rapid in the first two extraction steps, but when the extraction temperature is lowered the dissolution rate becomes more gradual. For the extraction at 60°C an approximately equal amount of bulk susceptibility ($\sim 22\%$) is lost in each step. Magnetite does not completely dissolve in four extraction steps at 60°C ($\sim 12\%$ of initial susceptibility left). During the first extraction step, maghemite dissolves distinctly less than in the second step where the highest loss of susceptibility occurs. Maghemite is completely dissolved after four extraction steps at all three temperatures. Therefore, it appears that only at

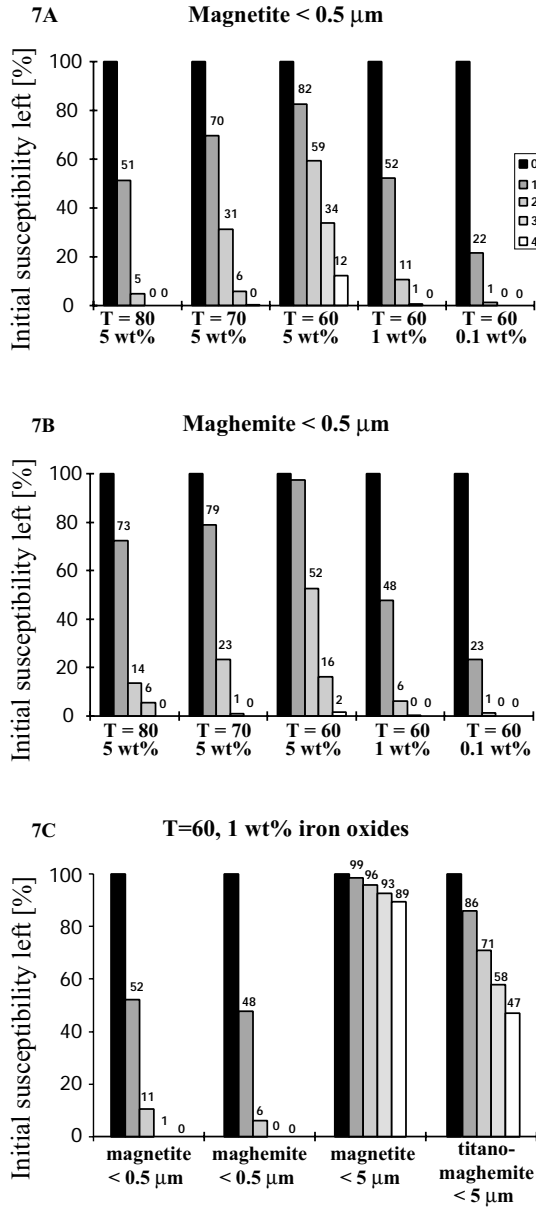


Figure 7: Average results of the CBD extraction experiments. For each experiment a total of 12 samples and an additional 4-6 blanks were extracted. Upper chart represents extractions of fine-grained magnetite, middle chart represents extractions of fine-grained maghemite, and the lower chart is a comparison of the extractions of fine-grained synthetic and coarse-grained natural iron oxides. In the first two charts (7A and 7B), the extraction protocol is given on the horizontal axis, in the lower chart (7C) the extraction temperature was 60°C and the concentration of iron oxides was 1 wt%.

lower temperatures (60°C) the extraction results enable some distinction between samples containing 5 wt% magnetite and those containing 5 wt% maghemite.

3.3.2 Effects of concentration variation

Figure 7 (the three most right-hand panels of charts A and B) gives the results of the experiments using different concentrations of magnetic minerals at an extraction temperature of 60°C. In the 0.1 wt% as well as the 1 wt% experiment magnetite as well as maghemite were completely dissolved within the 4 steps of the experiment. An increase in dissolution rate was noted for both minerals when the concentration in the samples was decreased. The dissolution rate in each extraction step was similar for both minerals at similar extraction conditions, indicating that distinction between magnetite and maghemite is impossible at low concentrations of fine-grained magnetic material. The results of extraction of samples containing 1 wt% magnetite or 1 wt% maghemite at 60°C were comparable to the results of the 5 wt% magnetite experiment at T=80°C. This indicates that comparison of different procedures is indeed complicated if not impossible. For samples initially containing 0.1 wt% maghemite, the dissolution rate in the first extraction step was much larger than that of any of the other experiments using maghemite.

The results of the extraction experiments could be influenced by differences in the magnetic minerals of the different batches. The 60°C extractions were performed with magnetic minerals of batch 2. Results show, however, that the dissolution rate increases consistently with increasing temperature, therefore the changes in dissolution rate do not primarily depend on the batch of magnetic minerals that was used. Apparently, the variations in the procedure have a much greater impact on the dissolution behaviour than differences in mineral structure of the different batches.

Our results confirm that not only temperature but also concentration of magnetic material has a significant influence on the results of the extraction experiments. A low concentration of very fine-grained magnetic minerals – the rule in sediments and soils – can make it virtually impossible to distinguish magnetite from maghemite in samples.

3.3.3 Effects of grain size variation

In figure 7C, the results of the extractions of iron oxides of different grain sizes are given. The first two panels represent the fine-grained synthetic oxides, while the right two panels represent the coarser grained natural oxides. There is a prominent difference in dissolution behaviour between fine-grained oxides (which dissolve easily) and coarse-grained oxides (which dissolve less fast). Of all samples, the natural magnetite dissolved the least. The final susceptibility is ~ 89% of the initial value indicating that, most likely, only the oxidised rims of these coarse grains have dissolved. The natural titanomaghemite also dissolves slowly compared to the fine-grained oxides. However, here ~ 53% of the initial susceptibility was lost after 4 extraction steps. Therefore, the coarse-grained titanomaghemite is more susceptible to the CBD extraction method than magnetite of the same grain size.

3.3.4 Comparison with previous studies

Our results partly agree with the findings of Hunt et al. (1995c) in that both fine-grained maghemite and fine-grained magnetite are dissolved with the CBD extraction method. However, we also found that some coarse-grained iron oxides also dissolve in the CBD method.

Also, Hunt et al. found that a reduction in the amount of dithionite used in the extraction, would make it possible to distinguish magnetite from maghemite dissolution because less magnetite will be extracted. A reduction in dithionite can be viewed as similar to an increase in magnetic mineral concentration. We have shown that an increase in concentration will decrease the amount of magnetic mineral extracted, allowing some distinction between the dissolution behaviour of maghemite and magnetite at the lowest extraction temperature used. These concentrations (5 wt%), however, are high as compared to most natural soil and sediment samples.

4. Conclusions

The new ultrasonic stirring method improved dispersion and reduced the average diameter of aggregates of fine-grained magnetic minerals in the sample. However, a perfectly homogeneous dispersion, with non-interacting magnetic particles (as in most natural samples), could not be obtained. Between batches of synthetic minerals, made in a seemingly similar way, the magnetic behaviour may vary. These variations, however, did not noticeably influence dissolution behaviour in our experiments.

Our results show that the outcome of the CBD extraction method depends not only on the extraction temperature, but also on the concentration and grain size distribution of magnetic minerals. Increased temperature will increase the extraction rate of the magnetic minerals. Similarly, decreased concentration of iron oxides (or increased dithionite/ferrimagnetic mineral ratio) increases the extraction rate of the magnetic minerals. At high oxide concentrations (5 wt%) some distinction between fine-grained magnetite and fine-grained maghemite dissolution can be made.

Increase in grain size will decrease the dissolution rate, for magnetite this decrease is stronger than for titanomaghemite. Of the coarse-grained magnetite, only the oxidised rims were dissolved. Therefore, differentiation between these two minerals is possible for CBD extraction of coarse grains.

The CBD method dissolves all fine-grained magnetite as well as maghemite. A distinction between these two minerals requires application of more than one extraction procedure. Even when using different procedures on the same set of samples distinction will be difficult, as is illustrated by the similar dissolution behaviour of 5 wt% magnetite at 80°C and 1 wt% maghemite or magnetite at 60°C. The CBD extraction treatment is not suitable for distinction between fine-grained magnetic iron oxides.

Acknowledgements

The authors wish to thank H. Plugers and H. van Roermund for their assistance with the SEM analysis, and T. Broer and T. Zalm for the XRD analyses. The reviewers Ö. Özdemir, M. Singer and an anonymous reviewer are thanked for their constructive comments. This paper was supported by the Netherlands Earth & Life Sciences Council (ALW) with financial aid from the Netherlands Organisation for Scientific Research (NWO).

Selective Dissolution of Magnetic Iron Oxides in the Acid-Ammonium-Oxalate/Ferrous-Iron Extraction Method; I. Synthetic Samples

In soil magnetism, the magnetic parameters alone are not always sufficient to distinguish the lithogenic from the pedogenic magnetic fractions. Sequential extraction methods have therefore been incorporated into magnetic studies to constrain the environmental interpretation. Here, we report on the dissolution behaviour of magnetite and maghemite in the acid ammonium oxalate method, to see whether the method is suitable for specific dissolution of magnetic minerals from soils and sediments. To prevent changes in the extraction mechanism during the experiments (see Appendix A) we used an adapted version of the acid ammonium oxalate (AAO) method, in which Fe^{2+} is added to the extraction solution prior to the experiment (the AAO- Fe^{2+} method). The procedure was divided into several 30-minute extraction steps to check the dissolution progress. Synthetic samples containing a quartz matrix with 0.1 wt% of iron oxides were extracted with the AAO- Fe^{2+} method. The iron oxides consisted of either magnetite or maghemite with grain sizes of $< 0.5 \mu\text{m}$ (fine-grained or SD/PSD) and $< 5 \mu\text{m}$ (coarse-grained or MD/PSD), or a 1:1 mixture of both minerals. Because only magnetite and maghemite were studied, the changes in magnetic characteristics could be monitored after each extraction step by analysis of the bulk susceptibility and hysteresis parameters measured at room temperature. The AAO- Fe^{2+} method preferentially dissolved the smaller iron oxides from the samples. For samples containing coarse-grained iron oxides there is a preference for dissolving maghemite rather than magnetite. Extractions of the samples containing mixtures of two different grain sizes or with different mineralogy show that the method preferentially dissolves the smaller grains before attacking the coarse grains in the sample.

I. Introduction

In environmental magnetism, palaeoclimate studies use the magnetic characteristics of sediments and soils to identify the climatic conditions that prevailed during their deposition or formation. It is possible to use magnetic climate proxies because firstly, iron is an important component in all rocks and their weathering products, and secondly, iron(hydr)oxide formation is strongly dependent on climatic factors such as rainfall and temperature (Maher, 1998). Unfortunately, the magnetic signal alone is not always adequate for

palaeoclimate reconstruction, and additional methods are needed to improve the interpretation of the magnetic parameters as climate proxy. Ideally, a method that can differentiate between maghemite and magnetite within soils.

These two iron oxides have a high magnetic signal compared to other magnetic iron oxides (for example: magnetite has a saturation magnetisation of 92 Am²/kg, while that of hematite is 0.4 Am²/kg). This causes the magnetite and maghemite in natural samples to often control the overall magnetic signal. However, the differences in coercivity between maghemite and magnetite are very small and therefore the distinction between these minerals by magnetic hysteresis methods only can be difficult. The susceptibility and magnetisation changes with temperature are difficult to interpret because natural maghemite can be thermally unstable due to differences in crystalline structure (for example the substitution of iron by aluminium or titanium can decrease the Curie temperature of maghemite). Furthermore, organic carbon present in most natural soils will oxidise upon heating and thus can influence the signal.

In environmental magnetism as well as in soil science it is imperative to differentiate between oxides formed as products of (recent) weathering and those inherited from the parent material. Within soil science, several sequential extraction methods have been developed that can identify iron(hydr)oxide phases such as total free iron (i.e. easily soluble iron), and X-ray amorphous iron. A method that is frequently applied in environmental magnetism is the citrate-bicarbonate-dithionite (CBD) extraction method, which is reported to dissolve predominantly (fine-grained) maghemite (Veresub et al., 1993; Hunt et al., 1995c; Sun et al., 1995). However, we have recently shown that the CBD method is only useful for identification of grain sizes of magnetite and maghemite in samples (van Oorschot and Dekkers, 1999).

Therefore, we started an investigation to find other extraction methods that would selectively dissolve iron oxides. Here, we discuss results of extractions of well-defined synthetic samples with the acid-ammonium-oxalate/ferrous-iron (AAO-Fe²⁺) extraction method (results of extractions of natural samples will be discussed in Chapter 6). The AAO method is reported to extract only the X-ray amorphous iron oxides from soils (Schwertmann, 1964; McKeague and Day, 1965; Fischer, 1972; Cornell and Schindler, 1987; Phillips and Lovley, 1987), and therefore has potential for application in environmental magnetism where it could be used to dissolve the secondary iron oxides from soils.

The original AAO extraction method uses a mixture of oxalic acid and ammonium oxalate, and was introduced by Tamm (1922; 1932). Schofield (1949) and Deb (1950) showed that the method, when performed in daylight, dissolved the same phases as dithionite (free iron oxides), but to a lesser extent. In UV light, the dissolution of free iron oxides by the AAO method was more extensive, and was shown to be caused by photocatalytic dissolution of iron oxides with oxalate (De Endredy, 1963). Schwertmann suggested to exclude light from the extraction experiments and demonstrated that only the X-ray amorphous iron oxides are dissolved when the method is performed in the dark (Schwertmann, 1959; Schwertmann, 1964). Other studies confirmed his results (McKeague and Day, 1965; McKeague et al., 1971).

The AAO method - as described by Schwertmann (1964) - has been frequently applied in soil science as well as in some environmental magnetism studies to determine the amorphous and poorly crystalline iron oxide content of soils (e.g. Torrent et al., 1980; Olson and Ellis, 1982; Schwertmann et al., 1982; Schwertmann et al., 1985; Phillips and Lovley, 1987; Fine and Singer, 1989; Borggaard, 1990; Canfield et al., 1992; Golden et al., 1994; Pinheiro-Dick and Schwertmann, 1996; Rozan et al., 1997). However, several studies have shown that crystalline iron oxides can be dissolved as well with the AAO method (e.g.

McKeague et al., 1971; Schwertmann, 1973; Walker, 1983; Borggaard, 1988; Fine and Singer, 1989; Borggaard, 1990). Others reported that the method can be applied to dissolve specific minerals, such as magnetite, and that differentiation on the basis of mineralogy would be possible with this method (Chao and Zhou, 1983; Golden et al., 1994). These results are in contrast with the original observation that the AAO-method only dissolves amorphous iron oxides. In the method proposed by Schwertmann (1964) the dissolution rate changes with time. This change in dissolution rate is related to the increasing concentration of Fe^{2+} in the extraction solution during the experiment (Fischer, 1972; see also Appendix A). A constant

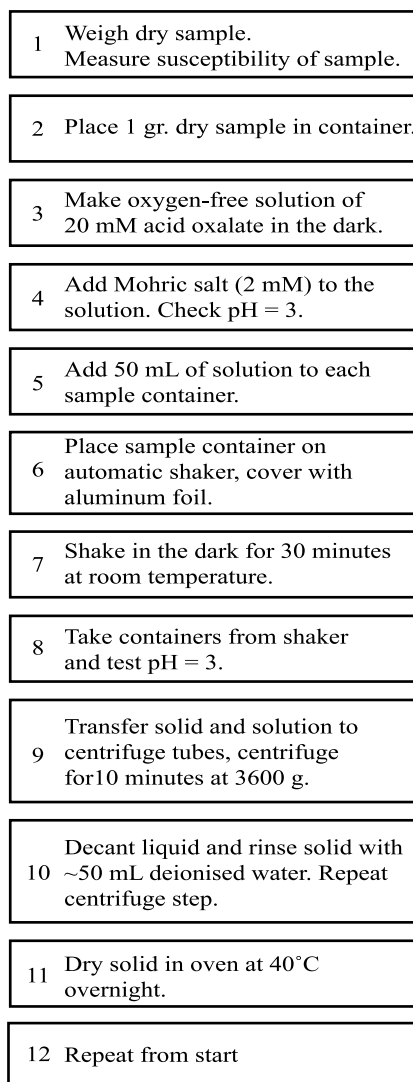


Figure 1: Flowchart of the AAO- Fe^{2+} extraction method, as used in the experiments of this study.

dissolution rate can be established by addition of a small amount of Fe^{2+} to the extraction solution prior to the experiment (e.g. Fischer, 1972; Blesa et al., 1987; Sulzberger et al., 1989; Grygar, 1997). This adapted method was used in our experiments and will be referred to as the AAO- Fe^{2+} method. Further aspects of this change in dissolution rate as well as the different extraction mechanisms of the AAO method are summarised in Appendix A.

We tested whether the AAO- Fe^{2+} method would dissolve crystalline iron oxides from synthetic samples by extracting dispersions of well-defined crystalline iron oxides in a quartz matrix. Furthermore, we studied whether the method would selectively dissolve specific minerals from our samples by conducting extractions of mixtures of iron oxides of different mineralogy.

2. Materials and methods

2.1 Extraction method

The procedure we use is based on the method of Schwertmann (1964), and the modifications described by Grygar (1997). It involves the use of a 20 mM acid ammonium oxalate solution with 2 mM Fe^{2+} added, as described in the extraction scheme of Figure 1. Table 1 compares the parameters of our procedure to those of Schwertmann and Grygar.

The extraction solution is prepared with deoxygenated water to prevent oxidation of Fe^{2+} in the extraction solution. The oxygen is removed from the water by boiling deionised water (~ 1.5 -2 L) until approximately 1 L is left, this is subsequently purged with Ar gas (~ 1 hour for 1 litre of water) and simultaneously cooled down to room temperature. This water is used to make a 1 L solution of 0.02 M

Author	Schwertmann ('64)	Grygar ('97)	this study
purging gas	none	nitrogen	argon
pH	3	2.7	3
concentration Ferrous Iron	none	2 mM	2 mM
concentration Acid Ammonium Oxalate	200 mM	20 mM	20 mM
volume of solution	100 mL	-	50 mL
extraction time	2 hours	-	30 minutes (per step)
sample mass	1-5 gr soil	5 mg iron oxide	1 gr synthetic sample 1 wt% iron oxides

Table 1: Specifications for three different methods of acid ammonium oxalate extraction.

oxalic acid/ammonium oxalate at pH 3 by adding 1.6 g ammonium oxalate ($(\text{NH}_4)_2\text{C}_2\text{O}_4 \cdot \text{H}_2\text{O}$) and 1.1 g oxalic acid ($\text{H}_2\text{C}_2\text{O}_4 \cdot 2\text{H}_2\text{O}$). Since pH plays an important role in the extraction mechanism (see appendix A) it is regularly checked throughout the preparation and extraction experiment. The bottle containing the solution is wrapped in aluminium foil to prevent photo-excitation of the oxalate, and the solution is continuously purged with Ar gas throughout the preparation. Then, the Fe^{2+} is added in the form of 0.784 g Mohric salt ($\text{Fe}(\text{NH}_4)_2(\text{SO}_4)_2 \cdot 6\text{H}_2\text{O}$) to make a concentration of 2 mM Fe^{2+} in solution. For each 1 g sample, 50 mL of this solution is required to perform one extraction step. A total of twelve samples as well as two blank samples are used for each samples series, requiring 700 mL of solution per extraction step. For each step a new solution is prepared.

After checking the pH of the solution, 50 mL is added with a dispenser to each of the sample containers. These 100 mL sample containers are made of brown glass, which prevents photo-catalytic dissolution of iron oxides during extraction. Subsequently, the containers are closed and placed on a mechanical shaker (Marius, type 71 SL) at room temperature and at medium speed for 30 minutes. Aluminium foil is wrapped around the containers and the shaker to prevent photochemical dissolution. After 30 minutes the samples are transferred to centrifuge tubes, and the liquid and solid phase are separated by centrifuging for 10 minutes at 3600 g (~ 4417 rpm, MSE Mistral 2000). The liquid is decanted (after checking pH, which remained at $\text{pH} = 3$ for all samples) and the samples are rinsed with ~ 50 mL deionised water and centrifuged again. The remaining solid is dried in air in an oven at 40°C for ~ 12 hours. The extraction step is repeated a maximum of two times, each sample series requiring one day for extraction and drying of the samples.

2.2 Synthetic samples

To keep control of as much of the experimental parameters as possible, we used synthetic samples made from a matrix of quartz (analytical grade, Merck) to which iron oxides are added. The quartz grains had an average grain size of 0.2 - 0.8 mm and contain < 0.05 % substances soluble in hydrochloric acid. The starting mass of the samples is ~ 1 g, the concentration of iron oxides is ~ 0.1 wt%.

The iron oxides were taken from a study by Hartstra (1982a), furthermore, we prepared fine-grained iron oxides according to the method described in Schwertmann & Cornell (1991). Table 2 shows the properties

Synthetic Iron Oxides	Natural Iron Oxides
Magnetite: - grain size $< 0.5 \mu\text{m}$ - $T_c \sim 580^\circ\text{C}$	Magnetite: - grain size $< 5 \mu\text{m}$ - $T_c \sim 580^\circ\text{C}$
Maghemite: - grain size $< 0.5 \mu\text{m}$ - $T_c \sim 640^\circ\text{C}$	Titanomaghemite: - grain size $< 5 \mu\text{m}$ - $T_c \sim 550^\circ\text{C}$ - $\text{Fe}_{(2-x)}\text{Ti}_x\text{O}_3$ ($x = 0.05; z = 0.8$)

Table 2: Properties and origin of the iron oxides used in this study. Synthetic iron oxides were prepared according to the protocol of Schwertmann and Cornell (1991), while the natural samples were taken from a study by Hartstra (1982a).

Iron oxide	χ_0 [10 ⁻⁸ m ³ kg ⁻¹]			M_{rs} [Am ² kg ⁻¹]			M_s [Am ² kg ⁻¹]			B_{cr} [mT]			B_c [mT]			M_{rs}/M_s			B_{cr}/B_c			
	A	B	C	A	B	C	A	B	C	A	B	C	A	B	C	A	B	C	A	B	C	
Syn. Magnetite		82.4			0.028			0.160			25.7			12.3			0.20			2.4		
Syn. Maghemite		54.4			0.029			0.106			27.3			15.4			0.29			1.8		
Nat. Magnetite	53.6	58.0		0.011	0.018		0.065	0.121		39.7	32.1	40	14.3	12.8	15.0	0.17	0.15	0.18	2.8	2.5	2.7	
Nat. Titanomaghemite	19.4	19.8		0.010	0.018		0.028	0.070		56.3	53.4		33.0	24.8		0.02	0.28		1.7	2.2		

Table 3: Initial susceptibility and hysteresis parameters of the iron oxides used in our study (column B). The data come from samples of iron oxides mixed with quartz (typically ~1 mg iron oxides in 1 g sample). Data for the < 5mm iron oxides are compared to data published by Hartstra (1982a; 1982b) in column A and data from Vlag et al. (1996) in column C.

of these oxides. The data for the natural iron oxides compare well with the original analyses by Hartstra (1982a) (see Table 3). The iron oxides were mixed with the matrix material by stirring both components in acetone in an ultrasonic bath for approximately two minutes (1999). After stirring, the samples were dried overnight in air in an oven at 40°C and stored. The samples contained either one of the mentioned iron oxides, or a mixture of two of these oxides (see Table 4). Each sample series consists of twelve samples and two blanks. The blanks contained only quartz and were handled in the same way as the other samples. After preparation the samples are transferred to the sample containers.

2.3 Magnetic methods

Prior to the start of the experiment and after each extraction step, the dry samples are weighed and bulk susceptibility as well as hysteresis parameters of the samples were measured. Bulk susceptibility was

Sample series	wt% synthetic magnetite ($\bar{\theta} < 0.5 \mu\text{m}$)	wt% synthetic maghemite ($\bar{\theta} < 0.5 \mu\text{m}$)	wt% natural magnetite ($\bar{\theta} < 5 \mu\text{m}$)	wt% natural titanomaghemite ($\bar{\theta} < 5 \mu\text{m}$)
syn. MN	0.1	-	-	-
syn. MH	-	0.1	-	-
nat. MN	-	-	0.1	-
nat. TiMH	-	-	-	0.1
mix 1	0.05	-	0.05	-
mix 2	0.05	-	-	0.05
mix 3	-	0.05	0.05	-
mix 4	-	0.05	-	0.05
blanks	-	-	-	-

Table 4: Composition of synthetic samples used in this study. All samples had a matrix of quartz and a total iron oxide concentration of 0.1 wt%. Total sample mass was 1.0 gr., and each series consisted of 12 samples.

measured with a KLY-2 susceptibility-bridge (AGICO). The sensitivity of the equipment is $4 \cdot 10^{-8}$ SI, and our data were at least a factor two higher. The susceptibility after each extraction step is normalised to the starting value of the susceptibility of the respective samples, to enable comparison between different sample series. The hysteresis loops were measured with an alternating gradient magnetometer (Micromag) with saturation field of 500 mT and a field increment of 5 mT. At 500 mT all samples had reached saturation magnetisation. The sensitivity of the Micromag is 1 nAm^2 , which is in the same range as the values for the M_{rs} of our blanks as well as of some of the mixtures after two extraction steps. All other samples had a magnetisation value of at least one order of magnitude higher than the sensitivity of the Micromag. The accuracy of each Micromag measurement is 2% versus the calibration, calibration was checked after each six measurements. All measurements were 70% slope corrected because of the high diamagnetic signal from the matrix. Backfield demagnetisation was performed in the same magnetometer with a field increment of 1 mT to a maximum field of -100 mT to determine the coercivity of remanence. A definition of all magnetic parameters used in this chapter can be found in the glossary of appendix B.

3. Results

In subsection 3.1 the magnetic properties of all sample series prior to extraction are presented. Subsequently, the results obtained from extractions of samples containing either one type of iron oxide (series 1-4 in Table 4, subsection 3.2) or mixtures of iron oxides (series 5-8 in Table 4, subsection 3.3) are presented.

3.1 Magnetic properties before extraction

The mass susceptibility of the original samples is given in Table 3. The hysteresis parameters (Table 5) show that all samples plot in different areas of the Day plot (Figure 2B). Typical values for the coarse-

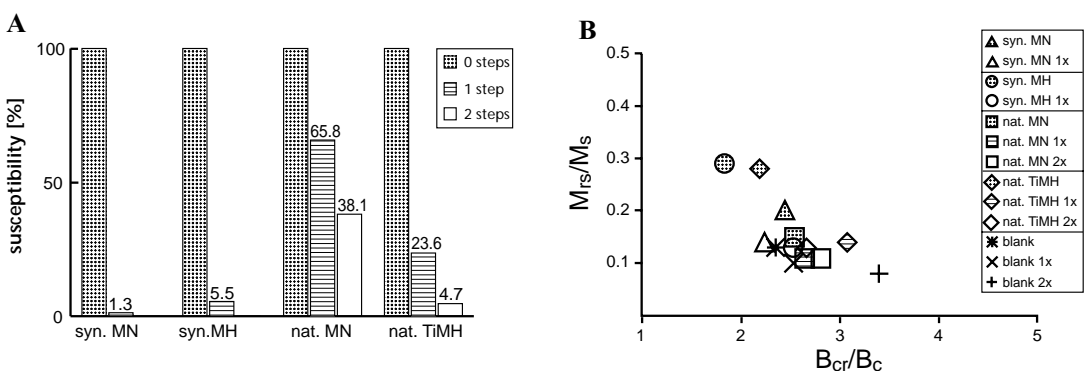


Figure 2: Magnetic parameters before and after extraction of synthetic samples containing a single type of iron oxide. Each sample series is represented by the average of twelve samples, the standard deviation ranges between 0.9–4.8 % depending on extraction step and sample series. (a) Percentage of initial susceptibility remaining after each extraction step. (b) Day plot. MN indicates magnetite, MH indicates maghemite and TiMH indicates titanomaghemite. Fine-grained iron oxides prepared according to Schwertmann and Cornell (1991) are indicated with 'syn', coarse-grained iron oxides from the study of Hartstra (1982a) are indicated with 'nat'.

grained magnetite are 0.15 for M_{rs}/M_s and 2.5 for B_{cr}/B_c , while coarse-grained titanomaghemite has values of 0.28 and 2.2 for M_{rs}/M_s and B_{cr}/B_c respectively. For fine-grained magnetite and for fine-grained maghemite our values are 0.20 and 0.29 for M_{rs}/M_s , and 2.4 and 1.8 for B_{cr}/B_c respectively, which is within the range published for magnetite by Dunlop and Özdemir (1997). The samples containing maghemite have a higher M_{rs}/M_s and a lower B_{cr}/B_c ratio than those containing magnetite. Samples of iron oxides with the same mineralogy show slightly higher M_{rs}/M_s and lower B_{cr}/B_c ratios for samples with fine grain size. Coercivity is high for unextracted samples, especially for the natural titanomaghemite ($B_{cr} = 53.4$ mT), and decreases via coarse-grained magnetite and fine-grained maghemite to the lowest value for the fine-grained magnetite ($B_{cr} = 25.7$ mT). The data for the coarse-grained minerals compare well to those published by Hartstra (1982a) and by Vlag et al. (1996).

3.2 Changes of magnetic properties with extraction

3.2.1 Susceptibility

After one extraction step, only a small percentage of the initial susceptibility remains in the samples containing fine-grained iron oxides (Figure 2). Loss of susceptibility is slightly higher for the samples with fine-grained magnetite than for those containing fine-grained maghemite. The susceptibility of the samples containing the coarse-grained iron oxides decreases more slowly. After two extraction steps almost all of the initial susceptibility in the samples with coarse-grained titanomaghemite has been removed, while ~ 40 % still remains in the samples containing coarse-grained magnetite.

3.2.2 Hysteresis parameters

The first extraction step causes the most significant change in hysteresis parameters (Table 5). The coercivities decrease to less than half the starting value for all fine-grained oxides and the coarse-grained titanomaghemite. The coercivity of the coarse-grained magnetite decreases to ~ 2/3 of the original value.

Iron oxide	M_{rs} [Am ² kg ⁻¹]			M_s [Am ² kg ⁻¹]			B_{cr} [mT]			B_c [mT]			M_{rs}/M_s			B_{cr}/B_c		
	0	1	2	0	1	2	0	1	2	0	1	2	0	1	2	0	1	2
Syn. Magnetite	0.028	0.001	-	0.16	0.01	-	25.7	14.1	-	12.3	6.8	-	0.20	0.13	-	2.4	2.0	-
Syn. Maghemite	0.029	0.002	-	0.11	0.01	-	27.3	15.0	-	15.4	6.1	-	0.29	0.13	-	1.8	2.5	-
Nat. Magnetite	0.018	0.007	0.004	0.12	0.06	0.04	32.1	19.5	17.7	12.8	7.3	6.6	0.15	0.12	0.11	2.5	2.6	2.8
Nat. Titanomaghemite	0.018	0.005	0.003	0.07	0.03	0.03	53.4	18.3	15.7	24.8	6.0	5.6	0.28	0.14	0.12	2.2	3.0	2.6
Blank	0.001	0.001	0.001	0.004	0.005	0.009	18.3	13.4	19.9	7.6	5.3	4.9	0.12	0.10	0.07	2.4	2.6	4.1

Table 5: Hysteresis parameters of samples before and after extraction. The number in the header indicates the number of extraction steps performed. All parameters are averages of 12 samples, the fine-grained samples were only extracted once.

For the fine-grained samples, M_{rs} is reduced to less than 1% of its original value after one extraction step. In the coarse-grained samples the reduction is $\sim 50\%$ for the magnetite and $\sim 34\%$ for the titanomaghemite.

A Day plot of the samples is given in Figure 2B. All samples shift from the pseudo single-domain (PSD) toward the multidomain (MD) range in the Day plot after extraction. This indicates that the PSD characteristics of the samples before extraction are most likely due to the contributions of a range of grain sizes, leading to an average grain size in the PSD range. During extraction the smallest grains are dissolved completely in the first extraction step, causing the average grain size to shift to a larger size. After two extraction steps, the samples with fine-grained iron oxides, show resemblance in hysteresis parameters to the data of the blanks. The samples with coarse grains of natural titanomaghemite also compare well with the blanks. All extracted samples show a decrease in M_{rs}/M_s ratio. This decrease is strongest for the samples containing maghemite. All samples, except those containing fine-grained magnetite, show an increase in B_{cr}/B_c ratio after extraction. The decrease in M_{rs}/M_s ratio is related to a strong decrease of both M_{rs} and M_s , but the value of M_{rs} decreases more rapidly. The increase in B_{cr}/B_c is related to a more rapid decrease in B_c .

3.3 Dissolution behaviour of iron oxide mixtures

In Figure 3A, the decrease in susceptibility with each extraction step is given for all mixtures. The susceptibility of the mixtures after extraction mostly reflects the contribution of the coarse-grained samples, indicating that the fine-grained oxides were preferentially dissolved. The mixtures containing coarse-grained titanomaghemite show a more rapid decrease in susceptibility than those containing coarse-grained magnetite. The contribution of the fine-grained iron oxides to the susceptibility of the samples after extraction appears limited. However, judging from the percentage of decrease in susceptibility for the different mixtures, the fine-grained maghemite dissolves more slowly from the samples than the fine-grained magnetite.

In Table 6 the hysteresis parameters of the mixtures before and after extraction are compiled. In all

Sample	M_{rs} [Am ² kg ⁻¹]			M_s [Am ² kg ⁻¹]			B_{cr} [mT]			B_c [mT]			M_{rs}/M_s			B_{cr}/B_c		
	0	1	2	0	1	2	0	1	2	0	1	2	0	1	2	0	1	2
mix 1 (syn. MN & nat. MN)	0.030	0.004	0.003	0.084	0.036	0.024	29.5	25.7	22.2	16.2	10.9	9.4	0.23	0.13	0.13	1.8	2.4	2.4
mix 2 (syn. MN & nat. TiMH)	0.015	0.006	0.003	0.053	0.069	0.030	35.4	37.3	19.6	20.6	14.0	7.7	0.28	0.16	0.11	1.7	2.9	2.7
mix 3 (syn. MH & nat. MN)	0.015	0.004	0.002	0.068	0.037	0.022	29.8	25.6	24.4	16.4	10.2	8.7	0.23	0.12	0.10	1.9	2.6	2.8
mix 4 (syn. MH & nat. TiMH)	0.016	0.003	0.001	0.056	0.013	0.009	35.5	41.1	34.6	19.6	17.0	10.2	0.28	0.22	0.14	1.8	2.6	2.9
Blank	0.001	0.001	0.001	0.004	0.005	0.009	18.3	13.4	19.9	7.6	5.3	4.9	0.12	0.10	0.07	2.4	2.6	4.1

Table 6: Hysteresis parameters of samples after extraction. All parameters are averages of 12 samples. Mix 1 and mix 3 are mixtures of coarse-grained magnetite with fine-grained magnetite and maghemite respectively. Mix 2 and 4 are mixtures of coarse-grained titanomaghemite with fine-grained magnetite and maghemite respectively. The number in the header represents the number of extraction steps performed.

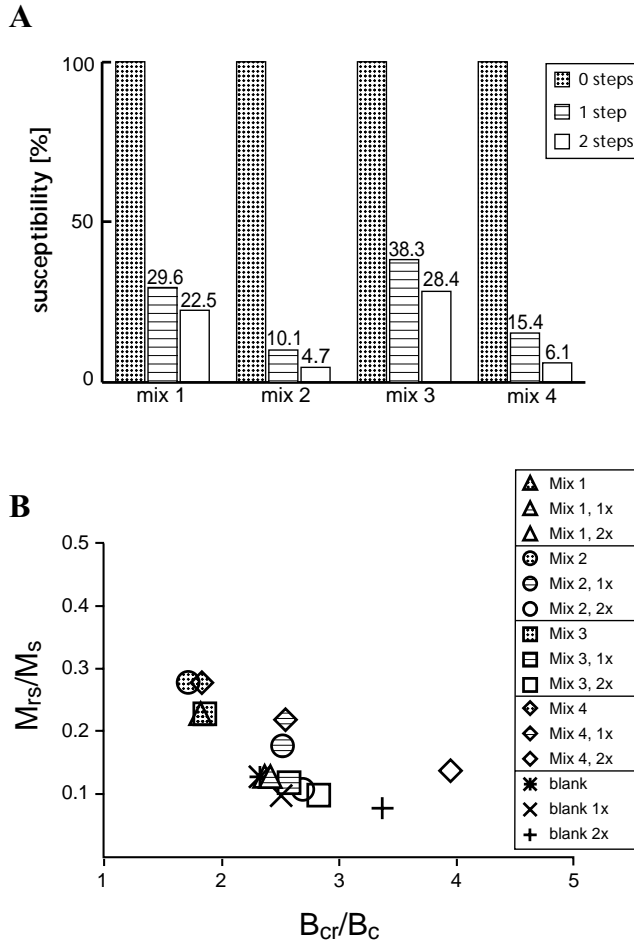


Figure 3: Magnetic parameters before and after extraction of synthetic samples containing a mixture of iron oxides. (a) Percentage of initial susceptibility remaining after each extraction step. (b) Day plot. Mix 1 and mix 3 are mixtures of coarse-grained magnetite with fine-grained magnetite and maghemite respectively. Mix 2 and 4 are mixtures of coarse-grained titanomaghemite with fine-grained magnetite and maghemite respectively. Fine-grained iron oxides prepared according to Schwertmann and Cornell (1991), coarse-grained iron oxides from the study of Hartstra (1982a). Each mixture is the average of a series of twelve samples, the standard deviation varies between 0.8 and 6.5 % depending on the extraction step and sample series.

mixtures, M_{rs} is almost reduced to zero ($\sim 10\%$ of the starting value) after one extraction step, while M_s is reduced to approximately 50% of its starting value. For those mixtures containing coarse-grained magnetite (mixture 1 and 3), B_c and B_{cr} behave very similar and decrease with each extraction step. For the samples with coarse-grained titanomaghemite (mixture 2 and 4), B_{cr} increases after one extraction step, and has the lowest value after two extractions. This final decrease in B_{cr} is strongest for the mixture with fine-grained magnetite. B_c of these mixtures decreases with each extraction step, but the decrease is most rapid for the mixture containing fine-grained magnetite.

The hysteresis parameters of the mixtures are shown in Figure 3B. Before extraction, all mixtures plot in the same part of the diagram, in the PSD range close to the single domain (SD) area. After extraction all samples show a decrease in M_{rs}/M_s ratio and an increase in B_{cr}/B_c ratio, and in the Day plot the samples move toward the MD area. This is an indication that the fine-grained oxides are preferentially removed from the mixture in the first extraction step, which changes the average grain size diameter to higher (more MD) values. The increase in coercivity ratio is strongest for the mixtures containing coarse-grained titanomaghemite, and weakest for the mixtures containing coarse-grained magnetite. The decrease in M_{rs}/M_s is strongest for the mixtures containing coarse-grained magnetite and weakest for the mixtures containing coarse-grained titanomaghemite. The fine-grained oxides do not appear to affect the hysteresis parameters of the extracted mixtures.

4. Discussion & conclusion

4.1 Synthetic samples

We have shown that the AAO-Fe²⁺ method can dissolve crystalline iron oxides of varying grain sizes. However, the dissolution behaviour of each mineral type and grain size is very distinct and they can be identified by magnetic analysis of the samples before and after extraction. With one extraction step, almost all fine-grained iron oxides are removed from the samples.

The results of our experiments show that with a combination of susceptibility and hysteresis data we can distinguish grain-size fractions as well as mineralogy of coarse grains in samples before and after extraction. All single oxide samples plot in different areas of the Day plot before extraction. After extraction we can make a distinction according to grain size from the susceptibility data, where the susceptibility decreases most strongly for the fine-grained iron oxides. Furthermore, we can make a distinction between magnetite and titanomaghemite samples from the susceptibility data, which show that the coarse-grained magnetite has the slowest decrease in susceptibility after extraction. Based on the susceptibility decrease, the dissolution rate can be classified as follows; fine-grained iron oxides > coarse-grained titanomaghemite > coarse-grained magnetite.

The mineralogy and grain sizes of the mixtures can be identified as well from the susceptibility data combined with the Day plot. The susceptibility data reflect the behaviour of the coarsest grain-size fraction in the mixtures, and here we can again distinguish between magnetite and titanomaghemite. We also see a more rapid decrease in susceptibility (2-10 % more loss of starting susceptibility) for the mixtures containing fine-grained magnetite compared to those with fine-grained maghemite. In the Day plot, the samples plot close together before extraction. However, the plot is useful to distinguish between the different mixtures after extraction. The data indicate that in mixtures of grain-size and mineralogy the preferential dissolution pathway is: fine-grained oxides first (with slight preference for magnetite), coarse-grained samples last (with preference for titanomaghemite).

4.2 Comparison with Citrate-Bicarbonate-Dithionite extraction

Like the citrate-bicarbonate-dithionite (CBD) method, the AAO-Fe²⁺ method preferentially dissolves the fine-grained iron oxides from synthetic samples. However, the results of the AAO-Fe²⁺ method give

more information about the type of iron oxides that are dissolved. The CBD method can only be used to differentiate fine from coarse grains (e.g. van Oorschot and Dekkers, 1999), while the AAO-Fe²⁺ method can identify both grain size and mineralogy. The most important parameter in the CBD method is the extraction temperature (e.g. van Oorschot and Dekkers, 1999), in the AAO-Fe²⁺ method light and pH can influence the extraction as well. The dissolution mechanism in the AAO-Fe²⁺ method is less aggressive and the results give more detail than the CBD method, therefore we would recommend this procedure for use in future studies.

4.3 Implications for the future

The AAO-Fe²⁺ extraction method has good potential as a tool in environmental magnetism. It may be suitable to dissolve all fine-grained pedogenic iron oxides from palaeosol samples in one extraction step, while leaving the lithogenic iron oxides virtually untouched. Because of the slightly preferential dissolution of fine-grained magnetite over fine-grained maghemite, the method could possibly differentiate between magnetite and maghemite within the pedogenic and lithogenic fractions. Before it can be used in environmental magnetism, however, the method needs to be tested on natural samples.

Acknowledgements

The manuscript was substantially improved by the constructive reviews of Dr. Stanjek and Dr. Kletetschka. This work is conducted under the programme of the Vening Meinesz Research School of Geodynamics (VMSG), and funded by the Netherlands Organisation for Scientific Research (NWO/ALW).

Appendix A: Extraction mechanism of the AAO vs. AAO-Fe²⁺ extraction method

AAO mechanism

The acid ammonium oxalate extraction mechanism (Schwertmann, 1964) is a ligand-promoted dissolution. As shown in Figure A-1A, oxalate adsorbs to a Fe(III) site at the crystal surface. The high polarity of the oxalate leads to a weakening of the bonds between the Fe(III) and the solid resulting in the slow release of the iron-oxalate complex into the solution. pH is an important factor in the AAO mechanism; protons facilitate the dissolution process by protonating OH⁻ groups on the mineral surface, thereby contributing to a weakening of the Fe-O bond. Thus, a decrease in pH will increase the dissolution rate. However, a decrease in pH increases the protonation of ligands in solution, thus a decrease in pH will decrease the adsorption of ligands to the mineral surface. As a result of these opposing processes, the AAO method has an optimum pH range of 2-4, where dissolution is maximum (Cornell and Schwertmann, 1996).

Another influence on the pH is the presence of calcium carbonate in samples. When calcium carbonate is present in a sample, it will buffer the acid from the extraction solution and thus increase the pH. At pH-values above 3 the rate of dissolution of iron will rapidly decrease (e.g. Parfitt, 1989; Campillo and Torrent, 1992). A simple calculation, assuming all acid in the extraction solution is used for the reaction of carbonate to CO₂, indicates that the calcium carbonate has to be present in amounts greater than 10 wt% to completely buffer the system. When calcium carbonate concentrations exceeds 10 wt%, it is advised to add more oxalic acid to the solution until the pH has stabilised at pH 3 (Campillo and Torrent, 1992).

In the method proposed by Schwertmann (1964) the dissolution rate changes with time. As shown in Figure A-2, the dissolution rate increases considerably after an initial period of slow dissolution (Fischer, 1972; Borggaard, 1990; Hering and Stumm, 1990). This change in dissolution rate is related to the increased concentration of Fe²⁺ in solution which has a catalytic effect on the dissolution mechanism (Borggaard, 1981). The Fe²⁺ combines with the oxalate in solution to form a complex that can dissolve iron from the solid more easily than an oxalate ion on its own. The oxalate in the complex acts a bridging ligand for the electron transfer between the Fe²⁺ of the complex and the Fe(III) in the solid surface. After dissolution of the iron from the solid, the Fe²⁺ will be released into the solution and can combine again with oxalate to form a new complex, which in turn can be used in the dissolution of more iron from the solid surface. By addition of a small amount of Fe²⁺ to the extraction solution at the start of the experiment, the initial slow rate of the AAO method disappears (Fischer, 1972; Baumgartner et al., 1983; Cornell and Schindler, 1987; Suter et al., 1988; Sulzberger et al., 1989; Borggaard, 1990; Hering and Stumm, 1990; Stumm and Sulzberger, 1992). Here, we refer to the adapted method, using Fe²⁺ as a catalyst, as the AAO-Fe²⁺ method.

AAO-Fe²⁺ mechanism

This dissolution mechanism has been described several times (Cornell and Schwertmann, 1996) and is given in Figure A-1B. The addition of Fe²⁺ to the extraction solution promotes the iron oxide dissolution because the Fe(II)-oxalate complex is a strong reductant. At low pH, both the Fe²⁺ and the surface of iron oxides are positively charged and repel each other electrostatically. The charge reversal of Fe²⁺ due to its

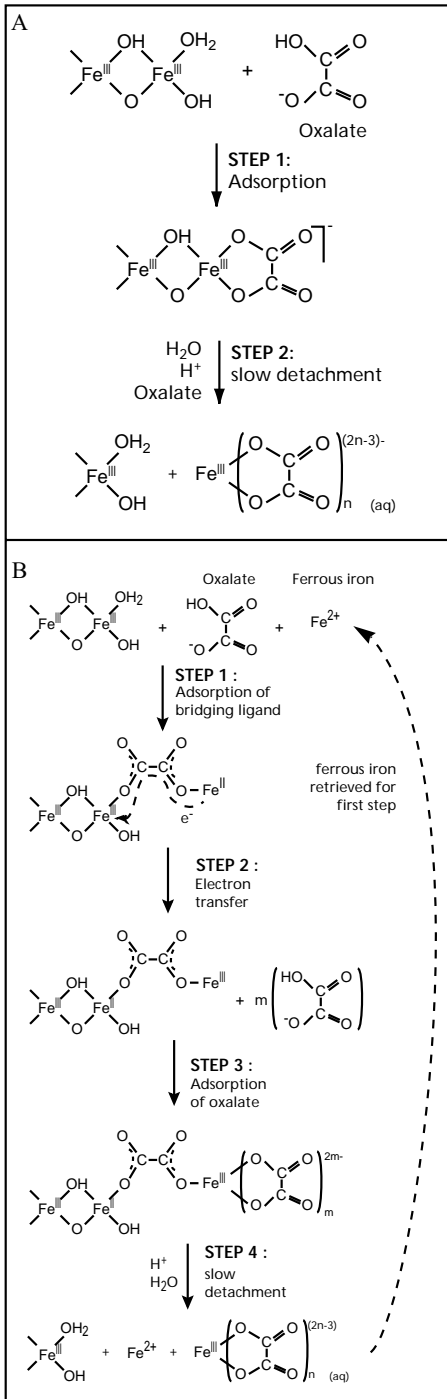


Figure A-1: Difference in dissolution mechanism for the AAO extraction method (A) and the AAO-Fe²⁺ extraction method (B) where Fe²⁺ is added to the extraction solution at the start of the experiment (modified after Hering and Stumm, 1990).

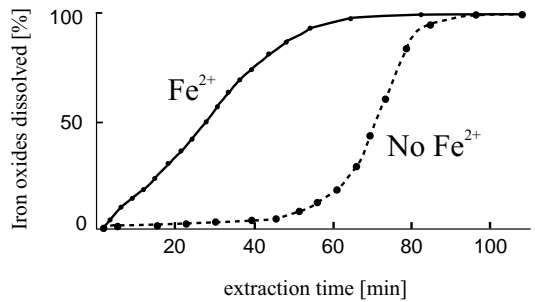


Figure A-2: Difference in dissolution rate caused by a change in extraction mechanism, for extraction of magnetite performed with a solution containing 0.1 mol/L oxalic acid and 6·10⁻⁶ mol/L Fe²⁺ (solid line) and a similar solution without Fe²⁺ added at the start of the experiment (dotted line) (modified after Baumgartner et al., 1983).

complexation with oxalate enables adsorption of the complex with the solid. The first step in the AAO-Fe²⁺ dissolution mechanism is the formation of a complex between Fe²⁺ and oxalate in solution. This complex adsorbs to a Fe(III) site on the mineral surface. The newly formed inner-sphere complex shifts the electron density towards the Fe(III) on the mineral surface and facilitates electron transfer with oxalate as the bridging ligand between the two iron atoms (Baumgartner et al., 1983; Cornell and Schindler, 1987; Stumm and Sulzberger, 1992). The reduced iron complex at the mineral surface can then be detached.

Appendix B: Glossary of magnetic terms used in this chapter

B_c	coercivity [mT] = the reverse field required to reduce the magnetisation to zero from saturation
B_{cr}	coercivity of remanence [mT] = the reverse field required to reduce the remanent magnetisation to zero after saturation
M_{rs}	saturation isothermal remanent magnetisation [$\text{Am}^2\text{kg}^{-1}$] = the magnetisation remaining in the absence of an external magnetic field after saturation
M_s	saturation magnetisation [$\text{Am}^2\text{kg}^{-1}$] = the strongest possible magnetisation which can be produced in a specimen by applying a field
χ	specific susceptibility [m^3kg^{-1}] = low field magnetic susceptibility expressed in terms of unit mass

Part II

Natural samples

Environmental magnetism-

Applications in natural loess-palaeosol sequences

This chapter introduces the principles and methods of environmental magnetism. It offers only a concise introduction to environmental magnetism, with a discussion of the parameters used to identify mineralogy, grain size and concentration, and a more specific focus on the use of environmental magnetic techniques in the determination of palaeoclimate proxies in loess-palaeosol sequences. The advantages and shortcomings of magnetic techniques for the determination of the climatic history of loess-palaeosol sequences are highlighted. Finally, the use of citrate-bicarbonate-dithionite (CBD) and acid-ammonium-oxalate (AAO) extraction methods in environmental magnetism studies is summarised.

1. Short history of environmental magnetism

The important role of iron oxides in soils was for a long time not recognised for two main reasons: they occur in low concentrations, and they are often amorphous and very fine grained. This makes it difficult to detect iron oxides in soils. The first report of soil hematite and goethite dates back to 1939, when Alexander et al. (1939) identified these minerals with X-ray diffraction (see also: Cornell and Schwertmann, 1996). It was not until 1951, however, that maghemite was identified in a soil for the first time by van der Marel (1951). This result was confirmed by Le Borgne in 1955, who attributed the increase in magnetic susceptibility in the topsoil to pedogenic formation of maghemite through forest fires (Le Borgne, 1955). His work is also the first report on magnetic enhancement within a soil profile, and it was not until the late 1970s that the importance of this discovery was fully understood. At this time, Mullins (1977) published a paper on the significance of magnetic susceptibility in identifying pedogenic and lithogenic ferrimagnetic minerals in soils. By then, it was generally realised that soils and sediments contain magnetic material that has been subject to transport, deposition or in situ transformation, and that the magnetic mineral composition of natural materials is influenced by environmental processes in the atmosphere, lithosphere, biosphere and hydrosphere. The first explicit description of environmental magnetism as a distinct field was in 1980 by Thompson et al. (1980). One of the landmark studies in this new field was the work of Heller and Liu (1982; 1984). They were the first to successfully construct a palaeomagnetic time-scale for the Chinese loess-palaeosol sequences. They used the information from their palaeomagnetic study to show that the pattern of magnetic susceptibility variation with depth in a Chinese loess-palaeosol sequence was in broad agreement with the oxygen isotope record in marine sediments, and that the high susceptibility layers (the palaeosols) were formed during interglacial stages. After this landmark study, many others started investigating how the magnetic signal in sediments is linked to climate. A more elaborate overview of the field is given by several authors, including the books of Thompson and Oldfield (1986) and Maher and Thompson (1999), as well as the reviews of Verosub and Roberts (1995), Heller and Evans (1995), or Dekkers (1997).

2. Magnetic properties related to grain size, mineralogy and concentration

To understand the influence of environment on magnetic minerals, one first has to develop methods to describe mineralogy, grain size and concentration of magnetic minerals in natural samples. Several mineral-magnetic parameters have been identified as being either dependent on mineralogy, grain size, concentration or on a combination of these characteristics. A list of common parameters and ratios used in environmental magnetism is given in table 1. Here, we will briefly discuss them. For a more detailed overview we refer to Thompson and Oldfield (1986) or Maher (1986).

symbol	Parameter description	dependent on / indicative of
χ	mass specific susceptibility [m^3/kg]	concentration of ferrimagnetic grains, and grain size
χ_{fd}	frequency dependence of susceptibility [%]	grain size
SIRM	saturation isothermal remanent magnetisation ($=M_{rs}$) [$\text{Am}^2\text{kg}^{-1}$] or [Am^{-1}]	concentration, grain size
M_s	saturation magnetisation [$\text{Am}^2\text{kg}^{-1}$] or [Am^{-1}]	concentration
B_{cr}	remanent coercive force [mT]	grain size, mineralogy (ferrimagnetic vs. antiferromagnetic)
B_c	coercive force [mT]	grain size, mineralogy (ferrimagnetic vs. antiferromagnetic)
$\text{IRM}_{0.3T}/\text{SIRM}_{1T}$	S-value [-]	mineralogy (ferrimagnetic vs. antiferromagnetic)
M_{rs}/M_s & B_{cr}/B_c	Day plot [-]	grain size (specifically for (titano-)magnetite)
T_C	Curie Temperature [$^{\circ}\text{C}$]	mineralogy
T_M	Morin transition temperature [$^{\circ}\text{C}$]	mineralogy (hematite)
T_V	Verwey transition temperature [$^{\circ}\text{C}$]	mineralogy (magnetite)
$\text{IRM}_{77-293\text{K}}$	isothermal remanent magnetisation (from 77 to 293 K) [$\text{Am}^2\text{kg}^{-1}$]	grain size, mineralogy
ARM	anhysteretic remanent magnetisation [$\text{Am}^2\text{kg}^{-1}$] or [Am^{-1}]	concentration of SD ferrimagnetic minerals
χ_{ARM}	ARM susceptibility [-]	concentration of SD ferrimagnetic grains
χ_{ARM}/χ	susceptibility ratio [-]	grain size
ARM/SIRM	magnetisation ratio [-]	grain size, concentration of SD remanence carrying particles
SIRM/χ	ratio of saturation IRM to susceptibility [10^3Am^{-1}]	concentration, grain size, mineralogy
χ/M_s	ratio of susceptibility to saturation magnetisation [mA^{-1}]	grain size

Table 1: A list of magnetic parameters that are commonly used in environmental magnetism to classify mineralogy, grain size and concentration of magnetic minerals.

2.1 Magnetic susceptibility (χ)

Magnetic susceptibility usually reflects the content of magnetic minerals of the sample, a high susceptibility indicates a high content of magnetic minerals (Thompson et al., 1980; Maher, 1986; Verosub and Roberts, 1995). It is a useful tool to quickly identify ferro- and ferrimagnetic minerals (which have a high susceptibility, see table 2). Since the susceptibility of diamagnetic minerals is very small and negative, and that of paramagnetic minerals is also small (but positive), they usually represent a very small fraction of the sample susceptibility. The susceptibility signal will thus be dominated by the ferri- and ferromagnetic minerals provided their concentration is large enough ($> 1 \text{ wt}\%$) (Mullins, 1977). However, there are certain settings, for example marine limestones and marls, in which the concentration of the ferri- and ferromagnetic minerals are very low. In these materials as much as $\sim 50\%$ up to even $\sim 90\%$ of the susceptibility signal originates from diamagnetic or paramagnetic minerals. The susceptibility not only reflects concentration of magnetic minerals, but can also express grain size. Superparamagnetic (SP) grains with a grain size close to the single-domain (SD) boundary have extremely high susceptibility (up to ~ 20

Mineral	Formula	Magnetism	χ [10^{-8} m ³ kg ⁻¹]
magnetite	Fe ₃ O ₄	ferrimagnetic	57000
maghemite	γ -Fe ₂ O ₃	ferrimagnetic	57000
hematite	α -Fe ₂ O ₃	antiferromagnetic	60-600
goethite	α -FeOOH	antiferromagnetic	70
pyrite	FeS ₂	paramagnetic	30
quartz	SiO ₂	diamagnetic	-0.6
feldspar	(Ca,K,Na,Al)Silicate	diamagnetic	-0.5
clay minerals	e.g. illite, kaolinite	dia-/paramagnetic	-2 to 100
calcium carbonate	CaCO ₃	diamagnetic	-0.5

Table 2: Formula, magnetic class and typical susceptibility values (at room temperature) for a number of common minerals.

times the value of the SD grains of the same mineral) (Mullins, 1977; King et al., 1982; Maher, 1988; Banerjee et al., 1993; Sun et al., 1995; Verosub and Roberts, 1995). This makes susceptibility a good indicator for the presence of (large) SP grains.

2.2 Frequency dependence of susceptibility (χ_{fd})

Since magnetic susceptibility is dependent on concentration as well as grain size, low concentrations of SP grains as well as high concentrations of SD grains can result in similar susceptibility signals. To determine whether the high susceptibility signal results from either concentration or grain size, we can use a susceptibility ratio known as frequency dependence of susceptibility. Magnetic susceptibility decreases with increasing operating frequency of the analytical equipment, but the small magnetic grains near the SP/SD boundary are much more sensitive to this increase in frequency than larger grains (Thompson and Oldfield, 1986; Verosub and Roberts, 1995). This means that these grains have an SP-like susceptibility signal at the low measurement frequency, but they have SD-like susceptibility at the high measurement frequency.

The frequency dependence of susceptibility can therefore be used to determine the contribution of SP material to the signal. The frequency dependence can be calculated with the following equation:

$$\chi_{fd} = \frac{\chi_{LF} - \chi_{HF}}{\chi_{HF}} \cdot 100\% \quad \text{Here, } \chi_{LF} \text{ is}$$

susceptibility measured at low frequency (usually ~ 460 Hz) and χ_{HF} is the susceptibility measured at high frequency (usually ~ 4600 Hz). It is important to know the measurement frequencies when comparing results of different studies. If the frequencies are not similar, the χ_{fd} values cannot be readily compared. The maximum value that can be achieved for χ_{fd} is $\sim 15\%$ (although empirical evidence suggests a maximum χ_{fd} of $\sim 30\%$ (Worm, 1998)), therefore this parameter is not a quantitative but only a qualitative measure for SP grains. For the SP/SD grain sizes, χ_{fd} lies in the range of 7-15%, while for MD grains χ_{fd} is $< 5-6\%$ (as measured in natural samples, e.g. Maher, 1988; Fine et al., 1993a).

2.3 Hysteresis parameters

All magnetic materials that can carry a remanent magnetic signal display hysteresis when subjected to a cyclic magnetic field. Hysteresis is a term for the lagging behind of the magnetisation of a material with the external inducing magnetic field. Hysteresis is most evident from a plot of the change in magnetisation in a cyclic field; this yields an open loop. The shape of a hysteresis loop indicates the dominant grain size or the presence of a mineral mixture (figure 1). Three mineral and grain-size specific components can be retrieved from such a plot: the saturation magnetisation (M_s), the remanent saturation magnetisation (M_{rs}) and the coercive force (B_c). M_s is a mineral specific parameter and represents the maximum magnetic moment (measured in a magnetic field) that can be induced in a magnetic material. B_c is indicative of mineralogy (it is high for hematite and goethite, but low for magnetite) as well as grain size (it is higher for SD and PSD particles than for MD particles of the same mineral) (Eyre and Shaw, 1994; Dunlop and Özdemir, 1997; Worm, 1998). Together with the remanent coercive force (B_{cr}), (derived from a backfield demagnetisation curve, see figure 2) these four parameters can be used to plot a ‘Day’ diagram of M_{rs}/M_s vs. B_{cr}/B_c (for an example see Chapter 3, figure 2). For the SD and PSD fields the boundaries are based on Stoner–Wohlfarth theory for uniaxial anisotropy (Stoner and Wohlfarth, 1948), while the boundary between PSD and MD fields is more or less arbitrary. In addition, Day et al. (1977) proposed boundaries that were experimentally determined for (titano)magnetite. Therefore, if the samples contain only magnetite or titanomagnetite, we can derive the dominant grain-size of these minerals from the Day plot. A Day plot of mixed grain sizes and/or mixed mineral types should be interpreted with caution.

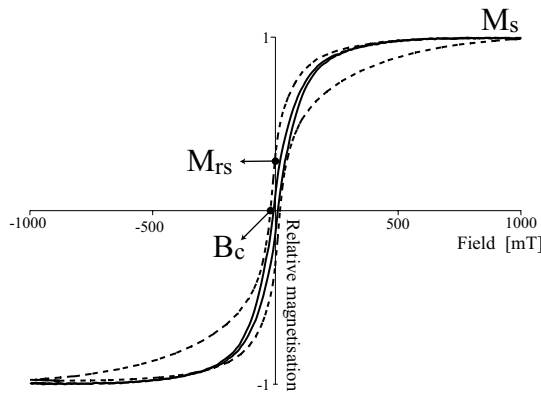


Figure 1: Examples of hysteresis loops, the solid line is an example of a coarse-grained monomineralic spinel-type sample (courtesy of Pauline Kruiver), and the dashed line represents a wasp-waisted loop (Tauxe et al., 1996) (courtesy of Sébastien Bailly). Wasp-waisted is the term for a loop that is narrow at low field values and more open or wider towards the maximum magnetisation before it closes at high field values. In the example the wasp-waistedness is caused by a mixture of magnetite and hematite. A mixture of SP and SD magnetite can also yield wasp-waisted hysteresis loops but in those cases the wasp-waistedness is restricted to much lower field values. The vertical axis shows the magnetisation normalised to the maximum magnetisation. The horizontal axis shows the field value in milli Tesla (mT). At a specific field strength the magnetisation will not increase anymore, this is the saturation magnetisation (M_s). The remanent saturation magnetisation (M_{rs}) is the maximum value for magnetisation, measured in a zero field, that remains in a sample after saturation. The field at which the magnetisation is equal to zero is called the coercive force (B_c).

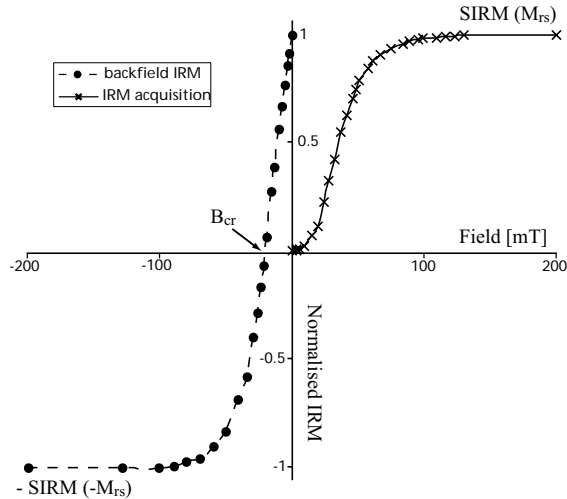


Figure 2: Example of an isothermal remanent magnetisation (IRM) acquisition curve, and a backfield demagnetisation curve. The IRM acquisition is achieved by submitting the sample to increasing field strengths and subsequently measuring the acquired remanent magnetisation. At a specific field strength the magnetisation will not increase anymore, this is the saturation isothermal remanent magnetisation (SIRM). The backfield curve is derived from the samples that have acquired an SIRM in one direction, and have subsequently been submitted to increasingly stronger magnetic field in the opposite direction. In this way the SIRM is slowly broken down, the field at which the remanent magnetisation is zero is called the remanent coercive force (B_{cr}). A low B_{cr} indicates that the minerals are easily magnetised: they have a soft magnetic component. A high B_{cr} indicates that the minerals have a hard magnetic component: they are not easily (de)magnetised.

2.4 Saturation remanent magnetisation (M_{rs} or SIRM) and the S-ratio

SIRM is the maximum remanent magnetisation that can be induced in a sample, it is an expression of the concentration and the domain state of remanence-carrying minerals (Maher, 1986; Eyre and Shaw, 1994; Hunt et al., 1995a). The grain size of a magnetic mineral will also influence the remanent magnetisation. SD particles have the strongest SIRM, while that of MD size particles is considerably weaker (Maher, 1986; Thompson and Oldfield, 1986). The domain state can be inferred from the M_{rs}/M_s ratio, when there is one dominant magnetic mineral present.

Ferrimagnetic minerals are more easily magnetised than antiferromagnetic minerals, therefore the former will reach their SIRM at lower field values than the latter (see also table 3). The ratio of IRM at different field values is often used to estimate the contribution of these two types of magnetic minerals. A widely used ratio is the S-value, which ranges between -1 and $+1$;

$$S_{-0.3T} = \frac{IRM_{-0.3T}}{IRM_{1T}} \quad (17)$$

When the ratio is close to one, the dominant magnetic minerals are ferrimagnetic, and it will decrease with increasing contribution of antiferromagnetic minerals (Maher, 1986; Verosub and Roberts, 1995). Bloemendal et al. (1992) introduced an alternative ratio that is more commonly used, which ranges between 0 and $+1$ and somewhat simplifies the interpretation;

Mineral	Saturation field [mT]
magnetite & maghemite	~ 100 mT (MD) 150 - 300 mT (SD) ^{1,2}
hematite	400 - 500 mT (MD) 800 - 2500 mT (SD) ^{2,3}
goethite	>3000 mT ⁴

¹Thompson & Oldfield, 1986

²Opdyke & Channell, 1996

³Walden et al., 1999

⁴Dekkers, 1989

Table 3: Typical values for the field at which SIRM is achieved, for several common magnetic minerals (adapted from: Thompson and Oldfield, 1986; Dekkers, 1989; Opdyke and Channell, 1996; Walden et al., 1999).

$$S_{-0.3T} = \frac{(-IRM_{-0.3T} / SIRM) + 1}{2} \tag{18.}$$

The ratio will be close to zero for the hard magnetic minerals such as hematite and goethite, and it will approach 1 for soft magnetic minerals such as magnetite. Some caution is advised when using these ratios; when the sample consists of a mixture of two or more mineral types or grain sizes the ratios can give ambiguous values (Kruiver and Passier).

2.5 Thermomagnetic behaviour

Magnetisation and susceptibility are examples of parameters that are subject to change on heating or cooling. Their thermomagnetic behaviour is in principle mineral specific, although solid solution (isomorphous substitutions) can complicate the interpretation of thermomagnetic curves. Thermomagnetic curves yield information on the Curie temperature (T_C), the temperature above which a magnetic mineral loses its collective magnetisation and becomes a paramagnetic mineral. Therefore, a plot of the changes in magnetisation with temperature can be used to determine mineralogy (Banerjee et al., 1993; Liu et al., 1995; Liu et al., 1999) (figure 3a). Diamagnetic or paramagnetic minerals with isolated magnetic moments only, do not show a Curie temperature. The induced magnetisation in diamagnetic particles is independent of temperature. Paramagnetic particles follow Curie’s law: the induced magnetisation is proportional to the inverse of the (absolute) temperature.

A Curie curve is usually measured in air, but the presence of oxygen can cause (partial or complete) oxidation of the sample during heating. This oxidation changes the composition of the magnetic mineral phase(s) and can lead to a false determination of T_C (see figure 3b). The change in magnetisation at a specific temperature then reflects a conversion to a different magnetic mineral, instead of representing a true Curie point. In a true Curie point, the magnetisation should reappear on cooling when the collective magnetisation sets in again. To verify the thermomagnetic curve, it is advised to perform the analysis in several incremental heating steps. If the magnetisation curve remains reversible after heating to a specific

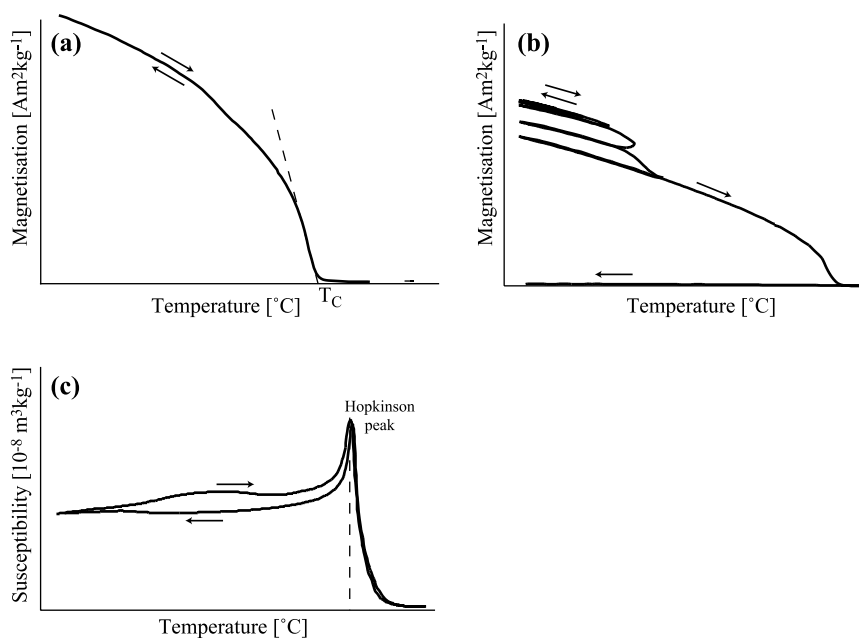


Figure 3: Examples of thermomagnetic curves. The values of the temperature and magnetisation axes are arbitrary. Panel (a) shows a typical Curie curve for magnetite, with a T_C of $\sim 580^\circ\text{C}$. Panel (b) shows a Curie curve of a sample that is chemically altered before reaching its true T_C . The heating is performed in segments, when the magnetisation behaviour over the temperature segment is irreversible, conversion of the magnetic mineral must have taken place. Panel (c) shows the behaviour of the initial susceptibility as a function of temperature in an Ar atmosphere. Just before the fast drop in susceptibility around 580°C , a distinct peak is observed. This peak is typical of SD grains where susceptibility is proportional to M_s/B_c . The peak is caused by a faster decrease in B_c during heating than the drop in M_s , and is known as the Hopkinson peak.

temperature, no chemical alteration has taken place. If the path is irreversible after heating, some chemical alteration must have occurred in that temperature interval. For hematite and goethite an irreversible path doesn't always indicate chemical or structural changes, because the magnetic domains in these minerals increasingly align themselves to the induced field and thus can give a higher magnetisation after heating (see also de Boer and Dekkers, 1998).

The behaviour of susceptibility at different temperatures is mineral-specific, but also depends on grain size and mineralogy. Like the Curie point (T_C) for magnetisation, the susceptibility has a mineral-specific temperature (referred to as the Hopkinson peak) after which it will decrease rapidly when the temperature is increased (figure 3c). The exact shape of the Hopkinson peak depends on the grain-size distribution, while the temperature of the peak depends on mineralogy (Thompson and Oldfield, 1986; Eyre and Shaw, 1994). Thermal analysis of the low-field susceptibility as well as thermomagnetic analysis can be performed in Ar or N_2 atmosphere, this strongly reduces or even prevents oxidation of the sample (conversion of magnetic minerals) and gives a true thermal signal.

The magnetisation can also be measured at low temperatures, without the disturbing influence of chemical alterations. At temperatures below 0°C , there are some mineral-specific changes in magnetic

properties, referred to as magnetic transitions. For example, while warming from low temperature back to room temperature, 'ideal' magnetite grains lose part of their magnetisation at the Verwey transition ($T_V \sim -150^\circ\text{C}$ or $\sim 120\text{K}$) (Verwey et al., 1947). The value for the Verwey temperature varies: when the magnetite is isomorphously substituted, or (partly) oxidised, T_V usually is lower than -150°C . Well-crystalline hematite also has a magnetic transition, known as the Morin transition, which occurs at $T_M \sim -10^\circ\text{C}$ ($\sim 263\text{K}$) in pure hematite (Morin, 1950). Below T_M the magnetisation of hematite drops considerably, caused by a change in the direction of the 'easy' magnetisation from within the basal plane to the hexagonal c-axis (Dunlop and Özdemir, 1997). At this point the canted antiferromagnetic structure of hematite gives way to a perfect antiferromagnetic structure with a much lower magnetisation.

Another important low-temperature magnetic phenomenon takes place in SP particles. Analogous to paramagnetic particles, the magnetisation of SP grains follows Curie's law for paramagnetic particles: it is inversely related to temperature (Dunlop and Özdemir, 1997). SP particles can carry a remanence at low temperatures (depending on their actual volume), while their remanent magnetisation is zero at room temperature. A comparison of IRM induced at room temperature and at -196°C (77 K) gives an indication of the presence of SP grains (Banerjee et al., 1993; Liu et al., 1995).

2.6 Anhyseretic remanent magnetisation (ARM)

The ARM is often considered as the closest laboratory analogue to the natural remanent magnetisation (NRM) of a sample. ARM is the remanent magnetisation acquired by subjecting a sample to a slowly decreasing alternating field in the presence of a small direct or steady magnetic field referred to as the DC bias field: typically $50\text{--}100\ \mu\text{T}$. For magnetite, ARM is proportional to the DC bias field up to $\sim 80\ \mu\text{T}$. The ARM is highly sensitive to the presence of SD grains of strongly ferrimagnetic minerals (in particular magnetite and maghemite), and increases with increasing concentration of these minerals (Oldfield, 1991; Verosub and Roberts, 1995). Division of the ARM (expressed per volume: $[\text{Am}^{-1}]$) by the DC bias field $[\text{Am}^{-1}]$ yields a dimensionless parameter that is called the susceptibility of ARM (χ_{ARM}). This parameter is similar to the initial susceptibility and a plot of χ_{ARM} versus χ_{in} may be used for granulometric purposes (King et al., 1982). The χ_{ARM}/χ ratio is a useful parameter for assessing the amount of fine versus coarse magnetic grains when magnetite is the dominant magnetic mineral (Verosub and Roberts, 1995). In this case, the ratio will vary inversely with magnetic grain size. However, the interpretation of this ratio can be complicated when the samples contain significant amounts of SP or paramagnetic material (Opdyke and Channell, 1996).

2.7 Ratios of remanence and susceptibility

As mentioned before, the mineral-magnetic parameters may depend on magnetic mineralogy, concentration or grain size. Magnetic mineralogy can be inferred from thermomagnetic analysis and also from thermal demagnetisation. At low magnetic mineral concentration (when magnetic interaction is not important), the rule in sediments and soils, coercivity parameters are concentration-independent; they express mineralogy and grain size. M_{rs} and susceptibility are concentration-dependent, but, these parameters also reflect mineralogy or grain-size differences. When a single magnetic mineral dominates in the samples, division of two concentration-dependent parameters yields a ratio that is independent of concentration. Then, grain-size trends may be interpreted.

Common ratios used for the determination of magnetic grain size or concentration are listed in table 1

(they are: ARM/SIRM, SIRM/ χ , χ_{ARM}/χ and χ/M_s). The ARM/SIRM ratio is highest for SD ferrimagnetic particles and can be used to identify their presence (Sugiura, 1979; Zhou et al., 1990; Hunt et al., 1995a; Hanesch and Petersen, 1999). Comparison of the ARM/SIRM ratio between studies should be treated with caution: ARM values depend on the applied DC-bias field and on the maximum alternating field (if saturation is not achieved), variations in the ARM/SIRM ratios may therefore be caused by differences in experimental settings rather than by differences in grain size.

The ratio of SIRM/ χ can also be used to monitor grain size or mineralogical changes. The ratio is high for hematite (~ 200 kA/m) and low for magnetite ($\sim 1.5\text{--}50$ kA/m), furthermore the presence of SP or paramagnetic grains will lower this ratio (Thompson et al., 1980; Maher, 1986; Verosub and Roberts, 1995). In natural settings the ratio usually remains below 30 kA/m. For monomineralic assemblages (without SP grains), the ratio is inversely correlated to grain size, and will decrease with increasing grain size (Opdyke and Channell, 1996).

Finally the χ/M_s ratio reveals the relative changes in susceptibility caused by SP grains. Since M_s is independent of grain size, and susceptibility is high in SP grains and much lower in SD-MD grains, the peaks in this ratio represent SP contributions (Banerjee et al., 1993; Hunt et al., 1995a).

3. Magnetic properties of loess-palaeosol sequences and their relation to climate

The composition of magnetic minerals in a natural setting will depend on a variety of factors, including source material, weathering, transport, humidity, temperature, and acidity. The type and size of mineral that survives or forms in a certain regime is therefore diagnostic for a specific environment. By analysing the mineralogy, concentration and grain size of the magnetic particles in natural samples we may be able to derive the environmental setting of these samples. In this thesis, the investigations have been restricted to loess and palaeosol samples, and the next sections describe in some more detail how the magnetic signal of a depositional or soil-forming setting can be related to palaeoclimate.

3.1 Magnetic susceptibility in modern soils

Le Borgne discovered that the magnetic susceptibility throughout a soil profile is not constant (Le Borgne, 1955). He also postulated that the iron content of soils often increases with increased pedogenesis. His conclusion therefore was, that the enhanced susceptibility and iron content of topsoil was related to the neoformation of an iron oxide. He argued that the iron oxide in question was most likely maghemite, and this was later confirmed by Mullins (1977). Le Borgne proposed a fermentation mechanism in which maghemite could be formed during pedogenesis (Table 4). Later studies, however, indicated that the magnetic enhancement can also be caused by the in situ formation of microcrystalline magnetite (Fine et al., 1989; Maher and Hounslow, 1999; Shenggao, 2000), or a combination of both magnetite and maghemite (Maher, 1998).

During the development of a soil profile, the magnetic enhancement usually occurs only in the topsoil (A-horizon or eluvial horizon). There are three ways in which the magnetic susceptibility can be enhanced: (1) by preferential accumulation of lithogenic minerals, (2) by formation of new pedogenic minerals, or (3) by deposition of airborne particles in polluted areas (Mullins, 1977; Fine and Singer, 1989; Fine et al., 1992;

proces	product
low T oxidation of magnetite (150-250°C) ¹	maghemite
burning: reduction of hematite or goethite to magnetite and subsequent oxidation to maghemite ^{1,2}	magnetite/maghemite
dehydration of lepidocrocite (275-410°C) common in mottles of gley soils ^{1,2}	maghemite
fermentation: reduction/oxidation of poorly crystalline iron oxides ^{1,2,3}	magnetite/maghemite
biogenic contribution ²	magnetite
atmospheric fall-out ²	hematite/magnetite

¹ Mullins 1977

² Maher 1998

³ Le Borgne 1955

Table 4: Processes responsible for the production of pedogenic magnetic minerals, as proposed by several authors (adapted from: Le Borgne, 1955; Mullins, 1977; Maher, 1998).

Verosub and Roberts, 1995; Shenggao, 2000). In the topsoil authigenic formation of pedogenic iron oxides is most favoured because the weathering of the lithogenic ferrimagnetic minerals and, more importantly, the weathering of iron-bearing silicates is more intensive (Fine and Singer, 1989; Fine et al., 1992; Cornell and Schwertmann, 1996).

Mineral	Major soils
Goethite (α -FeOOH)	Aerobic and anaerobic soils of all regions.
Lepidocrocite (γ -FeOOH)	Anaerobic, clayey, non-calcareous soils of cooler and temperate regions.
Ferrihydrite ($\text{Fe}_5\text{HO}_8 \cdot 4\text{H}_2\text{O}$)	Groundwater and stagnant water soils (gleys and pseudogleys) and podsoles of temperate and cool regions. Paddy soils.
Hematite (α -Fe ₂ O ₃)	Aerobic soils of subtropical, mediterranean and humid to subhumid tropical regions (lateritic and plinthitic soils, red mediterranean soils, oxisols, ultisols). Usually absent in soils of temperate and cool regions.
Maghemite (γ -Fe ₂ O ₃)	Aerobic soils of the tropics and subtropics.
Magnetite (Fe ₃ O ₄)	Can form both aerobically and anaerobically, therefore no limits on soil type.

Table 5: General summary of the occurrence of pedogenic iron oxides in various soils (adapted from Cornell and Schwertmann, 1996).

Specific environmental settings favour pedogenic formation of equally specific iron oxides. The soil magnetic minerals usually have very fine grain size and the crystallinity varies with the maturity of soils. Goethite and magnetite form in anaerobic as well as aerobic environments, and are common minerals in almost all soil types. In subtropical and tropical climates, maghemite and hematite are common minerals, while in cooler and dryer climates lepidocrocite and ferrihydrite are more common (Table 5). Well drained, intermittently wet and dry soils with a reasonable buffer capacity and a substrate source of Fe, are ideally suited for the formation of ferrimagnetic minerals, and the enhancement of magnetic susceptibility is strongest in these environments (Singer and Fine, 1989; Maher, 1998). Conversely, some environments inhibit abundant pedogenic formation of ferrimagnetic minerals. This is the case in excessively arid soils, perennially wet soils, or acid soils (Singer and Fine, 1989; Maher, 1998). In warm and humid climates the formation of SP magnetic minerals is dominant (Banerjee et al., 1993).

In addition to climate, the bedrock also determines whether or not enhancement of magnetic susceptibility occurs. In soils developed on sedimentary source rocks, the upper horizon usually shows magnetic enhancement caused by pedogenic formation of SP/SD sized ferrimagnetic minerals. Yet, when the source material has a low initial iron content (and therefore a low magnetic susceptibility), the pedogenic formation of ferrimagnetic material is limited and the profile will exhibit no magnetic enhancement (Shengqao, 2000).

3.2 Chinese loess-palaeosol sequences and the link with climate

The Chinese loess plateau is a 500,000 km² area of mostly Quaternary loess deposits in the North of China (Figure 4). The loess deposits are very thick (between 150 and 300 m) and they constitute one of the most complete and long-lasting (~ 2.6 Ma) terrestrial records of past climates (Zhou et al., 1990; Fine et al., 1993a; Heller et al., 1993; Verosub et al., 1993; Gallet et al., 1998; Kemp, 1999). The yellow or cream-coloured loess beds are periodically alternated by palaeosol beds of red or brown colour.



Figure 4: Distribution of the loess-palaeosol sequences in the world (indicated in grey). The Chinese loess plateau is indicated in black.

The first comprehensive study of variation in magnetic susceptibility of the loess–palaeosol sequences in China was published by Heller and Liu (1984). They showed that the alternations in maximum and minimum magnetic susceptibility match those of the warm and cold oxygen isotope stages of the marine sediment record. In China, high susceptibility values are mostly confined to the palaeosols, while low susceptibilities are mainly found in the loess deposits. Because the alterations of loess and palaeosol horizons are an expression of Milankovitch cycles, the magnetic susceptibility variations also reflect Milankovitch cycles (Hovan et al., 1989; Shackleton et al., 1991; Bloemendal et al., 1995; Fang et al., 1999a; Fang et al., 1999c; Heslop et al., 2000). Furthermore, the frequency dependence of magnetic susceptibility (χ_{fd}) shows variations within the palaeosol layers, which are interpreted to represent finer-scale variations in temperature and humidity within a single interglacial or interstadial period (Heller and Wang, 1991; Banerjee et al., 1993).

Throughout the profile, magnetite, maghemite, and hematite occur as the most important magnetic minerals. The concentration and grain-size of these three minerals vary throughout the profile, causing the differences in magnetic signal. The dominant carriers of the magnetic signal are the ferrimagnetic minerals (magnetite and maghemite), which are enriched in the palaeosol layers. The grain size of the magnetic minerals ranges from very fine-grained to approximately silt sized (SP to MD), but is predominantly SP in the palaeosols (Zhou et al., 1990; Maher and Thompson, 1991; Liu et al., 1992; Maher and Thompson, 1992; Heller et al., 1993; Liu et al., 1995; Vandenberghe et al., 1997; Fang et al., 1999c). The SP ferrimagnetic minerals in the palaeosols were probably formed during pedogenesis, although there is some debate about this issue (see section 3.3), while the SD/PSD/MD ferrimagnetic grains have a lithogenic origin (Heller and Wang, 1991; Maher and Thompson, 1991; Maher and Thompson, 1992; Banerjee et al., 1993; Evans and Heller, 1994; Liu et al., 1995; Liu et al., 1999; Vidic et al., 2000).

Originally it was thought that the pedogenic enhancement of magnetic material originates from a change in input of material during the interstadials and interglacials. The rationale was that in these periods the constant ‘rain’ of uniformly sized magnetite from the troposphere was emphasised because of a reduced input of less-magnetic wind-borne loess (Kukla et al., 1988). It soon became clear, however, that the warmer and more humid climate of the interglacial intervals intensified weathering and caused alteration of non-magnetic iron-bearing silicate minerals to strongly magnetic ultrafine ferrimagnetic grains (Singer and Fine, 1989; Zhou et al., 1990; Maher and Thompson, 1991; Hus and Han, 1992; Maher and Thompson, 1992; Banerjee et al., 1993). For a while, it was thought that the pedogenic enhancement was caused by fine-grained maghemite (Maher and Thompson, 1991; Liu et al., 1992; Evans and Heller, 1994; Eyre and Shaw, 1994; Sun et al., 1995), but this idea has now been challenged. New evidence indicates that it could also be caused by fine-grained pedogenic magnetite (Liu et al., 1994; Maher et al., 1994; Sun et al., 1995; Fang et al., 1999a; Liu et al., 1999). To this day, the mineralogy of the carriers of the pedogenic magnetic signal is hotly debated.

Clearly there is a link between magnetic signal and climate, but the intricacies of this link are still unknown. Currently, there are several possible mechanisms under investigation. The magnetic enhancement of the Chinese palaeosols is positively correlated to increased temperature and humidity (interglacial), therefore the idea was put forward to derive palaeoprecipitation values for the periods of palaeosol formation. Several approaches were proposed: (1) quantification of palaeoprecipitation by the concentration of SP ferrimagnetic minerals in the soil (Hunt et al., 1995a), (2) correlation of present-day precipitation with SP ferrimagnetic concentration in modern soils and extrapolating to the palaeosols

(Maher et al., 1994; Liu et al., 1995), (3) linking magnetic susceptibility directly to palaeoprecipitation (Meng et al., 1997; Fang et al., 1999c).

The climate in the Chinese loess plateau is mainly controlled by the Asian monsoonal circulation system (An et al., 1991; Xiao et al., 1995; Fang et al., 1999b). During winters, a combination of several atmospheric circulation patterns (the East Asian winter monsoon, the westerlies and the Tibetan winter monsoon) controls the input of aeolian particles from the Tibetan plateau. The western part of the Chinese loess plateau is mostly dominated by this system. During summers, a change in atmospheric circulation enhances the influence of the summer monsoon that brings in hot and humid air from the Pacific and Indian ocean, and increases pedogenesis. The influence of the summer monsoon is strongest in the central part of the loess plateau. The loess-palaeosol sequences have been linked to the change in monsoonal system, and it is generally believed that the palaeosol horizons are linked to periods when the summer monsoon was dominant, while the loess horizons represent periods of time when the winter monsoon dominated in the Chinese loess plateau (Fang et al., 1999c; Liu et al., 1999; Ding et al., 2001).

3.3 *Controversial issues*

Despite the large number of studies on the Chinese loess-palaeosol sequences, there remain a few controversial points concerning the interpretation of the magnetic signal. They can be divided into four categories:

(1) **The process of pedogenic formation of ferrimagnetic minerals**

There is an ongoing debate about the pedogenic processes that are responsible for the increase in fine-grained ferrimagnetic minerals in the palaeosols. Historically, there were three schools of thought (Oldfield, 1992; Sun et al., 1995). The first hypothesis involves the depositional dilution of a constant flux of tropospheric ultrafine magnetic particles during glacial periods by a reduced input of wind-borne loess particles of low magnetic susceptibility, which caused a fictitious enhancement of the magnetic susceptibility signal in the palaeosol (e.g. Kukla et al., 1988). The second hypothesis concerned the post-depositional pedogenic processes during interglacial periods, such as fermentation, formation by magnetotactic bacteria and weathering of Fe-bearing silicates (e.g. Zhou et al., 1990). Finally, the third hypothesis involves the physical enrichment of magnetic minerals in soils as a result of decalcification and soil compaction (e.g. Heller and Liu, 1984).

The sequences found in China, Central Europe and the USA all show an enhanced magnetic susceptibility signal in the palaeosol layers caused by an increase in the concentration of ferrimagnetic minerals. Conversely, in other areas such as Siberia, Alaska and Argentina, the palaeosol layers show a minimum susceptibility caused by a lack of neoformation of ferrimagnetic minerals in the palaeosols (Maher, 1998). These differences in magnetic enhancement have been related to variations in the pedogenic environment. A combination of dilution during interglacial stages and waterlogging of the soils (which prevents formation of new ferrimagnetic minerals) has been suggested to explain the low signal in the palaeosols (Liu et al., 1999).

A suite of physical, chemical and biological processes is involved in the enhancement of the magnetic signal. For different sites, or even different periods at the same site, any single hypothesis may not satisfactorily account for all the variations observed (Sun and Liu, 2000).

(2) The differentiation between local, regional and global signals

Although the magnetic record in the Chinese loess plateau is a proxy for the global climate as controlled by Milankovitch cycles, its expression is also controlled by regional and local climate. For example, locally-controlled signals such as the distance from the loess source area or the presence of other source areas determine the grain-size input for the loess (and thus the source material for the palaeosols). In some cases, the principal carrier of the magnetic signal in the palaeosols seems not to be the SD pedogenic minerals, but rather coarse-grained lithogenic magnetic minerals derived from local sources.

Regional signals such as the strength of the Asian monsoon systems also influence the soil formation (Banerjee et al., 1993). The climate in the Chinese loess is governed by two monsoonal systems: the cool and dry winter monsoon originating in the Tibetan plateau, and the warm and moist summer monsoon originating in the Pacific and Indian oceans. The winter monsoon is primarily responsible for the influx of loess from the Tibetan plateau, and its effects are strongest in the western loess plateau, which is closest to the Tibetan plateau. The summer monsoon is primarily responsible for the weathering of the loess and the formation of palaeosols, and its effects are strongest in the central loess plateau. Here, a second source area (the Gobi desert) also brings loess into the plateau.

The consequence of these mechanisms is that the magnetic signal in these loess-palaeosol sequences is not a straightforward expression of Milankovitch cycles, and it is more locally or regionally dominated than was originally thought (Sun and Liu, 2000). The distinction between orbital forcing and local or regional mechanisms has been difficult because the correlation of the loess-sequences to the orbital cycles was not straightforward. This was mainly caused by the fact that, prior to 1999, it was not realised that the position of the Bruhnes/Matuyama boundary in these sequences could be ambiguous. When it was discovered that the lock-in depths of geomagnetic reversals in these sequences was larger than expected (Zhou and Shackleton, 1999), a new tuning of the proxy-records to the astronomical time-scale for this period was possible (Heslop et al., 2000) (see also subsection (4)).

(3) The differentiation between magnetite and maghemite

Although rock-magnetic analysis provides detailed information about the composition of the magnetic fraction, for the ferrimagnetic spinel-type grains the results can be very similar and additional analyses are required to determine the amount and mineralogy of these grains. Differentiation between these minerals is of vital importance to the understanding of the composition of both loess and palaeosols. It would help in the determination of the mechanism(s) of neoformation of pedogenic magnetic minerals and thus help in understanding the environmental processes behind the palaeosol formation. Furthermore, it would improve the source-analysis for the loess horizons and aid in the detection of syndepositional alterations of magnetic minerals in the loess.

Usually, the concentrations of magnetite and/or maghemite are too low to measure them with X-ray diffraction or Mössbauer spectroscopy. These minerals have very similar physical properties and are difficult to distinguish from one another by field-dependent rock-magnetic techniques (Maher, 1988; Heller et al., 1991; Banerjee et al., 1993; Liu et al., 1999). Furthermore, it is still unclear whether the enhanced magnetic signal in the palaeosols arises from magnetite or maghemite (or possibly a combination of both), and whether the signal in the loess has been altered by oxidation after deposition. New rock-magnetic techniques have been developed recently: first-order-reversal-curve (FORC) analysis (Pike et al., 1999),

and improved isothermal remanent magnetisation (IRM) component analysis (Heslop et al., 2001; Kruijer et al., 2001). These techniques may aid in the distinction between these minerals, however, they are still based on the (rather similar) magnetic characteristics.

(4) Diagenetic factors

Since (in China), loess deposition continued during pedogenesis in interglacials and interstadials, loess units are subjected to weak soil processes syndepositionally, and will therefore retain at least some pedogenic signal (Kemp, 1999; Liu et al., 1999). The palaeosol horizons represent periods of time when pedogenic processes have dominated over loess deposition. Furthermore, it has been shown that the recording of the natural remanent magnetisation (NRM) in these deposits has a downward offset. For instance, the Matuyama/Brunhes boundary is found at variable levels in these sequences. The true boundary is located in soil horizon S7, but the change in direction of the NRM is usually found in the underlying L8 loess horizon, and it has also been detected in the even older S8 palaeosol. Zhou and Shackleton showed that the NRM in the loess was locked-in at a (substantial) depth below the surface (up to several meters), corresponding to a time lag of 10^3 - 10^4 years (Zhou and Shackleton, 1999). This demonstrates that the carriers of the magnetic signal in the loess have been affected by minor pedogenesis prior to lock-in of the magnetic signal. Therefore the magnetic signal is not necessarily carried by the 'true' lithogenic particles in the loess. The interpretation of the NRM signal in the loess-palaeosol sequences must be performed with caution; the correlation of magnetic enhancement signals with orbital forcing is influenced by the offset in lock-in of the NRM signal.

4. Chemical extraction methods on natural samples

The controversial issues that have risen during the investigation of the relationship between magnetic enhancement and global climate indicate that the results of rock-magnetic studies alone will not always suffice, and that other methods are required to derive a more complete interpretation of the signal. The rock-magnetic results can be complemented by other methods such as selective chemical extraction of magnetic particles.

4.1 Citrate-Bicarbonate-Dithionite (CBD) method

In natural samples, the iron oxides often form aggregates with clay, which inhibits a good analysis of the clay mineralogy by X-ray diffraction. For this purpose, Mehra and Jackson introduced the CBD method (Mehra and Jackson, 1960), which disaggregates these assemblages and dissolves the iron oxides. The first studies using CBD on natural soils indicated that it easily dissolved both crystalline and amorphous iron (McKeague and Day, 1965; McKeague et al., 1971; Bigham et al., 1978; Torrent et al., 1980). Further investigations revealed that the method had a preference for particular minerals and grain-size ranges. Goethite and hematite were dissolved preferentially over magnetite, but the fine-grained goethite and hematite dissolved completely, whereas coarser grains did not dissolve completely (McKeague et al., 1971; Walker, 1983). This preference for the complete dissolution of fine-grained hematite was not found in other studies, where it was only partly removed from the soil (Ericsson et al., 1984).

In later studies, the CBD method was used to make a distinction between lithogenic and pedogenic minerals. Fine and co-workers (1989; 1989) concluded that the lithogenic magnetite in their samples was completely resistant to CBD, while the pedogenic maghemite was dissolved. Their measurements of the magnetic susceptibility showed that the magnetically enhanced signal in the soil was lost after CBD extraction. This was attributed to the preferential loss of pedogenic minerals during the extraction. Further studies confirmed this result, and it appeared that the frequency dependence of susceptibility also decreased after extraction, confirming again the preferential dissolution of the very fine-grained (SP/SD) pedogenic minerals (Fine et al., 1989; Fine et al., 1992; Singer et al., 1992; Fine et al., 1993a; Verosub et al., 1993; Shenggao, 2000).

On the basis of the CBD results, the magnetic components in the Chinese loess-palaeosol sequence have been subdivided into three groups. One is a pedogenic component the other a non-CBD soluble lithogenic component, and the third is a weathered lithogenic component (oxidised rims on lithogenic magnetite) (Verosub et al., 1993). Other studies with soils and loess, however, have provided results that contradict the previous interpretations. In a study of Argentinean soils, the CBD method dissolved almost all iron oxides, without making a distinction in mineralogy or grain size (Venegas et al., 1994). Sun et al. (1995) performed extractions in which not only fine-grained maghemite had been dissolved from Chinese loess-palaeosol samples, but also coarse-grained maghemite and fine-grained magnetite had been removed. Maher found that in modern soils, the fraction dissolved by CBD exhibits no correlation with the magnetic signal (Maher, 1998). The method was therefore assumed to attack all maghemite grain sizes as well as fine-grained (pedogenic) magnetite, while leaving the (lithogenic) coarse-grained magnetite intact (Sun et al., 1995; Verosub and Roberts, 1995). This hypothesis was expanded by Liu, who argued that the CBD method has no preference for any mineral, but only dissolves a finite thickness of ferrimagnetic material from each grain, so that the finer grains are preferentially dissolved (Liu et al., 1999). A very recent study reveals that, although the CBD method dissolved iron oxides from both loess and palaeosol, it still dissolved more material from the soils, indicating a preference for fine-grained pedogenic minerals (Vidic et al., 2000). The smallest grain size of lithogenic magnetite in the loess-palaeosol sequence is not known, and since the CBD method is known to extract magnetite up to $\sim 1 \mu\text{m}$ in diameter, the lithogenic magnetic signal as recorded after CBD extraction could be underestimated, while the pedogenic signal is overestimated (Vidic et al., 2000). Nevertheless, it appears that the ratio of CBD dissolved iron versus total Fe_2O_3 content can be taken as a measure of the weathering degree of the soil (as suggested by Torrent et al., 1980), and it appears to be a legitimate proxy for climate change (Ding et al., 2001).

4.2 Acid-Ammonium-Oxalate (AAO) method

The AAO method as proposed by Tamm (1922; 1932), is performed in light, and was shown to dissolve crystalline goethite and hematite (Deb, 1950). Schwertmann (1964) proposed to perform the method in the dark, which resulted in the selective dissolution of all amorphous iron oxide phases. This was confirmed by AAO extraction of a range of modern soils (McKeague and Day, 1965; McKeague et al., 1971; Bigham et al., 1978; Torrent and Gomez-Martin, 1985). Further testing indicated that the dark AAO method preferentially dissolves specific minerals. Lepidocrocite, goethite and hematite dissolve slowly, while magnetite and ferrihydrite were preferentially dissolved (McKeague et al., 1971; Schwertmann et al., 1982; Walker, 1983). Walker (1983) further concluded that primary (= lithogenic) magnetite is dissolved by the

AAO method, and that dissolution occurs preferentially along the crystal edges. In Californian soil samples, maghemite dissolved much better than magnetite (Fine and Singer, 1989). According to the authors, maghemite was of pedogenic origin in these soils while the magnetite was purely lithogenic. Thus, the method could be used for the identification of pedogenic and lithogenic magnetic minerals.

The apparently controversial results obtained with this extraction method (does it have preference for specific minerals or for amorphous particles?), has stopped researchers of using it in environmental magnetism studies since the early 1990's, instead the CBD method has been used as preferred extraction tool.

4.3 *Extraction methods in this thesis*

The two extraction methods briefly discussed in the previous sections have yielded apparent contradictory results as to their mineral or grain-size specificity. It has been debated that the CBD method dissolves all available iron oxides, or only small grains of iron oxides, or only specific minerals. Similarly, the AAO method has been applied to dissolve only amorphous iron oxides, or only specific minerals.

However, since chemical extraction methods are usually very sensitive to changes in protocol, there is a possibility that these apparent controversies are related to differences in the application of these extraction methods, rather than to failure of the selective capacity of these methods. The primary aim of this thesis was to investigate the effects of changes in protocol on the outcome of the extraction experiments, and to determine whether and how the use of both methods could be optimised for selective dissolution of magnetic spinel-type iron oxides. Our studies of the selective dissolution of iron oxides from synthetic samples have shown that the CBD method does not differentiate between fine-grained magnetite and maghemite, but for coarser grains, there is a preference for the dissolution of magnetite over maghemite. The results of extractions with the AAO-Fe²⁺ method on synthetic samples, showed a preference for maghemite of all grain sizes.

In the next chapters we will discuss the results obtained from extractions of natural loess and palaeosol samples with both methods. These experiments were performed to verify the evidence acquired from the study of synthetic samples (part I). With the results, we hope to improve the interpretation of the rock-magnetic parameters that are used for the identification of the magnetic carriers of the palaeoclimatic signal in loess-palaeosol sequences. Individually, the chemical and magnetic methods are often insufficient for this purpose, but a combination of these methods distinctly enhances the diagnostic value of environmental magnetic research.

Dissolution of Iron Oxides from a Loess-Palaeosol Sequence with the Citrate-Bicarbonate-Dithionite Extraction Method

Here, with an optimised extraction protocol, we test whether the CBD method can discriminate lithogenic and pedogenic iron oxides in a loess-palaeosol sequence from South Moravia (Czech Republic). A low extraction temperature (60°C) was used to facilitate distinction between grain sizes. The composition of the samples was monitored with rock-magnetic (IRM component analysis, hysteresis, susceptibility, and FORC curves) as well as geochemical techniques (ICP-OES).

The samples were shown to contain a mixture of magnetite, fine-grained hematite, and Al-substituted goethite. The fine-grained magnetite as well as hematite and goethite are primarily associated with soil-formation, while the coarse-grained fraction of magnetite is most likely detrital. In the palaeosol samples, the CBD method dissolved almost all of the magnetite, as well as all Al-substituted goethite and part of the hematite, in the first extraction step. In the loess, hematite and the oxidised rims of magnetite were dissolved. Thus, the CBD method dissolved the pedogenic as well as part of the lithogenic fraction from the palaeosol samples, while in the loess samples the 'unstable' minerals were dissolved. This makes the distinction between lithogenic and pedogenic magnetic signals based on CBD data ambiguous.

I. Introduction

Selective extraction methods have been applied in several environmental magnetism studies (e.g. Walker, 1983; Fine and Singer, 1989; Hunt et al., 1995b; Sun et al., 1995; Vidic et al., 2000). The purpose of these methods is to distinguish the lithogenic from the pedogenic magnetic particles, and thus to retrieve information about the environmental magnetic signal. One of the extraction methods that is frequently used is the citrate-bicarbonate-dithionite (CBD) method. It was first introduced in 1960 by Mehra and Jackson (1960), to help improve the detection of silicate clays with X-ray diffraction by the removal of free iron oxides, it has since been implemented in soil science to give an estimate of the total free iron in the samples (e.g. McKeague and Day, 1965; Bigham et al., 1978; Schwertmann and Fechter, 1984; Ghabru et al., 1990; 1995; Sommer and Stahr, 1996). Early studies indicated that the method showed preference for specific minerals following the order: hematite > goethite > oxidised magnetite surface > magnetite (Mehra and Jackson, 1960; McKeague and Day, 1965; McKeague et al., 1971; Walker, 1983; Fine and Singer, 1989). Furthermore, Al-substituted oxides (hematite and goethite) were dissolved more slowly than their unsubstituted counterparts (Torrent et al., 1987; Borggaard, 1990; Trolard et al., 1995). It was later

discovered that the CBD method does not necessarily show a preference for mineral type, but rather for grain size, by preferentially dissolving all fine-grained iron oxides (Ericsson et al., 1984; Fine and Singer, 1989; Borggaard, 1990; Hunt et al., 1995c; Sommer and Stahr, 1996). Magnetite could also be dissolved by the CBD method, but it mainly attacks the fine-grained particles. The limited dissolution of coarse-grained magnetite has been attributed to the presence of “nonreducible Fe^{2+} impurities” in the magnetite structure, which would inhibit dissolution in a similar way as Al-for-Fe substitutions (Borggaard, 1990).

In many loess-palaeosol sequences, the magnetic susceptibility enhancement found in the palaeosol is associated with neof ormation of very fine-grained spinel-type iron oxides. The CBD method was reported to remove all pedogenic iron oxides from the samples without affecting the lithogenic fraction (Fine and Singer, 1989; Hunt et al., 1995c; Singer et al., 1995; Sommer and Stahr, 1996). However, later studies have shown that the method does not only attack fine-grained iron oxides, but it will also dissolve (part of) the coarser iron oxides (van Oorschot and Dekkers, 1999; Vidic et al., 2000). This will result in an overestimated pedogenic fraction in natural samples, although the effect is probably negligible in palaeosol samples (Vidic et al., 2000).

Besides controversial results concerning the exact phases dissolved by CBD treatment and the distinction between pedogenic and lithogenic magnetic minerals, the method has also been disputed because it is reported to dissolve Fe from silicate minerals as well. With the introduction of the CBD method, Mehra and Jackson (1960) found that 7-15% SiO_2 had dissolved after 1 hour of CBD treatment at 80°C. Nonetheless, they stated that the method was the most suitable one for the dissolution of secondary iron oxides from samples without greatly affecting silicates. Others confirmed these results and showed that the method attacks several silicate minerals such as amorphous iron silicates, illite, kaolinite and montmorillonite clays, biotite, olivine, as well as hornblende (McKeague and Day, 1965; Douglas, 1967; Bigham et al., 1978; Ericsson et al., 1984; Stucki et al., 1984; Su and Harsh, 1996; Rozan et al., 1997). Conversely, there is evidence that the major part of the Si that is dissolved by CBD comes from Si(OH)_4 , amorphous silica which is often associated with pedogenic iron and aluminium oxides (Weaver et al., 1968). The amount of Si and Al that is dissolved with CBD is usually highest in the B-horizons of soils (Ghabru et al., 1990).

Extractions of synthetic samples with different CBD protocols have shown that the method can not only be sensitive to grain size or mineralogy, but also to concentration of iron oxides and extraction temperature (van Oorschot and Dekkers, 1999). The samples with low iron-oxide concentration, which were extracted at low extraction temperatures (60°C), were most promising for selective dissolution of only fine-grained minerals. Therefore, samples from a loess-palaeosol sequence were extracted at 60°C to determine whether only the pedogenic minerals had been removed. Moreover, we measured the concentration of Si in our extraction solution, to see if and how the CBD method had affected the silicates in our samples.

2. Samples

We sampled a well-developed loess-palaeosol site just north of the town of Bořetice (Czech Republic), details of the site were described previously by van Oorschot et al. (2001) (see Chapter 6). It contains 4 palaeosols, each developed at a different time. The top of the site has been disturbed by landslides, therefore

we only sampled the lowermost palaeosol. The top part of the sampled section consists of an earthified Rotlehm, which formed from the loess during the Middle Pleistocene ($\sim 0.9 - 0.5$ Ma ago) close to the Bruhnes/Matuyama boundary, it has been identified as belonging to pedocomplex VII. The lower part of the section contains the original loess and dates from the Lower Pleistocene (Havlíček and Smolíkova, 1993). The A-horizon of the palaeosol has been eroded prior to the new deposition of loess.

Bulk samples were taken at 30-cm intervals starting at the top of the palaeosol and ending in the underlying loess. The samples were dried in air for 24 hours, and then stored in a refrigerator. Prior to use, the material was powdered with pestle and mortar and subsamples were taken for various analyses. For the extraction experiments, a sample series consisted of three 4.00 gr. samples from the same level in the section as well as one blank sample consisting of pure quartz (Merck, analytical grade). For the carbonate analysis, 0.5 - 1 gr. of material was used, from each level two subsamples were analysed (results have been reported previously in van Oorschot et al. (2001), see Chapter 6). The bulk material was also subsampled for isothermal remanent magnetisation (IRM) acquisition analysis. These samples (1-2 gr.) were weighed into plastic cylindrical cups (identical in size to standard palaeomagnetic samples) and mixed with epoxy resin (Araldit D, Ciba Specialty Chemicals).

3. Methods

For the chemical extraction, we used the adapted CBD method as discussed previously (van Oorschot and Dekkers (1999), see Chapter 2). A short version of the protocol is given in figure 1; 4 gr. sample was used with 45 mL extraction solution. The extraction temperature was kept low (60°C), to improve distinction between minerals as much as possible. After extraction, the samples were centrifuged and the decanted liquid was analysed with an ICP-OES (inductively coupled plasma optical emission spectrometer, Perkin Elmer-type Optima 3000). An aliquot (1 mL) was taken from the liquid and diluted 10 times with 1N HNO_3 . Accuracy and precision were checked with laboratory standards and duplicate analyses.

Before and after extraction, the samples were weighed and analysed with a range of rock-magnetic techniques. Bulk susceptibility was measured on a susceptibility bridge (KLY 2, AGICO). The sensitivity of the equipment is $4 \cdot 10^{-8}$ SI, and our data were at least a factor of two higher. The susceptibility after each extraction step was normalised to the original susceptibility of the sample to enable comparison between different samples. Thermomagnetic analysis was performed in air with a modified horizontal translation type Curie balance. Moreover, susceptibility changes with temperature were measured in nitrogen atmosphere on a susceptibility bridge equipped with a heating unit (KLY3/CS3, AGICO). Isothermal remanent acquisition (IRM) was induced with a PM4 pulse magnetiser, and measured with a JR5A spinner magnetometer (AGICO). The data was used for IRM component analysis with the programs of Kruiver et al. (2001) and Heslop et al. (2001). The IRM component analysis defines the magnetic composition of the samples with three parameters (SIRM, $B_{1/2}$ and DP) for each separate magnetic component. SIRM is the saturation (maximum) IRM of the component, and $B_{1/2}$ represents the field at which half the SIRM of the component has been acquired. $B_{1/2}$ is also known as the remanent acquisition coercive force (B_{cr} , as defined by Dankers (1978) and Hartstra (1982b)). DP represents one standard deviation in the log-Gaussian distribution. Hysteresis loops were measured on an alternating gradient magnetometer (Micromag), a

- 1 Place 4 gr sample in a 100 mL centrifuge tube.
- 2 Measure magnetic parameters.
- 3 Add 40 mL 0.3 M sodium citrate solution, add 5 mL 1 M sodium bicarbonate solution.
- 4 Stir the sample and place in a waterbath at 60°C.
- 5 Add 1 gr sodium dithionite, keep the sample at constant T for 15 minutes, stir the sample every 5 minutes.
- 6 Centrifuge at 3500 g (~ 4417 rpm) for 10 minutes, decant the liquid (use for ICP-OES analysis).
- 7 Rinse the sample with deionised water (50 mL), centrifuge again at the same settings.
- 8 Dry the sample at 40°C, weigh the dry samples.
- 9 Repeat step 2 - 8 (max. 4 times)

Figure 1: Protocol of the CBD extraction method, as described by van Oorschot and Dekkers (1999). Each batch of samples consisted of three samples from the same level in the section, as well as one quartz blank.

maximum field of 1 T and a field increment of 5 mT were chosen. All samples had reached saturation magnetisation at or before 500 mT. The sensitivity of the Micromag is 1 nAm², which is in the same range as the values for the saturation remanent magnetisation (M_{rs}) of our blanks (~ 1-4 nAm²) as well as for the samples after CBD extraction ($M_{rs} \geq 4$ nAm²). The unextracted samples had magnetisations of at least one order of magnitude higher. The samples were 70% slope corrected, due to the high diamagnetic signal of the silicate and carbonate minerals in the samples. The Micromag was also used to measure backfield demagnetisation to determine coercivity of remanence (B_{cr}). This was measured with a field increment of 2.5 mT up to a maximum field of -100 mT, saturation had been induced at 500 mT.

4. Results & Discussion

4.1 ICP-OES

The extraction solutions were analysed with ICP-OES (only the data for Fe, Al and Si were used in this study). The concentration of iron was very high in the first extraction solution (between ~ 650 and ~ 1900 ppm), but low in all subsequent extraction steps (around ~ 100 ppm, cf. Figure 2A). For the first extraction

step, the highest Fe concentration was found in the top of the palaeosol (Bo) and the lowest in the loess sample (B240). In the palaeosol from palaeosol to loess (B180 – B210), the Fe values remain approximately constant at ~1500 ppm after one extraction step. From the top of the palaeosol to the most enhanced zone (Bo to B150), the amount of Fe extracted in one CBD step slowly decreases (from ~1900 ppm to ~1000 ppm).

The concentration of extracted aluminium shows similar behaviour as that of iron (Figure 2B). Most of the aluminium was extracted in the first extraction step (~40 – 125 ppm), the pattern is similar to that of the concentration of iron after one CBD extraction step. The concentration is high in the top of the palaeosol (~125 ppm), and decreases steadily towards the enhanced zone (~60 ppm). In the enhanced zone the concentrations are also high (~125 ppm), and decrease again in the loess, which has the lowest concentration of all (~40 ppm). In all consecutive extractions, the concentration of aluminium is constant throughout the section and similar for each extraction step (~30 ppm).

The amount of silica dissolved with CBD remained constant for each extraction step. Therefore, Si is not related to the dissolution of iron oxides, but originates from the breakdown of silicate minerals (clays, amorphous silicate and/or quartz). However, the amount of Si dissolved throughout the section does vary: between ~40 and ~100 ppm per CBD step. In the loess the concentration of dissolved Si is low (~40 ppm), this can be explained by the high carbonate content compared to the palaeosol samples (25.8 wt% vs. 0.3–0.5 wt%, respectively), this decreases the relative contribution of silicate minerals. In the palaeosol, carbonate contents are much lower, furthermore, the silicate minerals could have already been partially weathered during pedogenesis. Both factors may contribute to silica being more easily dissolved by CBD in the palaeosol. The variations of silica dissolution in the palaeosol cannot be easily explained, but could be related to the degree of weathering.

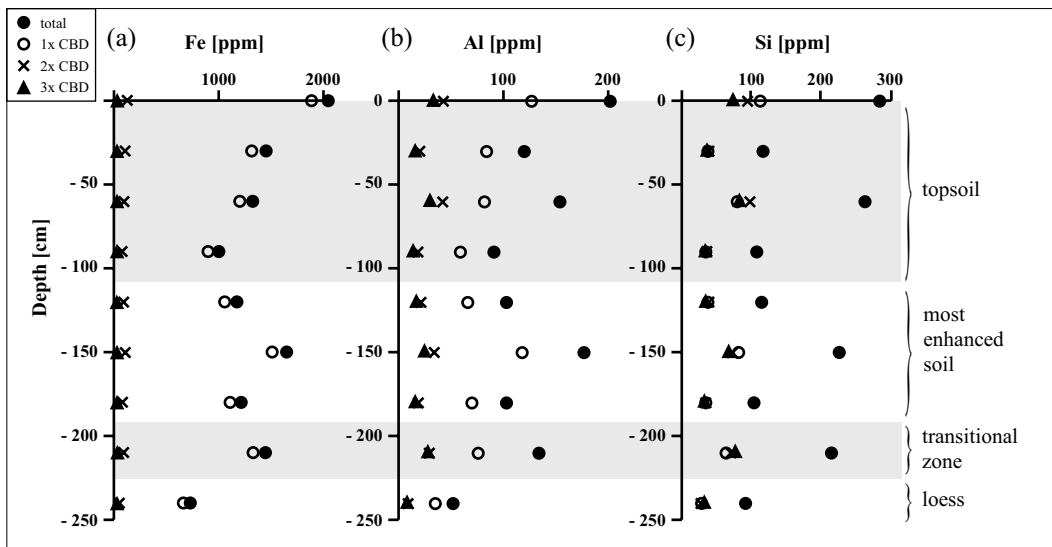


Figure 2: Results from ICP-OES analysis of the extraction solution after each extraction step: (a) dissolved iron, (b) dissolved aluminium, and (c) dissolved silicon. The values of each horizon are averages of three samples. Grey blocks indicate lithological horizons.

The similar concentration changes of Fe and Al in the extraction solution, indicates that these two may be linked to the same mineral phase, suggesting that the iron oxides that were removed by CBD have some Al-for-Fe substitutions. This is not uncommon for soil-derived iron oxides, and the degree of Al substitution increases with the degree of weathering (Cornell and Schwertmann, 1996). Furthermore, the degree of substitution may vary throughout a soil profile. The ratio of Al to (Al + Fe) is used to express the degree of Al-for-Fe substitutions. The average ratio for the first extraction step of this section is 0.05. The values for the lower part of the section are slightly lower (~ 0.04 for the loess), while those of the top of the palaeosol are 0.05 and the highest value is just above the start of the transitional zone (B150, ~ 0.06). Little Al-for-Fe substitution has occurred because the loess from which the palaeosol was formed is quartz-rich and does not contain much reactive Al. Furthermore, in the prevailing temperate climate Al-for-Fe substitution would have been marginal (Cornell and Schwertmann, 1996).

Fe and Al dissolve mainly in the first extraction step, while the dissolution rate of Si remains constant throughout the different extraction steps. This suggests that in the first step mainly (Al-substituted) iron

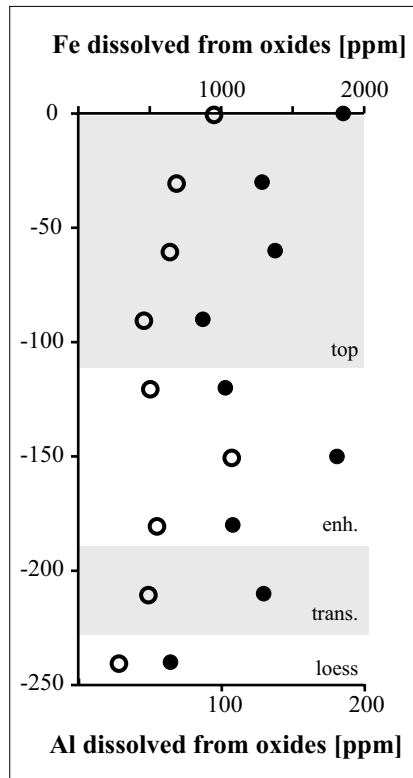


Figure 3: Total Fe and Al dissolved from oxides only. The values of Fe and Al dissolved in the third extraction step are subtracted from the values of Fe and Al dissolved in the first extraction step. The solid circles represent Fe, and the open circles represent Al. The data were calculated assuming that during the third extraction step Fe and Al are only dissolved from silicate minerals, and that the dissolution rate of silicate minerals is the same for each extraction step. Grey blocks indicate lithological horizons, 'enh.' is the most enhanced part of the palaeosol and 'trans.' indicates the transitional zone between palaeosol and loess.

oxides are dissolved, while in subsequent steps the dissolved Fe and Al originates mainly from the dissolution of silicate minerals. We can thus calculate the amount of Fe and Al dissolving from iron oxides in the first step by subtracting the amount of Fe and Al dissolving from silicate minerals in the last extraction step (Figure 3). The figure shows that Fe and Al still show a similar pattern across the section and thus are most likely components of the same mineral.

4.2 Susceptibility

The susceptibility trend in the original samples (Figure 4A) is similar to the behaviour of the dissolved iron of the first extraction step (Figure 2A). The initial susceptibility is low in the loess ($\sim 20 \cdot 10^{-8} \text{ m}^3 \text{ kg}^{-1}$) and enhanced in the palaeosol. The enhancement is strongest just above the transitional zone (B150 $\sim 100 \cdot 10^{-8} \text{ m}^3 \text{ kg}^{-1}$) and level at $\sim 60 \cdot 10^{-8} \text{ m}^3 \text{ kg}^{-1}$ in the top of the section. After three extractions, the susceptibility is constant throughout the whole section ($\sim 10 \cdot 10^{-8} \text{ m}^3 \text{ kg}^{-1}$) which corresponds to $\sim 40\%$ of the value for the unextracted loess. In the palaeosol samples about 75–85% of the original susceptibility had been lost after 1 CBD step. The final susceptibility after 3 CBD steps in the palaeosol samples varied between 8 and 15% of the original value, while the transitional layer (B180/B210) had retained up to $\sim 20\%$ of the original signal. The decrease in susceptibility is strongest in the first extraction step, and after the second step hardly any change in susceptibility could be observed (Figure 5). The signal of the loess samples decreases after one extraction step and then remained constant, while in the palaeosols, there was still a loss in susceptibility after the second extraction step. This could indicate that in the palaeosol coarse (lithogenic) magnetite grains were oxidised more severely than those in the loess.

These results indicate that the particles responsible for the high magnetic susceptibility signal are removed during the first extraction step. The constant susceptibility with depth, after three extractions, suggests that either all iron oxides were removed, or a small and stable (lithogenic) fraction remained in all samples.

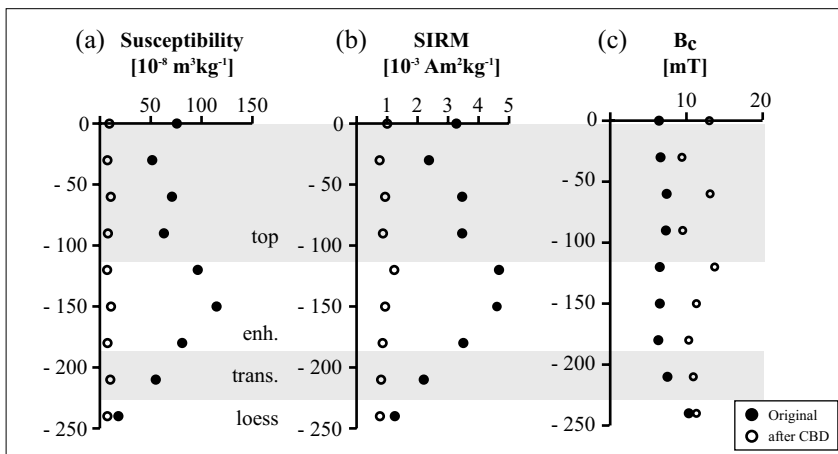


Figure 4: Magnetic characteristics of the original samples, and the samples after three CBD extraction steps; (a) bulk susceptibility, (b) SIRM, and (c) B_c . Grey blocks indicate lithological horizons, 'enh.' indicates the most enhanced part of the palaeosol and 'trans.' indicates the transitional zone between palaeosol and loess.

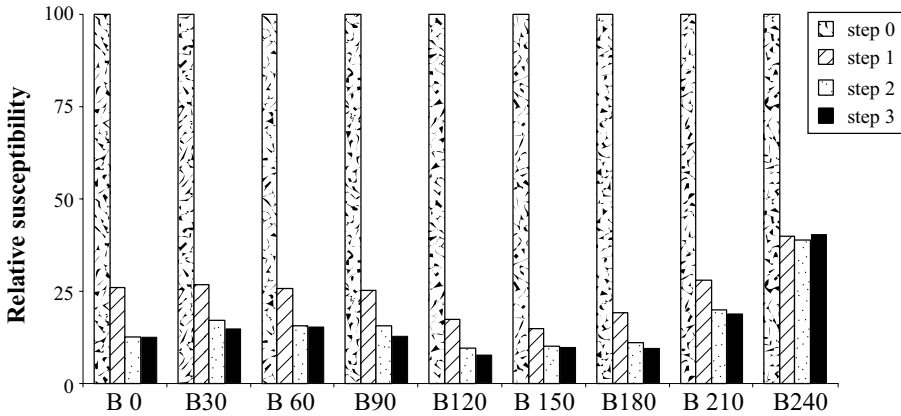


Figure 5: Relative loss in susceptibility after each CBD extraction step. The original susceptibility is set at 100%. For the absolute values: see figure 4A.

4.3 Thermomagnetic analyses

The thermomagnetic curves all show a slow decrease in magnetisation with increasing temperature, and a Curie point at $\sim 580\text{--}600^\circ\text{C}$ for all samples prior to extraction, indicating the presence of magnetite (Figure 6). The most enhanced parts of the palaeosol also have the highest magnetisation (e.g. B0 and B150), while the samples from the transition zone and loess (B240) have the weakest magnetisation. After heating, the cooling curve shows a decreased magnetisation at room temperature, indicating that some of the magnetite was converted to hematite during the measurement. The degree of magnetite conversion was calculated from the difference in magnetisation at room temperature before and after heating, this varies within the section (Table 1). The conversion is strongest in the top of the palaeosol (magnetisation decreased with $\sim 40\%$) and weakest in the loess ($\sim 10\%$ decrease in magnetisation). Furthermore, the cooling curve of the

Sample	original		extracted (3x CBD)	
	initial M_s [$\text{Am}^2\text{kg}^{-1}$]	conversion [%]	initial M_s [$\text{Am}^2\text{kg}^{-1}$]	conversion [%]
B 0	0.042	37.5	0.018	32.2
B 30	0.038	36.8	n.d.	n.d.
B 60	0.044	36.4	0.017	34.8
B 90	0.039	38.5	n.d.	n.d.
B 120	0.052	23.1	n.d.	n.d.
B 150	0.052	21.2	0.018	35.4
B 180	0.044	39.5	n.d.	n.d.
B 210	0.035	31.4	0.017	27.1
B 240	0.022	8.6	0.015	27.2

Table 1: Percentage converted magnetite (presumably to hematite) during the thermomagnetic analysis (based on the decrease in magnetisation at room temperature) and the initial magnetisation values for the unheated samples. The abbreviation 'n.d.' was used for samples that were not analysed. The percentages were determined for both extracted and unextracted samples, and in the unextracted samples they most likely reflect the fine-grained magnetite contribution throughout the section.

loess samples reflects only a paramagnetic signal (it is a straight line in a plot of magnetisation vs. $1/T$), indicating that the weak ferromagnetic signal in the loess has been removed during heating. The conversion degree was also calculated for the extracted samples (Table 1, last column). After three CBD extraction steps, the conversion of magnetite upon heating is approximately equal throughout the section, which suggests a similar composition of magnetic minerals throughout the section.

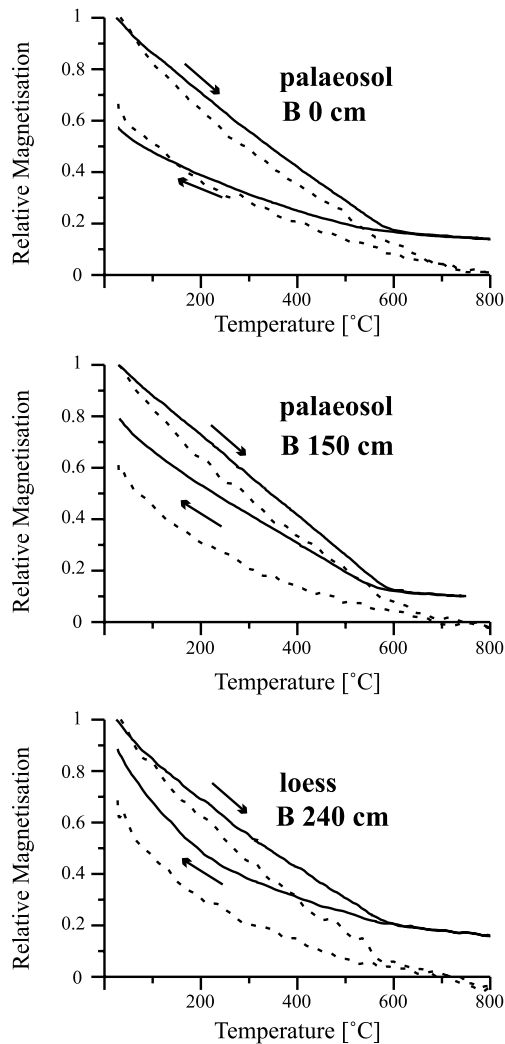


Figure 6: Thermomagnetic curves of representative samples before (solid line) and after (dashed line) 3 CBD extraction steps. The arrows indicate heating and cooling curves, all magnetisations were normalised with the initial value for the room-temperature magnetisation. The measurements were performed in air at a heating rate of $\sim 10^\circ\text{C}/\text{min}$. The initial magnetisation of the palaeosol samples (B 0 and B 150 in the figure) was $\sim 0.04 - 0.05 \text{ Am}^2\text{kg}^{-1}$ for the unextracted samples, and $\sim 0.02 \text{ Am}^2\text{kg}^{-1}$ for the CBD extracted samples. The initial magnetisation of the loess (B 240) was $\sim 0.035 \text{ Am}^2\text{kg}^{-1}$ and $0.015 \text{ Am}^2\text{kg}^{-1}$ for the original and the extracted samples respectively.

The extracted samples (3x CBD) have a lower initial magnetisation, but the curves are similar to the thermomagnetic behaviour of the original samples (Figure 6). However, the Curie temperature in the extracted palaeosol samples is generally higher than in the original samples. Because of the low magnetisation values, the Curie points are difficult to determine but fall in the range of 600 - 700°C for the palaeosol samples, and remain at ~ 580-600°C for the loess and transition zone samples. This indicates that

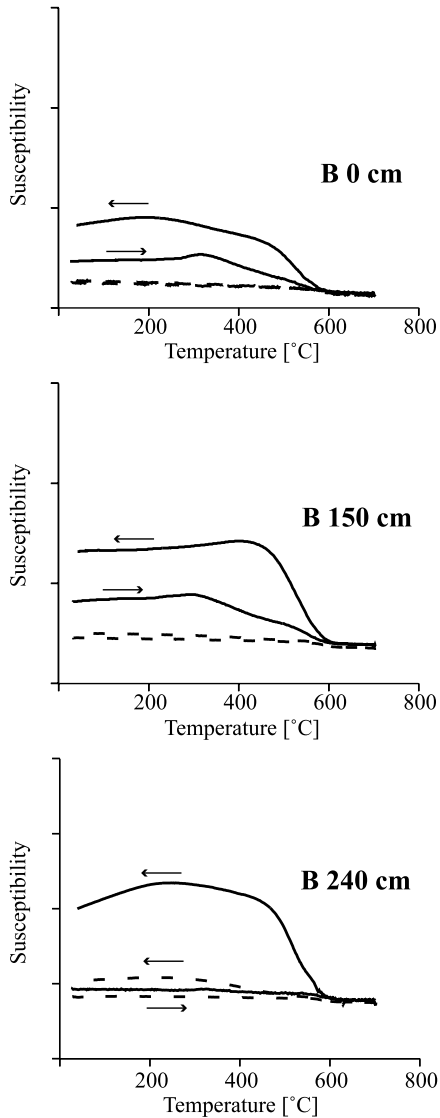


Figure 7: Susceptibility changes (arbitrary units) with temperature for samples before (solid line) and after (dashed line) three CBD extraction steps. All analyses were performed in Argon atmosphere at heating and cooling rates of ~ 10°C/min.

magnetite is present in the lower part of the section, while the palaeosol shows either the conversion of magnetite during heating or the existence of maghemite (or hematite) in the extracted samples. Some conversion does take place in all samples, indicating that the loss of magnetisation is most likely caused by the conversion of magnetite. The magnetisation at room temperature has decreased by 30–40 % for all samples.

Measuring the thermomagnetic behaviour of the samples in an inert atmosphere should provide an insight into the presence of maghemite in the extracted samples, because it is highly sensitive to spinel-type minerals. The samples all show an increase in susceptibility signal after heating in Ar atmosphere to 700°C (Figure 7, solid lines). Furthermore, all palaeosol samples show a small peak at ~ 350°C upon which the susceptibility starts to decrease. The small peak could be caused by iron sorbed to organic matter, which would explain the increase in susceptibility after heating to 700°C. Upon heating the organic matter starts to disintegrate around 350°C. Any sorbed iron will be released and can form magnetite (note that very little Fe is required to form a measurable amount of magnetite) (Hirt et al., 1993). The peak could also be caused by the presence of Ti-substituted magnetite. This titanomagnetite will exsolve into a non-magnetic Ti-oxide and pure magnetite upon heating to temperatures above 600°C and subsequent slow cooling (Collinson, 1983; O'Reilly, 1984). However, the Curie curve shows no indication for a low Curie point associated with titanomagnetite. Therefore we propose that the peak is related to the release of Fe from organic matter or clay minerals and subsequent conversion of this Fe to magnetite.

The curves of the extracted samples all show reversible behaviour and a slight decline in susceptibility around 580°C, suggesting that some of the magnetite still remains (Figure 7, dashed lines). The main magnetic component of the original samples is magnetite, while after extraction a minor amount of magnetite remains. The presence of maghemite, found in the Curie curves of the extracted samples, could not be confirmed by the measurements in Ar atmosphere. The loess sample shows irreversible behaviour with a slight increase in susceptibility after heating, suggesting some sorbed Fe has reacted as suggested for the unextracted samples.

4.4 IRM component analysis

IRM component analysis shows that the original as well as the extracted samples contain two magnetic components (Table 2). The contribution of each component to the total SIRM varies. Before extraction, component 1 is responsible for 85–90% of the total SIRM, while component 2 forms the other 10–15% of the SIRM signal. The first component has a low $B_{1/2}$ (~ 30 mT in the palaeosol and up to 50 mT in the loess), and originates most likely from (oxidised) magnetite. The second component has a high $B_{1/2}$ (~500 to 1000 mT) and therefore originates from goethite and/or hematite. The high coercivity suggests the presence of goethite, but this could not be confirmed by thermal analysis of the IRM (see also van Oorschot et al., 2001).

After extraction the SIRM of the first component has decreased by a factor of 3 to 5 in the palaeosol and a factor of 1–2 in the loess and transitional zone. Simultaneously, the second component has decreased by a factor of ~ 5. The relative contribution of the components has therefore shifted, ~ 90–99 % of the signal is now caused by component 1, while ~ 1–10% of the signal is formed by component 2. For component 1, $B_{1/2}$ in the palaeosol samples increased with ~ 10 mT (to ~ 40 mT), while in the loess and the transitional zone, $B_{1/2}$ decreased with ~ 10 mT (to ~ 40 mT) (Table 2). The decrease in SIRM combined with the

original samples					
Sample code	Total SIRM [10^{-3} Am ² /kg]	component 1 [%]	$B_{1/2}^1$ [mT]	component 2 [%]	$B_{1/2}^2$ [mT]
B 0	3.27	89.3	32 (9 - 107)	10.7	955 (468 - 1950)
B 30	2.37	90.4	36 (11 - 120)	9.6	1906 (776 - 4677)
B 60	3.46	85.3	29 (10 - 87)	14.7	589 (129 - 2692)
B 90	3.46	83.8	28 (10 - 81)	16.2	537 (112 - 2570)
B 120	4.67	91.4	28 (9 - 85)	8.6	1175 (380 - 3631)
B 150	4.60	91.3	28 (9 - 83)	8.7	1148 (309 - 4266)
B 180	3.50	88.6	28 (9 - 81)	11.4	1023 (295 - 3548)
B 210	2.20	90.9	41 (12 - 135)	9.1	1778 (676 - 4677)
B 240	1.25	84.8	49 (15 - 155)	15.2	501 (79 - 3162)
after 3x CBD extraction					
Sample code	Total SIRM [10^{-3} Am ² /kg]	component 1 [%]	$B_{1/2}^1$ [mT]	component 2 [%]	$B_{1/2}^2$ [mT]
B 0	1.01	92.3	41.7 (15 - 115)	7.7	354.8 (41 - 3090)
B 30	0.76	91.1	38.9 (13 - 117)	8.9	426.6 (45 - 4074)
B 60	0.94	97.9	43.7 (14 - 138)	2.1	1318.3 (275 - 6310)
B 90	0.87	88.2	38.0 (14 - 105)	11.8	239.9 (78 - 741)
B 120	1.24	93.8	41.7 (15 - 115)	6.2	363.1 (107 - 1230)
B 150	0.94	98.6	44.7 (14 - 141)	1.4	1778.3 (759 - 4169)
B 180	0.86	93.0	38.9 (14 - 110)	7.0	489.8 (89 - 2692)
B 210	0.81	95.3	37.2 (13 - 110)	4.7	436.5 (98 - 1950)
B 240	0.77	95.2	40.7 (14 - 117)	4.8	457.1 (141 - 1479)

Table 2: IRM component analysis of original and CBD extracted samples. All samples contain a two-component magnetic signal. $B_{1/2}$ represents the field value at which half of the SIRM of the component is reached. The numbers between brackets after $B_{1/2}$ for each component indicate $B_{1/2}$ plus or minus the antilog of the DP parameter, describing the width of the distributions.

increase in $B_{1/2}$ in the palaeosol samples, suggest that here mostly fine-grained magnetite (close to superparamagnetic (SP)) was dissolved, leading to a stronger expression of the fine-grained SD magnetite for component 1. The decrease in SIRM combined with the decrease in $B_{1/2}$ in the loess and transitional samples, suggest that fine-grained magnetite was removed in combination with the oxidised rims of the coarse magnetite, resulting in a more coarse-grained magnetite composition for component 1. This seems in agreement with the findings of van Velzen and Dekkers (1999) who show that in many loess-palaeosol sequences the loess contains more partially-oxidised magnetite than the overlying palaeosol.

For component 2, $B_{1/2}$ decreased to approximately half of its original value ($\sim 240 - 500$ mT) in the palaeosol samples and remains approximately the same in the loess samples (~ 450 mT). The decrease of $B_{1/2}$ suggests removal of a high-coercivity component (most likely goethite) during the extraction procedure,

while the decrease in SIRM indicates that most likely also hematite has been removed. However, after extraction some hematite still remains which was determined from the IRM component analysis as well as the higher Curie points in the Curie curves of the extracted samples.

4.5 Hysteresis (Day plot)

The hysteresis loops for the loess and transition zone are wasp-waisted, indicating a multicomponent magnetic signal. In the Day plot (Day et al., 1977), all samples plot in the PSD (pseudo-single domain) magnetite region, near the MD (multidomain) magnetite region (Figure 8). After one CBD extraction, the samples all show a decrease in B_{cr}/B_c and an increased M_{rs}/M_s ; they all move toward the SD (single-domain) magnetite region of the Day plot. This movement has been attributed to the loss of SP grains (Dunlop, 1999). For all subsequent extractions, the palaeosol samples plot in a position between that of the original and that of the once-extracted samples. In the loess, the B_{cr}/B_c decreases while M_{rs}/M_s changes little in the first extraction step. Subsequent extractions of the loess samples only decrease the M_{rs}/M_s ratio, and the signal moves downward in the Day plot. In these samples, the loss of oxidised rims of magnetite probably caused the shift in the Day plot.

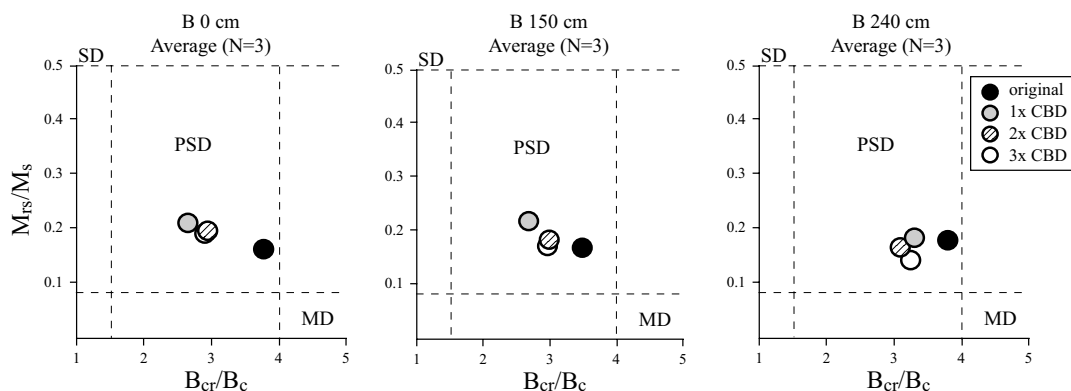


Figure 8: Day plots for several representative samples from the Boretice site; the SD, PSD and MD fields for pure magnetite are indicated. Black circles represent original samples, once-extracted samples are grey, twice-extracted samples are hatched, thrice-extracted samples are open circles. All circles represent averages of at least three samples.

5. Conclusions

The original samples contain a mixture of partly oxidised SD/PSD magnetite with fine-grained Al-substituted goethite and hematite, as concluded from IRM component analysis and ICP-OES results. After one CBD extraction step, almost all of the susceptibility, SIRM and easily dissolved iron and aluminium had been removed. The only cause of the loss in magnetic signal can be the loss of fine-grained magnetite. The loss of aluminium in coherence with iron suggests that Al-substituted goethite or hematite had also been dissolved in the first extraction step. After three extractions, only a weak magnetite signal could be identified in the palaeosol samples, while it was stronger in the loess samples (thermomagnetic curves). The

lack of further significant changes in magnetic characteristics suggest that the CBD method had removed all unstable magnetite and Al-goethite and part of the hematite from the palaeosols, while it had removed only a small fraction of hematite and the oxidised rims of magnetite from the loess samples. The analysis of the extraction solution furthermore showed that the CBD method also attacks silicate minerals. The dissolution preference as suggested by others: hematite > goethite > oxidised magnetite surface > magnetite (Mehra and Jackson, 1960; McKeague and Day, 1965; McKeague et al., 1971; Walker, 1983; Fine and Singer, 1989), is not supported by our results. Almost all minerals dissolved simultaneously in the first extraction step.

Extractions of the same samples with the AAO-Fe²⁺ extraction method showed very similar results (van Oorschot et al. (2001), see Chapter 6). With this method mostly the fine-grained magnetite was dissolved from the samples, and hematite or goethite did not dissolve. The removal of fine-grained magnetite by the CBD method was comparable to that of the AAO-Fe²⁺ method. Al-goethite and hematite were removed to a larger extent from the palaeosol and the loess by the CBD extraction. Neither of these methods preferentially dissolved only pedogenic particles. Subtraction of the signal of the AAO-Fe²⁺ extracted samples from that of the CBD extracted samples, could possibly result in a pure pedogenic signal (Al-goethite and hematite). However, this is not easily realised.

Acknowledgements

I. v. O. thanks Neli Jordanova, Adry van Velzen, Pavel Havlíček and Eduard Petrovský for their assistance in the field during the sampling in South Moravia. The labwork of Judith Beks, and the discussions with Guus Loch were greatly appreciated. This work was conducted under the programme of the Vening Meinesz Research School of Geodynamics (VMSG), and funded by the Netherlands Organisation for Scientific Research (NWO/ALW).

Selective Dissolution magnetic Iron Oxides With the Acid-Ammonium-Oxalate/Ferrous-Iron Extraction Method; II. Natural Loess and Palaeosol Samples

Chemical extraction methods are being introduced into environmental magnetism studies to aid in the interpretation of magnetic climate proxies. Previous studies have shown that the acid-ammonium-oxalate/ferrous-iron (AAO-Fe²⁺) extraction method can be used to selectively dissolve very fine-grained magnetite and maghemite from synthetic samples. Here, we present the results of a study of this extraction method to serve as a tool for selective dissolution of pedogenic magnetic minerals from a loess-palaeosol transect. Before and after extraction, the samples were subjected to standard mineral-magnetic methods (measurement of low-field susceptibility and hysteresis parameters), as well as first-order-reversal-curve (FORC) analysis. In addition, acquisition curves of the isothermal remanent magnetisation (IRM) were fitted with logarithmic distributions. These analyses showed the magnetic dominance of low-coercivity magnetic minerals. By subtracting the IRM remaining after extraction from that before extraction, the magnetic fraction that was dissolved could be characterised as well, serving as a check for the performance of the extraction method.

The method successfully dissolved the superparamagnetic and part of the single domain material from the palaeosol samples in one extraction step, repetition of the extraction hardly resulted in further changes to the magnetic content of the samples. The magnetic characteristics of the loess samples remained stable throughout the experiment. The combination of the AAO-Fe²⁺ extraction with mineral-magnetic analysis has successfully identified the pedogenic contribution in our samples. Therefore, potentially present variations in the lithogenic fraction in pedogenically enhanced intervals can be assessed, improving the merit of mineral-magnetic climate proxy parameters.

I. Introduction

Loess-palaeosol sequences have been the topic of many investigations over the past decades. The focus of most studies was originally on determining the (magneto)stratigraphy and correlation with other terrestrial and marine sequences (Busacca, 1989; Maher, 1998; Zhou and Shackleton, 1999), and later turned to the mineral-magnetic parameters that reveal the climatic history contained in the sequences (Heller and Liu, 1986; Singer and Fine, 1989; Liu et al., 1998; Fang et al., 1999c). Understanding the type of magnetic minerals and the grain-size fraction that carry the climatic information, will help constrain the interpretation of the magnetic climate proxies.

Several studies have shown that some magnetic parameters, such as the low-field susceptibility, correlate with the oxygen isotope curve, therefore they can be used as climate proxies (Heller and Evans, 1995; Liu et al., 1998; Maher, 1998). However, the interpretation of this correlation may be ambiguous, because in some geographical locations the magnetic signal in palaeosols is enhanced compared to that of the loess (like the sequences in China and Central Europe), while in other locations the reverse is true (for example in sequences in Siberia and Argentina, e.g. Maher, 1998).

The magnetic particles in loess are in principle deposited at the same time as the loess itself, and therefore give information about the source area of the loess. However, chemical alteration of the magnetic minerals in the loess after deposition cannot be ruled out (Maher, 1998). In contrast, the palaeosols have a complicated magnetic signal, it originates partly from the original magnetic minerals in the loess and partly from the magnetic particles formed and/or chemically altered during pedogenesis. Extensive pedogenesis may even downprint the palaeomagnetic signal (Zhou and Shackleton, 1999; Heslop et al., 2000). In the case of magnetically enhanced palaeosols, it is therefore necessary to differentiate between the lithogenic and pedogenic contribution of the magnetic signal to extract more meaningful climatic information from palaeosols. Subtraction of the magnetic signal from adjacent loess intervals may lead to erroneous conclusions, because the pedogenic signal is not uniquely based on neoformation of magnetic particles. Furthermore, the composition of the loess may have varied throughout deposition.

To identify the link between magnetic properties and climate change, an interpretation based on mineral-magnetic information only, is often insufficiently distinctive, and complementary techniques have been introduced to help constrain the interpretation (Hunt et al., 1995c; Singer et al., 1995). By dissolving the small particles, chemical extraction methods may offer more information on the changes that have taken place in the lithogenic fraction during the formation of the palaeosols. A number of extraction methods have been investigated in the past to determine the dissolution behaviour of fine- and coarse-grained iron oxides and to find the most suited method for the specific question at hand (Hunt et al., 1995c; Singer et al., 1995; van Oorschot and Dekkers, 1999; van Oorschot and Dekkers, 2001). The acid-ammonium-oxalate/ferrous-iron (AAO-Fe²⁺) extraction method has yielded promising results in synthetic samples (van Oorschot and Dekkers, 2001). The method readily dissolves fine-grained iron oxides, and attacks maghemite preferentially over magnetite. Furthermore, the results are not dependent on the concentration of magnetic iron oxides, which seems to be the case with the citrate-bicarbonate-dithionite extraction when the amount of iron oxides is high. In natural samples the AAO-Fe²⁺ method is expected to preferentially dissolve the smaller magnetic particles from the sample, leaving behind the coarse-grained particles that are of lithogenic origin. With magnetic analysis of samples before and after chemical extraction, more information can be obtained about possible alterations of the original lithogenic particles in the palaeosol.

Here, we aim to compare the results of the AAO-Fe²⁺ extraction method for natural samples with the outcome of a directly related study into the dissolution behaviour of synthetic samples (van Oorschot and Dekkers (2001), see Chapter 3), to see whether these behave in a similar way. The dissolution behaviour of magnetic minerals from a loess-palaeosol sequence from South Moravia (Czech republic) during treatment with the AAO-Fe²⁺ extraction method will be discussed. Besides conventional rock-magnetic techniques, two new methods are incorporated into our study; first-order-reversal-curve (FORC) analysis (Pike et al., 1999; Roberts et al., 2000) and automated isothermal remanent magnetisation (IRM) component analysis

(Heslop et al., 2001; Kruiver et al., 2001). In this way we obtained detailed information of the effects of the extraction method on the composition and grain-size distribution of magnetic minerals in our samples.

Loess-palaeosol sequences of Central Europe

Loess-palaeosol sequences of Quaternary age occur sporadically over a wide area in Europe, from sites in Normandy (France) to deposits as far east as the Ukraine (Stremme, 1998). In South Moravia, where the Czech Republic borders with Austria and Slovakia, loess-palaeosol sequences are abundant. The loess was deposited during the glacial phases of the Pleistocene. During the interglacial stages the climate became warmer and rainfall increased, this enabled soils to develop in the top of the loess deposits. Usually, during the following glacial stage the top of the newly formed soils was partly eroded and the soils were subsequently buried by younger loess deposits (Kraus, 1999). These fossil soils are referred to as palaeosols, and Rotlehm, Braunlehm and Chernozem soils are the most common types of palaeosol found in Moravia (classification according to Kubiena and Muckenhausen in: Kuntze et al., 1981).

The loess-palaeosol sequences of Central Europe are characterised by a small low-field susceptibility signal in the loess and enhanced low-field susceptibility in the palaeosol. This enhancement of magnetic susceptibility in the palaeosols has been correlated to neoformation of ferrimagnetic minerals (Mullins, 1977; Longworth et al., 1979; Fine et al., 1989; Forster and Heller, 1997). The causes of this neoformation

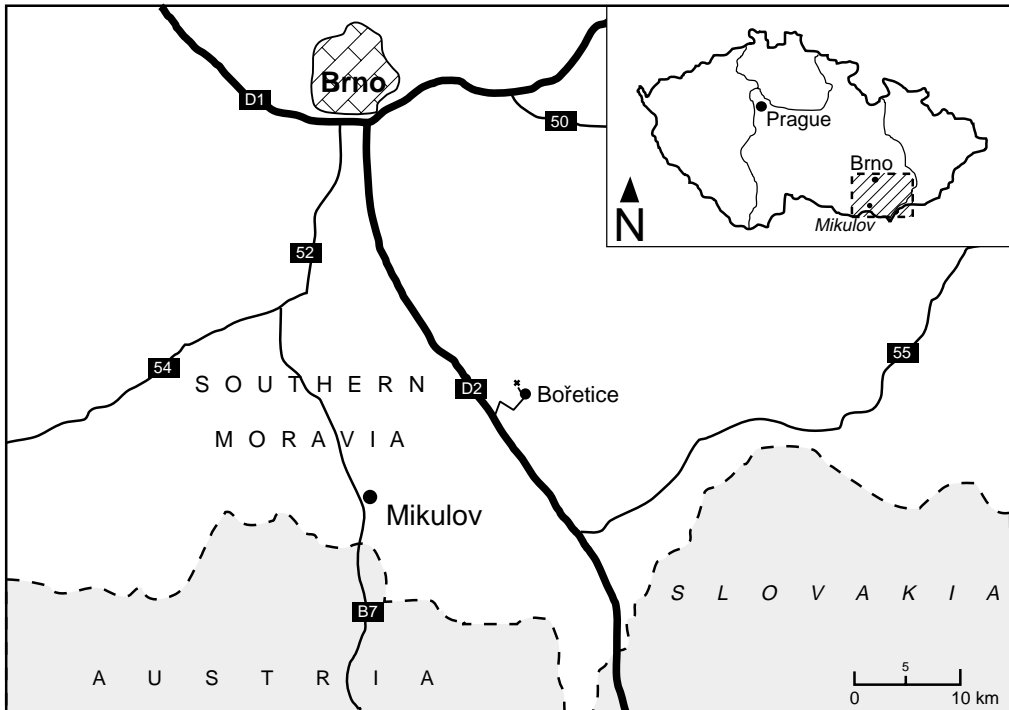


Figure 1: Topographical map of site location. The site is located at ~40 km SSE of Brno, just North of the town of Bofetice.

however, are still under debate. The enhanced magnetic signal has a variety of applications; it has been correlated to palaeorainfall (Maher and Thompson, 1992) and has also been used to indicate the extent of soil-development (Maher, 1998). The sequences in Moravia are grouped into soilcomplexes (also known as pedocomplexes or PK), with each complex representing a complete glacial-interglacial cycle. The soilcomplexes can contain more than one loess/palaeosol sequence. For example, soilcomplex PK IV dates from oxygen isotope stage 7, and is usually distinguished by a double pedocomplex consisting of a pair of lower reddish-brown Bt horizons (Parabraunerde) overlain by Chernozems, and these soils are intercalated by loess or redeposited loess (Frechen et al., 1999).

2. Material & Methods

2.1 Sample area

We sampled a site of well-developed loess with several palaeosols just north of the village of Bořetice (Fig. 1). This site contains 4 palaeosols, each developed at a different time. The top of the section has been partly disturbed by solifluction, therefore we only sampled the lowermost, oldest palaeosol and the loess underneath it. The sampled section is schematically represented in figure 2, a trench was dug to obtain fresh samples. The top part of the sampled section consists of an earthified Rotlehm, which formed from the loess during the Lower-Middle Pleistocene ($\sim 0.9 - \sim 0.5$ Ma ago) close to the Matuyama/Brunhes boundary, it has been identified as belonging to soilcomplex PK VII. The lower part of the section contains the original loess and dates from the Lower Pleistocene (Havlíček and Smolikova, 1993). The A-horizon of the palaeosol has been eroded prior to the new deposition of loess. Bulk susceptibility and colour were measured in the field at 2.5 and 5 cm intervals respectively, with a Bartington MS2F probe (sensitivity of $2 \cdot 10^{-6}$ SI) and a Minolta CM508i portable spectrophotometer. The low-field susceptibility is enhanced in the lower part of the Rotlehm compared to that of the loess, which is consistent with the observation that all central European palaeosols have an enhanced susceptibility (Sartori et al., 1999). The average carbonate content in the palaeosol is ~ 0.5 wt%, the loess horizon has an average carbonate content of ~ 26 wt%.

2.2 Samples

Bulk samples – to be chemically extracted – were taken at 30 cm intervals by digging into the surface of the trench and collecting the fresh material in plastic bags. To check whether the Matuyama/Brunhes boundary had been recorded in this section, oriented samples were taken every 15 cm by carefully pressing plastic cylinders with orientation marks into the surface of the section. The plastic cylinders (volume 8 cm^3) were identical in size to standard palaeomagnetic samples (25 mm diameter, height 22 mm). Prior to analysis, the oriented samples were stored in a refrigerator (at 4°C). The bulk samples were dried in air for 24 hours, and then stored in the refrigerator.

The bulk material was powdered with pestle and mortar and subsamples were taken for various analyses. For the extraction experiments, a sample series consisted of three 1.00 gr. samples from the same level in the section as well as one blank sample consisting of pure quartz (Merck, analytical grade). For the carbonate analysis, 0.5 – 1 gr. of sample was used, from each level two subsamples were analysed. The bulk material

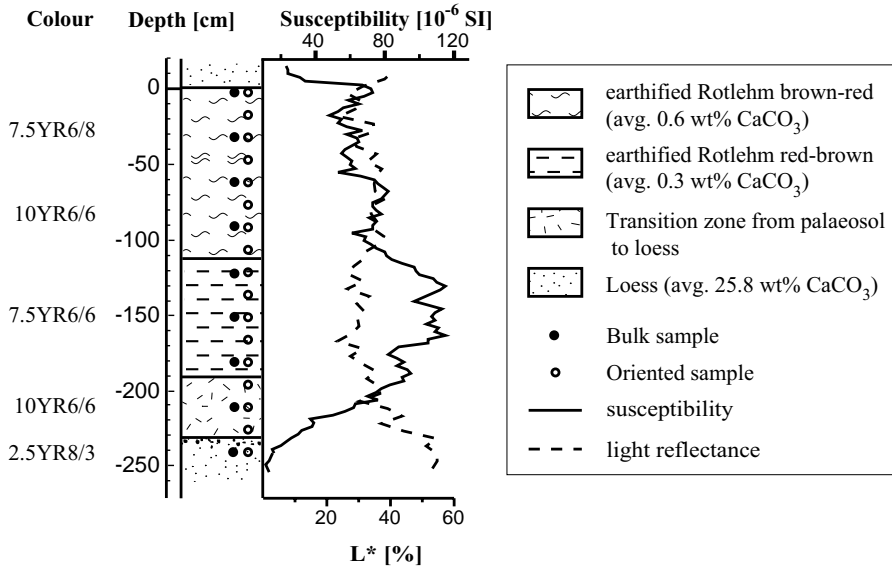


Figure 2: Schematic representation of the sampled section. Colour indications are according to the Munsell notation. The sampled levels are indicated with open circles (oriented samples) and closed circles (bulk samples). Susceptibility was measured in the field (every 2.5 cm) and is represented by the solid line, light reflectance (every 5 cm) is represented by the dashed line. There is a gradual change from the loess horizon towards the enhanced palaeosol between -230 and -190 cm depth. The carbonate content represents an average of the top of the palaeosol and the lower (most enhanced) part of the palaeosol with two samples measured for each sampled level. The standard deviation in the carbonate content was 0.1 for all samples.

was also subsampled for IRM acquisition analysis. These samples (1–2 gr.) were weighed into plastic cylindrical cups (the same as used to take oriented samples in the field) and mixed with epoxy resin (Araldite D, Hardener HY956, Ciba Specialty Chemicals). FORC analysis requires much smaller samples dictated by the sample probe of the MicroMag. Powdered samples containing typically 10 mg sample material, were mixed with the epoxy resin and cast in Teflon moulds which resulted in cylindrical samples with a diameter of ~ 1.5 mm and a length of maximum ~ 2 mm. Some of the extracted samples carried only a very weak magnetic signal, these were cast in a mould with a diameter of ~ 4.5 mm and a length of maximum ~ 4 mm (containing ~ 50 mg sample material) to improve data acquisition with the magnetometer.

2.3 Chemical analyses

The calcium carbonate content of the samples was determined with a Scheibler analyser, it involves the addition of 7 mL of 1 M hydrochloric acid solution to a weighed amount of sample. The volume of CO_2 -gas which is formed during the dissolution of calcium carbonate in the acid is used to determine the calcium carbonate content of the sample.

The AAO- Fe^{2+} extraction method has been described in detail by van Oorschot and Dekkers (2001) (Chapter 3). It uses a 20 mM acid ammonium oxalate solution with 2 mM ferrous iron added at pH 3. The extraction solution is prepared using deoxygenated water to prevent precipitation of the ferrous iron during the preparation and the extraction experiment. For each sample, 50 mL of this solution is required

to perform one extraction step, a fresh solution is prepared for each extraction step. The containers with the samples and the extraction solution are placed on a mechanical shaker at room temperature and at medium speed for 30 minutes. Aluminium foil is wrapped around the containers and the shaker to prevent photochemical dissolution. After 30 minutes the liquid and solid phase are separated by centrifuging for 15 minutes at 3600 g (~ 4417 rpm). The samples are rinsed with ~ 50 mL deionised water and centrifuged again. The remaining solid is dried in an oven at 40°C for ~ 12 hours. The extraction step is repeated a maximum of two times, each sample series requiring one day for extraction and drying of the samples.

2.4 Magnetic measurements

The natural remanent magnetisation (NRM) of the oriented samples was measured with a 2G Enterprises DC SQUID magnetometer (noise level $4 \cdot 10^{-12}$ Am²). Stationary three-axis AF demagnetisation was performed in a laboratory-built coil with a peak field of 300 mT, we used a maximum demagnetisation field of 250 mT. The oriented samples were also used to measure frequency dependence of the low-field susceptibility (χ_{fld}) on a Bartington MS2B dual frequency sensor (low frequency 460 Hz, high frequency 4600 Hz; sensitivity $2.5 \cdot 10^{-6}$ SI).

Prior to the start of the extraction experiment and after each extraction step, the dry samples are weighed and bulk susceptibility as well as hysteresis parameters of the samples were measured. Bulk susceptibility (χ_{in}) was measured with a KLY-2 bridge-type susceptometer (AGICO). The sensitivity of the equipment is $4 \cdot 10^{-8}$ SI, and our data were at least two orders of magnitude higher. The hysteresis loops were measured with an alternating gradient magnetometer (MicroMag) with saturation field of 500 mT and a field increment of 5 mT. At 500 mT all samples were magnetically saturated. The sensitivity of the Micromag is 1 nAm², which is at least two orders of magnitude lower than the magnetisation of our samples. All measurements were 70% slope corrected because of the high diamagnetic signal. Backfield demagnetisation was performed in the same magnetometer with a field increment of 1 mT to a maximum field of -100 mT to determine the coercivity of remanence.

IRM was induced by a PM4 pulse magnetiser and measured with a JR5A spinner magnetometer (AGICO). The sensitivity of the spinner magnetometer is $\sim 2.7 \cdot 10^{-11}$ Am², the minimum IRM measured during our experiments was at least two times stronger. IRM acquisition curves (completely saturated) were analysed with the Cumulative Log Gaussian (CLG) programme of Kruiver et al. (2001) and the automated analysis method by Heslop et al. (2001) to determine magnetic coercivity components in the samples. This involves fitting of a measured IRM acquisition curve with a number of logarithmically distributed coercivity distributions, each characterised by their midpoint ($B_{1/2}$), spreading or dispersion, and magnetic concentration. A statistical test is provided to determine the number of distributions required for an optimal fit. The fitting was also performed for the samples that had been extracted. The data were subsequently mass-corrected and subtracted taking into account the small but slightly varying contribution of the epoxy resin. The resulting IRM curve was analysed with the same programmes and represents the grains that had been dissolved with the extraction method. The grain-size variations of the magnetic minerals in the samples before and after extraction were studied as well with FORC analysis (Pike et al., 1999). Data acquisition was performed on the alternating gradient magnetometer.

3. Results

3.1 Magnetic characterisation of original samples

NRM. Because the palaeosol was formed during the Middle Pleistocene, the Matuyama/Bruhnes boundary may have been recorded in this section. However, the *NRM* data show that all samples have normal polarity (Fig. 3A); thus the boundary was not recorded in this section. AF demagnetisation revealed that most samples decay univectorially towards the origin (Fig. 3B), they have a one-component *NRM*. However, in some samples a viscous overprint presumably by the laboratory field is displayed by the low-coercivity *NRM* fraction (B90-A in Fig. 3B(ii) is an example). Viscous overprints are only found in the lower part of the palaeosol (-75 – -180 cm), the loess again has only a one-component *NRM*. The viscous overprint in the lower part of the palaeosol suggests a high concentration of SP grains in this part of the profile.

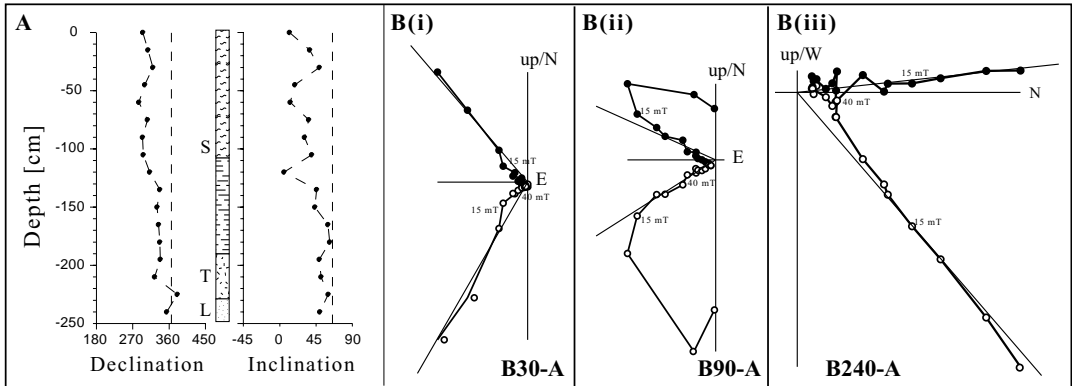


Figure 3: *NRM* for the oriented samples, AF demagnetisation was induced with fields of 5, 10, 15, 20, 25, 30, 35, 40, 50, 60, 80, 100, 150, 200, and 250 mT. Panel A gives declination and inclination throughout the section, the dashed lines represent the declination and inclination of the present geocentric axial dipole field for the site. A schematic representation of the sampled section is given in the column of panel A. Here, 'S' indicates the palaeosol, 'L' is the loess, and 'T' is the transitional zone between palaeosol and loess. Panels B(i) through B(iii) are Zijderveld diagrams of typical examples from the section. Closed (open) symbols represent projection to the horizontal (vertical) plane. All samples have a normal polarity *NRM* (panels B(i) and B(iii)) from the palaeosol and the loess respectively), while some samples show a viscous overprint presumably acquired during storage (panel B(ii)).

The intensity of the samples before AF demagnetisation was approximately constant throughout the section ($\sim 9 - \sim 12 \text{ mA m}^{-1}$) except for the bottom of the section (loess samples) which had a lower intensity (2 mA m^{-1}). After demagnetisation to 250 mT the average remaining intensity of the samples is $\sim 0.7 \text{ mA m}^{-1}$, but for the lower part of the section this value is even smaller (0.1 mA m^{-1}).

The *NRM* that remains after AF demagnetisation at 100 mT is an indication for the presence of hard magnetic components such as hematite or goethite. The samples between 0 – -50 cm and $\sim -165 - -210$ cm are completely demagnetised at fields of 30 – 40 mT (99% of their initial *NRM* intensity is lost). The palaeosol samples between -50 – -165 cm require 100 mT to be completely demagnetised (99% of their

initial NRM intensity is lost). The loess samples require AF demagnetisation at fields of 60 – 80 mT. In most samples the NRM decays in a two-stage fashion with a plateau at 40 – 60 mT (the NRM intensity at this field range is $\sim 1\text{--}2 \text{ mAm}^{-1}$).

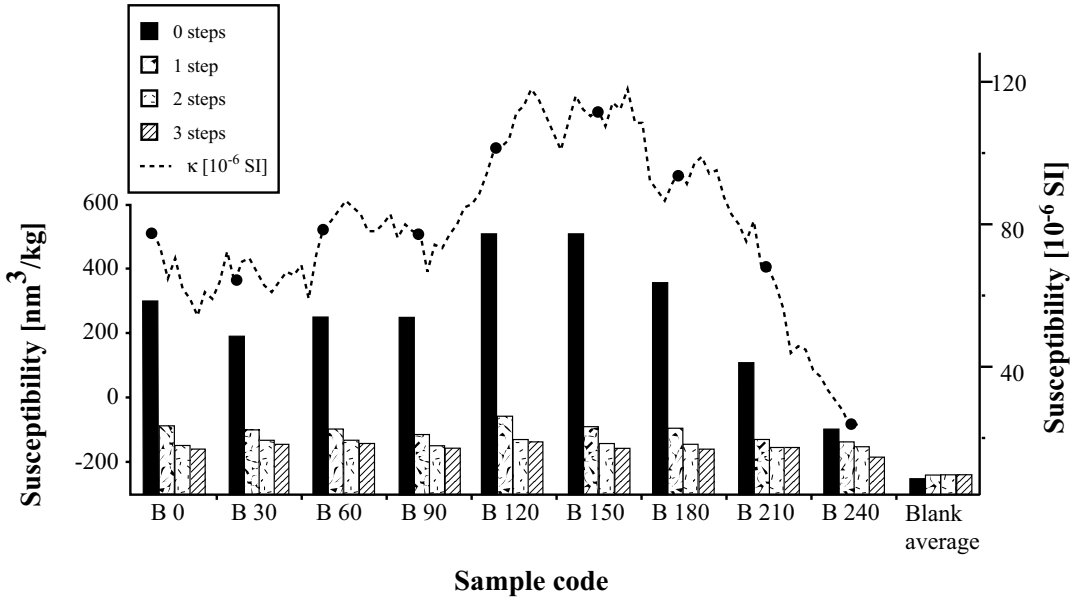


Figure 4: Susceptibility change of samples subjected to the AAO-Fe²⁺ extraction method. The bars give the susceptibility of the bulk samples before and after extraction. The black bars represent samples that have not been extracted. The numbers in the legend refer to the number of extraction steps performed (average of 3 samples per horizon, data of the blanks based on 9 samples (one for each sampled level)). The dotted line represents the bulk susceptibility as measured in the field, with the closed circles indicating the level at which each bulk sample was taken.

Low-field susceptibility. χ_{in} ranges between $\sim 500 \text{ nm}^3/\text{kg}$ in the most enhanced parts of the palaeosol to $\sim -100 \text{ nm}^3/\text{kg}$ in the loess (Fig. 4). Within the palaeosol, χ_{in} varies with depth. From 0 to $\sim -100 \text{ cm}$, χ_{in} is enhanced compared to that of the loess, between ~ -100 and $\sim -200 \text{ cm}$, the enhancement is even more pronounced. Between $\sim -190 \text{ cm}$ and $\sim -230 \text{ cm}$ the transition from palaeosol to loess occurs, this is reflected in a strong decrease in χ_{in} . The χ_{in} pattern found in the field matches that of χ_{in} measured in the laboratory (Fig. 4). The χ_{fd} measurements (Table 1) show that the concentration of SP grains in the palaeosol is higher than that of the loess samples (χ_{fd} is respectively 10–15 % and 4%). These values correspond with those of other studies of natural soils. Most enhanced soils have χ_{fd} in the range of 4–12%, while the C horizon usually has χ_{fd} of $\sim 0\text{--}4\%$ (Maher, 1998; Hanesch and Petersen, 1999). SP grains have a much higher susceptibility than coarser magnetite (Thompson and Oldfield, 1986; Dunlop and Özdemir, 1997), therefore, the enhanced χ_{in} in the soils originates at least in part from the presence of SP grains while the other part of the increased χ_{in} originates from the increased concentration of SD-like spinel iron oxides.

	frequency dependence (%)	absolute difference in frequency susceptibility ($\kappa_{lf} - \kappa_{hf}$)	low frequency susceptibility (κ_{lf} , 10^{-8} SI)
B0	10.0	7.2	72
B15	10.4	5.9	56.8
B30	9.5	5.3	55.5
B45	9.8	5	50.8
B60	9.9	6.9	69.6
B75	8.8	5.6	63.7
B90	9.2	5.9	64.3
B105	9.4	6	63.7
B120	10.2	9.5	92.8
B135	10.1	10.1	99.9
B150	10.4	9.1	87.1
B165	10.2	8.7	85.7
B180	9.7	7.2	74.4
B195	9.0	6	66.5
B210	9.1	4.3	47.1
B225	7.9	2.5	31.6
B240	3.7	0.5	13.4

Table 1: The frequency dependence of the low-field susceptibility of the unextracted, oriented samples. The loess level is represented by sample -240 cm, while the gradual change from loess to palaeosol is represented by samples -195 through -225 cm.

M_{rs}/M_s					B_{cr}/B_c				
Code	0	1	2	3	Code	0	1	2	3
B0	0.14	0.18	0.17	0.15	B0	4.0	3.2	3.7	4.6
B30	0.15	0.14	0.25	0.18	B30	3.7	3.6	3.3	4.3
B60	0.16	0.13	0.19	0.16	B60	3.4	3.7	3.2	3.9
B90	0.14	0.17	0.23	0.19	B90	3.6	3.2	3.1	3.7
B120	0.16	0.18	0.16	0.17	B120	3.7	2.9	3.3	3.6
B150	0.09	0.20	0.20	0.16	B150	3.4	3.3	3.2	3.5
B180	0.12	0.20	0.15	0.16	B180	4.4	3.3	3.7	3.6
B210	0.15	0.17	0.15	0.18	B210	4.1	3.4	3.5	3.2
B240	0.19	0.15	0.17	0.19	B240	3.6	3.2	3.6	3.9
Blank	0.10	0.10	0.08	0.17	Blank	3.6	3.4	7.1	3.0

Table 2: Change in magnetisation ratio (M_{rs}/M_s) and coercivity ratio (B_{cr}/B_c) for the samples before and after extraction with the AAO-Fe²⁺ method.

Hysteresis parameters. All samples have a magnetisation ratio (M_{rs}/M_s) of 0.1 – 0.2, and a coercivity ratio (B_{cr}/B_c) of 3 – 4 (Table 2), which means they plot in the pseudo-single-domain (PSD) region of the Day plot, close to the multidomain (MD) field (Day et al., 1977). The magnetisation ratio remains relatively constant in the top part of the palaeosol, and then starts to increase to reach the highest M_{rs}/M_s ratios in the loess. From top to bottom, the coercivity ratio decreases in the top part of the palaeosol and starts to increase in the enhanced lower part of the palaeosol. Going further down, the B_{cr}/B_c ratio decreases again toward the loess.

IRM components. The automated fitting of the IRM components (Heslop et al., 2001) shows that a two-component IRM yields statistically the best fit for all samples (see Fig. 5 for typical examples throughout the section, panel a-f). One component has a low coercivity (the soft component), and the other has a very high coercivity (the hard component). The relative contribution of the low- and high-coercivity

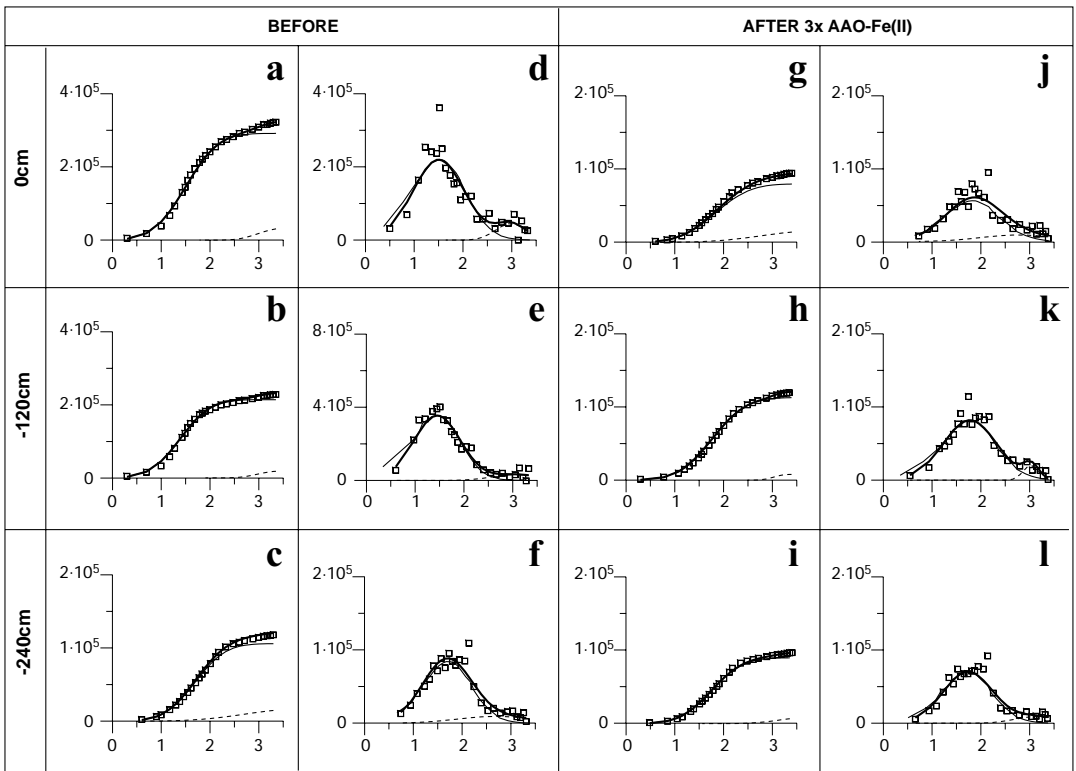


Figure 5: IRM component analysis for some typical palaeosol and loess samples. Data points are indicated by open squares. The sum of all components is represented by a thick black line, the thin solid line represents the soft component, the dotted line represents the hard component. Panels a-c are IRM acquisition curves of unextracted samples, panels g-i represent IRM acquisition curves of the same samples after three AAO-Fe²⁺ extraction steps. Panels d-f and j-l represent the IRM gradient analysis of original and extracted samples respectively. In all panels the vertical axis represents IRM, while the horizontal axis represents the ¹⁰log of the applied field (mT). Before fitting, all data were corrected for the IRM signal and mass of the epoxy resin in each sample.

		component 1				component 2			
	Sample	SIRM	B 1/2	DP	Contribution	SIRM	B 1/2	DP	Contribution
Before	Average soil	321143 ± 76500	30 ± 3	0.49 (10 - 93 mT) ± 0.03	88.6 ± 3	40657 ± 10815	1048 ± 455	0.52 (316 - 3470 mT) ± 0.14	11.4 ± 3
	loess	106000	49	0.50 (16 - 155 mT)	84.8	19000	501	0.80 (79 - 3161 mT)	15.2
After	Average soil	90857 ± 13600	58 ± 5	0.55 (16 - 206 mT) ± 0.02	84.8 ± 5.6	16000 ± 5690	920 ± 331	0.52 (278 - 3046 mT) ± 0.27	15.2 ± 5.6
	loess	90000	55	0.51 (17 - 178 mT)	90.0	10000	1413	0.44 (513 - 3892 mT)	10
Dissolved	Average soil	241571 ± 70470	25 ± 1	0.46 (9 - 72 mT) ± 0.01	94.7 ± 1.8	13000 ± 4320	1597 ± 369	0.33 (747 - 3414 mT) ± 0.09	5.3 ± 1.8
	loess	22100	45	0.59 (12 - 175 mT)	99.1	210	1259	0.18 (832 - 1906 mT)	0.9

Table 3: The average values of SIRM (10^{-8} Am²/kg), $B_{1/2}$ (mT), DP, and relative contribution (%) of the IRM components in the palaeosol and in the loess samples. The DP is given in logfield values (mT values are given in brackets). The first values are from unextracted samples, the second set of values are of extracted samples, and the final set is from the dissolved fraction (before-after). The average of the palaeosol samples is determined from samples between 0 and -180 cm, while the loess value is determined from samples at -240 cm. The standard deviation of the average samples is given in smaller font size.

components in the palaeosol samples is $\sim 90\%$ and $\sim 10\%$ respectively ($\sim 3.2 \cdot 10^{-3}$ vs. $\sim 0.4 \cdot 10^{-3}$ Am²/kg, see table 3). The loess samples have a slightly higher contribution of high-coercivity material, $\sim 15\%$, and $\sim 85\%$ of low-coercivity material ($\sim 1 \cdot 10^{-3}$ vs. $\sim 0.2 \cdot 10^{-3}$ Am²/kg, see table 3).

The low-coercivity component in the palaeosol has a lower $B_{1/2}$ than that of the loess (respectively ~ 30 mT and ~ 50 mT), while both components have a similar dispersion of 0.5. The dispersion is given in logfield units, therefore the dispersion of the $B_{1/2}$ of the soft component in the palaeosol is $\sim 10 - \sim 93$ mT and in the loess this is $\sim 16 - \sim 155$ mT. This component originates most likely from SD to pseudo-single-domain (PSD) magnetite. The lower $B_{1/2}$ in the palaeosol compared to that of the loess samples cannot originate from the low-temperature oxidation of magnetite, for this would lead to increase in coercivity (van Velzen and Dekkers, 1999). The difference is likely due to an increased abundance of finer grains including superparamagnetic (SP) grains; this decreases the overall $B_{1/2}$ of the sample, because the coercivity of SP grains is close to zero (Dunlop and Özdemir, 1997).

The average $B_{1/2}$ of the high-coercivity component in the palaeosol is ~ 1050 mT with a dispersion of 0.5 (= 316–3470 mT). In the loess, the $B_{1/2}$ of the hard component is ~ 500 mT and the dispersion is wider (0.8 = 79–3161 mT). This hard component is either hematite or goethite. The mineralogy was verified with thermal demagnetisation of a tri-axial IRM (Lowrie, 1990). The saturation IRM of some representative samples from the section was split into three orthogonally directed components in the sample. The a-axis contained the hard component with $B_{cr} > 126$ mT, the b-axis contained the intermediate component ($30 < B_{cr} < 126$ mT) and the c-axis contained the soft component ($B_{cr} < 30$ mT). These field values were based on the results of the IRM fitting. The samples were subsequently thermally demagnetised at 60, 80, 100, 120 and 140°C. The decrease in IRM with increasing temperature is gradual for all components (Fig. 6), this indicates that the hard component could not have originated from goethite which has a Néel temperature of $\sim 120^\circ\text{C}$. An IRM residing in goethite would decay rapidly at low temperatures and show a break in slope at 100–120°C.

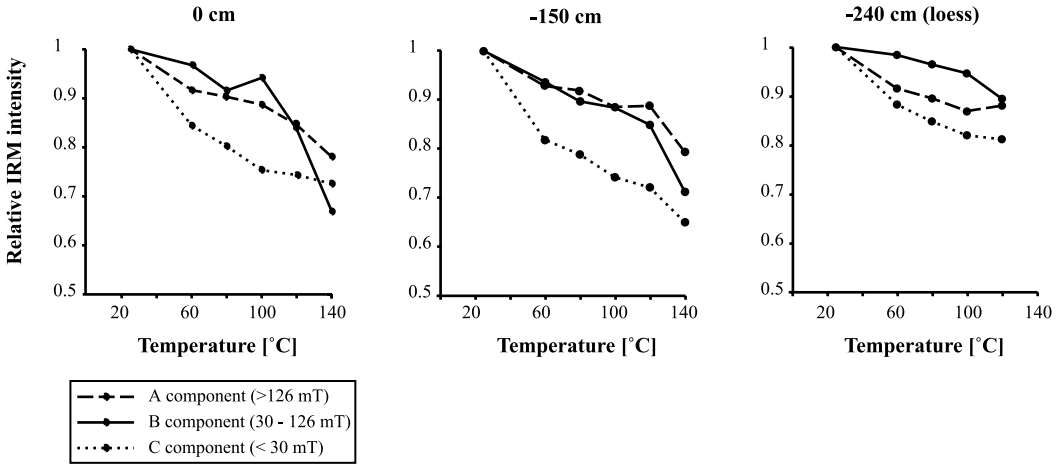


Figure 6: Thermal demagnetisation of tri-axial IRM. The two left panels are two palaeosol samples, the right panel is a loess sample. On the vertical axis is the relative IRM intensity, the horizontal axis shows the temperature steps used for the thermal demagnetisation. The 140°C step for the loess samples is not given, the plastic container with the orientation marks that holds the sample had partly molten during this final heating step making it impossible to determine the IRM. The dashed line represents the hard component (A), the solid line indicates the intermediate IRM component (B), and the dotted line represents the soft component (C). The intensity of the hard component was the lowest, and that of the soft component was always highest. The initial intensity for the different components in the 0 cm sample was 1410, 2600 and 3430 nAm² (A, B, and C component respectively). In the -150 cm sample this was 1240, 4320 and 5030 nAm² and in the loess sample (-240 cm) this was 500, 1090 and 1250 nAm² (A, B, and C respectively).

FORC distribution. A FORC distribution is a contour plot that allows the user to evaluate magnetic hardness and interaction separately in a sample. The horizontal axis H_c represents the coercivity, and the vertical axis H_u represents the magnetic interaction in the sample (Pike et al., 1999). Non-interacting samples have narrow distributions centred on $H_u = 0$. SD particles centre on their H_c , close to the ordinate of the plot they have no contour density (Pike et al., 1999; Roberts et al., 2000). Modelling has shown that thermal relaxation of SP (and small SD) particles yields vertical contour lines with the maximum contour density at $H_c = 0$ (Pike et al., 2001). Preliminary modelling of MD grains indicate vertical contour lines centred on H_c of the particles (Pike et al. in press PEPI). In practise small MD grains have contour lines shaped like an acute triangle with the base at an angle $\neq 0$ with the horizontal axis (\Rightarrow) (Roberts et al., 2000). The contour density is spread over a comparatively large H_u interval because the domains within MD particles interact with each other.

The FORC distribution of the palaeosol (Fig. 7 upper panel) and loess (Fig. 7 lower panel) samples indicates dominant fine-grained SD magnetite. In the palaeosol sample the increased contour density close to the ordinate axis might be interpreted as indicative of the presence of SP particles. The triangular shape of the contours indicates a minor presence of MD grains as well. The wide distribution in coercivity (up to ~ 50 mT), and the narrow vertical distribution (most contours within ± 2 mT) indicate the presence of well dispersed SD grains. There is no displacement along the vertical axis, confirming that there is little magnetic interaction in the sample.

The loess sample shows slightly larger grains: there are more contours with MD-like triangular shape, and the distribution is more centred to the left. Also the vertical distribution is larger (most contours within ± 4 mT). The presence of SP grains cannot be evaluated because the weak magnetic signal required a large smoothing factor to produce the FORC diagram shown. This makes the left-most part of the diagram less reliable. In both palaeosol and loess the magnetic dominance of magnetite precludes a meaningful determination of high-coercivity components.

3.2 Characterisation of extracted samples

Low-Field susceptibility. In the palaeosol samples, χ_{in} decreased most significantly after one AAO-Fe²⁺ extraction step (Fig. 4). After one extraction the susceptibility varied between -60 nm³/kg for the most enhanced part of the palaeosol, -120 nm³/kg for the other palaeosol samples and -140 nm³/kg for the loess sample and that from the transitional zone between the loess and the palaeosol. After two extractions, the bulk susceptibility of all samples remained constant at ~ -150 nm³/kg. The data for the blank samples remained constant at -240 nm³/kg.

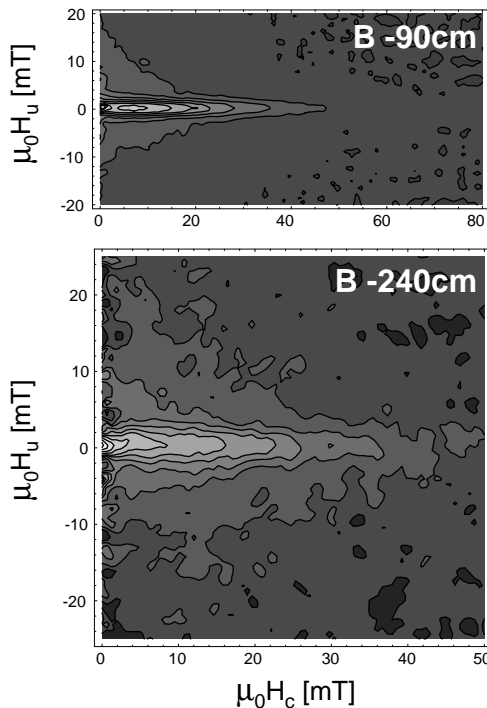


Figure 7: FORC diagram of some representative samples of unextracted bulk material. On the horizontal axis is $\mu_0 H_c$ (indicative of grain-size range), the vertical axis represents $\mu_0 H_u$ (indicative of magnetic interaction). The saturation field for both diagrams was 500 mT, and 106 FORC curves were measured. The top diagram is an example from the palaeosol (measurement averaging time = 2 sec), the lower diagram is from the loess horizon (measurement averaging time = 1 sec).

χ_{fd} could not be determined for the extracted samples, because low- and high-frequency measurements yielded essentially the same value (the potentially present difference appeared to be below the resolution of the instrument), resulting in a χ_{fd} equal to zero.

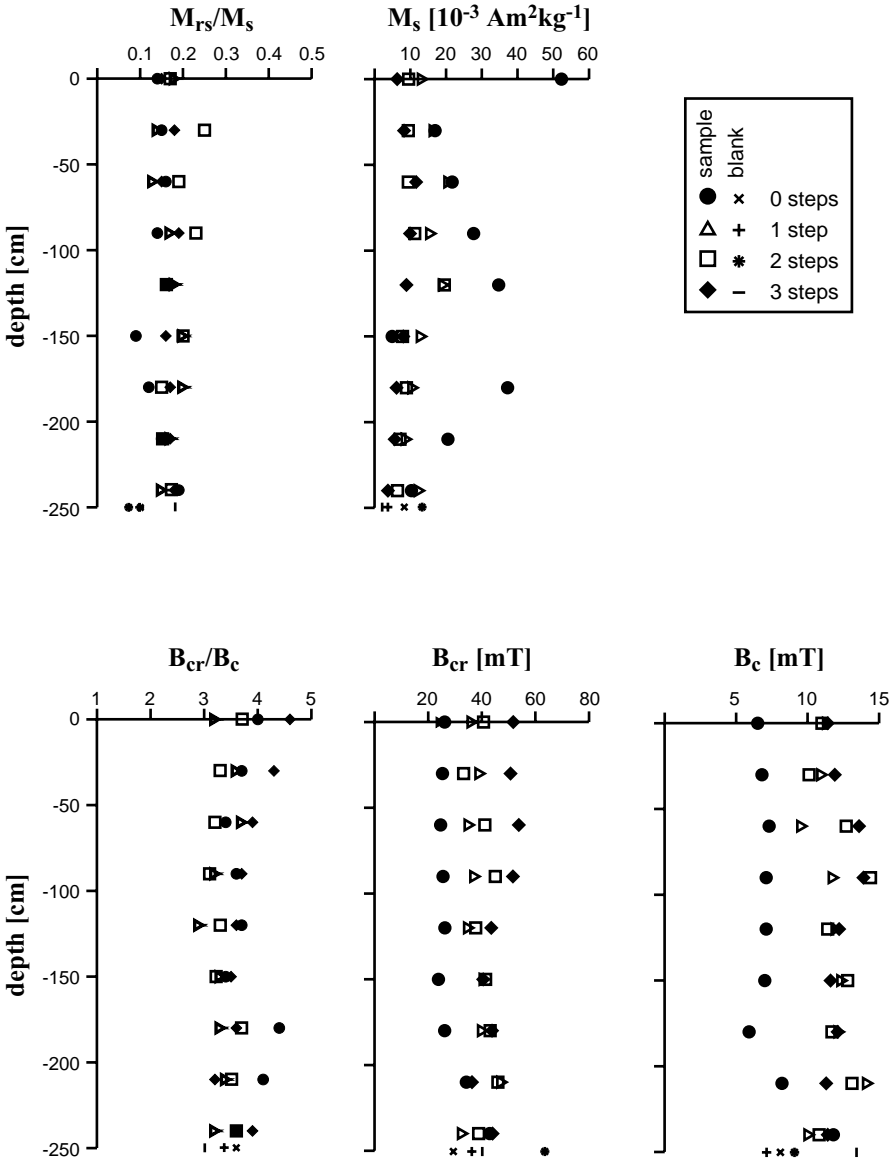


Figure 8: Change in hysteresis parameters (M_{rs}/M_s , M_s , B_{cr}/B_c , $B_{c'}$ and B_{cr}) with depth of the section as well as with each extraction step. Closed circles represent the non-extracted samples, closed diamonds represent the same samples after three extraction steps. The open triangles and squares are from extraction step 2 and 3 respectively.

Hysteresis parameters. A similar change in hysteresis parameters after one extraction step is observed for all palaeosol samples: the coercivity ratio decreases, while the magnetisation ratio increases slightly (Table 2). Figure 8 shows that both B_{cr} and B_c increase after extraction. The value of B_c doesn't change further with more extraction steps and remains at a value of ~ 12 mT. B_{cr} keeps increasing after each extraction step with endvalues of ~ 40 – 50 mT in the palaeosol samples. The coercivity ratio first decreases due to the relatively fast increase in B_c compared to B_{cr} , but the stabilisation of B_c after one extraction step causes the coercivity ratio to start increasing again. The magnetisation ratio increased slightly, the most noticeable increase in

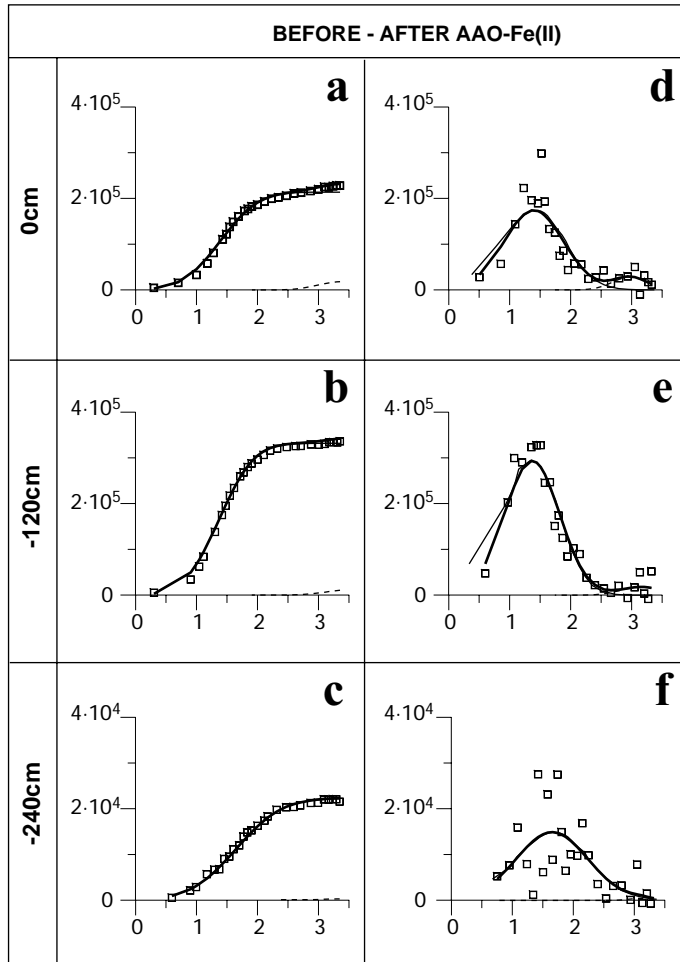


Figure 9: IRM component analysis for the difference in IRM acquisition before and after extraction for some typical palaeosol and loess samples. Data points are indicated by open squares. The sum of all components is represented by a thick black line, the thin solid line represents the soft component, the dotted line represents the hard component. Panels a-c are IRM acquisition curves, panels d-f represent the IRM gradient analysis of the subtracted dataset. In all panels the vertical axis represents IRM, while the horizontal axis represents the $^{10}\log$ of the applied field (mT). Before fitting, all data were corrected for the IRM signal and mass of the epoxy resin in each sample.

magnetisation ratio is for the most enhanced part of the palaeosol (Fig. 8). The increase in magnetisation ratio is related to the strong decrease in M_s for all sample except the loess samples. After one extraction step, the palaeosol samples have lost 50–80% of their original M_s . More extraction steps hardly affect the M_s and it remains at $\sim 1 \cdot 10^{-2} \text{ Am}^2/\text{kg}$, similar to the M_s of the loess samples and the quartz blanks. M_{rs} also decreases less rapidly in the second and third extraction step, this causes the magnetisation ratio to stabilise at a slightly higher value than that of the original samples.

The samples in the lower part of the section (loess and transition from palaeosol to loess) behave differently, here B_{cr} hardly changes with extraction and the coercivity ratio remains constant. The M_s decreases slightly in the loess samples but the magnetisation ratio remains constant. The loess samples show a decrease in both magnetisation and coercivity ratio. The samples have very similar B_{cr} and M_s as the quartz blanks, which could indicate all iron oxides have been removed from the sample, but H_c is slightly higher than that of the blanks.

IRM components. After extraction, all samples still have a two-component IRM distribution (Fig. 5, panel g-l). In the palaeosol samples the relative contribution of the components has changed to $\sim 85\%$ for the soft component and $\sim 15\%$ for the hard component ($\sim 9 \cdot 10^{-4}$ vs. $\sim 1.6 \cdot 10^{-4} \text{ Am}^2/\text{kg}$, see table 3). This indicates

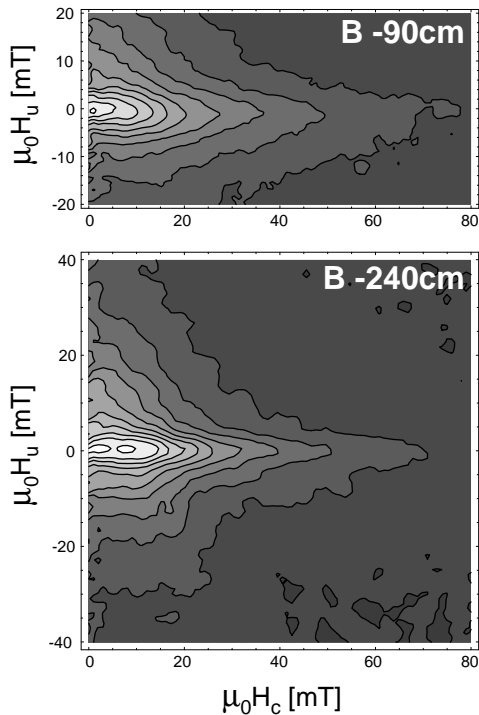


Figure 10: FORC diagram of some representative samples after three AAO-Fe²⁺ extraction steps. On the horizontal axis is $\mu_0 H_c$, the vertical axis represents $\mu_0 H_u$. The saturation field for both diagrams was 500 mT, and 106 FORC curves were measured. The measurement averaging time was 2 sec. The top diagram is an example from the palaeosol, the lower diagram is from the loess horizon.

that the soft component has been preferentially dissolved from the soil samples. The soft component in all palaeosol samples has an average $B_{1/2}$ value of ~ 58 mT, the hard component has a decreased $B_{1/2}$ value of ~ 900 mT. Both components in the palaeosol samples have dispersions of ~ 0.5 (component 1: 16–206 mT; component 2: 278–3046 mT).

The relative contribution of the soft component has increased in the loess samples ($\sim 90\%$ or $9 \cdot 10^{-4}$ Am²/kg) while the contribution of the hard component has decreased ($\sim 10\%$ or $1 \cdot 10^{-4}$ Am²/kg). The average $B_{1/2}$ of the soft component in the loess is ~ 55 mT with a dispersion of 0.51 (17–178 mT), the hard component has an increased $B_{1/2}$ value of ~ 1400 mT and has a more narrow dispersion of 0.44 (513–3892 mT).

The dissolved magnetic fraction is represented in the curve of the difference in IRM acquisition between original and extracted samples (Fig. 9). Analysis of these curves show that mainly the soft component dissolved during the extraction. The contribution of the soft component to the dissolved fraction is $\sim 95\%$ ($2.4 \cdot 10^{-3}$ Am²/kg) in the average of the palaeosols (7 samples) and even $\sim 99\%$ in the loess samples ($2.2 \cdot 10^{-4}$ Am²/kg). The $B_{1/2}$ of the dissolved soft component is 25 mT in the palaeosol samples, and 45 mT in the loess (dispersions are 0.46 (or 9–72 mT) and 0.59 (or 12–175 mT) respectively). The $B_{1/2}$ of the dissolved hard component is ~ 1600 mT in the palaeosol samples, and ~ 1250 mT in the loess (dispersions are 0.33 (or 747–3414 mT) and 0.18 (or 832–1906 mT) respectively). Only 1–5% of the hard component has dissolved from the loess and the palaeosol samples respectively ($2 \cdot 10^{-6}$ and $1.3 \cdot 10^{-4}$ Am²/kg, see table 3). It seems the loss in magnetic particles is most likely related to dissolution of newly formed pedogenic iron oxides as well as the dissolution of the weathered surface of particles in the loess.

FORC distribution. The FORC diagrams of the extracted samples show a pattern with a wider vertical distribution (max. 40 mT) but no vertical displacement of the centre of distribution (Fig. 10). The magnetic signal was weak requiring rather high smoothing factors to produce the plots shown. It is remarkable that the coercivity contour distribution along the horizontal axis goes up to values of ~ 80 mT (before extraction this was up to ~ 50 mT), this may hint at the presence of high-coercivity material. The FORC diagrams with their increased triangular shape, thus show an increase in MD character after extraction, with increased magnetic (intraparticle) interaction. The wider distribution of coercivities may be caused by the dissolution of magnetite during the extraction experiments. The partial disappearance of the SD magnetite signal facilitates the expression of the weakly magnetic hematite.

4. Discussion and Conclusions

The normal polarity of all samples indicate that the section was formed during the Brunhes; the pedocomplex assignment precludes formation during the Jaramillo subchron. Viscous resetting of the NRM is unlikely, because the declinations in particular deviate from the geocentric axial dipole direction for the site. The higher NRM intensity of the palaeosol samples is consistent with its enhanced susceptibility, indicating that enhancement originates from increased concentration of ferrimagnetic particles in the palaeosol. In the top of the palaeosol, most of the NRM is lost after applying a field of only ~ 40 mT, indicating that the main carrier of the magnetic signal in the top of the palaeosol is magnetite of

large SP or PSD/MD size. The high χ_{fd} pleads for the former. In the more enhanced part of the palaeosol (between -50 – -165 cm) as well as in the loess, most of the NRM is lost after applying a field of 80-100 mT indicative of SD to PSD size magnetite. Here, the hysteresis parameters plot in the PSD region as well. The high-coercivity component determined by the IRM component analysis does not emerge in the NRM behaviour.

IRM component analysis shows that all samples contain a two-component IRM. The low-coercivity component is interpreted to be SD magnetite, and the high-coercivity component originates from hematite. The higher value of $B_{1/2}$ and narrow dispersion of the hard component in the palaeosol compared to that in the loess, indicates neoformation of fine-grained hematite in the former. This is confirmed by the higher intensity of NRM in the palaeosol samples after demagnetisation to 250 mT (which is 4 to 10 times higher in the palaeosol samples than in the loess samples).

The FORC diagrams follow the pattern of the soft IRM component and display predominantly well-dispersed SD magnetite. However, the presence of hematite can be inferred from the fairly high coercivity values found in FORC diagrams of extracted samples.

After extraction, the susceptibility in all samples has decreased, the decrease was strongest after one extraction step. The loess samples were hardly affected, indicating a small portion of very fine magnetic grains in the loess. The susceptibility of the palaeosol samples after extraction was comparable to that of the loess samples. From the second extraction step onward, palaeosol and loess samples behaved along similar lines. Therefore, all pedogenic iron oxides have likely been removed from the samples during the first extraction step. Also, the AAO-Fe²⁺ extraction method has not greatly affected the coarser lithogenic particles in the samples, a behaviour that concurs with the results obtained for synthetic samples (van Oorschot and Dekkers (2001), see Chapter 3).

The hysteresis parameters confirm that predominantly small SP/SD grains were removed by the extraction method (magnetisation ratio increased, while coercivity ratio decreased). The data also show that the loess samples have lost some SD grains (both magnetisation and coercivity ratios decreased). The dissolution of fine-grained magnetite was also detected with the IRM component analysis. After extraction, the relative contribution of hematite to the IRM signal of the palaeosol had increased, indicating that the soft component had been preferentially removed.

The loess samples also lost part of the hematite during extraction, as indicated by the decrease in dispersion and the absolute IRM contribution of the hard component. The FORC diagrams of extracted samples all showed an increase in MD character, evidenced by increased magnetic (intraparticle) interaction. The SP/SD material had been removed from the samples concurring with the example shown by Roberts et al. (2001) for the citrate-bicarbonate-dithionite (CBD) extraction. χ_{fd} of the samples after extraction unfortunately fell below the resolution of the instrument, thus precluding confirmation by χ_{fd} behaviour.

It is shown here that the AAO-Fe²⁺ extraction method is expected to dissolve fine-grained (SP/SD) ferrimagnetic minerals from palaeosol samples in one extraction step. This method is slightly less aggressive than the CBD method and offers a better discrimination in the ultrafine grain-size range. The relative stability of the magnetic parameters in the loess before and after extraction supports this discrimination. The method has successfully dissolved the pedogenic component from the palaeosol samples as well as the oxidised rims of the lithogenic magnetic minerals in the loess.

Acknowledgements

The authors greatly appreciated the help of all participants in the field trip to Moravia, and would especially like to thank Adry van Velzen, Neli Jordanova and Eduard Petrovský. The authors also wish to thank Pauline Kruiver and David Heslop for their assistance with the IRM component analysis as well as for fruitful discussions of the results. The help of Chris Pike with the FORC analysis was greatly appreciated. This work is conducted under the programme of the Vening Meinesz Research School of Geodynamics (VMSG), and funded by the Netherlands Organisation for Scientific Research (NWO/ALW).

Part III

Voltammetry of Microparticles

An introduction to electrochemistry

While searching for a mineral-specific analytical tool to use in environmental magnetism, electrochemical techniques have shown to be promising. With voltammetric techniques, the reductive dissolution of fine-grained magnetic material can be monitored both qualitatively as well as quantitatively. The methods are fast and comparatively straightforward to interpret, and require little amount of sample. This chapter contains a concise introduction to the basic principles of electrochemistry, followed by a more detailed description of voltammetry. The final section explains how voltammetry has been used in electrochemistry and shows the benefits for application in environmental magnetism. For more detailed information on electrochemistry, the reader is referred to Kissinger and Heineman (1984), Atkins (1989), or Scholz and Meyer (1998). A glossary of electrochemical terms is included at the end (terms listed in the glossary are printed in *italic* in the text when used for the first time).

1. Basic principles of electrochemistry

Electrochemistry describes the use of chemical reactions to produce electricity and the use of electricity to produce chemical change (Atkins, 1989). An example of the first is the galvanic cell or ordinary battery, where an electrical *current* is generated via controlled chemical reactions. Electricity is also used to produce a reaction, for example in silver plating, where a thin film of silver is deposited on a metal by applying a current (= *electrolysis*). These techniques all require a comparatively simple electrochemical system with two electrodes of opposite charge (figure 1). One electrode is the *cathode*, where reduction takes place; the other is the *anode*, and here oxidation occurs. *Electrons* leave the *cell* through the anode (hence the minus sign in the figure), travel through the external circuit, and enter the cell again through the cathode (hence the plus sign) where they bring about reduction (Atkins, 1989). The electrodes are usually suspended in a salt solution (the *electrolyte*) where the ions can move freely between the two electrodes.

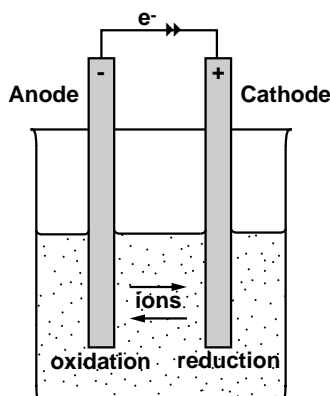


Figure 1: Set-up of a standard electrochemical cell.

The amount of energy released by the movement of electrons is called the *potential*. A high cell potential signifies that the cell reaction has a strong tendency to generate a current of electrons. By measuring the cell potential with a voltmeter, we can deduce the type of reaction occurring in the cell. However, electrochemistry has a wider application than mentioned above. It can be used to study the mechanism and kinetics of reactions that require an exchange of electrons (redox reactions). For this type of application the electrochemical system has to be expanded. The system should contain three electrodes suspended in one electrolyte (figure 2). One electrode is the *working electrode*, at which the reaction will occur, the second electrode is the *counter electrode*, which acts either as a sink or distributor of electrons, and the third electrode is the *reference electrode*. The potential of a cell is measured by a voltmeter, which must be connected to two terminals, i.e. it measures the difference between the two. This means that the potential of a single electrode can never be measured, unless a reference electrode is used to which we assign a zero potential. The reference electrode represents a standard potential to which the reaction potential of the working electrode can be compared.

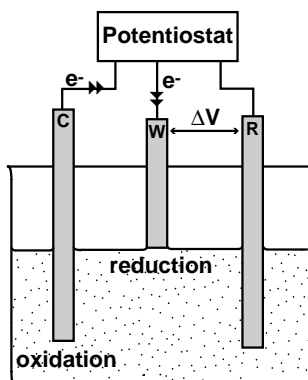


Figure 2: Set-up of a standard electrochemical cell used in voltammetry. C is the counter electrode (usually a Pt wire), W is the working electrode (usually a PIGE), and R is the reference electrode (usually SCE). All electrodes are connected to a potentiostat, which regulates the potential of the working electrode and measures the current. By adjusting the potential, reductive dissolution can occur at the working electrode, causing current to flow between counter and working electrode.

Because the reactivity of a compound depends on its composition and structure, this information can be deduced from electrochemical measurements (Scholz and Meyer, 1998). Thus, information on the concentration, dissolution behaviour and chemical state of the reactants, as well as the reaction kinetics and mechanism can be obtained (Scholz and Meyer, 1998). This is achieved by using the Nernst equation, the standard electrochemical equation (for a derivation and discussion, see Atkins, 1989):

$$E = E^0 - \frac{RT}{nF} \ln Q = E^0 - \frac{0.0592}{n} \log Q \quad (19.)$$

Where E stands for cell potential [V], E^0 is the standard cell potential [V], R is the gas constant [8.3143

$\text{J}\cdot\text{K}^{-1}\cdot\text{mol}^{-1}$], T is temperature [K], n is the amount of electrons used in the reaction, F is Faraday's constant [$9.64853\cdot 10^4 \text{ C}\cdot\text{mol}^{-1}$], and Q is the reaction quotient which expresses the ratio of dissolved product versus dissolved reactant. The Nernst equation is used for the determination of the concentration of the reactants and products in the cell, or for the prediction of the cell potential from the concentration of reactants in the electrolyte.

2. Voltammetry of microparticles

2.1 Introduction and brief history

In *voltammetry*, the current at an electrode is measured as a function of the potential applied to the electrode. If a voltammetric measurement is made using a mercury drop electrode, the method is termed polarography, when solid electrodes are used the method is called voltammetry. Electrochemical techniques are commonly used to analyse species in solution, however, voltammetry of microparticles (VMP) involves the electrochemical analysis of solid particles.

Initially, much of the electrochemical research was focused on detection and analysis of aqueous species, and it was believed that it is difficult to carry out electrochemical experiments on solid phases. The result would depend too much on the state of the surface studied, its crystallographic orientation, its chemical or electrochemical pre-treatment, and the adsorption of foreign compounds (Scholz and Meyer, 1998). Nevertheless, the development of electrography by Glazunov and Fritz (Jirkovsky, 1934) had shown that electrochemical analysis of solids can be reliable and reproducible. This technique could thus be used to study solid material, and from this moment other researchers have tried to optimise the identification of solids by electrochemical methods (Allen et al., 1979; Brainina and Vydrevich, 1981; Scholz et al., 1989a; Grygar et al., 1995). The electrochemical methods can be complementary to standard tools for identification of powdered solids (such as X-ray diffraction, IR-spectroscopy, or Mössbauer spectroscopy). In addition, they are also rapid, simple, and work on a microscale. Ideally, the methods are useful for analysing metal alloys, pigments, superconductors, and pure minerals, but application to mixtures of inorganic compounds or even natural soil and rock samples should also be possible. For example, the method was used to test the electrochemical corrosion behaviour of dental amalgams of different compositions at varying pH (Scholz and Meyer, 1994).

Since the 1950's several types of electrode have been developed for solid state electrochemistry. All methods involve an electrode containing the compound to be studied, usually mixed with graphite. These are called *compact electrodes* and *carbon paste electrodes*. Adams (1958) was one of the first to make a compact electrode which consisted of a mixture of magnetite, graphite and paraffin wax pressed together to form a cylinder. He used the electrode to study the electrochemical behaviour of magnetite. This mineral plays an important role in the formation of the protective oxide layers, which form on steel in high-pressure aqueous environments. Many people followed his example and used compact electrodes to study the electrochemical behaviour of solids (Hickling and Ives, 1975; Allen et al., 1979; Allen et al., 1980; Brainina and Vydrevich, 1981).

These methods were very successful in the analysis of solids, but they could only be used on solids that were metals, alloys or semiconductors. In 1989, Scholz and co-workers introduced a new method where

the solid was not incorporated into the working electrode but immobilised on the electrode surface (Scholz et al., 1989a). They used a paraffin impregnated graphite rod (*PIGE*) as working electrode, and deposited the sample onto the lower end of the electrode. This was subsequently placed in an electrolyte and subjected to a voltammetry technique, which involves a stepwise increase or decrease in potential while the current of the system is monitored. This method was named voltammetry of microparticles (*VMP*).

With this new technique, information on the electroactive compounds in the sample can be obtained by scanning over a certain potential range and looking for peaks in the current. If there are none, then there was no reaction. When peaks in current do occur, the potential is indicative of the compounds that have reacted, and the peak area is directly proportional to the amount of this electroactive species (Kissinger and Heineman, 1984).

2.2 Procedure

The procedure for voltammetry of microparticles is discussed in detail by Scholz and co-workers in several publications (1989a; 1994; 1998). The following subsections give a short description of the electrode and sample preparation, the voltammetric measurement, and the cleaning of the electrode.

2.2.1 *PIGE* (electrode) preparation

Before the electrode is used, it is impregnated with paraffin. This will help keep down the background current and prevents contamination of the electrode with dissolved species from the electrolyte. For the impregnation, a graphite rod of ~ 5 cm length and ~ 5 mm diameter is placed in a container with molten paraffin. Subsequently, the air is pumped out of the container to create a vacuum atmosphere, this will facilitate the impregnation of the graphite by the molten paraffin. When air bubbles stop evolving from the electrode, it is fully impregnated. The electrode is taken out of the paraffin and cooled on filter paper. After cooling, the lower end of the electrode (which will be used to deposit the sample onto) is carefully polished on ordinary smooth notebook paper or filter paper. The other end of the electrode is connected to the *potentiostat* with a crocodile clip.

Samples are ground to fine powder in a mortar, which is especially important when a mixture of electroactive compounds is studied (the rule when dealing with natural samples), to prevent preferential uptake of one compound by the electrode (Scholz and Meyer, 1998). The powdered sample is placed on a flat surface (preferably filter paper) and the electrode is rubbed over the sample spot. In this way, the sample particles are embedded in the soft surface of the graphite electrode. The total amount of sample that is thus transferred onto the lower end of the electrode lies in the range of 0.1–2 μg (Grygar, 1995). By mixing an internal standard (with known mass and peak potential) into the sample before applying it to the electrode, it is possible to (semi-) quantitatively analyse the sample composition.

2.2.2 Measurement

The cell is prepared following the diagram in figure 2. The working electrode is dipped into the electrolyte solution and then slightly raised to make the solution adhere to the electrode surface. When the electrode is dipped deeper into the electrolyte, it will cause an increase in the background current as well as deteriorate the reproducibility of the experiment. For reductive dissolution of the sample, the potential of the system is varied at a constant *scan rate* (v) from more positive to more negative and thus more reducing

values (EG & G, 1984), and the resulting current is measured. The scan rate is usually in the range of 1–50 mV/sec. A high scan rate will increase the peak current (see also equation 21), but it will simultaneously decrease the time in which a certain reaction can occur. This may distort the peaks into barely distinguishable kinks in the background current. Conversely, a low scan rate will increase the background current, therefore it is best to empirically determine the optimum scan rate for each experiment.

The range of the potential is limited to the chemical characteristics of the electrolyte. Since the electrolyte is usually an acid dissolved in water, the potential is limited by the reduction of H^+ to H_2 at potentials beyond -1 V against a *saturated calomel electrode* (SCE). This reaction causes an exponential increase in the background current.

For a current to flow between the working and counter electrodes, a reaction must take place (EG&G). The plot of the potential versus the current is called a *voltammogram* (for an example see figure 3). The current peaks and starts to decrease when a significant amount of the reacting species is consumed. Each peak occurs at a potential characteristic of the reacting species, the type of supporting electrolyte, and the type of working electrode (EG&G). Depending on the scan rate, the potential range, reaction kinetics, and particle size, the voltammetry measurement is usually very rapid and can be performed in 10 minutes or less (Scholz et al., 1989a). After the measurement, the electrode is cleaned by rubbing it on filter paper. Whether the cleaning was sufficient, can be tested by measuring a voltammogram of the cleaned electrode; this should give no peaks. The same electrolyte solution can be used for numerous analyses.

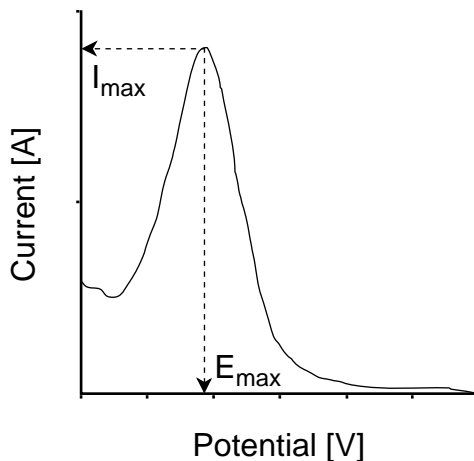


Figure 3: Example of a voltammogram. The horizontal axis represents the potential range, and the vertical axis is the resulting current. E_{\max} is the mineral specific reaction potential, where current peak height is maximum (I_{\max}).

2.3 Advantages of VMP over previous methods

The advantages of the VMP method are considerable: the same electrode can be used to study several different solids, or several subsamples from the same solid. Single solids as well as mixtures of electroactive compounds can be analysed, thus the method can be used on synthetic as well as natural material (Scholz and Meyer, 1998).

The success of solid-state electrochemistry, however, depends on two factors. First, the small sample volume will induce localised production or consumption of comparatively large amounts of electric charge by the reacting solid, which may lead to bad signal resolution. The second problem is the possibility of low electrical conductivity of the working electrode, which can lead to an undesired build-up of charge at the end of the electrode. To circumvent these difficulties, one should use as little sample amount as possible to allow the best possible electric contact between the sample and the working electrode. The VMP method meets these two requirements, because the sample is embedded into the working electrode surface, and contact between electrolyte and working electrode is limited to the surface on which the sample is embedded.

Several different electrodes (such as glassy carbon electrodes, metal electrodes and basal plane pyrolytic graphite electrodes) have been tested for use in VMP, but the PIGE still is the most universal (Scholz and Meyer, 1998). Graphite is an inert conductor, therefore the PIGE has a wide potential range, and consequently a wide analytical range. The wax in the PIGE inhibits pollution of the electrode by salts from the electrolyte, it reduces the residual currents, and it improves reproducibility (Kissinger and Heineman, 1984). VMP is applicable to a wide range of scientific questions: it can be used to identify mineralogical composition, and to study dissolution mechanisms and kinetics. Moreover, the results can be used to derive specific mineralogical or crystallographic information, such as isomorphous substitutions and defects in the crystal lattice (Grygar, 1996a).

3. VMP in electrochemistry and environmental magnetism

A number of metal oxides and hydroxides can be reductively dissolved to form soluble species with a lower oxidation state, rather than being reduced to the elementary metal. Therefore, these oxides are very suitable for analysis with VMP, a good example of these are iron(oxy)(hydr)oxides (Scholz and Meyer, 1998).

Grygar (1995) has studied the reductive dissolution behaviour of several synthetic iron oxides and (oxy)hydroxides (hematite, magnetite, maghemite and goethite). He found that these minerals could be reductively dissolved from the working electrode at different potentials typical of each phase (Table 1),

Compound	E_{\max} [mV]
hematite	-400
magnetite	-60
maghemite	0
goethite (two peaks)	-80 & -220
ferrihydrite	105 to 0

Table 1: Peak potential for several synthetic iron oxides and hydroxides. With Ag/AgCl reference electrode, OIGE (silicon oil impregnated graphite electrode) working electrode, scan rate 10 mV/sec, and electrolyte: 0.1 M HClO₄ + 0.1 M NaClO₄ (after Grygar, 1995).

illustrating the diagnostic power of the VMP technique. For example, the dissolution of goethite was shown to be governed by its structure and shape (Grygar, 1995; Grygar et al., 1995). The voltammogram of goethite contains two peaks at different potential (~ -80 mV and ~ -220 mV vs. Ag/AgCl standard reference electrode), the occurrence of these peaks is related to the dominant type of crystalline planes in the goethite. Particles with a well-developed (021) plane dissolve extremely slow at ~ -80 mV and only show the second peak. Conversely, particles with well-developed (110) and (010) planes dissolve rapidly at ~ -80 mV and do not show the second peak (Grygar et al., 1995).

It is possible to quantify concentrations of different minerals within a mixture, by making a calibration curve with mixtures of known amounts of well-defined minerals (Grygar, 1995; Grygar et al., 1995). Grygar also deduced which parameters in a voltammogram were influenced by grain shape, size and homogeneity (Grygar, 1996a). The width and the height of the voltammetric peak are related to the homogeneity of the sample (γ) as well as the *charge-transfer coefficient* (α), while the potential of the voltammetric peak depends on the charge-transfer coefficient and the rate constant at the reference potential (k_0) (Grygar, 1996a; Grygar, 1996b). Grygar (1996a) showed that the overall reaction rate of a mixture of particles with a continuous uniform distribution in grain size or surface reactivity can be written as:

$$I = kQ_0 \left(\frac{Q}{Q_0} \right)^\gamma \quad (20.)$$

With I denoting the current of the reaction [A], Q the *charge* during the course of the reaction [A·sec], Q_0 the charge at the onset of the reaction [A·sec], k the *rate constant* [sec^{-1}], and γ the *homogeneity factor*. The homogeneity factor is related to the grain-size distribution and the composition of the sample. When γ is high, the grain-size distribution or the composition of the sample is very heterogeneous. This homogeneity factor can be determined by plotting $\ln(I/k \cdot Q_0)$ vs. $\ln(Q/Q_0)$ (as follows from equation 20). This yields a straight line, the slope of which is the homogeneity factor γ .

The height and width of the peak are related to the charge-transfer coefficient α and to the homogeneity factor γ . Grygar (1996a) showed empirically that for synthetic iron oxides this relation is:

$$\left(\frac{I_p}{Q_0} \right)_{meas.} = 0.2 \frac{\alpha n F}{RT} \nu (1 - 0.5 \ln \gamma) \quad (21.)$$

Here, I_p is the peak current and Q_0 the charge at the start of the experiment, α is the charge-transfer coefficient and n is the number of electrons in the reaction, F is Faraday's constant, R is the gas constant and T is the absolute temperature. The parameter ν is the scan rate, and γ is the homogeneity factor. A plot of $\gamma(I_p/Q_0)$ vs. potential (as forced by the potentiostat) will give the reaction peak. When γ increases (indicating increased heterogeneity of the sample), the height of the peak decreases, while its width increases (figure 4). The peak height will also increase as a consequence of higher γ (indicating more reactive species).

The position of the peak potential is not related to the homogeneity of the sample, but only to its reactivity (expressed in α) and the rate constant at the potential of the reference electrode (k_0). The rate

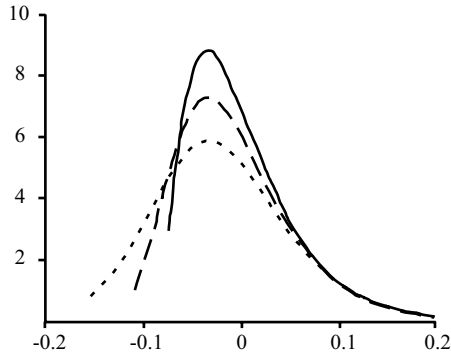


Figure 4: example of the changes in voltammetric peak shape with different values for the homogeneity factor (γ). The curves were calculated for charge-transfer coefficient (α) = 0.5, rate constant at reference potential (k_0) = $1 \cdot 10^{-2} \text{ sec}^{-1}$ and scan rate (ν) = 1 mV/sec. The solid line had a γ of 2/3, the dashed line a γ of 1 and the dotted line had a γ of 1.5. (after Grygar 1996b).

constant k is related to k_0 and the potential E by the following equation:

$$k = k_0 \exp\left(-\frac{\alpha n F}{RT} E\right) \quad (22.)$$

From this, we can derive an equation describing the dependence of the peak potential on α and k_0 :

$$E_p = E_0 - \frac{RT}{\alpha n F} \ln\left(\frac{\alpha n F}{RT} \nu\right) + \frac{RT}{\alpha n F} \ln(k_0) \quad (23.)$$

This equation has been derived to describe the position of the voltammetric peak during the reaction of solid monodisperse particles. However, Grygar has shown that the equation can be applied to the voltammetric dissolution of a variety of particles, when γ is used to characterise the particle homogeneity and phase composition (Grygar, 1996a; 1996b). For the complete derivation of these equations we refer to Grygars work (Grygar, 1995; 1996a; Grygar et al., 1995).

The results of the electrochemical studies of reductive dissolution, and comparison with normal reductive dissolution experiments, have shown that there is a close similarity between chemical and electrochemical dissolution of iron oxides, including the relative reactivity of individual iron oxides and influence of the particle size (Grygar, 1997). Electrochemical methods are therefore a valid tool for studying reductive dissolution.

In environmental magnetism, qualitative and quantitative identification of the magnetic minerals is essential to a successful understanding of the mineral-magnetic climate proxies. As noted in previous chapters, the strongly magnetic ferrimagnetic minerals often suppress the expression of other magnetic minerals. By careful application of a number of different rock-magnetic techniques, the magnetic mineralogy of a sample can be derived. However, this is a time-consuming procedure, and unfortunately often yields non-unique results. In principle, the VMP method makes it possible to derive the composition

and characteristics of the magnetic minerals in a matter of minutes. For weakly magnetic material such as hematite and goethite, VMP could complement standard mineral-magnetic techniques. However, the method has as yet only been tested on synthetic material. In the next chapters, we present the results of a pilot study of the method applied to natural samples.

Glossary of terms (Units between parentheses where appropriate)

Anode	= electrode at which oxidation occurs, and where electrons leave the cell.
Carbon paste electrode	= electrode made of high-quality graphite powder mixed with organic binders, such as silicone oil, to form a paste. In modified carbon paste electrodes, the sample is mixed into the paste.
Cathode	= electrode at which reduction occurs, and where electrons enter the cell.
Cell	= an electrochemical system, usually consisting of a container with electrodes that are suspended in an electrolyte.
Charge (Q)	= current \times time = measure of the number of electrons involved in the reaction, [C].
Charge-transfer coefficient (α)	= the speed at which an electron is transferred from one material to another.
Compact electrode	= electrode made up of the sample, a chemically inert electrical conductor and a binding agent, all pressed together to form a cylinder.
Counter electrode	= the electrode which provides the current path in an electrochemical cell.
Current (I)	= magnitude of the electron flow in a system [A].
Electrolyte	= a conductive solution in which the electrochemical reactions of interest take place.
Electrolysis	= the use of an electric current to bring about a chemical reaction.
Electron (e^-)	= negatively charged subatomic particle.
Homogeneity factor (γ)	= parameter that reflects the homogeneity of the sample (grain size, mineralogy)
PIGE	= paraffin impregnated graphite electrode, used in voltammetry of microparticles.
Potential (E)	= amount of electrical force or energy in a system [V].
Potentiostat	= an electrochemical instrument which controls the potential applied to the working electrode.
Rate constant (k or k_0)	= rate determining factor that influences the current at the peak potential of a reaction [sec^{-1}]
Reference electrode	= the electrode against which the potential of the working electrode is measured.
Scan rate (v)	= the speed at which the potential is being changed [V/sec].
SCE	= saturated calomel electrode, commonly used reference electrode
VMP	= voltammetry of microparticles.
Voltammetry	= measurement of the change in current in an electrochemical cell when the potential of the working electrode is changed.
Voltammogram	= a plot of the potential versus the current detected during voltammetry
Working electrode	= the electrode where the reaction of interest takes place.

Detection of Low Concentrations of Fine-Grained Iron Oxides by Voltammetry of Microparticles

Mineralogical discrimination of iron oxides in soils and sediments is not a trivial task, mainly because of their small grain size and low concentrations. With mineral-magnetic techniques, highly magnetic ferrimagnetic spinels can be determined with a very low detection limit (~10 ppm). Unfortunately, the magnetic signal of natural samples is often dominated by magnetite, and in particular the expression of weakly-magnetic antiferromagnetic minerals is suppressed by this high signal. In contrast, electrochemical techniques, such as voltammetry of microparticles (VMP) are not affected by these differences in magnetic signal.

VMP makes use of the electrochemical law that iron(oxy)(hydr)oxides can be reductively dissolved at potentials that are specific for their mineralogy and reactivity. Therefore, by scanning over a potential range and monitoring the potential at which a reaction occurs, one can specify the type of minerals present. VMP can be applied to samples without requiring any form of pre-treatment. The method is rapid, comparatively straightforward to interpret, and requires little amount of sample (micrograms). However, the detection limit of VMP on natural samples has not yet been investigated. Here, we present a pilot study of the use of VMP in the identification of the ferric oxides of natural samples from Spanish red beds of Miocene age. A standard addition method with pyrolusite enabled semi-quantitative analysis of the samples; concentrations of (anti)ferromagnetic iron(oxy)(hydr)oxides down to ~0.1 wt% could be detected.

1. Introduction

Qualitative and quantitative identification of magnetic minerals is essential to a successful understanding of mineral-magnetic climate proxies. The presence of strongly magnetic ferrimagnetic minerals in a sample – the rule in natural samples – suppresses the expression of the weakly magnetic antiferromagnetic minerals. By careful application of a number of different rock-magnetic techniques (i.e. first-order-reversal-curve (FORC) analysis, isothermal remanent magnetisation (IRM) component analysis, thermomagnetic analysis, and determination of the frequency dependence of susceptibility), the magnetic mineralogy of a sample can be derived. However, this is a fairly time-consuming procedure, and it unfortunately does not always yield unambiguous results. More generally applied mineralogical identification methods such as X-ray diffraction and Mössbauer spectroscopy, are often not suited for use on natural material, because the magnetic components are of low concentration and usually fall below the detection limit of these techniques. Conversely, selective extraction methods have yielded promising results for the identification of the magnetic carriers in natural samples (Fine et al., 1993a; Sun et al., 1995; van Oorschot et al., 2001). However, these methods still require additional mineral-magnetic techniques for a complete understanding

of the sample composition. To avoid possible ambiguity in the interpretation, as well as laborious analytical procedures, a mineral-specific analytical technique is needed, which can identify different types of magnetic minerals, even at low concentrations.

Voltammetry of microparticles

Electrochemistry describes the use of chemical reactions to produce electricity, and the use of electricity to produce a chemical change (Atkins, 1989). Thus, it can be used to study the mechanism and kinetics of redox reactions. For a long time, it was generally accepted that only species in solution could be studied with electroanalytical techniques. However, in 1989, Scholz and co-workers (1989a) introduced a method of sufficient reproducibility and lucidity, where the solid sample was immobilised on the electrode surface and subsequently analysed. This method was named abrasive stripping voltammetry (AbrSV), later the name was changed to voltammetry of microparticles (VMP).

With VMP, information on the electroactive compounds in the sample is obtained by scanning over a specified potential range and looking for peaks in the current, which indicate the occurrence of electrochemical reactions. The current peaks and starts to decrease when a significant amount of the reacting species is consumed. The plot of the potential versus the current is called a voltammogram or VA curve. The peak potential is indicative of the compounds that have reacted, and the peak area (or charge) is proportional to the amount of electroactive species (Kissinger and Heineman, 1984). In this way, information on the concentration and chemical state of the solid reactants, as well as on the reaction kinetics and mechanism can be obtained (EG&G; Scholz and Meyer, 1998). Voltammetry is complementary to standard techniques for identification of powdered solids (e.g. X-ray diffraction, IR-spectroscopy, Mössbauer spectroscopy), but it is also rapid, simple, and works on a microscale. It is suitable for analysing metal alloys, pigments, superconductors, and pure minerals, but application to mixtures of inorganic compounds or even natural soil and rock samples is possible as well (Scholz and Meyer, 1998).

Grygar (1995) studied the reductive dissolution behaviour of several synthetic iron oxides and oxyhydroxides (hematite, magnetite, maghemite and goethite) with VMP. He found that these minerals are reductively dissolved from the working electrode at different potentials typical of each phase, illustrating the diagnostic power of this technique. It is also possible to quantify concentrations of different minerals within a mixture, by making a calibration curve with mixtures of known amounts of well-defined minerals (Grygar, 1995; Grygar et al., 1995). Comparison of the results of the electrochemical studies of reductive dissolution with normal reductive dissolution experiments has shown that there is a close similarity between the chemical and electrochemical dissolution of iron oxides, including the relative reactivity of individual iron oxides and the influence of the particle size. Electrochemical methods are therefore a valid alternative to more laborious and time-consuming methods of mineral identification through selective dissolution.

VMP could make it possible to derive the composition and characteristics of the ferric oxides in a sample within a matter of minutes. Furthermore, the technique is simple and no sample pre-treatment is required (apart from grinding in a pestle and mortar). In particular for weakly magnetic material such as hematite and goethite, VMP would complement standard mineral-magnetic techniques. However, the method has as yet only been tested on synthetic material and on some lateritic samples containing high concentrations of iron oxides (Grygar, 1997; 1998; Grygar et al., 1997). Here, we present the results of a pilot study concerning the analysis of the magnetic mineral composition in natural samples containing low concentrations of Fe_2O_3 .

2. Experimental procedures

2.1 Samples and magnetic methods

Samples were taken from a 25 m long transect of continental red bed deposits in La Gloria, Teruel basin, Spain (Figure 1a). This section dates from the Middle to Late Miocene (~8.3 – ~11.4 Ma), and consists mainly of red silty clays with intercalations of red sands and conglomerates which are capped by white lacustrine limestones (Krijgsman et al., 1996) (Figure 1b). During red bed deposition, the climate in the Teruel Basin was warm and semi-arid to arid (Alonso-Zarza and Calvo, 2000). The samples are labelled as GLOxxA, with xx the number of the sample starting with 01 at the bottom of the section. The samples used in this study come from an interval close to the middle of the transect at ~10 m stratigraphic level, this part of the section was formed in the Late Miocene (~9.8 Ma), and contains an alternation of red clay, red sands and sandy conglomerates. In Table 1, some geochemical and lithological characteristics of the samples are presented.

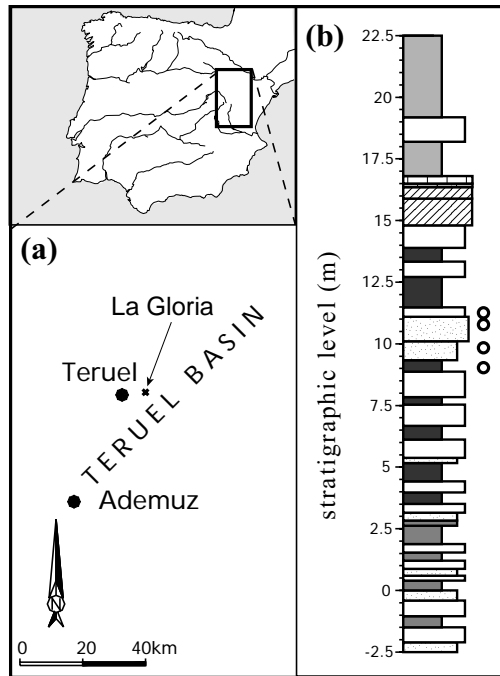


Figure 1: (a) Topographical map of the location, the inset (b) shows the lithological column. The La Gloria section consists of a sequence of red clays (black and grey) intercalated with red sands (dotted) and limestones or caliches (white). The open circles adjacent to the lithological column, indicate the levels from which samples were taken for this study.

The magnetic composition of the samples was analysed by isothermal remanent magnetisation (IRM) component analysis and first-order reversal curve (FORC) distribution analysis. The samples (1–2 gr) for IRM component analysis were weighed into plastic cylindrical cups and mixed with epoxy resin (Araldit

Sample code	stratigraphic level [cm]	lithology	colour	CaCO ₃ [wt%]	Fe	Al	k [10 ⁻⁶ SI]
GLO059A	900	dark red clay	5YR4/8	4.6	~ 3 wt%	~ 6 wt%	230
GLO062A	975	sandy red clay	5YR4/4	1.2	~ 1 wt%	~ 2.5 wt%	50
GLO065A	1080	limestone	5YR6/4	41.0	-	-	110
GLO066A	1120	caliche	5YR5/6	18.2	-	-	150

Table 1: Some lithological, mineral-magnetic and geochemical parameters of the samples used in this study. Colour is categorised with Munsell's system for soil colour, iron and aluminium content of the samples is determined with total destruction (dissolution in HF, HNO₃ and HClO₄). Minus signs are given when no data was acquired.

D, Hardener HY956, Ciba Specialty Chemicals). IRM was induced by a PM4 pulse magnetiser and measured with a JR5A spinner magnetometer (AGICO). The sensitivity of the spinner magnetometer is $\sim 2.7 \cdot 10^{-11}$ Am², the minimum IRM measured during our experiments was at least two times stronger. IRM acquisition curves (completely saturated) were analysed with the Cumulative Log Gaussian (CLG) programme of Kruiver et al. (2001) and the automated analysis method by Heslop et al. (2001) to determine magnetic coercivity components in the samples. This involves fitting of a measured IRM acquisition curve with a number of logarithmically distributed coercivity distributions, each characterised by their midpoint ($B_{1/2}$), spreading or dispersion, and magnetic concentration. A statistical test is provided to determine the number of distributions required for an optimal fit.

For the FORC analysis, samples (~ 10 mg) were mixed with epoxy resin and cast in Teflon moulds, which resulted in cylindrical samples with a diameter of ~ 1.5 mm and a length of maximum ~ 2 mm. Data acquisition was performed on an alternating gradient magnetometer (Micromag), and the results were plotted in a FORC diagram according to the methods described by Pike et al. (Pike et al., 1999; 2001; Roberts et al., 2000). A FORC distribution is a contour plot that allows the user to separately evaluate magnetic hardness and interaction in a sample. The horizontal axis ($\mu_0 H_u$) represents the coercivity, and the vertical axis ($\mu_0 H_v$) represents the magnetic interaction in the sample.

2.2 VMP procedure

The procedure for voltammetry of microparticles is discussed in detail by Scholz and co-workers (1989a; 1994; 1998). The following is a short description of the electrode and sample preparation, the voltammetric measurement, and the cleaning of the electrode. The specific settings for analysis of iron oxides were discussed by Grygar (1996b; 1996a; 1997; 1998; Grygar and Ruan, 1998), and a brief summary of the settings is given in Fig. 2. Calculation of the concentration of measured compounds is done by using an internal standard as proposed by Grygar and van Oorschot (in press, see also Chapter 9), the details are discussed in subsection 2.2.3.

The sensitivity of the VMP technique is essential for the purpose of application to natural samples. We tested the sensitivity by comparing untreated samples and samples that were extracted for a maximum of four times with the acid-ammonium-oxalate/ferrous-iron extraction method described by van Oorschot and Dekkers (2001, see also Chapter 3). Previous mineral-magnetic studies have shown that this method preferentially attacks very fine-grained ferrimagnetic iron oxides, and thus enhances the magnetic signal of weakly magnetic antiferromagnetic hematite and goethite (van Oorschot et al., 2001).

2.2.1 Preparation of the PIGE electrode and electrochemical cell

In VMP, the background current must be kept as low as possible. This current is partly controlled by the electrical conductivity of the working electrode. By using a good conductor (such as graphite) the background current is kept low. To further reduce the background current and to prevent contamination of the working electrode by material uptake from the electrolyte solution, paraffin impregnated graphite electrodes (PIGE) are used (Scholz and Meyer, 1998). A graphite rod of ~ 5 cm length and ~ 5 mm diameter is placed in a container with molten paraffin. Subsequently, the air is pumped out of the container to create a vacuum atmosphere, and thus facilitate the impregnation of the graphite by the molten paraffin. When air bubbles stop evolving from the electrode (after a few tens of minutes up to a few hours, depending on the original porosity of the graphite), it is fully impregnated. The electrode is taken out of the paraffin and cooled on filter paper. The lower end of the PIGE (which will be used to deposit the sample onto) is carefully polished on filter paper. The other end of the electrode is connected to a potentiostat with a crocodile clip.

The samples are ground to fine powder in an agate mortar to prevent preferential uptake of one compound by the electrode, this is especially important when a mixture of electroactive compounds is studied (the rule when dealing with natural samples) (Scholz and Meyer, 1998). A small amount (mg) of the powdered sample is placed on a flat surface (preferably filter paper) and the electrode is rubbed over the sample. In this way, the sample particles are embedded into the soft surface of the graphite electrode. The total amount of sample that is in this way transferred onto the lower end of the electrode lies in the range of $0.1\text{--}2\ \mu\text{g}$ (Grygar, 1995). By mixing an internal standard (with known mass and peak potential) into the sample before applying it to the working electrode, it is possible to quantitatively analyse the sample composition (Grygar and van Oorschot (in press), see also subsection 2.2.3).

The PIGE is the working electrode on which the reactions take place. The electrochemical cell (Fig. 2)

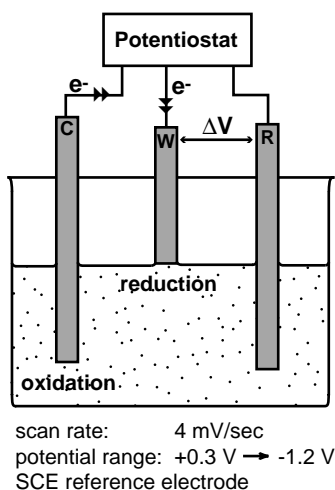


Figure 2: Schematic representation of the electrochemical cell used in this study. 'C' is the counter electrode (platinum wire), 'W' is the working electrode (PIGE) and 'R' the reference electrode (saturated calomel). The potentiostat controls the potential of the working electrode and measures the current flowing through the electrode. The electrolyte is a de-aerated mixture of acetic acid and acetate (1:1), with a total concentration of 0.2 M acetate.

further consists of a platinum wire, which serves as counter electrode and provides electrons necessary for the reduction of iron. The reference electrode is a saturated calomel electrode (SCE), the supporting electrolyte is a N₂-deaerated acetate buffer (acetic acid: acetate ratio 1:1, total acetate 0.2 M).

2.2.2 Measurement

The PIGE working electrode is dipped into the electrolyte solution and then slightly raised to make the solution adhere to the electrode surface. When the electrode is dipped deeper into the electrolyte during measurement, it will cause an undesired increase in the background current and therefore worsen reproducibility. For reductive dissolution of the sample, a potentiostat (μ Autolab, EcoChemie) is used to vary the potential of the system at a constant scan rate, from more positive to more negative and thus more reducing values (EG&G, 1984), and the resulting current is measured. The potential range is limited to the chemical characteristics of the electrolyte. Since the electrolyte is usually an acid dissolved in water, the negative frame of the potential window is limited by the reduction of H⁺ to H₂ at potentials beyond -1 V vs. SCE. This reaction causes an exponential increase in the background current. In this study, the potential range was set between 0.3 and -1.2 V against SCE. Despite the rapid increase in background current over the -1 to -1.2 V interval, sometimes peaks could be discerned in this range. The scan rate in VMP is usually in the range of 1–50 mV/sec. A high scan rate increases the peak current, but it also decreases the time in which a certain reaction can occur. This can cause distortion of the peaks to barely distinguishable kinks in the background current. On the other hand, a low scan rate will increase the background current, therefore it is best to empirically determine the optimum scan rate for each study. Here, the scan rate was set at 4 mV/sec.

Depending on the scan rate, the potential range, reaction kinetics, and particle size, a voltammetry measurement is usually very rapid and can be performed in 10 minutes or less (Scholz et al., 1989a). The maximum measurement time in our experiments was ~6 minutes per scan. The samples all reacted fully in one scan, all consecutive scans were similar in shape and showed only the background current. To reduce the contribution of the background current, we scanned each sample twice and subtracted these two currents.

After the measurement, the electrode is cleaned by rubbing it on filter paper. Whether the cleaning was sufficient can be tested by measuring a voltammogram of the cleaned electrode, this should give no peaks. From time to time it is recommendable to use a fine abrasive material for electrode cleaning. Here, we used SiO₂ powder (particle size ~10 μ m) on a filter paper. The cleaned electrode can be used again to measure other samples. Because of the cleaning and polishing of the electrode surface, the PIGE will gradually decrease in size after each experiment. This has no significant effect on the measurement, and each electrode can be used numerous times. The same is valid for the electrolyte solution; because the ratio of solution to solid is very high, numerous analyses can be performed before the electrolyte is saturated or interferes with the analysis.

2.2.3 Qualitative analysis and semi-quantitative analysis

Qualitative analysis. To identify the ferric oxide species in the samples, we compared their peak potentials to those of synthetic samples of known composition. These samples were made from synthetic iron oxides mixed into a quartz matrix with iron oxide contents varying between 0.1 and 3 wt-% (Table 2). Discrimination between goethite and hematite in the voltammograms is not straightforward, because of the overlap in the reaction potential range. Similar reactivity of both minerals can result in a similar reaction

Sample code	Original Ep vs. SCE [V]	Heated (300°C) Ep vs. SCE [V]	Enhancement factor
Ferrihydrite	-0.33	-0.33 *	2
Magnetite	-0.26 (sh), -0.92	-0.28 (sh), -0.85	3
Goethite 1	-0.72	-0.44 *	6
Goethite 2	-0.69	-0.40 *	11
Goethite 3	-0.54	-0.35 *	8
Goethite 4	-0.73	-0.60 *	7
Hematite 1	-0.76	-0.75	10
Hematite 2	-0.72	-0.71	10
Hematite 3	-0.76	-0.76	3
Hematite 4	-0.83	-0.83	4

* converted to hematite

Table 2: Synthetic samples used to determine specific reaction potentials of iron(hydr)oxides studied as well as for semi-quantitative analysis. All samples were mixed with quartz, and the concentration of iron(hydr)oxides varied between 0.1 and 3 wt%. The first column shows the peak potentials for the original samples, while the second column shows the change in peak potential after heating at 300°C for 15 min. The last column gives the relative enhancement of each signal compared to the signal expected from the peak height of the pyrolusite internal standard. All peak potentials were derived under the experimental conditions as described in the text.

potential. By heating the samples for 15 minutes at 300°C, goethite is converted to poorly crystalline hematite. This causes a shift of the peak potential toward more positive values (Grygar, 1996b). Comparison of the voltammograms of original and heated samples allows discrimination between these two minerals (Grygar and van Oorschot, in press).

Semi-quantitative analysis. The amount of sample deposited on the working electrode cannot be exactly determined, this complicates the quantitative evaluation of voltammetric curves. Grygar and van Oorschot (in press, see also Chapter 9) explored standard addition as a quantification method and judged pyrolusite ($\beta\text{-MnO}_2$) to be the best internal standard for the (semi-)quantitative analysis of iron(oxy)(hydr)oxides. Mn(III,IV)-oxides are reductively dissolved under similar conditions as iron oxides (Bakardjieva et al., 2000) but at potentials by at least 0.5 V more positive (all potentials mentioned are valid for the experimental conditions as described in the previous sections, and are measured against SCE). The pyrolusite peak occurs at +0.30 V, therefore there is no interference with the peaks from our samples (Figure 3a). However, VMP tests of the samples made with synthetic iron oxides and an internal standard, surprisingly showed that the peak heights of Mn- and Fe-oxide reductive dissolution were not in the proportion expected based on the oxide weight and the stoichiometry of the corresponding dissolution reaction. The areas of the iron oxide peaks were 2 to 10 times larger than theoretically expected (Table 2). Magnetite, ferrihydrite, and Al-doped hematite were least increased, while the peaks of goethite and pure hematite were enhanced 7 to 10 times. Because these ‘enhancements’ were reproducible, we used these factors in the quantification of our natural samples. The tests further showed that the VMP detection limit for the synthetic samples with quartz matrix is ~0.1 wt% for hematite and goethite.

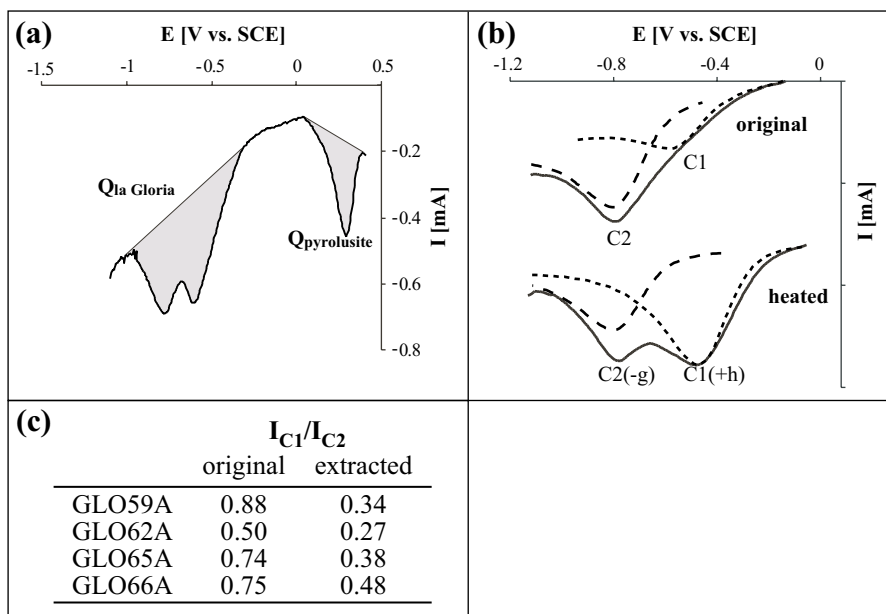


Figure 3: Example of the calculation of the iron oxide concentrations, as well as the contribution of the different oxides to the C2 peak. (a) shows a voltammogram of GLO62A, with pyrolusite added as an internal standard. The pyrolusite peak occurs at $\sim +0.3$ V (vs. SCE). The charge of the pyrolusite peak can be related to its concentration. Subsequently, the charge of the other peaks is used to make an estimate of the concentration of iron oxides in the sample. (b) shows an example of the calculation of the separate C1 and C2 signals from the total peak current of the overlapping two peaks. With Butler-Volmer fitting, the actual peaks are reconstructed (dotted line represents the C1 peak model curve, dashed line represents that of C2). The same is done for the voltammogram of the heated samples. The changes in the individual peak currents are related to the conversion of goethite to hematite upon heating, and can be expressed as I_{C1}/I_{C2} . Comparison of this ratio for the original and the heated sample can be used to calculate the contribution of goethite to the C2 peak. Here, I_{C1}/I_{C2} of the original samples reflects the ratio of poorly crystalline hematite to well crystalline (hematite + goethite), and the same ratio for the heated samples represents the ratio of (poorly crystalline hematite + converted goethite) to well crystalline hematite. (c) shows the difference in voltammogram of original and extracted samples as expressed by the current ratios. Here, the change in current ratio expresses the change in contribution of the poorly crystalline C1 hematite compared to the C2 species. The decrease in ratio reflects the decrease in contribution of the C1 species after extraction.

The voltammetric curves of all samples with the internal standard were processed with the GPES 4.4 code as supplied by the manufacturer of the potentiostat (EcoChemie). This programme is suitable for the evaluation of currents of fully separated peaks. However, voltammetric peaks overlapped in the la Gloria samples, therefore a different approach was used for these samples. A model fit with kinetics of the general reaction order between 0.9 and 1.5 was used. The model was based on Butler-Volmer kinetics of the charge transfer, combined with a finite amount of reactive sites on the dissolving surface as well as a continuous distribution of the size and reactivity of the dissolving particles (Grygar, 1996a; 1998). In this way individual peaks could be modelled (figure 3b) and from the changes in charges, the separate contributions of the peaks to the total signal could be calculated. Comparison of the I_{C1}/I_{C2} ratio between original and extracted samples gives an indication of the species that was dissolved by the AAO-Fe²⁺ extraction method (figure 3c).

3. Results

3.1 Magnetic measurements

The total SIRM values of these samples vary in the same way as their susceptibility, with high values for GLO59A and GLO66A and low values for GLO65A (Table 3). The behaviour of sample GLO62A is slightly different, with a minimum in susceptibility but not a minimum in SIRM. This suggests a different magnetic composition than the other samples, which was confirmed by the IRM component analysis. The magnetic composition of all samples is that of a two-component system with single domain (SD) to pseudo single-domain (PSD) magnetite and hematite or goethite. The contribution of magnetite ($B_{1/2} \sim 25$ mT) is ~ 45 - 50% , while that of hematite ($B_{1/2} \sim 450$ mT) is 50 - 55% . Because of the differences in magnetisation between magnetite and hematite/goethite, the concentration of the former must therefore be much smaller than that of the latter minerals. GLO62A deviates in magnetic composition; it has a higher contribution of magnetite ($\sim 72\%$ of the total SIRM) as well as a higher average coercivity for both components ($B_{1/2}$ of ~ 56 and ~ 660 mT respectively).

Original samples						
Sample code	k [10^{-6} SI]	Total SIRM [10^{-3} Am ² /kg]	component 1 [%]	$B_{1/2}$ 1 [mT]	component 2 [%]	$B_{1/2}$ 2 [mT]
GLO059A	230	3.73	43.4	26.3 (11 - 63)	56.6	427 (151 - 1202)
GLO062A	50	1.75	72.2	56.5 (19 - 170)	27.8	659 (347 - 1259)
GLO065A	110	1.41	43.9	26.3 (10 - 69)	51.1	479 (209 - 1096)
GLO066A	150	2.28	48.9	25.7 (12 - 55)	56.1	437 (162 - 1175)
samples after AAO-Fe ²⁺ extraction						
Sample code	k [10^{-6} SI]	Total SIRM [10^{-3} Am ² /kg]	component 1 [%]	$B_{1/2}$ 1 [mT]	component 2 [%]	$B_{1/2}$ 2 [mT]
GLO059A	135	2.89	42.9	91.2 (23 - 363)	57.1	416.9 (132 - 1318)
GLO062A	138	1.15	8.7	34.7 (15 - 81)	91.3	467.7 (166 - 1318)
GLO065A	112	1.16	40.5	32.4 (12 - 89)	59.5	524.8 (194 - 1413)
GLO066A	117	1.90	41.6	39.8 (15 - 110)	58.4	512.9 (170 - 1549)

Table 3: IRM component analysis for the samples before and after extraction. Component 1 is the soft magnetic component, component 2 is the hard component. Beside the total SIRM of the samples and the relative contribution of each component, $B_{1/2}$ is given as the average $B_{1/2}$ value plus or minus one standard deviation (in brackets).

After extraction with the AAO-Fe²⁺ method, the samples have lost part of both components and the contributions to the total signal have not changed greatly. However, in GLO62A, the dramatic change in relative contribution and $B_{1/2}$ of the soft component, indicates that here almost all fine-grained magnetite had been dissolved. For the other samples, the slight increase in $B_{1/2}$ of the soft component, suggests that part of the outer rims of the larger grains had been dissolved. Of the hard component, mostly poorly crystalline hematite was dissolved during extraction ($B_{1/2}$ increased slightly while its relative contribution

remains approximately constant). However, in the GLO62A samples, the contribution of the hard component increased considerably, while the $B_{1/2}$ decreased, this suggests the dissolution of goethite in these samples.

FORC diagrams are shown in Fig. 4. The presence of a soft magnetite component is evident as well as a much harder component. B_c of magnetite centres on ~ 16 mT in the FORC diagrams. Like in the IRM component analysis, the FORC diagram of GLO62A deviates from that of the other samples. The soft component shows a slightly lower B_c value, and there is a smoother transition toward the hard component. The magnetite could have a larger average grain size, it has a broader vertical spread in contours than the other GLO samples, indicating more interaction. There is more contour density closer to the left-hand side of the plot hinting at the presence of finer grains, possibly including SP grains.

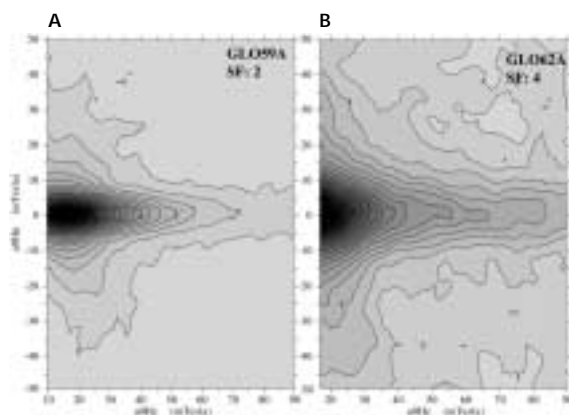


Figure 4: FORC diagrams of La Gloria samples. The distribution along the horizontal axis is an indication for grain size (coercivity), while the distribution along the vertical axis represents magnetic interaction within the samples. Panel (a) is representative for all samples except GLO62A (panel (b)). The flat vertical distribution in panel (a) indicates the presence of SD magnetite centred on $\mu_0 H_c$ of ~ 15 mT, while the wide distribution along the horizontal axis is caused by the presence of a hard magnetic component (hematite and/or goethite). In panel (b) the signal is centred on lower field values, indicating the possible presence of SP grains. The vertical distribution is wider in panel (b), this can be caused by the presence of larger (PSD) magnetite grains or by a stronger signal from the hard magnetic component (hematite or goethite).

3.2 Voltammetric measurements

The voltammetric curves of the samples from the La Gloria transect are clear, narrow and well reproducible. Voltammetry of the original samples exhibits two partly separated peaks C1 (~ -0.60 V) and C2 (~ -0.78 V) indicating the presence of at least two ferric oxide components (Figure 5A and Table 4). Sample GLO62A only exhibits the C2 peak. There are no indications of voltammetric kinks or shoulders at ~ -0.9 V in all samples, and therefore there is no voltammetric evidence for the presence of iron spinel oxides. The concentration lies below the detection limit of < 0.2 wt% for VMP.

The peak potential of C1 is indicative of poorly crystalline, soil ferric oxides. The C2 peak is comparable to peaks of well-crystalline synthetic goethite or hematite (Table 2, adopted from Grygar and van Oorschot (in press, Chapter 9)). The C1 peak disappears after AAO- Fe^{2+} extraction (Table 4, Fig. 5B), showing that

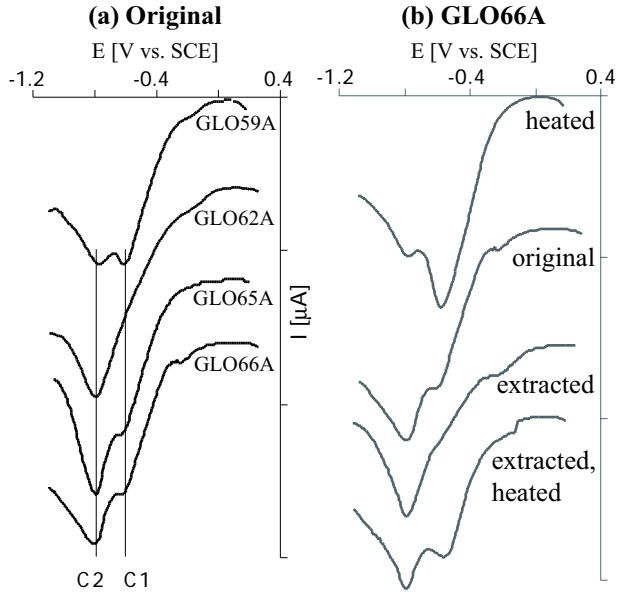


Figure 5: (a) Voltammograms of the La Gloria samples. C1 and C2 denote the individual reductive dissolution peaks. (b) Voltammograms of sample GLO66A; original, heated at 300°C, extracted by AAO-Fe²⁺, and extracted and subsequently heated at 300°C. In both panels, the curves were offset for clarity.

the chemical reactivity of this ferric oxide fraction is bigger than that of the phases causing peak C2. After heating at 300°C, peak C1 only slightly shifts cathodically, therefore we attribute this peak to the reaction of poorly crystalline hematite. In contrast, the signal of C2 is redispersed to C1 and C2 after heating. This indicates that it is made up of a signal of several minerals, of which one converts hematite (C1 peak) upon heating. One of the minerals making up the signal of C2 has to be goethite, which is converted upon heating, thus decreasing the original C2 signal and increasing the C1 signal. Therefore, we attribute the C2 peak to a goethite-hematite assemblage, in which both phases have practically equal dissolution reactivity. Because the extraction removed a substantial part of the poorly crystalline hematite, C1 disappears by extraction and reappears after heating due to the conversion of the remaining crystalline goethite to

Sample code	lithology	Original		Heated (300°C)		Extracted AAO-Fe ²⁺		Extracted & Heated	
		C1	C2	C1	C2	C1	C2	C1	C2
GLO059A	dark red clay	-0.61	-0.76	-0.56	-0.82 (sh)	(sh)	-0.77	-0.6 (sh)	-0.81
GLO062A	sandy red clay	(sh)	-0.78	-0.49	-0.80	(np)	-0.77	-0.55 (sh)	-0.81
GLO065A	sandstone	-0.60 (sh)	-0.79	-0.57	-0.82	(sh)	-0.78	-0.58	-0.80
GLO066A	caliche	-0.60	-0.79	-0.57	-0.81	(sh)	-0.76	-0.58	-0.79

Table 4: Peak potentials [V] detected in the VMP experiments for all samples (before and after extraction with AAO-Fe²⁺, as well as after heating to 300°C). C1 and C2 are the more positive and more negative cathodic peaks, respectively, (sh) denotes an unresolved peak or a shoulder, (np) indicates the absence of a voltammetric peak.

hematite. Here, as in the magnetic analysis, the behaviour of GLO62A deviates from that of the other samples. The C1 peak is absent in the original GLO62A sample, and it appears after heating, while in the other samples the C1 peak is enhanced after heating.

The development of the voltammetric peaks of original, extracted, heated, and extracted+heated samples was used to estimate the fractions of the ferric oxide species present in the samples as illustrated in figure 3. We confirmed this estimate by comparing the charges of C1 and C2 in the extracted and heated samples. GLO59A has the highest concentration of free ferric oxides and the smallest fraction of goethite (Table 5), which is in line with the estimate of ~ 3 wt% total Fe in the sample and the lowest $B_{1/2}$ for component 2 of all La Gloria samples. GLO62A has the smallest fraction of poorly crystalline hematite, which was confirmed by the low contribution of hard magnetic minerals in the IRM component analysis. However,

Sample code	Fe ₂ O ₃ [%]	Hematite (C1)	Hematite (C2)	Goethite (C2)
GLO059A	0.6-2.0	0.5	0.4	0.1
GLO062A	0.2-0.6	0.1	0.4	0.5
GLO065A	0.1-0.5	0.4	0.3	0.3
GLO066A	0.2-0.8	0.5	0.25	0.25

Table 5: Estimates of the concentration of the three separate ferric oxide phases detected in the La Gloria samples. The second column gives the absolute percentage of iron oxides, columns 3-5 give the relative contributions of the different iron oxide phases.

this sample also has the highest concentration of goethite, which is reflected in the high $B_{1/2}$ of the hard component. In GLO65A and GLO66A the ratio of the components of the goethite-hematite assemblage is very similar, which is reflected in the magnetic characteristics as well.

4. Discussion

Magnetic analyses indicate all samples contained a mixture of magnetite and a hard component inferred to be hematite and/or goethite. VMP showed the hard component consisted of well-crystalline goethite and hematite as well as poorly crystalline hematite. Magnetite could not be detected by VMP, indicating it is below the detection limit of 0.2 wt%. Assuming an SIRM for SD magnetite of 45 Am²/kg, we can calculate that the average magnetite concentration in our samples is ~ 0.002 wt%. This is in agreement with the VMP results.

In the samples, the magnetite is presumably of detrital origin. The crystalline hematite and goethite probably formed during deposition of the clay and sand in a warm and dry climate. Usually hematite and goethite are formed from dehydration of ferrihydrite. In warm and dry climates, the formation of hematite is favoured over that of goethite (Cornell and Schwertmann, 1996). The poorly crystalline hematite could have been created during a separate soil-forming phase, hence its poor crystallinity and small grain size. GLO62A does not contain the poorly crystalline hematite phase, but it is a sandy horizon, poor in clay, and has probably undergone little additional soil formation.

The VMP peaks are very distinct and allowed for semi-quantitative analysis of the separate contributions of these three mineral phases. The estimates of the amount of free ferric oxides obtained by voltammetry (0.1 – 2 wt%) were comparable to those obtained from total iron extraction (1–3 wt%) (Grygar and van Oorschot, in press). This lends further support for the internal standard technique that was used in our experiments. The total amount of hematite in the samples varied from ~0.2 wt% to ~1.8 wt%, and could be detected by magnetic methods as well. Contrarily, the goethite was not detected by other rock-magnetic techniques, probably due to the low concentrations of ~0.2 to 0.6 wt% as well as the low magnetic signal of goethite compared to that of hematite. Only the magnetic signal of sample GLO62A indicated the possible presence of goethite, by an increased $B_{1/2}$ compared to the other GLO samples.

5. Conclusion

The sensitivity of voltammetry to ferric oxides is an order of magnitude better than that of XRD, and therefore we were able to detect goethite and hematite in the natural samples with total free $\text{Fe}_2\text{O}_3 \geq 0.1$ –0.2 wt%. Beside the detection itself, voltammetry provided more detailed information about the ferric oxides, based on the distribution of their dissolution reactivity.

Voltammetry demonstrated that AAO- Fe^{2+} extraction attacked at least part of the poorly crystalline (pedogenic) hematite in the samples. The magnetic data showed that the AAO- Fe^{2+} extraction had removed the fine-grained magnetite, and in some cases it had also dissolved part of the hard magnetic fraction (hematite) (van Oorschot and Dekkers, 2001; van Oorschot et al., 2001). VMP showed that the more crystalline goethite and hematite were preserved after this treatment. The magnetic analyses are particularly suited for magnetite characterisation, but the information on the ferric oxide phases (hematite and goethite) is substantially more detailed in the VMP data. Addition of an internal standard (pyrolusite) enables semi-quantitative evaluation of the concentration of ferric oxides.

Acknowledgements

Pauline Kruiver kindly supplied us the La Gloria samples and corresponding magnetic data. M.J.D. acknowledges CEREGE for support during his sabbatical stay. Part of this work was conducted under the programme of the Vening Meinesz Research School of Geodynamics (VMSG), and funded by the Netherlands Organisation for Scientific Research (NWO/ALW).

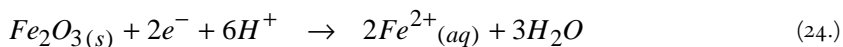
Voltammetric identification of pedogenic iron oxides in palaeosol and loess

Voltammetry of immobilised microparticles was used to detect low concentrations of goethite and hematite in palaeosol and loess samples. The total content of iron oxides in the natural samples was below 2 wt% and below the detection limit of X-ray powder diffraction. Goethite was distinguished from hematite due to the different electrochemical reactivity of the product of thermal dehydroxylation of goethite (very fine-grained crystalline hematite). The voltammetric analysis was tested using synthetic samples of ferrihydrite, goethite, hematite, magnetite, or Mg-ferrite with SiO₂ and a natural sample of smectite with an admixture of goethite. The detection is most sensitive for goethite and hematite (detection limit about 0.1 wt%), and approximately an order of magnitude better than X-ray powder diffraction analysis.

I. Introduction

Pedogenic (formed in soil) ferrihydrite, $\text{Fe}_2\text{O}_3 \cdot n\text{H}_2\text{O}$, goethite ($\alpha\text{-FeOOH}$), and hematite ($\alpha\text{-Fe}_2\text{O}_3$) play an important role in the chemistry of iron in soils (Cornell and Schwertmann, 1996). Ferrihydrite is a metastable product of fast hydrolysis of dissolved iron. Goethite and hematite are the final products of aging of ferrihydrite and other metastable ferric oxides, and their ratio reflects the conditions under which the soil was formed, such as rainfall, temperature, and Al/Fe ratio (Trolard and Tardy, 1987; Cornell and Schwertmann, 1996). Generally, hematite prevails over goethite in soils formed in warmer and drier climate. The identification of small amounts of these minerals is, however, not an uncomplicated task (Cornell and Schwertmann, 1996). Ferrihydrite and sometimes also goethite are poorly crystalline minerals and/or present in small amounts only. Therefore, they cannot be easily identified by X-ray diffraction analysis. Similarly, the success of Mössbauer spectroscopic analysis is complicated by non-stoichiometry, Al-for-Fe substitution, and the small particle size of these species (Komadel et al., 1998; Vandenberghe et al., 2000). Diffuse reflectance spectroscopy is sufficiently sensitive and specific to determine soil ferric oxides (Malengreau et al., 1996; Scheinost et al., 1998), but it is not very common in analytical practice. Rock-magnetic methods (Dekkers, 1997) can detect ferrimagnetic magnetite (Fe_3O_4) and maghemite ($\gamma\text{-Fe}_2\text{O}_3$) with extraordinary sensitivity, but the contribution of imperfectly antiferromagnetic goethite and hematite to the overall magnetic properties is usually insignificant compared to the signal of magnetite even when the magnetite content is small. In addition, ferrihydrite is paramagnetic at room temperature so it cannot be detected by remanent magnetic measurements.

The total content of ferric oxides is routinely evaluated by chemical extraction methods, such as citrate-dithionite-bicarbonate or oxalate extractions (Cornell and Schwertmann, 1996). The dissolution is based on the increase of the dissolution rate of ferric oxides after their reduction to Fe(II) that is finally converted to soluble Fe^{2+} by action of acids and/or ligands



The source of the electrons is a chemical agent, such as dithionite or ferrous oxalate. The interpretation of extraction methods is not so straightforward as it was believed after introducing them in the 1960's and 1970's. Not only phase composition, but also particle size and Al-for-Fe substitution significantly affect the dissolution reactivity of ferric oxides (Trolard et al., 1995; Malengreau et al., 1996; van Oorschot and Dekkers, 1999). A reliable but comparatively laborious approach to ferric-oxide analysis is a combination of chemical extraction with other methods such as Mössbauer spectroscopy (Komadel et al., 1998), elemental analysis and diffuse-reflectance spectroscopy (Malengreau et al., 1996), or elemental analysis and X-ray diffraction (Trolard et al., 1995). The aim of the present work was to test whether the combination of magnetic characterisation methods and chemical and electrochemical dissolution can lead to a successful identification of the mineralogical composition of natural samples.

Voltammetry, usually employing redox dissolution reactions, was proposed several times as an analytical tool for powdered solids, for which traditional analysis is not convenient, or should be shortened, simplified, and/or done with a small amount of samples available (Scholz et al., 1989b; 1991; Lange et al., 1993; Komorsky-Lovric, 1998; Domenech-Carbo et al., 2000). In the last decade, the technique referred to as voltammetry of microparticles has been applied to analysis of metals, metal oxides and chalcogenides (Scholz and Meyer, 1994; 1998), including ferric oxides (Grygar, 1996b; 1997; 1998). Electrochemical dissolution of ferric oxides proceeds analogous to the chemical reaction described by equation 24 but the electrons are supplied by the working electrode. Voltammetry of microparticles has not yet been used to characterise the ferric oxides in natural samples except for a few cases of laterites (Grygar, 1997; Grygar et al., 1997), in which well-crystalline iron oxides, easily detectable by X-ray diffraction, form one of the major components. In the present study, we focused on early Quaternary loess containing ferric oxides in concentration of about 1 wt%, i.e. below the detection limit of X-ray diffraction analysis. To distinguish goethite from hematite of a similar reactivity we propose to heat the samples to 300°C, which causes transformation of goethite to poorly crystalline hematite, that is more reactive in dissolution (Grygar, 1996b).

2. Experimental

We sampled a well-developed loess section with several palaeosols just North of the village of Bořetice, South Moravia, Czech Republic. This site contains four palaeosols, each developed at a different time. The top of the section has been partly disturbed by solifluction, therefore we only sampled the lowermost, oldest palaeosol. The top part of the documented section consists of an earthified Rotlehm, which formed from the loess during the Lower-Middle Pleistocene (~ 0.9 – 0.5 Ma ago), it has been identified as belonging to soil complex PK VII. The lower part of the section contains the original loess and dates from the Lower Pleistocene (Havlíček and Smolikova, 1993). The A-horizon of the palaeosol has been eroded prior to the new deposition of loess. The magnetic susceptibility is enhanced in the palaeosol compared to that of the loess, which is consistent with the observation that all central European palaeosols have

enhanced susceptibility compared to the original loess (Sartori et al., 1999). The average carbonate content in the palaeosol is ~0.5 wt%, the loess horizon has an average carbonate content of ~26 wt%. Bulk samples were taken at 30-cm intervals over the entire length of the section, samples were dried and stored in a laboratory refrigerator prior to use. The samples are labelled as Bx, with x the level in centimetres at which the sample was taken. The zero level was set at the top of the palaeosol. The loess is located at the bottom of the section, around -240 cm. Between approximately -190 and -230 cm there is a gradual change from palaeosol to loess, which is not only reflected in a gradual change in colour, but also by changes in magnetic signal as well as mineralogical composition.

To evaluate the total amount of chemically reactive ferric oxides and Al-for-Fe substitution, the samples were extracted by the citrate-bicarbonate-dithionite (CBD) procedure in three steps (van Oorschot and Dekkers, 1999) and after each step the concentration of Al, Fe, and Si in the extracts was analysed by ICP. X-ray diffraction analysis (Siemens D5005, CuK α radiation) was performed to characterise the mineralogical composition of natural samples.

Bulk susceptibility was measured with a KLY-2 susceptibility-bridge (AGICO, sensitivity $4 \cdot 10^{-8}$ SI, susceptibility of the samples was at least two orders of magnitude higher). Subsamples were mixed with epoxy resin and used for isothermal remanent magnetisation (IRM) acquisition analysis. The IRM was induced by a PM4 pulse magnetiser and measured with a JR5A spinner magnetometer (AGICO). A review on rock-magnetic measurements and their analytical applications can be found in Dekkers (1997) with a more detailed discussion of the methodology and analytical implications.

To test the voltammetric analysis we used sample VZS-6 (here denoted Smectite-1) characterised in Komadel et al. (1998). Smectite-1 is a natural aluminosilicate containing an admixture of goethite in the concentration 0.82 wt% (by Mössbauer spectroscopy) or 1.2 wt% (by chemical dissolution). In addition to natural samples, some synthetic samples were analysed for two main reasons: (1) to be able to directly compare the electrochemical response of more crystalline synthetic material to supposedly less crystalline solid material, and (2) to look for the most suitable internal standard. Commercially available pigments Bayferrox 306 (magnetite) and 140 (hematite-1) were used without further pretreatment. Hematite-2 and goethite-1 were prepared by oxidative hydrolysis of a ferrous sulphate solution. Hematite-3 and Al-doped hematite-4 were prepared by evaporation of a solution of Fe- (hematite-3) and Al- and Fe-nitrates (hematite-4), with citric acid (NO_3^- and citric acid in molar ratio 1.5:1) and calcination of the dry foam at 600°C. Hematite-4 contained 10 mol-% Al. Goethite-2, 3, and 4 were obtained by aging ferrihydrite in a strongly alkaline solution at 70°, 4°, and 70°C, respectively. Goethite-4 contained 8 mol-% Al. Hematite-2 and the synthetic goethites have been used previously for voltammetric studies (Grygar, 1996b; 1997). Ferrihydrite was the product of forced hydrolysis of ferric nitrate solution. Mg-ferrite was prepared by solid-state synthesis from MgO and Fe₂O₃ at 1100°C. βMnO_2 was prepared by thermal decomposition of Mn(II) nitrate, and birnessite ($\text{K}_{0.25}\text{MnO}_2$) by the sol-gel procedure from potassium permanganate and glucose (Bakardjieva et al., 2000). Electrochemical dissolution of the manganese oxides was also reported in Bakardjieva et al. (2000). The phase purity of synthetic samples was checked by powder X-ray diffraction. Before the voltammetric experiments, synthetic ferric and manganese oxides were carefully mixed with SiO₂ (particle size 13 μm) in an agate mortar to dilute the analyte to a level similar to that in natural loess and palaeosol samples.

For the electrochemical study, a N₂-deacrated acetate buffer (acetic acid: acetate ratio 1:1, total acetate 0.2

M) was used as supporting electrolyte. A paraffin-impregnated graphite working electrode was used. All potentials are referred to saturated calomel reference electrode (SCE). Voltammetric analysis of the pure synthetic iron oxides was described in Grygar (1996b; 1997; 1998).

3. Results and discussion

The natural samples were mainly composed of common clay minerals (smectite, kaolinite, mica-illite) and relic minerals (quartz, feldspars). The overall amount of kaolinite was relatively low. As for the actual feldspars and clay minerals, B₀, B₃₀, and B₉₀ were similar in composition. B₆₀, B₁₂₀ and B₁₅₀ exhibited the largest diffraction lines of various feldspars and less developed clay minerals. The content of smectite and kaolinite continuously increased from B₁₅₀ to B₂₄₀ (the loess sample). B₂₄₀ contained a significant amount of calcite, which is typical of loess, and the highest amount of kaolinite and mica-illite. No free iron oxides (hematite, goethite, magnetite-maghemite) were detected by powder X-ray diffraction. The sum of reactive Fe represented approximately 2% of the sample mass as follows from the results of CBD extraction given in table 1. The considerable amount of extracted Si showed that clay minerals were also partially dissolved, and so not all Al (and maybe Fe) extracted was bound in the ferric oxides.

Magnetic characterisation revealed that all natural samples contained two magnetic components. One component, with low coercivity and high saturation isothermal remanent magnetisation (SIRM), was most likely pseudo single-domain magnetite, i.e. with particle size close to 1 μm (Dekkers, 1997). The other component had a very high coercivity and its contribution to the SIRM was in the order of 10%. This second component was most likely fine-grained hematite, i.e. with particles <1 μm , which is typical for pedogenic iron oxides. Because the SIRM of magnetite is about three-orders of magnitude higher than that of hematite, magnetite will dominate the signal even if it is present in ten-times smaller concentration than hematite. Hence, the rock-magnetic methods revealed fine-grained pedogenic hematite with a substantially smaller amount of fine-grained (SD/PSD) magnetite (of lithogenic as well as pedogenic origin). Goethite would not be detected under these conditions due to very small remanent magnetism (antiferromagnetic structure) and the relatively low magnetic field used for IRM acquisition. The rock-magnetic behaviour of these samples will be detailed in a separate contribution (see Chapter 5 and/or 6).

	1st step		Total of three steps		
	Fe	Al	Fe	Al	Si
B ₀	2.12	0.14	2.30	0.23	0.32
B ₃₀	1.48	0.09	1.63	0.14	0.13
B ₆₀	1.58	0.10	1.72	0.19	0.30
B ₉₀	1.01	0.07	1.13	0.10	0.12
B ₁₂₀	1.19	0.07	1.32	0.12	0.13
B ₁₅₀	2.07	0.15	2.23	0.21	0.30
B ₁₈₀	1.25	0.08	1.37	0.12	0.12
B ₂₁₀	1.49	0.09	1.63	0.15	0.24
B ₂₄₀	0.75	0.04	0.82	0.06	0.11

Table 1: Percentage of Fe, Al, and Si extracted by CBD of natural samples.

Voltammetry was applied in the same manner as reported previously (Grygar, 1996b; 1997; 1998). Scanning started at open circuit potential and continued to negative potentials at scan rate 4 mV/s. An example of a typical voltammetric curve of the natural samples is shown in fig. 1 (B60). Each scan was repeated three times and the difference between the first and second one, and the second and the third scan are shown as well in figure 1. Obviously, the background current was very high with respect to the net current of ferric oxide dissolution. The subtraction of two subsequent scans solved this problem and resulted in clear voltammograms of ferric oxides in all natural samples (fig. 2, table 2). Differential pulse voltammetry could also be used to suppress the large background, but the interpretation of the resulting voltammograms is not so straightforward as in the case of common linear-sweep measurement – for example, it requires empirical calibration curves (Scholz et al., 1991). We therefore preferred linear sweep voltammetry although we were not successful in decreasing the background current by changing scan rate or solution pH. All voltammograms discussed in this report were obtained by the subtraction of the first two scans.

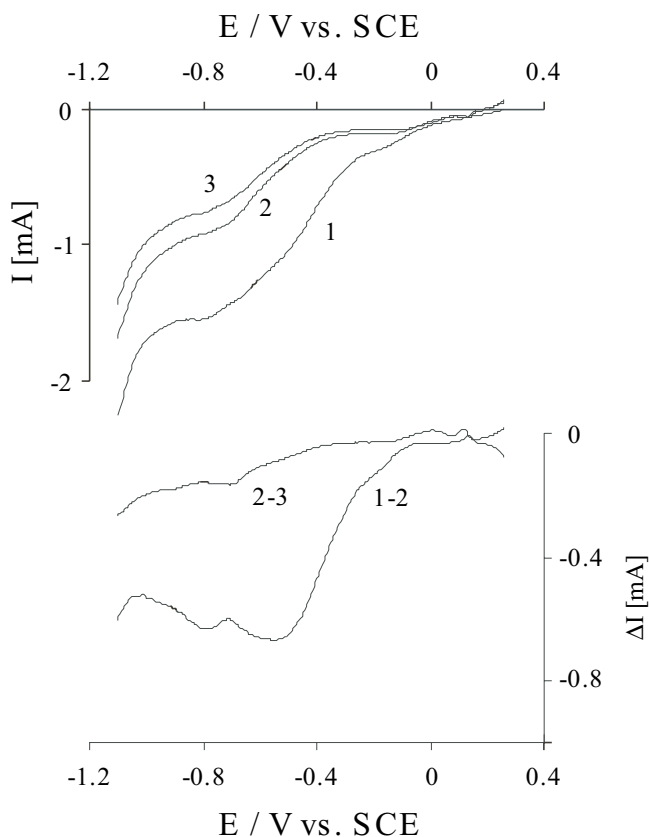


Fig. 1: Voltammetric curves of palaeosol B60. Upper part: 1st, 2nd, and 3rd linear-sweep voltammetric scans; lower part: subtraction of 1st minus 2nd, and 2nd minus 3rd scans.

Sample	As received	After heating	Iron oxide present
B0	-0.46	-0.49, -0.9 (sh)	h, sp (?)
B30	-0.60, -0.95 (sh)	-0.48, -0.8 (sh)	g, sp (?)
B60	-0.55, -0.7 (sh)	-0.48, -0.8 (sh)	h
B90	-0.48, -0.6 (sh)	-0.47	h
B120	-0.45	-0.48	h
B150	-0.45	-0.48	h
B180	-0.47	-0.46	h, g (?)
B210	-0.4 (sh), -0.61	-0.45, -0.8 (sh)	h, g
B240	-0.60, -0.9 (sh)	-0.44, -0.85 (sh)	g, sp (?)

Table 2: Voltammetric peak potentials E_p (V vs. SCE) of loess samples as received and after heating at 300°C for 15 minutes. Start at OCP (about 0.25 V), 4 mV/s. A possible minor peak or shoulder is denoted (sh). Iron oxide denotation: h- hematite, g- goethite, sp- magnetite or ferrite.

To identify the ferric oxide species in the natural samples, we compared their peak potentials to those of synthetic samples of known composition. The parameters of voltammetric peaks of synthetic iron oxides in an SiO_2 matrix (iron oxide content 0.1 to 3 wt-%) were summarised in table 3. In correspondence with previous reports (Grygar, 1996b), goethite and hematite had similar reactivity, and so they are further referred to as α -phases. The peak potentials of the ferric oxides in the natural samples (table 2) were similar to that of poorly crystalline synthetic α -phases (table 3, goethite-3). A minor amount of magnetite-like oxides or very well-crystalline goethite or hematite was probably responsible for a shoulder at about -0.9 V (B60 and B210). Ferrihydrite was not present in a detectable amount, which is conceivable given the Pleistocene age of the soils and loess. The VA peaks at about -0.5 V hence represented the most important ferric oxide species in the natural samples. The area of the shoulder at about -0.9 V represented 1-10% of the dominant peak, and so if spinel oxides such as magnetite were responsible for it, their content is about one to two orders of magnitude lower than that of the α -phases. This is in general agreement with the results of rock-magnetic measurements.

Sample	As received samples		Heated samples
	Sensitivity	E_p (V vs. SCE)	E_p (V vs. SCE)
Ferrihydrite	2	-0.33	-0.33
Magnetite	3	-0.26 (sh), -0.92	-0.28, -0.85
MgFe_2O_4	3	-1.01 (sh)	-0.96 (sh)
Goethite-1	6	-0.72	-0.44
Goethite-2	11	-0.69	-0.40
Goethite-3	8	-0.54	-0.35
Goethite-4	7	-0.73	-0.60
Hematite-1	10	-0.76	-0.75
Hematite-2	10	-0.72	-0.71
Hematite-3	7	-0.76	-0.76
Hematite-4	3	-0.83	-0.83

Table 3: Voltammetric peak potential and relative sensitivity of original ferric oxides with respect to manganese oxide internal standard and peak potential of samples after heating at 300°C for 15 min. Start at OCP (about 0.25 V), 4 mV/s.

To discriminate between the two α -phases, we used the method of Grygar (1996b), which is based on the fact, that at relatively low temperatures goethite is dehydrated to reactive, defect-rich hematite, for which the VA peak is shifted anodically with respect to its parent goethite. This phenomenon is demonstrated in fig. 2 with natural Smectite-1 and synthetic Goethite-3 heated at 300°C for 15 minutes in air. We also processed the other natural samples in this way, and evaluated the changes of the voltammetric peaks caused by the heating. In the majority of the samples, such as B0 and B90, the only effect of heating was ‘activation’ of ferric oxides, leading to sharper VA peaks at similar potentials as in the original samples. In such cases, we can identify hematite as the main α -phase. In samples B240 and B210 and possibly in B180 and B30, the anodic shift of the voltammetric peak was indicating the presence of goethite. Samples B180 to B240 were similar from a mineralogical viewpoint, moreover they exhibited increased degree of weathering of feldspars, and an increased amount of pedogenic goethite could hence be expected in these samples.

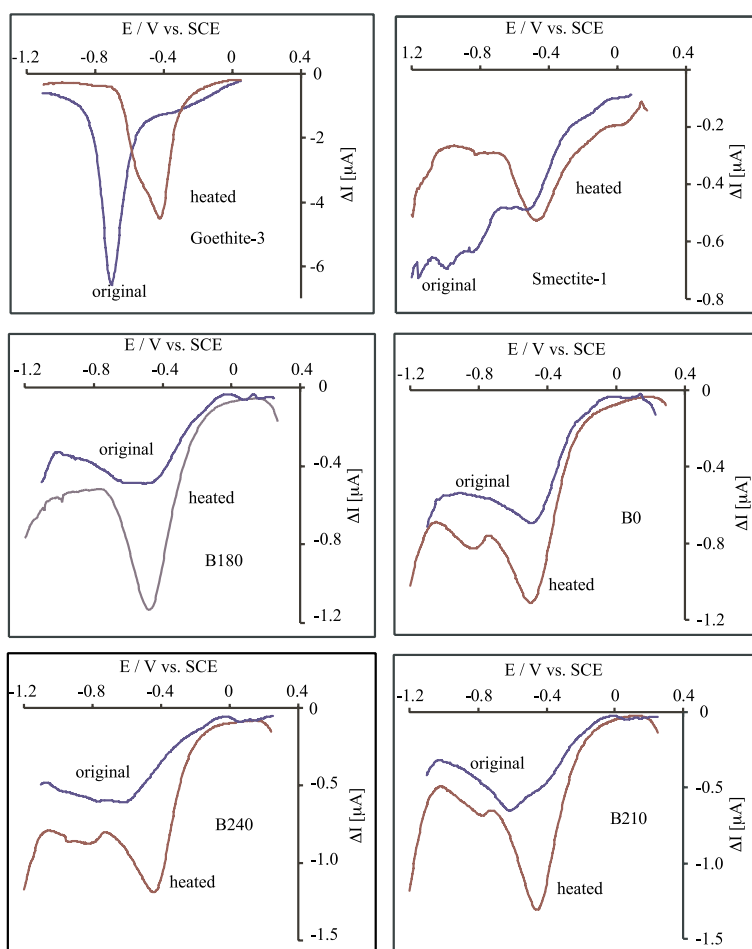


Fig. 2: Voltammetric curves of palaeosols B0, B90, B210, B240 and Smectite-1 and synthetic Goethite-3. The original samples and the samples heated to 300°C for 15 min are shown.

The amount of Al extracted by the first step of CBD (table 1) corresponded to about 12 mol-% Al in dissolved ferric oxides, which is common for soil hematites (Cornell and Schwertmann, 1996). Such a level of substitution could possibly affect the dissolution reactivity of ferric oxides. For example, Al-for-Fe substitution was found to decrease dissolution reactivity of goethite, and above 10 mol-% of Al, goethite loses its electroactivity (Grygar, 1997). Cr- and Mn-substitution in hematite have a similar effect (Grygar et al., 1999; in print), but Al-doped hematite has not yet been subjected to voltammetric analysis. We hence prepared and tested a series of Al-doped hematites with Al content up to 10 mol-%. Electrochemical properties of pure hematites 1-3 and 10 mol-% Al doped hematite-4 are also given in table 3. All Al-doped hematites were electroactive and yielded well-defined voltammetric peaks without a significant change of peak potential. However, the peak area of Al-doped Hematite-4 was decreased. We can therefore confirm that Al-for-Fe substitution found in the soil and loess samples does not endanger voltammetric detection of hematite.

The semi-quantitative evaluation of VA curves is complicated by the fact that the actual overall amount of deposited sample is not known. We hence tested the possibility to use additions of an internal standard for a quantitative evaluation. To avoid peak overlap of the standard and iron oxides, we chose manganese oxide additions. Mn(III,IV)-oxides are dissolved reductively under similar conditions as iron oxides (Bakardjieva et al., 2000) but at potentials by at least 0.5 V more positive. β - MnO_2 (pyrolusite) and $\text{K}_{0.25}\text{MnO}_2$ (birnessite) were tried as internal standards, yielding peaks at +0.30 and +0.41 V, respectively. The tests performed with synthetic samples surprisingly showed that the charges of Mn- and Fe-oxide reductive dissolution were not in the proportion expected on the base of the oxide weight and the stoichiometry of the corresponding dissolution reaction. The areas of the iron oxide peaks were 2 to 10 times larger than theoretically expected (table 3, column 'sensitivity'). Magnetite and ferrihydrite were increased the least, while the peaks of both α -phases were enhanced 7 to 10 times. It is probably related to a catalytic reaction, either a hydrogen-

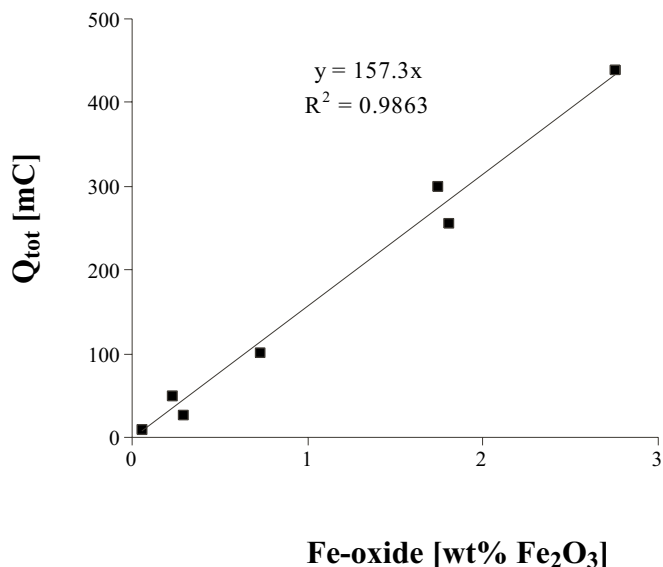


Fig. 3: The areas of voltammetric peaks of ferric oxides in synthetic mixtures of α -phases with SiO_2 . The concentration of FeOOH was expressed as Fe_2O_3 .

evolution side reaction (Mancey et al., 1993) or the reduction of oxygen (Vago et al., 1994). The 'sensitivity' did not depend substantially on the particle size of ferric oxides.

We used an internal standard to examine the limit of voltammetric detection of ferric oxides. In synthetic physical mixtures of iron and manganese oxides with SiO_2 , samples with a concentration of goethite and/or hematite larger than 0.1 wt% yielded clear VA peaks with the charge ratios of Mn- and Fe-oxide dissolution not affected by dilution. In figure 3, the charges of the dissolution peaks of goethite or hematite in synthetic mixtures were plotted against their concentration, showing the lower concentration range suitable for the detection of the α -phases. The plot also indirectly shows reproducibility of the sample deposition on the working electrode. At concentrations below 0.1%, the voltammetric peaks of α -phases disappeared.

In addition we tried to use the internal standard to estimate the total amount of reactive ferric oxides in loess samples. Because the quantitative analysis of iron oxides in loess by X-ray diffraction was impossible, we can consider the amount of Fe dissolved by CBD (table 1) as the upper estimate of the ferric oxide content. For this experiment we used the natural samples heated at 300°C that improved the peak shape of the ferric oxides, and mixed the subsamples of preheated samples with the internal standard (about 1 wt% β - MnO_2). We compared the charge ratio of Mn and iron oxide dissolution assuming that enhancement of the Fe response was equal to those of synthetic Al-doped hematite-4 (table 3). This yielded an amount of Fe in ferric oxides in soil and loess samples between 0.6 wt% (B240) and 1.2 wt% (Bo). X-ray diffraction is able to detect more than about 1 wt% crystalline phases, and the detection limit of diffuse reflectance spectroscopy is ~0.5 wt% of ferric oxides (Scheinost et al., 1998).

4. Conclusions

An assemblage of α -phases (goethite and hematite) was found in the palaeosol and loess samples. The overall content of ferric oxides was below 2 wt%, probably close to 1 wt%. To distinguish goethite and hematite, the samples were heated at 300°C and the voltammograms of the original and heated samples were compared. Hematite was identified to be the major component of the ferric oxide assemblage. In the loess sample (about 0.5 wt% of Fe in ferric oxides) we found a significant amount of goethite. The limit of voltammetric detection of these two phases in synthetic samples was about 0.1 wt%, which is sufficient for detection of pedogenic ferric oxides in soils and loess. The sensitivity of voltammetry to detect microparticles of goethite and hematite is hence comparable to that of diffuse reflectance spectroscopy and it is about an order of magnitude better than that of X-ray powder diffraction analysis. The voltammetric detection of goethite and hematite is enhanced by a catalytic side reaction that, on the one hand, excludes exact quantitative determination by using an internal standard, but on the other hand, enables to detect several tenths of percent of the electroactive species in a mixture without further sample pretreatment.

Acknowledgements

I. v. O. wishes to thank Judith Beks for her work on the CBD extraction of the natural samples, and Helen de Waard for the ICP analyses. The field-assistance of Neli Jordanova, Adry van Velzen, Pavel Havlíček and Eduard Petrovský during the sampling in South Moravia was greatly appreciated. We wish to thank Mark Dekkers for useful discussions of this manuscript. T. G. thanks Eduard Petrovský (Institute of geophysics, Prague Czech Republic) and David Hradil (Institute of Inorganic Chemistry, Řež, Czech Republic) for useful comments on rock-magnetic and mineralogical characterisation of natural samples. Part of this work was conducted under the programme of the Vening Meinesz Research School of Geodynamics (VMSG), and funded by the Netherlands Organisation for Scientific Research (NWO/ALW).

Epilogue

At the end of this thesis, I feel it is appropriate to give a synthesis of its three parts, and to attempt to outline the course of future work in this field, in particular with regard to the combination of (electro)chemical methods and mineral-magnetic techniques. Mineral-magnetic analysis is highly sensitive, especially for spinel-type, strongly magnetic oxides. It can be applied to all types of natural samples since all Earth materials contain at least trace amounts of iron(oxy)(hydr)oxides. Unfortunately, the results are not always unambiguous when dealing with magnetite (Fe_3O_4) and/or maghemite ($\gamma\text{-Fe}_2\text{O}_3$). These minerals have very similar mineral-magnetic properties and are therefore difficult to distinguish from each other. Because their formation or provenance depends on climate and environment, distinction between these minerals is essential for a better understanding of magnetic climate-proxies. The research presented in this thesis was performed to help reduce the ambiguity in the identification of magnetite and maghemite, and thus to enhance the diagnostic power of environmental-magnetic techniques. Complementary non-magnetic methods were introduced from other disciplines (such as soil science and electrochemistry) to help clarify the mineral-magnetic signal.

The purpose of the first two parts of this thesis was to establish a reliable protocol for the (chemical) identification of pedogenic and lithogenic magnetic iron oxides. In our search for the 'perfect solution' we studied two extraction methods (CBD and AAO- Fe^{2+}) and determined the optimum conditions for selective dissolution of iron oxides. The results show that the combination of mineral-magnetic and extraction data certainly leads to a better understanding of the origin of the strongly magnetic minerals in natural samples. Furthermore, with a new technique developed in electrochemistry called voltammetry of microparticles (VMP), we were able to identify and characterise the weakly magnetic minerals in some loess and palaeosol samples in the third part of this thesis.

CBD method

The results from Chapter 2 show that the CBD method is rather aggressive in the dissolution of iron oxides, and a clear distinction between fine-grained magnetite and maghemite is virtually impossible. From the study on synthetic samples we concluded that the method has a preference for fine-grained iron oxides, followed by coarse-grained titanomaghemite, and the method has little effect on coarse-grained magnetite. The CBD method further showed to be very sensitive to changes in temperature and iron oxide concentration. At higher temperatures, the dissolution rate of iron oxides increased, while at higher iron oxide concentration, the dissolution rate decreased.

When tested on natural samples (Chapter 5), the results show that the method again mainly dissolves the fine-grained iron oxides as well as the oxidised (maghemitised) rims of coarse-grained magnetite. Furthermore, the results show that silicate minerals were attacked as well. The aggressive dissolution mechanism of the CBD method attacks fine-grained pedogenic and lithogenic iron oxide particles without any mineralogical preference. Therefore, we must conclude that the method is only suited for the distinction between fine-grained and coarse-grained iron oxides. However, our results also show that when the concentration of iron oxides is high enough (≥ 5 wt%) the method can be used to distinguish fine-grained magnetite from fine-grained maghemite. Therefore we recommend to only apply this method (with a low extraction temperature of 60°C) for specific dissolution of pedogenic iron oxides when the concentration of iron oxides in the sample is very high.

AAO-Fe²⁺ method

The AAO-Fe²⁺ method appeared to be distinctly less aggressive than the CBD method, but the results of both methods on synthetic samples were quite similar. The AAO-Fe²⁺ method also removed mainly the fine-grained spinel-type iron oxides and showed a clear distinction between coarse-grained magnetite and titanomaghemite. Only with extensive rock-magnetic analysis was it possible to make distinctions in the dissolution rate of the fine-grained oxides. In Chapter 3, we showed that the effects of the method are not limited to amorphous minerals only – as it was designed to be – but that it was also capable of dissolving crystalline iron oxides from our synthetic samples. Furthermore, the method proved to be strongly dependent on pH and the presence of light. The results of AAO-Fe²⁺ extractions of natural samples (Chapter 6) are concurrent with the results from our synthetic samples. The method primarily dissolved very fine-grained (SP/SD) magnetite and the oxidised rims from the lithogenic coarse-grained magnetite. Of the ferromagnetic minerals, goethite was preferentially dissolved over hematite. Although this method does show a preference for specific minerals (such as magnetite and goethite), it does not specifically remove pedogenic particles. However, since it does not affect the silicate minerals (like the CBD method does), it is more suitable to study magnetic mineral compositions than the CBD method is.

Voltammetry of microparticles

Since neither of the extraction methods could be used to make a good distinction between fine-grained magnetite and maghemite, we searched for other techniques that would allow for this. The results obtained by electrochemists on voltammetry of microparticles (VMP) of pure oxides were promising, and we therefore started a pilot study to see whether the method would work on natural samples where iron oxides are present in much lower concentrations.

The results of our experiments with natural samples of two different sites (Chapters 8 and 9) show that it is possible to detect ferric oxides in natural samples, with a detection limit of only 0.1–0.2 wt%. The strongly magnetic particles could, however, not be detected. For regular soils and sediments VMP could therefore not discriminate between magnetite and maghemite, our original aim, but the method did provide more information on the weakly magnetic (pedogenic) particles (hematite and goethite), and thus considerably improved the knowledge of the composition of our samples. Moreover, the information that could be obtained about goethite and hematite was more detailed than that from magnetic analysis, because in the latter they are usually swamped by the signal from the strongly magnetic iron oxides. With the VMP method, distinction between hematite and goethite (mineralogy, crystallinity and reactivity) is possible. By addition of an internal standard, the method is even suitable for semi-quantitative analysis.

Future goals

The complexity of the mechanisms behind climatically controlled magnetic enhancement makes it inevitable to integrate methods from different scientific disciplines into environmental magnetism. The results of our extractions on natural samples show that both extraction methods (CBD and AAO-Fe²⁺) remove part of the pedogenic minerals, although in a varying degree. Neither method was able to remove the newly formed pedogenic particles with sufficient efficiency without affecting the lithogenic fraction as well. Nevertheless, in combination with new mineral-magnetic techniques (FORC diagrams and IRM component analysis) the extraction methods did provide valid information about the composition of the

samples, which could not be retrieved from standard rock-magnetic data alone. The combined use of these mineral-magnetic techniques with CBD and AAO-Fe²⁺ methods are therefore suitable tools in identifying the composition of both lithogenic and pedogenic magnetic fractions in natural samples. Finally, because of the strong dependence of the outcome of these extractions on their protocol parameters, we recommend that the extraction methods be applied with a standardised protocol. For the CBD method we suggest the use of a low extraction temperature (60°C), low dithionite concentration (1 gr), and short extraction times (15 min.). For the AAO-Fe²⁺ method the exclusion of light and the buffering of the pH (between 2 and 4) are of vital importance. The reduction of the extraction time from 2 hours to steps of 30 minutes also improves the interpretation.

The current protocols of the CBD and AAO-Fe²⁺ extraction methods have now been optimised for use in environmental magnetism, but they are not performing satisfactorily in view of our original aims. We therefore need to continue the search for other (extraction) methods that will allow an unambiguous distinction between fine-grained magnetite and maghemite. Chemical sequential extraction methods are also being used in other scientific fields such as (marine) geochemistry and soil science. A joint effort will undoubtedly expand the ideas for an even more meaningful application of extraction methods. However, the dissolution kinetics of the very fine-grained magnetic minerals are mostly dominated by their grain size. Thus, most chemical extraction methods will not be very suitable for a mineralogical distinction between minerals of such small grain size, and the 'perfect solution' is probably not to use chemical extraction methods for the purpose of distinguishing fine-grained magnetite from maghemite.

The VMP technique can identify weakly magnetic minerals, even at very low concentrations. This technique shows exceptional promise for the field of environmental magnetism, and can aid, in particular, in the study of red beds and other sediments comparatively rich in (anti)ferromagnetic minerals. Furthermore, it can be used to study reactivity, mineralogy and composition of synthetic iron oxides used for fundamental rock-magnetic research. It also has many applications in other fields of earth sciences where information is needed on the composition of iron oxides in natural or synthetic samples. For example, in soil science it can be used for studying the development and maturity of modern soils. Finally, it would be very interesting to develop a portable system that could be taken into the field to measure in situ.

Over the past years several new analytical techniques have been developed which show great promise for use in environmental magnetism. Mineral-magnetic methods such as FORC diagrams and IRM component analysis have opened up new possibilities for determining grain size and mineralogy of (small amounts of) natural materials. Just recently, the electron spin resonance (ESR) method has proven to be very useful for the detection of low concentrations of ferrimagnetic minerals in samples dominated by diamagnetic minerals. The way forward for mineral identification in environmental magnetism will be – in my opinion – the combination of these new techniques (VMP, ESR, FORC diagrams and IRM component analysis) with standard mineral-magnetic measurements. This undoubtedly will provide new insights into the magnetic composition of natural materials and inevitably lead to improved magnetic climate-proxies.

References

- Adams, R.N., 1958. *Analytical Chemistry*, 30: 1576.
- Agemian, H. and Chau, A.S.Y., 1977. *A study of different analytical extraction methods for nondetrital heavy metals in aquatic sediments*. *Archives of Environmental Contamination and Toxicology*, 6: 69-82.
- Aguilera, N.H. and Jackson, M.L., 1953. *Iron oxide removal from soils and clays*. *Soil Science Society of America - Proceedings*, 17: 359-364.
- Alexander, L.T., Hendricks, S.B. and Nelson, R.A., 1939. *Minerals present in soil colloids: II. Estimation in some representative soils*. *Soil Science*, 48: 273-279.
- Allen, P.D., Hampson, N.A. and Bignold, G.J., 1979. *The electro-dissolution of magnetite - Part I. The electro-chemistry of Fe₃O₄/C discs - Potentiodynamic experiments*. *Journal of Electroanalytical Chemistry*, 99: 299-309.
- Allen, P.D., Hampson, N.A. and Bignold, G.J., 1980. *The electro-dissolution of magnetite - Part II. The oxidation of bulk magnetite*. *Journal of Electroanalytical Chemistry*, 111: 223-233.
- Alonso-Zarza, A.M. and Calvo, J.P., 2000. *Palustrine sedimentation in an episodically subsiding basin: the Miocene of the northern Teruel Graben (Spain)*. *Palaeogeography, Palaeoclimatology, Palaeoecology*, 160: 1-21.
- An, Z.-S., Kukla, G.J., Porter, S.C. and Xiao, J., 1991. *Magnetic susceptibility evidence of monsoon variation on the loess plateau of central China during the last 130,000 years*. *Quaternary Research*, 36: 29-36.
- Atkins, P.W., 1989. *General Chemistry*. Scientific American Books, New York.
- Atkins, P.W., 1990. *Physical Chemistry*. Oxford University Press, Oxford.
- Bakardjieva, S., Bezdicka, P., Grygar, T. and Vorm, P., 2000. *Journal of Solid State Electrochemistry*, 4: 306.
- Banerjee, S.K., Hunt, C.P. and Liu, X.-M., 1993. *Separation of local signals from the regional paleomonsoon record of the Chinese loess plateau: a rock-magnetic approach*. *Geophysical Research Letters*, 20: 843-846.
- Baumgartner, E., Blesa, M.A., Marinovich, H.A. and Maroto, A.J.G., 1983. *Heterogeneous electron transfer as a pathway in the dissolution of magnetite in oxalic acid solutions*. *Inorganic Chemistry*, 22(16): 2224-2226.
- Bigham, J.M., Golden, D.C., Bowen, L.H., Buol, S.W. and Weed, S.B., 1978. *Iron oxide mineralogy of well-drained Ultisols and Oxisols: I. Characterisation of iron oxides in soil clays by Mössbauer spectroscopy, X-ray diffractometry, and selected chemical techniques*. *Soil Science Society of America - Journal*, 42: 816-825.
- Blesa, M.A., Marinovich, H.A., Baumgartner, E.C. and Maroto, A.J.G., 1987. *Mechanism of dissolution of magnetite by oxalic acid-ferrous ion solutions*. *Inorganic Chemistry*, 26: 3713-3717.
- Bloemendal, J., King, J.W., Hall, F.R. and Doh, S.J., 1992. *Rock magnetism of Late Neogene and Pleistocene deep-sea sediments: relationships to sediment source, diagenetic processes, and sediment lithology*. *Journal of Geophysical Research*, 97(B4): 4361-4375.
- Bloemendal, J., Liu, X.-M. and Rolph, T.C., 1995. *Correlation of the magnetic susceptibility stratigraphy of Chinese loess and the marine oxygen isotope record: chronological and palaeoclimatic implications*. *Earth and Planetary Science Letters*, 131: 371-380.
- Borggaard, O.K., 1981. *Selective extraction of amorphous iron oxides by EDTA from soils from Denmark and Tanzania*. *Journal of Soil Science*, 32: 427-432.
- Borggaard, O.K., 1988. *Phase identification by selective dissolution techniques*. In: J.W. Stucki, B.A. Goodman and U. Schwertmann (Editors), *Iron in Soils and Clay Minerals*. Reidel Publishing, Dordrecht, pp. 83-98.
- Borggaard, O.K., 1990. *Kinetics and mechanism of soil iron oxide dissolution in EDTA, oxalate and dithionite*. *Sciences Géologiques - Mémoire*, 85: 139-148.
- Borradaile, G.J., 1996. *Experimental stress remagnetisation of magnetite*. *Tectonophysics*, 261: 229-248.
- Boudreau, B.P. and Ruddick, B.R., 1991. *On a reactive continuum representation of organic matter diagenesis*. *American Journal of Science*, 291: 507-538.
- Bradshaw, P.M.D., Thomson, I., Smee, B.W. and Larsson, J.O., 1974. *The application of different analytical extractions and soil profile sampling in exploration geochemistry*. *Journal of Geochemical Exploration*, 3: 209-225.

- Brainina, K.Z. and Vydrevich, M.B., 1981. *Stripping Analysis of Solids (Review)*. Journal of Electroanalytical Chemistry, 121: 1-28.
- Busacca, A.J., 1989. *Long Quaternary record in eastern Washington, U.S.A., interpreted from multiple buried palaeosols in loess*. Geoderma, 45: 105-122.
- Campillo, M.C.d. and Torrent, J., 1992. *A rapid acid-oxalate extraction procedure for the determination of active Fe-oxide forms in calcareous soils*. Zeitschrift fur Pflanzenernahrung und Bodenkunde, 155: 437-440.
- Canfield, D.E., Raiswell, R. and Bottrell, S., 1992. *The reactivity of sedimentary iron minerals toward sulfide*. American Journal of Science, 292: 659-683.
- Chao, T.T. and Zhou, L., 1983. *Extraction techniques for selective dissolution of amorphous iron oxides from soils and sediments*. Journal of the Soil Science Society of America, 47: 225-232.
- Chester, R. and Hughes, M.J., 1967. *A chemical technique for the separation of ferro-manganese minerals, carbonate minerals and adsorbed trace elements*. Chemical Geology, 2: 249-262.
- Cisowski, S., 1981. *Interacting vs. non-interacting single domain behaviour in natural and synthetic samples*. Physics of the Earth and Planetary Interiors, 26: 56-62.
- Collinson, D.W., 1983. *Methods in Rock Magnetism and Palaeomagnetism: Techniques and Instrumentation*. Chapman and Hall, New York, 503 pp.
- Cornell, R.M. and Schindler, P.W., 1987. *Photochemical dissolution of goethite in acid/oxalate solution*. Clays and Clay Minerals, 35(5): 347-352.
- Cornell, R.M. and Schwertmann, U., 1996. *The iron oxides*. VCH Publishers, Weinheim, 573 pp.
- Cox, A., Doell, R.R. and Dalrymple, G.B., 1963. *Geomagnetic polarity epochs and Pleistocene geochronometry*. Nature, 198: 1049-1051.
- Dankers, P.H.M., 1978. *Magnetic properties of dispersed natural iron-oxides of known grain-size*. PhD Thesis, Utrecht University, Utrecht, 143 pp.
- Day, R., Fuller, M. and Schmidt, V.A., 1977. *Hysteresis properties of titanomagnetites: grain-size and compositional dependence*. Physics of the Earth and Planetary Interiors, 13: 260-266.
- de Boer, C.B., 1999. *Rock-magnetic studies on hematite, maghemite and combustion-metamorphic rocks*. Ph.D. Thesis, Utrecht University, Utrecht, 254 pp.
- de Boer, C.B. and Dekkers, M.J., 1996. *Grain size dependence of the rock magnetic properties for a natural maghemite*. Geophysical Research Letters, 23(20): 2815-2818.
- de Boer, C.B. and Dekkers, M.J., 1998. *Thermomagnetic behaviour of hematite and goethite as a function of grain size in various non-saturating magnetic fields*. Geophysical Journal International, 133: 541-552.
- De Endredy, A.S., 1963. *Estimation of free iron oxides in soils and clays by a photolytic method*. Clay Mineralogy Bulletin, 5: 209-217.
- Dearing, J.A., Bird, P.M., Dann, R.J.L. and Benjamin, S.F., 1997. *Secondary ferrimagnetic minerals in Welsh soils: a comparison of mineral magnetic detection methods and implications for mineral formation*. Geophysical Journal International, 130: 727-736.
- Deb, B.C., 1950. *The estimation of free iron oxides in soils and clays and their removal*. Journal of Soil Science, 1(2): 212-220.
- Dekkers, M.J., 1989. *Magnetic properties of natural goethite—I. Grain-size dependence of some low- and high-field related rock magnetic parameters measured at room temperature*. Geophysical Journal of the Royal Astronomical Society, 97(2): 323-340.
- Dekkers, M.J., 1997. *Environmental magnetism: an introduction*. Geologie en Mijnbouw, 76: 163-182.
- Ding, Z.L., Yang, S.L., Sun, J.M. and Liu, T.S., 2001. *Iron geochemistry of loess and red clay deposits in the Chinese Loess Plateau and implications for long-term Asian monsoon evolution in the last 7.0 Ma*. Earth and Planetary Science Letters, 185: 99-109.
- Domenech-Carbo, A., Domenech-Carbo, M.T., Gimeno-Adelantado, J.V., Moya-Moreno, M. and Bosch-Reig, F., 2000. *Electroanalysis*, 12: 120.

- Douglas, L.A.**, 1967. *Sodium-citrate-dithionite-induced alteration of biotite*. *Soil Science*, 103(3): 191-195.
- Dunlop, D.J.**, 1986. *Hysteresis properties of magnetite and their dependence on particle size: A test of pseudo-single-domain remanence models*. *Journal of Geophysical Research*, 91(B9): 9569-9584.
- Dunlop, D.J.**, 1999. *Simulation of Mrs/Ms and Hcr/Hc values (Day Plot) for mixtures of superparamagnetic, single-domain, multidomain and PSD grains*, IUGG XXII General Assembly, Birmingham U.K.
- Dunlop, D.J. and Özdemir, Ö.**, 1997. *Rock Magnetism: Fundamentals and Frontiers. Studies in Magnetism*. Cambridge University Press, Cambridge, 573 pp.
- EG&G**, *A Review of Techniques for Electrochemical Analysis. Application Note E-4*, EG&G Princeton Applied Research, Electrochemical Instruments Group.
- EG&G**, 1984. *Basics of Voltammetry and Polarography. Application Note P-2*, EG&G Princeton Applied Research, Applied Instruments Group.
- Erel, Y., Harlavan, Y., Stein, M. and Blum, J.D.**, 1997. *U-Pb dating of Fe-rich phases using a sequential leaching method*. *Geochimica et Cosmochimica Acta*, 61(8): 1697-1703.
- Ericsson, T., Linares, J. and Lotse, E.**, 1984. *A Mössbauer study of the effect of dithionite/citrate/bicarbonate treatment on a vermiculite, a smectite and a soil*. *Clay Minerals*, 19: 85-91.
- Evans, M.E. and Heller, F.**, 1994. *Magnetic enhancement and palaeoclimate: study of a loess/palaeosol couplet across the loess plateau of China*. *Geophysical Journal International*, 117: 257-264.
- Eyre, J.K. and Shaw, J.**, 1994. *Magnetic enhancement of Chinese loess—the role of γ -Fe₂O₃* *Geophysical Journal International*, 117: 265-271.
- Fabian, K. and Dobeneck, T.V.**, 1997. *Isothermal magnetisation of samples with stable Preisach function: A survey of hysteresis, remanence, and rock magnetic parameters*. *Journal of Geophysical Research*, 102(B8): 17659-17677.
- Fang, X.-M. et al.**, 1999a. *Millennial-scale climatic change during the last interglacial period: Superparamagnetic sediment proxy from palaeosol S1, western Chinese Loess Plateau*. *Geophysical Research Letters*, 26(16): 2485-2488.
- Fang, X.-M., Li, J.-J. and Voo, R.v.d.**, 1999b. *Rock magnetic and grain size evidence for intensified Asian atmospheric circulation since 800,000 years B.P. related to Tibetan uplift*. *Earth and Planetary Science Letters*, 165: 129-144.
- Fang, X.-M. et al.**, 1999c. *Asian summer monsoon instability during the past 60,000 years: Magnetic susceptibility and pedogenic evidence from the western Chinese Loess Plateau*. *Earth and Planetary Science Letters*, 168: 219-232.
- Fine, P. and Singer, M.J.**, 1989. *Contribution of ferrimagnetic minerals to oxalate- and dithionite-extractable iron*. *Soil Science Society of America - Journal*, 53: 191-196.
- Fine, P., Singer, M.J., Ven, R.L., Verosub, K. and Southard, R.J.**, 1989. *Role of pedogenesis in distribution of magnetic susceptibility in two California chronosequences*. *Geoderma*, 44: 1195-1199.
- Fine, P., Singer, M.J. and Verosub, K.L.**, 1992. *Use of magnetic-susceptibility measurements in assessing soil uniformity in chronosequence studies*. *Soil Science Society of America - Journal*, 56: 1195-1199.
- Fine, P., Singer, M.J., Verosub, K.L. and TenPas, J.**, 1993. *New evidence for the origin of ferrimagnetic minerals in loess from China*. *Journal of the Soil Science Society of America*, 57(S5): 1537-1542.
- Fine, P., Verosub, K.L. and Singer, M.J.**, 1995. *Pedogenic and lithogenic contributions to the magnetic susceptibility record of the Chinese loess/palaeosol sequence*. *Geophysical Journal International*, 122: 97-107.
- Fischer, W.R.**, 1972. *Die Wirkung von zweiwertigem Eisen auf Lösung und Umwandlung von Eisen(III)-hydroxiden, Pseudogley & Gley - Genesis and use of hydromorphic soils*. VCH, Weinheim, pp. 37-44.
- Forster, T. and Heller, F.**, 1997. *Magnetic enhancement paths in loess sediments from Tajikistan, China and Hungary*. *Geophysical Research Letters*, 24(1): 17-20.
- Förstner, U. et al.**, 1981. *Chemical speciation of heavy metals in solid waste materials (sewage sludge, mining wastes, dredged materials, polluted sediments) by sequential extraction*, Heavy metals in the environment. C.E.P. Consultants, Edinburgh, U.K., Amsterdam, the Netherlands, pp. 698-704.

- Frechen, M., Zander, A., Cilek, V. and Lozek, V., 1999. Quaternary Science Reviews, 18: 1467-1493.
- Furrer, G. and Stumm, W., 1986. *The coordination chemistry of weathering: I. Dissolution kinetics of δ -Al₂O₃ and BeO*. Geochimica et Cosmochimica Acta, 50: 1847-1860.
- Galabutskaya, E. and Govorova, R., 1934. *Bleaching of kaolin*. R. Min. Suire., 9(4): 27-.
- Gallet, S., Jahn, B.-M., Vliet-Lanoë, B.v., Dia, A. and Rossello, E., 1998. *Loess geochemistry and its implications for particle origin and composition of the upper continental crust*. Earth and Planetary Science Letters, 156: 157-172.
- Ghabru, S.K., St.Arnaud, R.J. and Mermut, A.R., 1990. *Association of DCB-extractable iron with minerals in coarse soil clays*. Soil Science, 149(2): 112-120.
- Goldberg, E.D. and Arrhenius, G.O.S., 1958. *Chemistry of Pacific pelagic sediments*. Geochimica et Cosmochimica Acta, 13: 153-212.
- Golden, D.C., Ming, D.W., Bowen, L.H., Morris, R.V. and Lauer, H.V., 1994. *Acidified oxalate and dithionite solubility and color of synthetic, partially oxidized Al-magnetites and their thermal oxidation products*. Clays and Clay Minerals, 42(1): 53-62.
- Grygar, T., 1995. *Kinetics of electrochemical reductive dissolution of iron (III) hydroxy-oxides*. Collections of Czechoslovak Chemical Communications, 60: 1261-1273.
- Grygar, T., 1996a. *The electrochemical dissolution of iron(III) and chromium(III) oxides and ferrites under conditions of abrasive stripping voltammetry*. Journal of Electroanalytical Chemistry, 405: 117-125.
- Grygar, T., 1996b. *Electrochemical dissolution of iron(III) hydroxy-oxides: more information about the particles*. Collections of Czechoslovak Chemical Communications, 61: 93-106.
- Grygar, T., 1997. *Dissolution of pure and substituted goethites controlled by the surface reaction under conditions of abrasive stripping voltammetry*. Journal of Solid State Electro-chemistry, 1: 77-82.
- Grygar, T., 1998. *Phenomenological kinetics of irreversible electrochemical dissolution of metal-oxide microparticles*. Journal of Electroanalytical Chemistry, 2(3): 127-136.
- Grygar, T., Bakardijeva, S., Bezdicka, P. and Vorm, P., in press. *Ceramics-Silikaty*.
- Grygar, T., Bezdicka, P. and Caspary, E.-G., 1999. *Journal of the Electrochemical Society*, 146: 3234.
- Grygar, T., Kral, R., Nekovarik, C. and Zelenda, P., 1997. *Journal of the Czech Geological Society*, 42: 121.
- Grygar, T. and Ruan, H.D., 1998. *Dissolution of anisotropic and anisometric prismatic particles: limits of common kinetic laws*. Models in Chemistry, 135(1-2): 31-43.
- Grygar, T., Subrt, J. and Boháček, J., 1995. *Electrochemical dissolution of goethite by abrasive stripping voltammetry*. Collections of Czechoslovak Chemical Communications, 60: 950-959.
- Grygar, T. and van Oorschot, I.H.M., in press. *Voltammetric identification of pedogenic iron oxides in paleosol and loess*. Electroanalysis.
- Hanesch, M. and Petersen, N., 1999. *Magnetic properties of a recent parabrown-earth from Southern Germany*. Earth and Planetary Science Letters, 169: 85-97.
- Hartstra, R.L., 1982a. *Grain-size dependence of initial susceptibility and saturation magnetization-related parameters of four natural magnetites in the PSD-MD range*. Geophysical Journal of the Royal Astronomical Society, 71: 477-495.
- Hartstra, R.L., 1982b. *Some rockmagnetic parameters for natural iron-titanium oxides*. PhD Thesis, Utrecht University, Utrecht, 145 pp.
- Havlíček, P. and Smolková, L., 1993. *A loess series near Boretice (South Moravia)*. Bulletin of the Czech Geological Survey, 68(1): 19-24.
- Heller, F. and Evans, M.E., 1995. *Loess magnetism*. Reviews of Geophysics, 33: 211-240.
- Heller, F. and Liu, T.-S., 1982. *Magnetostratigraphical dating of loess deposits in China*. Nature, 300: 431-433.
- Heller, F. and Liu, T.-S., 1984. *Magnetism of Chinese loess deposits*. Geophysical Journal of the Royal Astronomical Society, 77: 125-141.
- Heller, F. and Liu, T.-S., 1986. *Palaeoclimatic and sedimentary history from magnetic susceptibility of loess in China*. Geophysical Research Letters, 13: 1169-1172.

- Heller, F., Liu, X.-M., Liu, T.-S. and Xu, T.-C., 1991. *Magnetic susceptibility of loess in China*. Earth and Planetary Science Letters, 103: 301–310.
- Heller, F. et al., 1993. *Quantitative estimates of pedogenic ferromagnetic mineral formation in Chinese loess and palaeoclimatic implications*. Earth and Planetary Science Letters, 114: 385–390.
- Heller, F. and Wang, J., 1991. *Magnetism of Quaternary sediments: loess in China*. INQUA Abstracts of Papers and Posters, 13: 88–97.
- Henkel, O., 1964. *Remanenzverhalten und wechselwirkungen in hartmagnetischen teilchen-kollektiven*. Physica Status Solidi, 7: 919–929.
- Hering, J.G. and Stumm, W., 1990. *Oxidative and Reductive Dissolution of Minerals*. In: M.F. Hochella Jr. and A.F. White (Editors), Mineral-water interface geochemistry. Reviews in Mineralogy. Mineralogical Society of America.
- Heslop, D., Dekkers, M.J., Kruiver, P.P. and van Oorschot, I.H.M., 2001. *Analysis of isothermal remanent magnetisation acquisition curves using an expectation-maximisation algorithm*. Geophysical Journal International (in press).
- Heslop, D., Langereis, C.G. and Dekkers, M.J., 2000. *A new astronomical timescale for the loess deposits of Northern China*. Earth and Planetary Science Letters, 184: 125–139.
- Hess, H.H., 1962. *History of ocean basins*. In: A.E.J. Engel et al. (Editors), *Petrologic studies*. Geological Society of America, pp. 599–620.
- Hickling, A. and Ives, D.J.G., 1975. *The electrochemical behaviour of iron oxides in dilute sulphuric acid and the interpretation of the flade potential of iron*. Electrochimica Acta, 20: 63–69.
- Hilton, J., Lishman, J.P. and Chapman, J.S., 1986. *Magnetic and chemical characterisation of a diagenetic magnetic mineral formed in the sediments of productive lakes*. Chemical Geology, 56: 325–333.
- Hirt, A.M., Banin, A. and Gehring, A.U., 1993. *Thermal generation of ferromagnetic minerals from iron-enriched smectites*. Geophysical Journal International, 115: 1161–1168.
- Hovan, S.A., Rea, D.K., Piasis, N.G. and Shackleton, N.J., 1989. *A direct link between the China loess and marine $d18O$ records: aeolian flux to the north Pacific*. Nature, 340: 296–298.
- Hunt, C.P. et al., 1995a. *Rock-magnetic proxies of climate change in the loess-paleosol sequences of the western Loess Plateau of China*. Geophysical Journal International, 123: 232–244.
- Hunt, C.P., Moskowicz, B.M. and Banerjee, S.K., 1995b. *Magnetic properties of rocks and minerals*. In: T.J. Ahrens (Editor), *A Handbook of Physical Constants, vol. 3*. American Geophysical Union, Washington, DC, pp. 189–204.
- Hunt, C.P., Singer, M.J., Kletetschka, G., TenPas, J. and Verosub, K.L., 1995c. *Effect of citrate-bicarbonate-dithionite treatment on fine-grained magnetite and maghemite*. Earth and Planetary Science Letters, 130: 87–94.
- Hus, J.J. and Han, J.-M., 1992. *The contribution of loess magnetism in China to the retrieval of past global changes—some problems*. Physics of the Earth and Planetary Interiors, 70: 154–168.
- Jackson, M.L., 1956. *Soil Chemical Analysis - Advanced Course*. Dept. of Soils, University of Wisconsin, Madison, Wisconsin, 991 pp.
- Jirkovsky, R., 1934. *Mikrochemie*, 15(9): 331.
- Jonker, A.R.T., 2000. *North by Northwest - Seafaring, science, and the Earth's magnetic field (1600-1800), Volume 1*. Cuvillier Verlag, Goettingen, Germany, 542 pp.
- Kapicka, A., 1992. *Magnetic susceptibility under hydrostatic pressure of synthetic magnetite samples*. Physics of the Earth and Planetary Interiors, 70: 248–252.
- Kemp, R.A., 1999. *Micromorphology of loess-paleosol sequences: a record of paleoenvironmental change*. Catena, 35: 179–196.
- King, J.W., Banerjee, S.K., Marvin, J.A. and Özdemir, Ö., 1982. *A comparison of different magnetic methods for determining the relative grain size of magnetite in natural materials: some results from lake sediments*. Earth and Planetary Science Letters, 59: 404–419.

- Kissinger, P.T. and Heineman, W.R. (Editors), 1984. *Laboratory techniques in Electroanalytical Chemistry. Monographs in Electroanalytical Chemistry and Electrochemistry*, 5. Marcel Dekker, New York, 751 pp.
- Komadel, P., Grygar, T. and Mehner, H., 1998. *Clay Mineralogy*, 33: 593.
- Komorsky-Lovric, S., 1998. *Croatica Chemica Acta*, 71: 263.
- Kraus, M.J., 1999. *Paleosols in clastic sedimentary rocks: their geologic applications*. *Earth-Science Reviews*, 47: 41-70.
- Krijgsman, W. et al., 1996. *A new chronology for the middle to late Miocene continental record in Spain*. *Earth and Planetary Science Letters*, 142: 367-380.
- Kruijver, P.P., Dekkers, M.J. and Heslop, D., 2001. *Quantification of magnetic coercivity components by the analysis of acquisition curves of isothermal remanent magnetisation*. *Earth and Planetary Science Letters*, 189(3-4): 269-276.
- Kruijver, P.P. and Passier, H.F., submitted. *Coercivity analysis of magnetic phases in sapropel S1 related to variations in redox conditions: what the S-ratio cannot explain*. *Geochemistry, Geophysics, Geosystems (G3)*.
- Kukla, G.J. et al., 1988. *Pleistocene climates dated by magnetic susceptibility*. *Geology*, 16: 811-814.
- Kuntze, H., Niemann, J., Roeschmann, G. and Schwerdtfeger, G., 1981. *Bodenkunde*. Eugen Ulmer GmbH & Co., Stuttgart, 407 pp.
- Landau, L.D. and Lifshitz, E.M., 1935. *On the theory of the dispersion of magnetic permeability in ferromagnetic bodies*. *Physikalische Zeitschrift der Sowjetunion*, 8: 153-167.
- Lange, B. et al., 1993. *International Laboratory*, 23: 23.
- Langereis, C.G. and Krijgsman, W. (in press). *Geomagnetic Polarity Time Scale, Encyclopaedia of Ocean Sciences*, Academic Press.
- Le Borgne, E., 1955. *Susceptibilit e magn tique anormale du sol superficielle*. *Annales De Geophysique*, 11: 399-419.
- Liu, X.M., Hesse, P. and Rolph, T., 1999. *Origin of maghemite in Chinese loess deposits: aeolian or pedogenic*. *Physics of the Earth and Planetary Interiors*, 112: 191-201.
- Liu, X.M., P. Hesse, Liu, T.S. and Bloemendal, J., 1998. *High resolution climate record from the Beijing area during the last glacial-interglacial cycle*. *Geophysical Research Letters*, 25(3): 349-352.
- Liu, X.-M., Rolph, T., Bloemendal, J., Shaw, J. and Liu, T.-S., 1994. *Remanence characteristics of different magnetic grain size categories at Xifeng, central Chinese loess plateau*. *Quaternary Research*, 42: 162-165.
- Liu, X.-M., Rolph, T., Bloemendal, J., Shaw, J. and Liu, T.-S., 1995. *Quantitative estimates of palaeoprecipitation at Xifeng in the loess plateau of China*. *Palaeogeography, Palaeoclimatology, Palaeoecology*, 113: 243-248.
- Liu, X.-M., Shaw, J., Liu, T.-S., Heller, F. and Baoyin, Y., 1992. *Magnetic mineralogy of Chinese loess and its significance*. *Geophysical Journal International*, 108: 301-308.
- Longworth, G. et al., 1979. *Mossbauer and magnetic studies of secondary iron oxides in soils*. *Journal of Soil Science*, 30: 93-110.
- Loveland, P.J., 1988. *The assay for iron in soils and clay minerals*. In: J.W. Stucki, B.A. Goodman and U. Schwertmann (Editors), *Iron in soils and clay minerals*. Reidel Publishing, Dordrecht, pp. 99-140.
- Lowrie, W., 1990. *Identification of ferromagnetic minerals in a rock by coercivity and unblocking temperature properties*. *Geophysical Research Letters*, 17: 159-162.
- Maher, B.A., 1986. *Characterisation of soils by mineral magnetic measurements*. *Physics of the Earth and Planetary Interiors*, 42: 76-92.
- Maher, B.A., 1988. *Magnetic properties of some synthetic sub-micron particles*. *Geophysical Journal*, 94: 83-96.
- Maher, B.A., 1998. *Magnetic properties of modern soils and Quaternary loessic paleosols: paleoclimatic implications*. *Palaeogeography, Palaeoclimatology, Palaeoecology*, 137: 25-54.
- Maher, B.A. and Hounslow, M.W., 1999. *The significance of magnetotactic bacteria for the palaeomagnetic and rock magnetic record of Quaternary sediments and soils*. In: D.H. Tarling and P. Turner (Editors), *Palaeomagnetism and Diagenesis in Sediments*. Special Publications. Geological Society, London, pp. 43-46.

- Maher, B.A. and Thompson, R.**, 1991. *Mineral magnetic record of the Chinese loess and paleosols*. *Geology*, 19: 3–6.
- Maher, B.A. and Thompson, R.**, 1992. *Paleoclimatic significance of the mineral magnetic record of the Chinese loess and paleosols*. *Quaternary Research*, 37: 155–170.
- Maher, B.A. and Thompson, R. (Editors)**, 1999. *Quaternary climates, environments and magnetism*. Cambridge University Press, Cambridge, U.K., 390 pp.
- Maher, B.A., Thompson, R. and Zhou, L.-P.**, 1994. *Spatial and temporal reconstructions of changes in the Asian palaeomonsoon: a new mineral magnetic approach*. *Earth and Planetary Science Letters*, 125: 462–471.
- Malengreau, N., Bedidi, A., Muller, J.-P. and Herbillon, A.J.**, 1996. *European Journal of Soil Science*, 47: 13.
- Mancey, D.S., Shoesmith, D.W., Lipkowski, J., McBride, A.C. and Noel, J.**, 1993. *Journal of the Electrochemical Society*, 140: 637.
- Martin, J.M., Nirel, P. and Thomas, A.J.**, 1987. *Sequential extraction techniques: promises and problems*. *Marine Chemistry*, 22: 313–341.
- McKeague, J.A., Brydon, J.E. and Miles, N.M.**, 1971. *Differentiation of forms of extractable iron and aluminum in soils*. *Proceedings of the Soil Science Society of America*, 35: 33–38.
- McKeague, J.A. and Day, J.H.**, 1965. *Dithionite- and oxalate-extractable Fe and Al as aids in differentiating various classes of soils*. *Canadian Journal of Soil Science*, 46: 13–22.
- Mehra, O.P. and Jackson, M.L.**, 1960. *Iron oxide removal from soils and clays by a dithionite-citrate system buffered with sodium bicarbonate*. In: A. Swineford (Editor), *Clays and Clay Minerals*. *Proceedings of the 7th national conference on clays and clay minerals*, Washington D.C., October 1958, pp. 317–327.
- Meng, X., Derbyshire, E. and Kemp, R.A.**, 1997. *Origin of the magnetic susceptibility signal in Chinese loess*. *Quaternary Science Reviews*, 16(8): 833–839.
- Merrill, R.T., McElhinny, M.W. and McFadden, P.L.**, 1996. *The magnetic field of the earth - Palaeomagnetism, the core and the deep mantle*. *International Geophysics Series*, Volume 63. Academic Press, San Diego, U.S.A., 531 pp.
- Morel, F.M.M. and Hering, J.G.**, 1993. *Principles and applications of aquatic chemistry*. John Wiley & Sons Inc., New York.
- Morin, F.J.**, 1950. *Magnetic susceptibility of α -Fe₂O₃ and γ -Fe₂O₃ with added titanium*. *Physical Reviews*, 78: 819–820.
- Mullender, T.A.T., van Velzen, A.J. and Dekkers, M.J.**, 1993. *Continuous drift correction and separate identification of ferrimagnetic and paramagnetic contributions in thermomagnetic runs*. *Geophysical Journal International*, 114: 663–672.
- Mullins, C.E.**, 1977. *Magnetic susceptibility of the soil and its significance in soil science - A review*. *Journal of Soil Science*, 28: 223–246.
- Nagata, T.**, 1961. *Rock Magnetism*. Maruzen company Ltd., Tokyo, Japan, 350 pp.
- Néel, L.**, 1949. *Influence des fluctuations thermiques sur l'aimantation de grains ferromagnétiques très fins*. *Comptes rendus hebdomadaires des séances de l'Académie des Sciences (Paris), Série B*, 228: 664–666.
- Néel, L.**, 1955. *Some theoretical aspects of rock magnetism*. *Advances in Physics*, 4: 191–243.
- Norrish, K. and Taylor, R.M.**, 1961. *The isomorphous replacement of iron by aluminium in soil goethites*. *Journal of Soil Science*, 12(2): 294–306.
- Oldfield, F.**, 1991. *Environmental magnetism: a personal perspective*. *Quaternary Science Reviews*, 10: 73–85.
- Oldfield, F.**, 1992. *The source of fine-grained magnetite in sediments*. *The Holocene*, 2(2): 180–182.
- Oldfield, F. and Robinson, S.G.**, 1985. *Geomagnetism and palaeoclimate*. In: M.J. Tooley and G.M. Sheail (Editors), *The Climatic Scene*. Allen & Unwin, Herts U.K.
- Olson, R.V. and Ellis, R.**, 1982. *Iron*. In: A.L. Page (Editor), *Methods of Soil Analysis, Part 2. Chemical and Microbiological Properties*. *Agronomy Monograph no. 9*. American Society of Agronomy - Soil Science Society of America, Madison, WI, USA, pp. 301–312.
- Opdyke, N.D. and Channell, J.E.T.**, 1996. *Magnetic Stratigraphy*. *International Geophysics series, Volume 64*. Academic Press Inc., San Diego, U.S.A., 346 pp.
- O'Reilly, W.**, 1984. *Rock and Mineral Magnetism*. Blackie, Glasgow, 220 pp.

- Özdemir, Ö., 1990. *High-temperature hysteresis and thermoremanence of single-domain maghemite*. *Physics of the Earth and Planetary Interiors*, 65: 125-136.
- Özdemir, Ö. and Banerjee, S.K., 1984. *High temperature stability of maghemite (γ -Fe₂O₃)*. *Geophysical Research Letters*, 11(3): 161-164.
- Parfitt, R.L., 1989. *Optimum conditions for extraction of Al, Fe, and Si from soils with acid oxalate*. *Communications in Soil Science and Plant Analysis*, 20(7&8): 801-816.
- Parry, L.G., 1980. *Shape-related factors in the magnetisation of immobilised magnetite particles*. *Physics of the Earth and Planetary Interiors*, 22: 144-154.
- Phillips, E.J.P. and Lovley, D.R., 1987. *Determination of Fe(III) and Fe(II) in oxalate extracts of sediments*. *Journal of the Soil Science Society of America*, 51: 938-941.
- Pike, C.R., Roberts, A.P. and Verosub, K.L., 1999. *Characterizing interactions in fine magnetic particle systems using first order reversal curves*. *Journal of Applied Physics*, 85(9): 6660-6667.
- Pike, C.R., Roberts, A.P. and Verosub, K.L., 2001. *FORC diagrams and thermal relaxation effects in magnetic particles*. *Geophysical Journal International*, 145(3): 721-730.
- Pinho-Dick, D. and Schwertmann, U., 1996. *Microaggregates from Oxisols and Inceptisols: dispersion through selective dissolutions and physicochemical treatments*. *Geoderma*, 74: 49-63.
- Postma, D., 1993. *The reactivity of iron oxides in sediments: A kinetic approach*. *Geochimica et Cosmochimica Acta*, 57: 5027-5034.
- Press, F. and Siever, R., 1986. *Earth*. W.H. Freeman & Co, New York.
- Raiswell, R., Canfield, D.E. and Berner, R.A., 1994. *A comparison of iron extraction methods for the determination of degree of pyritisation and the recognition of iron-limited pyrite formation*. *Chemical Geology*, 111: 101-110.
- Reeuwijk, L.P.v. (Editor), 1995. *Procedures for soil analysis. Technical Paper, 9*. International Soil Reference and Information Centre.
- Roberts, A.P., Pike, C.R. and Verosub, K.L., 2000. *First-order reversal curve diagrams: A new tool for characterising the magnetic properties of natural samples*. *Journal of Geophysical Research*, 105: 28461-28475.
- Rozañ, T.F., Benoit, G. and April, R.H., 1997. *A selective dissolution analysis optimized for measurement of weathering products in a soil*. *Soil Science Society of America - Journal*, 61: 949-958.
- Ryan, J.N. and Gschwend, P.M., 1991. *Extraction of iron oxides from sediments using reductive dissolution by Titanium(III)*. *Clays and Clay Minerals*, 39(5): 509-518.
- Sartori, M. et al., 1999. *Magnetic properties of loess grain size fractions from the section at Paks (Hungary)*. *Physics of the Earth and Planetary Interiors*, 116: 53-64.
- Scheinost, A.C., Chavernas, A., Barron, V. and Torrent, J., 1998. *Clays and Clay Minerals*, 46: 528.
- Schofield, R.K., 1949. *Effect of pH on electric charges carried by clay particles*. *Journal of Soil Science*, 1: 1-8.
- Scholz, F., Lange, B., Jaworski, A. and Pelzer, J., 1991. *Fresenius Journal of Analytical Chemistry*, 340: 140.
- Scholz, F. and Meyer, B., 1994. *Electrochemical solid state analysis: State of the art*. *Chemical Society Reviews*: 341-347.
- Scholz, F. and Meyer, B., 1998. *Voltammetry of solid microparticles immobilized on electrode surfaces*. In: A.J. Bard and I. Rubinstein (Editors), *Electroanalytical Chemistry - A series of Advances*. Marcel Dekker Inc., New York, pp. 1-86.
- Scholz, F., Nitschke, L. and Henrion, G., 1989a. *A new procedure for fast electrochemical analysis of solid materials*. *Naturwissenschaften*, 76: 71-72.
- Scholz, F., Nitschke, L., Henrion, G. and Damaschun, F., 1989b. *Fresenius Journal of Analytical Chemistry*, 335: 189.
- Schwartz, M., Lund, S.P., Hammond, D.E., Schwartz, R. and Wong, K., 1997. *Early sediment diagenesis on the Blake/Bahama outer ridge North Atlantic ocean, and its effects on sediment magnetism*. *Journal of Geophysical Research*, 102(B4): 7903-7914.
- Schwertmann, U., 1959. *Die fraktionierte Extraktion der freien Eisenoxyside in Boden, ihre mineralogischen Formen und ihre Entstehungsweisen*. *Zeitschrift für Pflanzenernährung, Düngung und Bodenkunde*, 84: 194-202.

- Schwertmann, U.**, 1964. *Differenzierung der Eisenoxide des Bodens durch photochemische Extraktion mit saurer Ammoniumoxalat-Lösung*. Zeitschrift für Pflanzenernährung, Düngung und Bodenkunde, 105: 194-202.
- Schwertmann, U.**, 1973. *Use of oxalate for Fe extraction from soils*. Canadian Journal of Soil Science, 53: 244-246.
- Schwertmann, U., Cambier, P. and Murad, E.**, 1985. *Properties of goethites of varying crystallinity*. Clays and Clay Minerals, 33(5): 369-378.
- Schwertmann, U. and Cornell, R.M.**, 1991. *Iron oxides in the laboratory - Preparation and characterisation*. VCH Publishers, Weinheim, 137 pp.
- Schwertmann, U. and Fechter, H.**, 1984. *The influence of aluminum on iron oxides: XI. Aluminum-substituted maghemite in soils and its formation*. Soil Science Society of America Journal, 48: 1462-1463.
- Schwertmann, U., Schulze, D.G. and Murad, E.**, 1982. *Identification of ferrihydrite in soils by dissolution kinetics, differential X-ray diffraction, and Mössbauer spectroscopy*. Journal of the Soil Science Society of America, 46: 869-875.
- Segal, M.G. and Sellers, R.M.**, 1984. *Redox reactions at solid-liquid interfaces, Advances in inorganic and bioinorganic mechanisms*, pp. 97-129.
- Shackleton, N.J., Kukla, G.J. and An, Z.-S.**, 1991. *Correlation of the Chinese loess sequence with the marine oxygen isotope record and astronomical calibration, 2.6 Ma to present (abstract)*. INQUA Abstracts of Papers and Posters, 13: 322.
- Shannon, R.D. and White, J.R.**, 1991. *The selectivity of a sequential extraction procedure for the determination of iron oxyhydroxides and iron sulfides in lake sediments*. Biogeochemistry, 14: 193-208.
- Shenggao, L.**, 2000. *Lithological factors affecting magnetic susceptibility of subtropical soils, Zhejiang Province, China*. Catena, 40: 359-373.
- Singer, M.J., Bowen, L.H., Verosub, K.L., Fine, P. and TenPas, J.**, 1995. *Mössbauer spectroscopic evidence for citrate-bicarbonate-dithionite extraction of maghemite from soils*. Clays and Clay Minerals, 43(1): 1-7.
- Singer, M.J. and Fine, P.**, 1989. *Pedogenic factors affecting magnetic susceptibility of Northern California soils*. Soil Science Society of America - Journal, 53: 1119-1127.
- Singer, M.J., Fine, P., Verosub, K.L. and Chadwick, O.A.**, 1992. *Time dependence of magnetic susceptibility of soil chronosequences on the California coast*. Quaternary Research, 37: 323-332.
- Sommer, M. and Stahr, K.**, 1996. *The use of element:clay-ratios assessing gains and losses of iron, manganese and phosphorus in soils of sedimentary rocks on a landscape scale*. Geoderma, 71: 173-200.
- Spósito, G.**, 1989. *The chemistry of soils*. Oxford University Press, New York, 277 pp.
- Stacey, F.D.**, 1992. *Physics of the earth*. Brookfield Press, Brisbane, Australia, 513 pp.
- Stacey, F.D. and Banerjee, S.K.**, 1974. *The physical principles of rock magnetism. Developments in Solid Earth Geophysics 5*. Elsevier Scientific Publishing Company, Amsterdam, 195 pp.
- Stoner, E.C. and Wohlfarth, E.P.**, 1948. *A mechanism of magnetic hysteresis in heterogeneous alloys*. Phil. Trans. Roy. Soc. (London), A 240: 599-642.
- Stremme, H.E.**, 1998. *Correlation of Quaternary pedostratigraphy from western to eastern Europe*. Catena, 34: 105-112.
- Stucki, J.W., Golden, D.C. and Roth, C.B.**, 1984. *Effects of reduction and reoxidation of structural iron on the surface charge and dissolution of dioctahedral smectites*. Clays and Clay Minerals, 32(5): 350-356.
- Stucki, J.W., Goodman, B.A. and Schwertmann, U. (Editors)**, 1988. *Iron in soils and clay minerals*. Reidel Publishing, Dordrecht, 893 pp.
- Stumm, W. and Furrer, G.**, 1987. *The dissolution of oxides and aluminum silicates: Examples of surface-coordination-controlled kinetics*. In: W. Stumm (Editor), Aquatic surface chemistry. J. Wiley and Sons Inc, New York, pp. 197-219.
- Stumm, W. and Sulzberger, B.**, 1992. *The cycling of iron in natural environments: Considerations based on laboratory studies of heterogeneous redox processes*. Geochimica et Cosmochimica Acta, 56: 3233-3257.

- Su, C. and Harsh, J.B., 1996. *Alteration of Imogolite, Allophane, and acidic soil clays by chemical extractants*. Journal of the Soil Science Society of America, 60: 77-85.
- Sugiura, N., 1979. *ARM, TRM, and magnetic interactions: concentration dependence*. Earth and Planetary Science Letters, 42: 451-455.
- Sulzberger, B., 1990. *Photoredox reactions at hydrous metal oxide surfaces; a surface coordination chemistry approach*. In: W. Stumm (Editor), *Aquatic Chemical Kinetics*. Wiley-Interscience, New York.
- Sulzberger, B., Suter, D., Siffert, C., Banwart, S. and Stumm, W., 1989. *Dissolution of Fe(III)(hydr)oxides in natural waters; laboratory assessment on the kinetics controlled by surface coordination*. Marine Chemistry, 28: 127-144.
- Sun, J. and Liu, T., 2000. *Multiple origins and interpretations of the magnetic susceptibility signal in Chinese wind-blown sediments*. Earth and Planetary Science Letters, 180: 287-296.
- Sun, W., Banerjee, S.K. and Hunt, C.P., 1995. *The role of maghemite in the enhancement of magnetic signal in the Chinese loess-paleosol sequence: An extensive rock magnetic study combined with citrate-bicarbonate-dithionite treatment*. Earth and Planetary Science Letters, 133: 493-505.
- Suter, D., Siffert, C., Sulzberger, B. and Stumm, W., 1988. *Catalytic dissolution of iron(III)(hydr)oxides by oxalic acid in the presence of Fe(II)*. Naturwissenschaften, 75: 571-573.
- Tamm, O., 1922. *Eine Methode zur Bestimmung der anorganischen Komponenten des Gelkomplexes in Boden*. Medd. Statens Skogsforsöksanstalt, 19: 385-404.
- Tamm, O., 1932. *Über die Oxalatmethode in der chemischen Bodenanalys*. Medd. Statens skogsforsöksanstalt, 27: 1-20.
- Tauxe, L., Mullender, T.A.T. and Pick, T., 1996. *Potbellies, wasp-waists, and superparamagnetism in magnetic hysteresis*. Journal of Geophysical Research B: Solid Earth, 101: 571-583.
- Tessier, A., Campbell, P.G.C. and Bisson, M., 1979. *Sequential extraction procedure for the speciation of particulate trace metals*. Analytical Chemistry, 51(7): 844-851.
- Thompson, R. et al., 1980. *Environmental applications of magnetic measurements*. Science, 207: 481-486.
- Thompson, R. and Oldfield, F., 1986. *Environmental Magnetism*. Allen & Unwin, London, 227 pp.
- Torrent, J. and Gomez-Martin, F., 1985. *Incipient podzolization processes in humic Acrisols of southern Spain*. Journal of Soil Science, 36: 389-399.
- Torrent, J., Schwertmann, U. and Barron, V., 1987. *The reductive dissolution of synthetic goethite and hematite in dithionite*. Clay Minerals, 22: 329-337.
- Torrent, J., Schwertmann, U. and Schulze, D.G., 1980. *Iron oxide mineralogy of some soils of two river terrace sequences in Spain*. Geoderma, 23: 191-208.
- Trolard, F., Bourrie, G., Jeanroy, E., Herbillon, A.J. and Martin, H., 1995. *Trace metals in natural iron oxides from laterites: A study using selective kinetic extraction*. Geochimica et Cosmochimica Acta, 59: 1285-1297.
- Trolard, F. and Tardy, Y., 1987. *The stabilities of gibbsite, boehmite, aluminous goethites and aluminous hematites in bauxites, ferricretes and laterites as a function of water activity, temperature and particle size*. Geochimica et Cosmochimica Acta, 51: 945-957.
- Vago, E.R., Calvo, E.J. and Stratman, M., 1994. *Electrochimica Acta*, 39: 1655.
- van der Marel, H.W., 1951. *γ -Ferric oxide in sediments*. Journal of Sedimentary Petrology, 21: 12-21.
- van Oorschot, I.H.M. and Dekkers, M.J., 1999. *Dissolution behaviour of fine-grained magnetite and maghemite in the citrate-bicarbonate-dithionite extraction method*. Earth and Planetary Science Letters, 167: 283-295.
- van Oorschot, I.H.M. and Dekkers, M.J., 2001. *Selective dissolution of magnetic iron oxides in the acid-ammonium-oxalate/ferrous-iron extraction method; I. synthetic samples*. Geophysical Journal International, 145(3): 740-748.
- van Oorschot, I.H.M., Dekkers, M.J. and Havlíček, P., 2001. *Selective Dissolution of Iron Oxides With the Acid-Ammonium-Oxalate/Ferrous-Iron Extraction Technique; II. Natural Loess and Palaeosol Samples*. submitted to: Geophysical Journal International.

- van Velzen, A.J. and Dekkers, M.J., 1999. *Low-temperature oxidation of magnetite in loess-paleosol sequences: A correction of rock magnetic parameters*. *Studia Geophysica et Geodetica*, 43: 357-375.
- Vandenbergh, J., Zhisheng, A., Nugteren, G., Huayu, L. and van Huissteden, J., 1997. *New absolute time scale for the Quaternary climate in the Chinese loess region by grain-size analysis*. *Geology*, 25(1): 35-38.
- Vandenbergh, R.E., Barrero, C.A., da Costa, G.M., Van San, E. and De Grave, E., 2000. *Hyperfine Interactions*, 126: 247.
- Venegas, R. et al., 1994. *Analysis of iron state in some Argentinean soils by dissolution methods and Moessbauer spectroscopy*. *Hyperfine Interactions*, 83: 451-455.
- Verosub, K.L., Fine, P., Singer, M.J. and TenPas, J., 1993. *Pedogenesis and paleoclimate: interpretation of the magnetic susceptibility record of Chinese loess-paleosol sequences*. *Geology*, 21: 1011-1014.
- Verosub, K.L. and Roberts, A.P., 1995. *Environmental magnetism: past, present, and future*. *Journal of Geophysical Research B: Solid Earth*, 100(B2): 2175-2192.
- Verwey, E.J., Haayman, P.W. and Romeijn, F.C., 1947. *Physical properties and cation arrangements of oxides with spinel structure*. *Journal of Chemical Physics*, 15: 181-187.
- Vidic, N.J., TenPas, J.D., Verosub, K.L. and Singer, M.J., 2000. *Separation of pedogenic and lithogenic components of magnetic susceptibility in the Chinese loess/palaeosol sequence as determined by the CBD procedure and a mixing analysis*. *Geophysical Journal International*, 142: 551-562.
- Vine, F.J. and Matthews, D.H., 1963. *Magnetic anomalies over ocean ridges*. *Nature*, 199: 947-949.
- Vlag, P., Rochette, P. and Dekkers, M.J., 1996. *Some additional hysteresis parameters for a natural (titano)magnetite with known grain size*. *Geophysical Research Letters*, 23(20): 2801-2806.
- Walden, J., Oldfield, F. and Smith, J. (eds), 1999. *Environmental magnetism: a practical guide. Technical Guide No. 6*. Quaternary Research Association, London, 243 pp.
- Walker, A.L., 1983. *The effects of magnetite on oxalate- and dithionite-extractable iron*. *Journal of the Soil Science Society of America*, 47: 1022-1026.
- Weaver, R.M., Syers, J.K. and Jackson, M.L., 1968. *Determination of silica in citrate-bicarbonate-dithionite extracts of soils*. *Journal of the Soil Science Society of America*, 32: 497-501.
- Weeks, R.J. et al., 1995. *Normalised natural remanent magnetisation intensity during the last 240,000 years in piston cores from the central North Atlantic Ocean: geomagnetic field intensity or environmental signal?* *Physics of the Earth and Planetary Interiors*, 87: 213-229.
- White, A.F., Peterson, M.L. and Hochella, M.F., 1994. *Electrochemistry and dissolution kinetics of magnetite and ilmenite*. *Geochimica et Cosmochimica Acta*, 58(8): 1859-1875.
- Worm, H.-U., 1998. *On the superparamagnetic - stable single domain transition for magnetite, and frequency dependence of susceptibility*. *Geophysical Journal International*, 133: 201-206.
- Xiao, J.-L., Porter, S.C., An, Z.-S., Kumai, H. and Yoshikawa, S., 1995. *Grain size of quartz as an indicator of winter monsoon strength on the loess plateau of central China during the last 130,000 yr*. *Quaternary Research*, 43: 22-29.
- Zhou, L.P. and Shackleton, N.J., 1999. *Misleading positions of geomagnetic reversal boundaries in Eurasian loess and implications for correlation between continental and marine sedimentary sequences*. *Earth and Planetary Science Letters*, 168: 117-130.
- Zhou, L.-P., Oldfield, F., Wintle, A.G., Robinson, S.G. and Wang, J.T., 1990. *Partly pedogenic origin of magnetic variations in Chinese loess*. *Nature*, 346(6286): 737-739.
- Zinder, B., Furrer, G. and Stumm, W., 1986. *The coordination chemistry of weathering: II. Dissolution of Fe(III) oxides*. *Geochimica et Cosmochimica Acta*, 50: 1861-1869.

Samenvatting in het Nederlands (summary in Dutch)

Milieu-magnetisme bestudeert onder andere het verband tussen klimaatsveranderingen en de eigenschappen van magnetische deeltjes in gesteenten, bodems en sedimenten. De standaard magnetische metingen zijn soms niet specifiek, en dat belet een duidelijke identificatie van de magnetische deeltjes die de klimaatsinformatie met zich dragen. In dit proefschrift worden verschillende aanvullende methoden uit scheikunde en bodemkunde onder de loep genomen om te zien of ze kunnen bijdragen tot de verbetering van het vaststellen van magnetische klimaatsindicatoren. In deze samenvatting krijgt de lezer eerst een korte introductie over de geschiedenis van magnetisch onderzoek. Dit historisch overzicht wordt gevolgd door een korte introductie over het verband tussen wereldwijde klimaatsveranderingen en magnetische mineralen. Tenslotte wordt een samenvatting gegeven van de doelstellingen en resultaten van dit proefschrift.

Geschiedenis van de ontdekking van magneten en van het aardmagneetveld

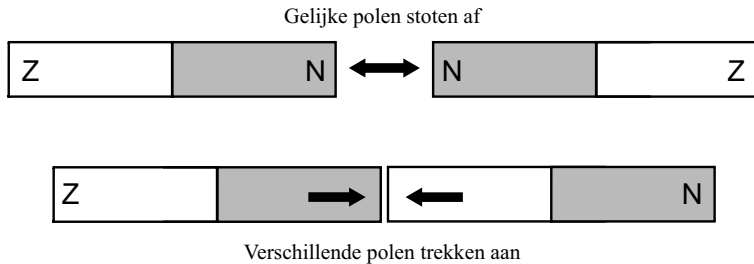
Vanaf het moment van de ontdekking van het bestaan van magneten zijn mensen al gefascineerd door hun ‘magisch’ gedrag. Wie heeft er niet gespeeld met twee magneten en was verwonderd over de manier waarop ze elkaar kunnen aantrekken en afstoten tegelijk? In de antieke Griekse en Chinese culturen was de aantrekkingskracht van de zogenaamde zeilsteen al algemeen erkend. Zeilsteen is een ouderwetse naam voor een natuurlijke magneet, de naam is waarschijnlijk afgeleid van het gebruik van deze steen voor de navigatie op zee. Zeilsteen is een ijzererts dat rijk is aan (geoxideerd) magnetiet (Fe_3O_4), een veel voorkomend magnetisch mineraal. Normaal gesproken zullen magnetiet-ertsen geen sterk magnetisch gedrag vertonen zoals zeilstenen dat doen. Deze stenen danken hun magnetische ‘kracht’ aan twee factoren: 1. de configuratie en concentratie van magnetiet kristallen 2. de bliksem is ingeslagen op het gesteente en dit heeft een tijdelijk en sterk magnetisch veld opgewekt waardoor het erts gemagnetiseerd is. Een belangrijke vindplaats van zeilsteen was de oude Griekse stad Magnesia (in Klein Azië of het tegenwoordige Turkije). Volgens de legende zou een Griekse herder genaamd Magnus rond 900 voor Christus door een veld met zwarte stenen zijn gelopen. De magnetische kracht van deze stenen trok de ijzeren nagels uit zijn sandalen en ook de ijzeren punt van zijn herdersstaf. Maar de unieke eigenschap van deze ‘lapis vivas’ (levende steen), namelijk dat deze het magnetische noorden kan aanduiden en dus kan worden gebruikt voor navigatiedoeleinden, werd door de Grieken van de Oudheid niet herkend.

Dit was anders in China, hier werd het eerste kompas rond 83 na Christus uitgevonden door Luan Te. Hij had een bordspel waarin een van de stukken een lepel was die gemaakt was van *ci shi* of ‘liefdessteen’ (= zeilsteen). Wanneer hij de andere metalen speelstukken bij het bord liet vallen begon de lepel te draaien, en als deze stopte was het handvat altijd naar het zuiden gericht. Na deze ontdekking begonnen de Chinezen het kompas te ontwikkelen en de zeilsteen te bestuderen om haar kracht te kunnen begrijpen. Ze beseften dat, zolang de zeilsteen vrij kon draaien, deze altijd naar het noorden wees. Rond het jaar 600 na Christus ontdekten ze dat zeilsteen gebruikt kan worden om andere ijzernaaldjes magnetisch te maken, maar deze naalden verloren hun magnetisatie na enige tijd weer. Hun grootste ontdekking was daarom dat ze ijzeren naalden een permanente magnetische kracht konden geven door ze eerst tot witheet te verhitten en ze vervolgens snel af te laten koelen in een noord-zuid oriëntatie. Met deze kennis konden ze de laatste versie van hun kompas verbeteren. Deze versie bestond uit een zeilsteen in de vorm van een vis, die vrij kon bewegen in een kom water. Ze vervingen de ‘vis’ door een gemagnetiseerde ijzeren naald en zo ontstond het ‘moderne’ kompas: een gemagnetiseerde naald die vrij kan draaien in een vloeistof. De eerste geschreven referentie naar zo’n kompas dateert van 1086 en staat in ‘Essays van de storm der dromen’ van

Shen Kua, en kort daarna wordt het kompas ook genoemd in de Europese literatuur. De kennis van het kompas is vermoedelijk naar de Westerse wereld gebracht door Marco Polo via de oude ‘zijde route’. Maar er is geen direct bewijs voor deze veronderstelling, het is ook mogelijk dat deze kennis via zee naar de Arabische en Europese landen is gebracht, of zelfs via de Vikingen.

In Europa werden magneten in het algemeen gezien als magische stenen met bijzondere krachten. De eerste expliciete referentie naar magneten staat in de ‘Roman d’Enéas’ (1155-1160 AD). Deze roman is geschreven door een anonieme Normandische dichter, hij schrijft: “De muren van Carthago zijn bezet met magneten zodat alle mannen in wapenuitrusting die te dicht bij de muur komen naar deze muur toetrokken worden en worden vastgehouden”. Deze dichter gebruikt een andere benaming voor zeilsteen: ‘adamant’ ofwel liefdessteen (hieruit is het franse woord voor magneet ‘aimant’ ontstaan). In die dagen geloofden mensen dat als je je geliefde een stuk ‘liefdessteen’ gaf dat hij of zij altijd bij je terug zou komen.

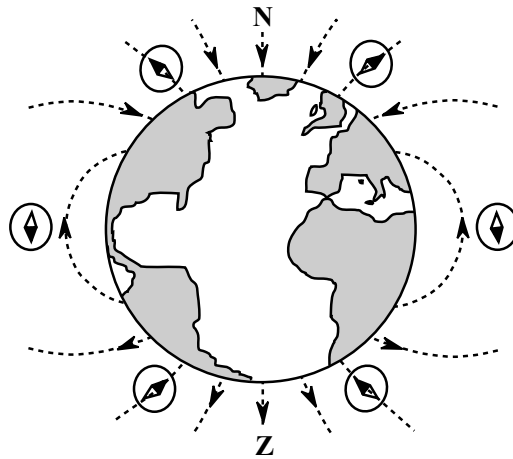
De eerste westerse referentie naar het gebruik van kompassen als navigatiemiddel stamt uit 1190-1199 AD, ongeveer een eeuw nadat in China het ‘moderne’ kompas was ontwikkeld. De referentie komt uit een boek van Alexander Neckam, een Augustijner abt. In zijn boek ‘De naturis rerum’ (Over alle natuurlijke zaken) beschrijft hij een apparaat dat werd gebruikt om te navigeren op zee als het bewolkt was. Met de introductie van het kompas word de zeilsteen ineens erg interessant voor Europese wetenschappers en in 1269 publiceert Pierre de Maricourt (beter bekend als Petrus Peregrinus ofwel Petrus de Pelgrim) een onderzoek naar kompassen en magneten dat als referentiewerk zal dienen voor de komende eeuwen. In zijn ‘Epistola de Magnete’ schrijft hij brieven naar zijn vriend Sygerus van Foucaucourt, waarin hij beschrijft hoe hij ontdekte dat een bol van zeilsteen zich gedraagt als een dipool: tegengestelde polen trekken elkaar aan, en gelijke polen stoten elkaar af (figuur 1). Zijn werk is het eerste wetenschappelijke onderzoek naar magneten dat ons bekend is: hij doet (nauwkeurige) experimenten en gebruikt alleen zijn observaties om een theorie te formuleren.



Figuur 1: Gelijke polen stoten elkaar af, terwijl verschillende polen elkaar aantrekken.

Eeuwenlang hebben wetenschappers zich afgevraagd wat de oorsprong van de magnetische kracht van zeilsteen is, en allen gingen ervan uit dat deze uit de hemel moest komen. Ze dachten dat de kracht kwam van de enige ster in de hemel die niet van positie veranderde: de poolster. Maar in 1600 verandert dit, in dit jaar publiceert William Gilbert (die het jaar erop de lijfarts wordt van koningin Elisabeth I) het resultaat van 18 jaar onderzoek naar magneten: ‘De Magnete, Magneticisque Corporibus, et de Magno Magnete Tellure – Physiologia Nova, Plurimis et Argumentis, et Experimentis Demonstrata’². Hij is de eerste wetenschapper

² Over Magneten, Magnetische Lichamen, en de Grote Magneet Aarde – Een Nieuwe Fysiologie, Gedemonstreerd aan de hand van Vele Argumenten en Experimenten

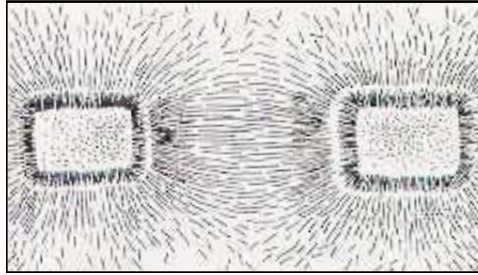


Figuur 2: Dipool weergave van het aardmagneetveld, de veldlijnen zijn weergegeven met stippellijnen. De hoek die een kompasnaald maakt t.o.v. het horizontale vlak hangt af van de geografische positie, zoals weergegeven in de voorbeelden voor hoge en lage breedtegraden.

die zich realiseert dat de Aarde zelf zich als een grote dipool magneet gedraagt met noord- en zuidpolen, en dat een kompasnaald zich richt naar het magnetisch veld dat wordt opgewekt door de aarde (figuur 2). Hij was de eerste onderzoeker die de aarde een fysieke eigenschap toebedeelde. Ook was hij de eerste die de oorsprong van het magneetveld vanuit een hemelse locatie (de poolster) naar de kern van de aarde verplaatste. Gilbert toonde verder aan dat de magnetische polen van de Aarde niet gelijkvallen met de geografische polen. Door zijn wetenschappelijke aanpak kon hij ook veel misverstanden en bijgeloof over magneten ontcrachten. Zo bestreed hij het wijdverbreide volksgeloof dat de magnetische kracht van een zeilsteen kan worden weggenomen door het met knoflook in te smeren. Hoewel het nog meer dan honderd jaar zou duren voordat het niet meer strafbaar was voor een Britse stuurman om knoflook te eten voordat hij ging werken omdat men bang was dat hij met zijn adem het scheepskompas zou demagnetiseren.

Het werk van Gilbert diende als uitgangspunt voor vele andere belangrijke ontdekkingen. Edmond Halley (van de komeet) was op zoek naar een verklaring voor de oorsprong van het aardmagneetveld. In 1692 stelde hij dat het binnenste van de aarde bestond uit verschillende lagen. Elke bol had een eigen magnetisatie, en elke bol draaide langzaam ten opzichte van de anderen. Hoewel dit geen goede verklaring voor de werking van het aardmagneetveld bleek te zijn, was hij wel de eerste die bedacht dat de aarde uit lagen bestaat. Deze bewering is bewezen met geofysisch onderzoek zo'n twee eeuwen nadat Halley het had bedacht.

Hans Christian Oersted (1777-1851) bestudeerde ook magnetisme, en hij ontdekte dat een magnetische naald zich loodrecht richt op een elektrische stroom die door een draad loopt. Zijn idee werd opgepakt door André-Marie Ampère (1775-1836), die aantoonde dat als een stroom door een spoel wordt geleid het een magnetisch veld produceert. Deze observaties waren van groot belang voor de ontwikkeling van ideeën over de oorsprong van het aardmagneetveld, waarvan we inmiddels weten dat het ontstaat in de vloeibare buitenste kern van de aarde (d.m.v. een dynamoproses). Door de hoge temperatuur in de kern van de Aarde zou elke magneet hier zijn magnetische kracht verliezen, dus de oorzaak van het aardmagneetveld is anders dan de aanwezigheid van een sterke magneet in de kern van de aarde. Deze

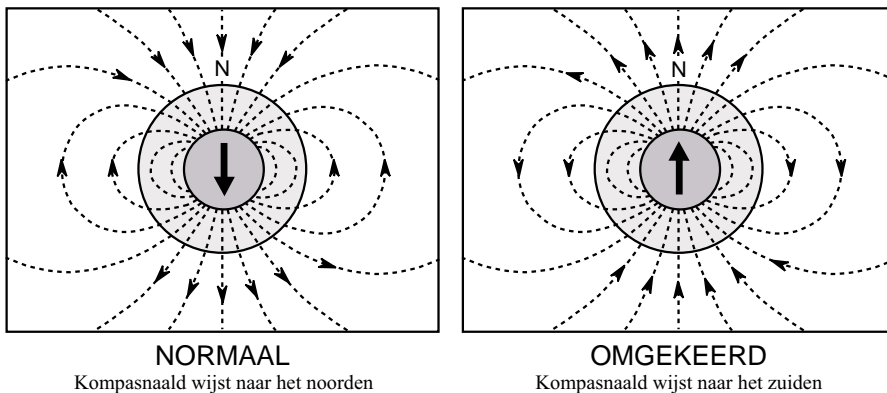


Figuur 3: Magnetische veldlijnen kunnen zichtbaar gemaakt worden door het plaatsen van 1 of meer magneten op een stuk papier dat is bedekt met ijzervijzel. Het ijzervijzel zal zich oriënteren volgens de veldlijnen die door de magneten worden opgewekt, net zoals een kompasnaald zich richt volgens de veldlijnen van het aardmagneetveld.

oorzaak is, simpel gezegd, de circulatie van elektrisch geleidende vloeistoffen in de vloeibare buitenkern van de aarde, een proces dat vergelijkbaar is met de cirkelvormige elektrische stromen in Ampère's experimenten. Rond diezelfde tijd (in 1838) ontwikkelt de Duitse wiskundige Carl Friedrich Gauss een mathematische beschrijving van het aardmagneetveld die tegenwoordig nog steeds wordt toegepast.

Michael Faraday was de eerste die een visuele presentatie (veldlijnen) maakte van de magnetische kracht van een magneet (figuur 3). Zijn tijdgenoot James Clerk Maxwell schiep in 1855 een mathematisch model dat alles wat bekend was over elektrische en magnetische velden combineerde en beschreef. Tot op de dag van vandaag vormen de wetten van Maxwell een van de belangrijkste pijlers van natuurkundig onderzoek; ze verklaren fenomenen zoals radiogolven, röntgenstralen en microgolven (van de magnetron).

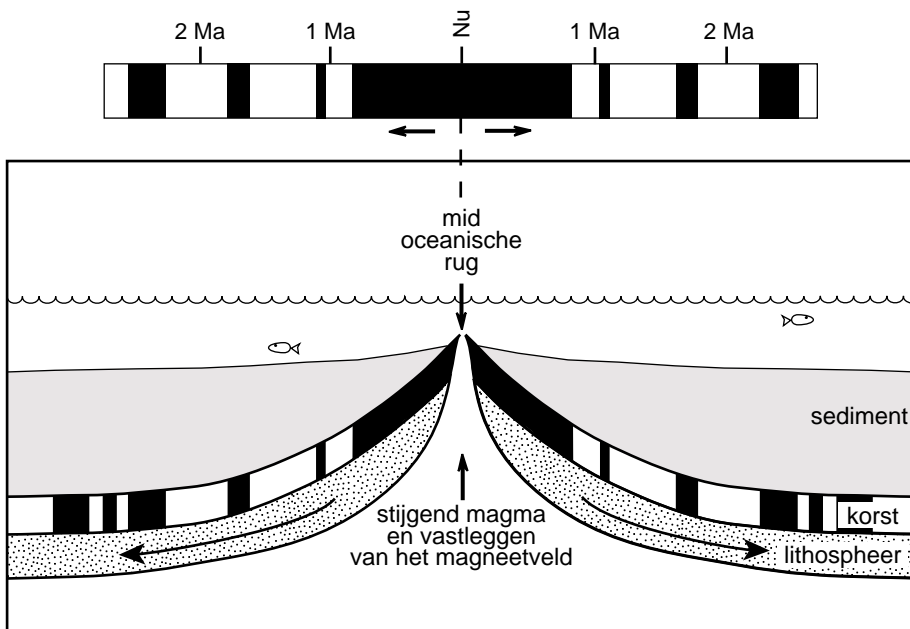
Nadat was ontdekt dat de aarde zelf een magneetveld produceert duurde het nog tot de twintigste eeuw voordat het belangrijkste kenmerk van het aardmagneetveld werd ontdekt: de eigenschap om van polariteit te wisselen. De Franse fysicus Bruhnes (1906) ontdekte dat de richting van de magnetisatie in een gestolde lavastroom en de aangrenzende gebakken klei precies tegenovergesteld was aan het huidige magneetveld (figuur 4). Hij suggereerde dat het aardmagneetveld omgekeerd moest zijn geweest ten tijde van het



Figuur 4: De belangrijkste eigenschap van het aardmagneetveld is de omkering van de richting. Het linker paneel laat de 'normale' huidige richting van het aardmagneetveld zien, en in het rechter paneel staat de omgekeerde situatie (vrij naar: Langereis & Krijgsman (in press)).

uitvloeiën van deze lava: het magnetisch noorden moet het magnetisch zuiden zijn geworden en vice versa. Later onderzoek door Mercanton (1926) en Matuyama (1929) bevestigde deze observaties. Zij vonden omgekeerde richtingen in gesteenten van over de hele wereld en Matuyama ontdekte dat de omgekeerde richtingen alleen voorkwamen in oudere gesteenten. Vervolgens werden steeds meer omkeringen gevonden en in 1955 stelde de Nederlander Hospers voor dat het patroon van omkeringen gebruikt kan worden om stratigrafische secties van over de hele wereld met elkaar te correleren en te dateren (zo ontstond de magnetostratigrafie).

Met de komst van betrouwbare dateringsmethoden voor gesteenten in de jaren zestig kon ook de geologische ouderdom van magnetische omkeringen bepaald worden (Cox et al., 1963). Dit leidde tot de ontwikkeling van een geomagnetische polariteit tijdschaal (GPTS); een tijdschaal gebaseerd op het specifieke patroon van omkeringen van het aardmagneteveld. Inmiddels hadden wetenschappers de patronen van magnetische richtingen die vastgelegd zijn in gesteenten over de hele wereld bestudeerd. Ze kwamen er achter dat de richting van het aardmagnetisch veld en de bijbehorende positie van de magnetische polen niet alleen met de tijd maar ook met de geografische positie had gevarieerd. Dit kon alleen verklaard worden met twee verschillende theorieën: ofwel had de magnetische pool zich verplaatst (true polar wander ofwel zwervende polen) of waren de continenten van plaats veranderd (continental drift



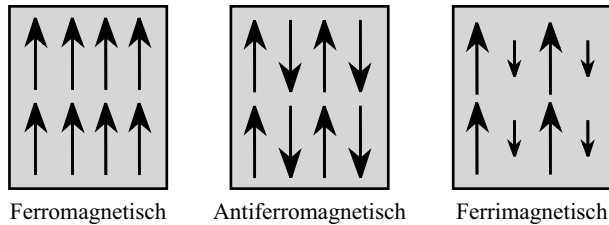
Figuur 5: Een diagram van het mid-oceanische rug (MOR) systeem (onderste paneel). Magma stijgt op in het midden van de rug en drijft de twee oceanische platen uiteen waardoor 'continental drift' ontstaat. Terwijl nieuw oceanische korst wordt gevormd in het centrum van de MOR, zullen de magnetische domeinen in het nieuwe gesteente zichzelf oriënteren naar het heersende aardmagneteveld. Dit resulteert in een patroon van normale en omgekeerde magnetische signalen (vergelijkbaar met de streepjescode op een produkt uit de supermarkt) die parallel lopen aan de MOR en aan weerszijden van deze MOR symmetrisch zijn (zoals in het bovenste paneel). De tijdschaal in het bovenste paneel is aangegeven in miljoenen jaren (Ma = Mega annum = 1 miljoen jaar) (vrij naar: Langereis & Krijgsman (in press)).

/ apparent polar wander ofwel verschuiving van continenten / schijnbaar zwerfende polen). In de daaropvolgende jaren was er heel wat ophef en discussie, maar er kon geen eenduidig bewijs gevonden worden voor de ene noch de andere theorie, totdat uiteindelijk via palaeomagnetisch onderzoek werd bewezen dat de continental drift theorie zoals eerder voorgesteld door Alfred Wegener (1912) correct was. Het mechanisme verantwoordelijk voor continental drift was echter nog onduidelijk. Gedurende de jaren vijftig hadden marine onderzoeksschepen al ontdekt dat het magnetisch signaal in de oceaanbodem in lange stroken, parallel aan de mid-Atlantische rug, was vastgelegd (figuur 5). De mid-Atlantische rug maakt deel uit van een wereldomvattend systeem van oceanische berggruggen. De structuur en verdeling van het magnetisch signaal in de zeebodem leken uitzonderlijk symmetrisch aan beide kanten van deze rug. Naar aanleiding van de hypothese over zeebodemspreiding van Hess (1962), namen Fred Vine en Drummond Matthews (1963) beide observaties samen en veronderstelden ze dat de zeebodem in constante beweging was en wegdreef van de centrale oceaanrug waar nieuwe oceaanbodem werd gevormd. Ze hadden het mechanisme ontdekt dat verantwoordelijk is voor continental drift. We noemen dit plaattektoniek en het is de grondgedachte van de moderne aardwetenschappen.

De stichters van gesteentemagnetisme

Veel oorspronkelijk onderzoek in palaeomagnetisme was gericht op het beschrijven van het aardmagneetveld, maar aan het einde van de achttiende eeuw begonnen onderzoekers te bestuderen hoe dit signaal werd vastgelegd in gesteenten en mineralen. Rond die tijd hadden onderzoekers al vastgesteld dat sommige gesteenten extreem sterke remanente magnetisatie hadden, maar deze effecten werden toegeschreven aan de gevolgen van blikseminslag door Alexander von Humboldt in 1797. De eerste observatie dat bepaalde gesteenten worden gemagnetiseerd in dezelfde richting als het aardmagneetveld werd gedaan door Dellesse in 1849 en door Melloni in 1853. Pierre Curie (die trouwde met Marie Curie in 1895) was ook gefascineerd van magnetisme voordat hij met zijn vrouw begon met onderzoek naar straling. Hij ontdekte dat magneten hun magnetische kracht verliezen boven een bepaalde temperatuur (die temperatuur noemen we nu Curie punt).

In Frankrijk publiceerde Paul Langévin zijn werk over de atoomtheorie van paramagnetisme in 1905. Hij liet zien dat paramagnetische mineralen een magnetische kracht vertonen die gelijk is aan het magneetveld waarin ze verblijven. Ze verliezen hun magnetische kracht zodra er geen extern magnetisch veld is. Ook toonde hij aan met zijn theorie dat de richting van die magnetische kracht verstoord zal worden bij hogere temperatuur. Zijn tijdgenoot, Pierre Ernst Weiss, werkte ook aan magnetisme. In 1907 publiceerde hij zijn moleculaire veld theorie waarin hij een verklaring geeft voor de oorsprong van magnetische momenten in mineralen. Hij stelde voor dat magnetische mineralen interne magnetische velden (domeinen) hebben. Bij gebrek aan een extern veld, zullen deze domeinen elkaar opheffen, terwijl ze zullen roteren of vergroten ten koste van andere domeinen als zelfs maar een klein extern veld wordt aangewend. Hij vond zo een verklaring van het magnetisch gedrag van ferromagneteten (figuur 6). De experimenten van Heinrich Georg Barkhausen (1919) bevestigden het bestaan van deze magnetische domeinen en ook van het verschuiven van domeinwanden. Hij liet zien dat wanneer een ferromagnetisch materiaal door een spoel bewogen wordt het een verandering in de positie van de domeinwanden veroorzaakt (dit fenomeen staat bekend als de Barkhausen sprongen), wanneer een versterker wordt gebruikt kun je dit verspringen van domeinwanden zelfs horen.



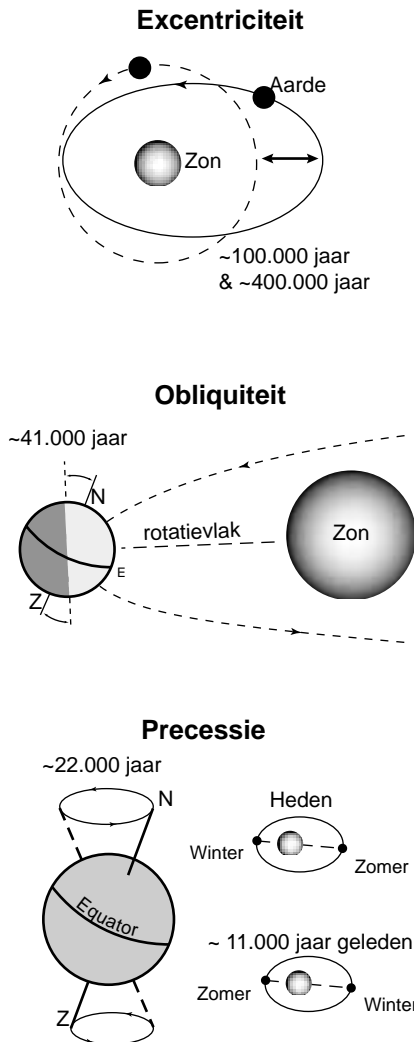
Figuur 6: Verschillende vormen van koppeling van spinmomenten resulteren in verschillend magnetisch gedrag. In ferromagnetische materialen zijn alle momenten hetzelfde gericht en dit resulteert in een netto magnetisch moment in dezelfde richting als alle afzonderlijke momenten. Metallisch ijzer is een voorbeeld van een ferromagnetisch materiaal. In antiferromagnetische mineralen zijn de afzonderlijke momenten in de verschillende sub-roosters van gelijke waarde, maar de richtingen zijn tegengesteld dus werken ze elkaar tegen. Dit resulteert in een netto magnetisch moment dat gelijk is aan nul. Gewoonlijk hebben antiferromagnetische materialen geen perfecte momenten en zijn de tegengesteld gerichte momenten niet helemaal parallel, dit noemen we gekanteld antiferromagnetisme. In zulke gevallen is het netto magnetisch moment niet nul. Hematiet is een voorbeeld van een mineraal met een gekanteld antiferromagnetisch moment. In ferrimagnetische materialen zijn de tegengestelde subrooster momenten niet van gelijke grootte waardoor er een netto magnetisch moment overblijft in de richting van het dominante sub-rooster moment. Magnetiet en maghemiet zijn voorbeelden van ferrimagnetische mineralen (vrij naar: Langereis & Krijgsman (in press)).

Het onderzoek naar het magnetisch gedrag van mineralen en naar het aardmagneetveld hebben zich afzonderlijk van elkaar ontwikkeld, tot in de jaren dertig, toen ze samen werden gebracht door onder anderen Koenigsberger, Thellier, Nagata en Néel. Deze wetenschappers onderzochten de processen die verantwoordelijk zijn voor de magnetisatie van gesteenten vanuit een fysisch oogpunt en ze probeerden deze magnetisaties te reproduceren in het laboratorium. Dit type onderzoek kreeg van Nagata (1953) de naam gesteentemagnetisme en het is nu de grondslag voor palaeomagnetisch onderzoek en ook van dit proefschrift. Ze ontdekten dat ze een magnetisatie konden opwekken in een gesteente monster door het bloot te stellen aan hitte en het vervolgens af te laten koelen in een (in het lab opgewekt) magneetveld. Dit is vergelijkbaar met de Chinese methode van het permanent magnetisch maken van kompas naalden. Néel (1949) toonde vervolgens aan dat deze thermoremanente magnetisatie (TRM) in het monster werd vastgelegd bij een specifieke temperatuur die afhangt van grootte en vorm van de magnetische korrels (deze temperatuur is later Néel temperatuur genoemd en heeft veel weg van het Curie punt voor ferromagnetische mineralen) (Néel, 1949). Ondanks de voorspelling van Landau en Lifschitz (1935) dat ferromagnetisme de enige mogelijke vorm van natuurlijk magnetisme kon zijn, gebruikte Néel de theorieën van Weiss om aan te tonen dat magnetische mineralen niet allemaal dezelfde verdeling van magnetische domeinen hebben, en zijn theorie voor single-domain (enkel-domein) mineralen is nog altijd geldig. Hij ontdekte ook een fenomeen dat inmiddels bekend staat als viskeuze magnetisatie: de langzame verandering van magnetisatie met tijd en constante temperatuur. Daarnaast onderscheidde hij ferrimagnetische en anti-ferromagnetische mineralen (Néel, 1955). In 1970 kreeg hij een Nobel prijs voor zijn werk.

Verband tussen klimaat en magnetische mineralen

Het klimaat op aarde varieert zowel op locale als op wereldwijde schaal, en we weten dat in het verleden er zich een aantal ijstijden hebben voorgedaan. In de jaren twintig verklaarde Milutin Milankovitch het voorkomen van zulke drastische veranderingen in het wereldklimaat door de variatie in de baan (= orbit)

van de aarde met de tijd te berekenen. Zijn theorie staat tegenwoordig bekend als de orbitaal of Milankovitch cycli. Hij ontdekte dat er drie belangrijke cycli zijn die de distributie van de warmte van de zon over de aarde bepalen: excentriciteit, obliquiteit en precessie (figuur 7). De excentriciteit cyclus bepaalt de vorm van de baan van de aarde rond de zon; die verandert van rond (lage excentriciteit) naar elliptisch (hoge excentriciteit) in periodes van 100.000 en 400.000 jaar. Tijdens periodes met een ronde baan is het contrast van seizoenen op het noordelijk en zuidelijk halfrond erg klein. Het contrast is groter tijdens periodes met een sterk elliptische baan, en dan is ook de lengte van de seizoenen anders.



Figuur 7: De drie Milankovitch cycli: excentriciteit, obliquiteit en precessie. De combinatie heeft invloed op het klimaat op aarde (vrij naar: Langereis & Krijgsman (inpress)).

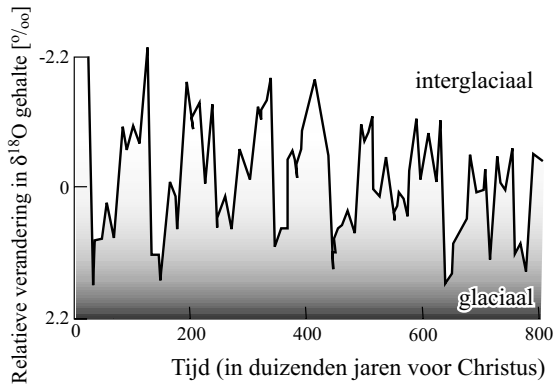
De obliquiteit beschrijft de verandering van de hoek die de rotatie-as van de aarde maakt ten opzichte van het vlak waarin de aarde rond de zon draait. Deze hoek varieert tussen 22° en 24.6° over een periode van ongeveer 41.000 jaar. De obliquiteit heeft meer effect op hogere breedtegraden dan aan de evenaar. Hoe kleiner de hoek met het draaivlak, hoe minder contrast in seizoenen: dus mildere winters en koele zomers bij een kleine hoek en koude winters en hete zomers bij maximale obliquiteit.

De klimaatprecessie cyclus duurt ongeveer 21.700 jaar en beschrijft de positie van de rotatie-as van de aarde ten opzichte van de zon. Het wiegelen van deze as heeft effect op de positie van de equinox (het tijdstip waarop de zon direct boven de evenaar staat). Dit betekent dat op sommige momenten in de precessie cyclus, de midzomernacht (op het noordelijk halfrond) het dichtst bij de zon is, terwijl tegelijkertijd de midwinternacht het verst van de zon af is (zie ook figuur 7). Ongeveer 11.000 jaar later is dit precies omgekeerd. Het gevolg is dat in de eerste situatie (op het noordelijk halfrond) de winters koud zijn omdat de midwinternacht het verst van de zon af is, terwijl de zomers heet zijn omdat de midzomernacht het dichtst bij de zon is. In de tweede situatie zal de winter mild zijn en de zomer koel, dit is de huidige situatie.

Van het gecombineerd effect van deze drie cycli kan de insolatie curve berekend worden, die geeft weer hoeveel energie de aarde ontvangt van de zon voor elke breedtegraad. Deze curve varieert door de tijd omdat de drie cycli allemaal verschillende perioden hebben en dus kunnen ze elkaar zowel versterken als uitdoven. De meest gunstige condities voor de groei van de ijskappen en het ontstaan van ijstijden zijn bij koele zomers, dus is de baan van de aarde rond de zon (ook wel orbital forcing genoemd) een van de belangrijkste oorzaken van het cyclisch groeien en krimpen van de ijskappen op de polen. Een ijstijd zal waarschijnlijk ontstaan in periodes van minimale obliquiteit, maximale excentriciteit en wanneer de aarde het verst van de zon staat tijdens de midzomernacht. Hoewel we momenteel in een warme (interglaciale) periode zitten, suggereert de huidige trend van de orbitale cycli dat we een nieuwe ijstijd zullen krijgen op het noordelijk halfrond. Desalniettemin, weten we niet precies wanneer deze nieuwe ijstijd zal plaatsvinden, met name omdat het nog steeds niet duidelijk is of de recente (door mensen veroorzaakte) toename in broeikasgassen het effect van de orbital forcing kan tegengaan en zo de afkoeling van het klimaat kan stoppen.

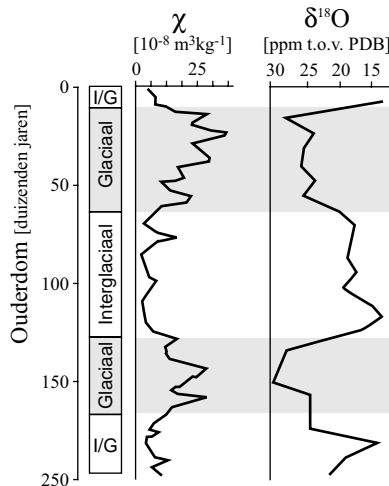
De theorie van Milankovitch verklaart het mechanisme van periodieke klimaatsveranderingen in het verleden. De veranderingen in de distributie van zonne-energie heeft een belangrijk effect gehad op klimaat en milieu, en dus ook op factoren zoals neerslag, windrichting en -sterkte, vegetatie, enzovoorts. Deze factoren hebben op hun beurt effect gehad op snelheid van vertering van gesteenten, de hoeveelheid stof die door de wind kan worden meegevoerd, de groei en het afsmelten van gletsjers, de groei van kalkriffen in zee, en vele andere fenomenen die zijn vastgelegd in het geologisch archief van de aarde. Op die manier is het patroon van klimaatsveranderingen uit het verleden vastgelegd in de gesteenten en sedimenten die we nu overal aantreffen. Een van de toetsstenen van het aardse klimaat die men terug kan vinden in sedimenten is de variatie in concentratie van stabiele zuurstofisotopen (^{18}O en ^{16}O). Oceaan sedimenten vormen een vrijwel continu archief van het geologisch verleden, en ze bevatten vele fossielen van planktonische foraminiferen (kleine zeediertjes met een kalkhoudende schaal). Deze diertjes nemen zuurstof op uit het oceaanwater om hun kalkschaal te maken, en de verdeling ($\delta^{18}\text{O}$) van zware zuurstof (^{18}O) tegen lichte zuurstof (^{16}O) isotopen is een maat voor de hoeveelheid ijs op de polen. Dat komt doordat de lichte zuurstof makkelijker verdampt uit de oceanen dan de zware zuurstof (zeker bij lage temperatuur aan het oceaan oppervlak), dit lichte zuurstof wordt daarom preferent opgeslagen in de ijskappen op de polen. Een toename in de concentratie zwaar zuurstof (^{18}O) in de oceanen, en dus een

toename in de $\delta^{18}\text{O}$ waarde in de kalkschaal van forams betekent dus een vergroting van de ijskappen en dus een kouder klimaat (figuur 8).



Figuur 8: Het zuurstofisotopen signaal van de afgelopen 800.000 jaar. Een toename van $\delta^{18}\text{O}$ ratio duidt op een ijstijd (glaciaal), en een afname van deze ratio wordt veroorzaakt door een warme periode (interglaciaal).

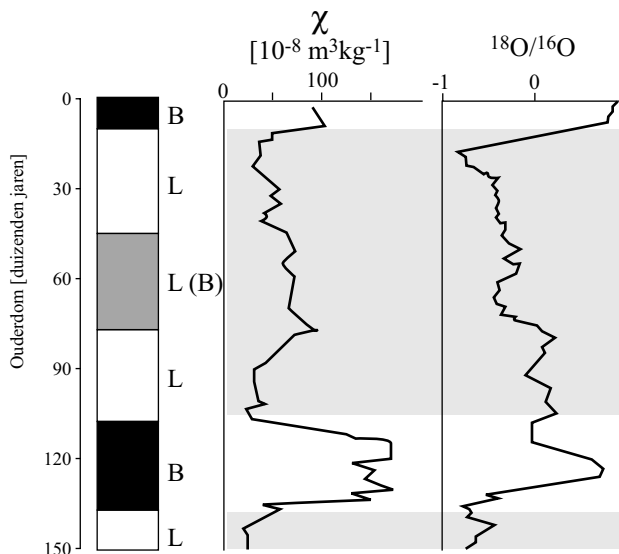
De waarneming dat de variatie in $\delta^{18}\text{O}$ in oceanische sedimenten ook een corresponderende variatie in magnetische eigenschappen vertoont, stimuleerde veel klimaatgericht palaeomagnetisch onderzoek. Deze ontdekking moest betekenen dat het magnetisch signaal in gesteenten en sedimenten niet allen maar een weerspiegeling is van het aardmagneetveld (richting en sterkte), maar ook van het klimaat. Het was duidelijk dat de veranderingen in magnetisch signaal in de oceanische sedimenten meestal het patroon van klimaatsverandering volgden (figuur 9). Een verklaring zou kunnen zijn dat tijdens ijstijden de invoer van



Figuur 9: Voorbeeld van de correlatie tussen de magnetische susceptibiliteit en de zuurstofisotopen ratio in een diepzee sediment. Ijstijden zijn aangegeven met grijs en hebben een hoge zuurstofisotopen ratio, terwijl de interglaciale periode een lage ratio hebben. De magnetische susceptibiliteit in deze sectie is sterker in niveaus die gevormd zijn tijdens ijstijden, en zwakker in niveaus die zijn gevormd tijdens interglacialen (vrij naar: Thompson & Oldfield 1986, fig 12.7).

foraminiferen (als oceanisch kalk) lager was vanwege het koude klimaat, op die manier zou de aanvoer van wind-getransporteerd en detritisch materiaal ogenschijnlijk zijn vergroot. Tijdens warmere perioden zou deze aanvoer juist worden verdund door de verhoogde aanvoer van kalk via foraminiferen en het magnetisch signaal is dan zwakker in sedimenten uit warmere perioden. Een andere verklaring is dat er tijdens ijstijden minder vegetatie is op het land, of misschien zijn er veranderingen in de windrichting, waardoor er meer of een veranderde aanvoer is van continentaal materiaal. Beide mechanismen zouden het magnetisch signaal in de oceanen tijdens ijstijden versterken.

De verandering in $\delta^{18}\text{O}$ en ook in magnetische eigenschappen van diepzee sedimenten zijn dus een indicatie voor klimaat. Het was echter moeilijk om een vergelijkbaar geologisch archief van klimaatsverandering te vinden op het land. Dit veranderde toen in de jaren tachtig de loess afzettingen in China werden gedateerd met behulp van magnetostratigrafie. Deze Chinese afzettingen dateren uit het Quartair en bestaan uit opeenvolgingen van loess die worden onderbroken door palaeobodems. Vervolgens werd aangetoond dat het magnetisch signaal in deze afzettingen zich vergelijkbaar gedroeg met het $\delta^{18}\text{O}$ signaal van mariene sedimenten (bijvoorbeeld: Heller and Liu, 1984). Het magnetische signaal van deze afzettingen varieert met het type gesteente; het is laag in de loess en hoog in de palaeobodems. De loess is afgezet tijdens ijstijden, terwijl in de warmere periodes de neerslag en temperatuur toenamen zodat bodemvorming kon optreden en sterk magnetische mineralen werden gevormd in de palaeobodems (figuur 10).



Figuur 10: Voorbeeld van de correlatie tussen de versterkte magnetische susceptibiliteit (toename in aantal fijnkorrelige magnetische mineralen) en het zuurstofisotopen signaal. De linker kolom toont het type gesteente van de loess-palaeobodem sectie. De palaeobodems zijn in zwart weergegeven. In het midden van de sectie zit een verweerde loess met een licht verhoogde magnetische susceptibiliteit die niet is gerelateerd aan het zuurstofisotopen signaal. Over het algemeen correleert de magnetische susceptibiliteit goed met het signaal van de zuurstofisotopen: het is hoog tijdens interglacialen (lage zuurstofratio) en laag tijdens ijstijden (hoge zuurstofratio, grijze stukken) (vrij naar Liu et al. 1995).

Dit proefschrift

Een belangrijk hulpmiddel bij het achterhalen en begrijpen van mineraalmagnetische eigenschappen en hun oorsprong is gesteentemagnetisme. Hierbij bestudeert men niet alleen de fundamentele magnetische eigenschappen van natuurlijke en synthetische mineralen, maar ook de relatie tussen magnetisme en mineralogie, korrelgrootte, korrel vorm, kristalliniteit, chemische samenstelling en temperatuur wordt gebruikt om het magnetisme van mineralen en gesteenten te begrijpen. Deze parameters kunnen vervolgens ook worden gebruikt om de concentratie en samenstelling van magnetische deeltjes in natuurlijke monsters te bepalen. Gesteentemagnetisme lijkt daarom ideaal voor de identificatie van pedogene (= in de bodem gevormde) magnetische deeltjes. Maar het signaal van ferrimagnetische deeltjes is vaak zo sterk dat het dat van andere (zwak magnetische) deeltjes overstemt, en dit belet een nauwkeurige bepaling van de magnetische samenstelling aan de hand van enkel gesteentemagnetische metingen. Andere technieken zijn daarom noodzakelijk om de exacte samenstelling te kunnen bepalen. Daarom zijn extractiemethoden geïntroduceerd in magnetische studies, omdat werd aangenomen dat deze selectief bepaalde mineralen of korrelgrootte fracties oplossen. De resultaten van een aantal van dergelijke onderzoeken hebben echter laten zien dat er soms controversiële resultaten waren over welke mineralen nu precies in oplossing gaan met deze methoden.

De Chinese loess-palaeobodem sequenties vormen de eerste continue continentale 'archieven' van klimaatsverandering die als zodanig herkend werden en al snel zijn vergelijkbare afzettingen ook in andere delen van de wereld aangetroffen. In deze sequenties kan de verandering van het magnetisch signaal met de diepte worden gecorreleerd aan de verandering in het klimaat (net zoals in oceanische sedimenten). In bepaalde gebieden zoals Alaska en Siberië, zijn echter tegengestelde magnetische patronen gevonden aan die van China: met hogere magnetische susceptibiliteit in de loess en lagere in de palaeobodems. Het mechanisme dat verantwoordelijk is voor dit versterkte magnetische signaal is dus niet overal hetzelfde geweest. Maar toch kan het magnetisch signaal van deze sedimenten gebruikt worden als indicator van wereldwijd veranderend klimaat, zelfs als de lokale mechanismen sterk variëren. Om te kunnen begrijpen waarom deze magnetische signalen per regio verschillen, is het belangrijk om te begrijpen welke processen hebben geleid tot de tegenovergestelde waarnemingen van hetzelfde klimaatsignaal. Bijvoorbeeld waarom en hoe magnetische mineralen worden gevormd tijdens bodemvorming en welke mineralen van het oorspronkelijke materiaal komen. Omdat de vorming van nieuwe mineralen (en de verwerking van de oorspronkelijke mineralen) afhangt van factoren zoals klimaat, zuurgraad en vochtigheid van de bodem, is het belangrijk om de samenstelling en concentratie van de pedogene (bij de bodem horende) magnetische mineralen te kunnen vaststellen, omdat deze de klimaatsgeschiedenis van de sectie voor een belangrijk deel weergeven.

Het voornaamste doel van dit proefschrift is om een beter begrip te ontwikkelen van de werking van chemische extractiemethoden, zodat we hun werking kunnen verbeteren en op die manier een betere identificatie van de bodem-mineralen kunnen maken. Daarom ligt de nadruk van dit werk op het onderscheid tussen twee veelvoorkomende ferrimagnetische oxiden: magnetiet en maghemiet. Naast het onderzoek naar de effectiviteit van bestaande extractiemethoden was het ook belangrijk om vast te stellen of er soms andere technieken waren (bijvoorbeeld technieken die gebruikt worden in bodemkunde of scheikunde) die geschikt zouden kunnen zijn voor de identificatie van magnetische mineralen. Een zoektocht langs verschillende disciplines leidde ons naar elektrochemie waar een nieuwe veelbelovende

methode was ontwikkeld voor de identificatie van ijzeroxides: voltammetrie van microdeeltjes (VMP).

Dit proefschrift is onderverdeeld in drie delen. In onze zoektocht naar de 'ideale oplossing' hebben we twee extractiemethoden bestudeerd: de CBD methode en de AAO-Fe²⁺ methode. Voor beide methoden hebben we eerst de optimale condities bepaald voor het selectief oplossen van ijzeroxiden (deel I). Om dit te bereiken hebben we gebruik gemaakt van synthetische monsters waarvan de magnetische samenstelling nauwkeurig bekend was. De resultaten laten zien dat door de combinatie van gesteentemagnetische analyse en extractie resultaten we een beter inzicht kregen in de samenstelling en het oplosgedrag van de ijzeroxides.

Vervolgens moesten we testen of de methoden hetzelfde resultaat geven voor natuurlijke monsters (Deel II). Hiervoor hebben we monsters genomen van een loess-palaeobodem sequentie in Tsjechië. Dezelfde extractiemethoden zijn op deze monsters toegepast, en met behulp van de gesteentemagnetische analyses kon ook van deze monsters een goed beeld geschetst worden van hun magnetische samenstelling.

Tenslotte hebben we een veelbelovende nieuwe techniek (voltammetrie van microdeeltjes) uit de elektrochemie voor het eerst getest op natuurlijke monsters. Deze VMP techniek bleek uitermate geschikt voor de identificatie van zwak magnetische mineralen, die normaliter met behulp van gesteentemagnetische analyses niet goed konden worden geïdentificeerd omdat het signaal van de sterke mineralen hun aanwezigheid vaak overstemt.

CBD methode

De resultaten van hoofdstuk 2 laten zien dat deze methode nogal agressief werkt en alle ijzeroxides oplost. Het enige onderscheid dat met deze methode kan worden gemaakt is tussen de snel oplopende fijnkorrelige mineralen en de langzaam oplopende grofkorrelige mineralen. Het bleek ook dat de experimentele condities een grote impact hebben op de werking van deze methode: bij een hogere extractiemethode lost alles sneller op, en bij een hogere ijzeroxide concentratie lost alles minder snel op. De resultaten van de natuurlijke monsters (hoofdstuk 5) laten zien dat ook hier voornamelijk de fijnkorrelige mineralen worden opgelost. Maar de geoxideerde randen van grofkorrelige mineralen worden ook opgelost, net als sommige silicaatmineralen. Dit betekent dat deze methode helemaal niet zo selectief is als eerder werd aangenomen en deze methode is dan ook niet geschikt voor de identificatie van een specifiek mineraal. Het onderzoek toonde echter wel aan dat als de concentratie ijzeroxides maar hoog genoeg is (groter dan 5%), er wel onderscheid kan worden gemaakt tussen fijnkorrelige magnetiet en maghemiet.

AAO-Fe²⁺ methode

Deze methode was een stuk minder agressief dan de CBD methode, maar de resultaten waren wel vergelijkbaar. De AAO-Fe²⁺ methode loste ook preferent de fijnkorrelige ijzeroxides op en gaf een goed onderscheid tussen grofkorrelige magnetiet en maghemiet (hoofdstuk 3). Met een uitgebreide gesteentemagnetische analyse was het echter wel mogelijk om te zien dat deze methode ook onderscheid maakt tussen fijnkorrelige magnetiet en maghemiet.

De methode was ontwikkeld om de niet-kristallijne mineralen preferent op te lossen, maar onze resultaten tonen aan dat de methode geen onderscheid maakt op kristalliniteit. Ook deze methode bleek gevoelig voor de experimentele condities, bij verhoging van de pH werden nauwelijks ijzeroxides opgelost. De resultaten van de natuurlijke monsters kwamen overeen met die van de synthetische monsters

(hoofdstuk 6). Ook hier was geen goed onderscheid tussen het preferent oplossen van bodemgerelateerde oxides over loess-gerelateerde deeltjes. Het mineralogisch onderscheid was meer dat magnetiet preferent werd opgelost in alle monsters. Ondanks dit tegenvallend resultaat is de methode toch beter geschikt voor gebruik dan de CBD methode omdat de laatste ook silicaatmineralen oplost.

Voltammetrie van microdeeltjes

Omdat geen van de extractiemethoden selectief de bodemgerelateerde mineralen verwijdert, moesten we op zoek naar een methode die deze deeltjes wel kon onderscheiden van de loess-gerelateerde mineralen. VMP is recent ontwikkeld binnen elektrochemie en is voornamelijk gebruikt op monsters die alleen bestonden uit ijzeroxides. Omdat de resultaten van deze methode zeer gunstig waren, besloten we de methode voor het eerst uit te testen op natuurlijke monsters. Dit was op de eerste plaats belangrijk om te bepalen wat de detectielimiet van deze methode was, en op de tweede plaats om te zien of er geen storende factoren zouden optreden bij metingen aan natuurlijke monsters.

We hebben getest met monsters van twee verschillende geologische locaties (hoofdstuk 8 en 9), en de resultaten zijn zeer positief. De sterk magnetische mineralen konden met deze methode niet worden geïdentificeerd, maar er kon wel heel gedetailleerde informatie verkregen worden over de (normaal slecht te meten) zwakke magnetische mineralen. Bovendien werd aangetoond dat de detectielimiet van deze methode veel lager is dan die van andere analysemethoden (0.1 %). De informatie die kon worden verkregen over de zwakke mineralen was veel gedetailleerder dan we normaal met standaard gesteentemagnetische metingen kunnen verkrijgen. Hierdoor kregen we veel meer inzicht in de magnetische samenstelling van de monsters en konden we specifieker zijn over de herkomst en klimaatgeschiedenis van beide geologische locaties. Bovendien konden we voor het eerst de concentratie van magnetische mineralen bepalen door middel van een interne standaard.

De resultaten van het onderzoek aan extractiemethoden tonen aan dat deze misschien niet de 'ideale oplossing' zijn voor het identificeren van specifieke magnetische mineralen. De VMP resultaten zijn echter veelbelovend, en in de toekomst zullen waarschijnlijk steeds meer technieken uit andere disciplines worden geïntegreerd in milieu-magnetisme om zo het onderzoek naar magnetische klimaatsindicatoren te verbeteren.

Dankwoord

In de jaren die ik op het fort heb doorgebracht zijn er een aantal mensen geweest die – actief dan wel passief – geholpen hebben bij de totstandkoming van dit proefschrift. Via deze weg wil ik hiervoor mijn dank uitspreken.

Mark, als mijn begeleider en co-promotor heb je me een entree gegeven tot de wondere wereld van het gesteentemagnetisme. Ik heb grote waardering voor de vrijheid en het vertrouwen dat je mij gaf tijdens de uitvoering van dit project. Mede dankzij jouw innovatieve instelling, heb ik in dit onderzoek veel nieuwe wegen kunnen bewandelen. Daarnaast heb ik bewondering voor je bijna encyclopedische kennis van het vakgebied, waar ik menig keer gebruik van heb kunnen maken. Je (vaak gedetailleerde) reviews hebben de kwaliteit van mijn werk altijd positief beïnvloed.

Mijn promotor, Cor Langereis, wil ik allereerst danken voor de vrijheid die ik van hem kreeg bij de uitvoering van dit onderzoek. Daarnaast ben ik hem dank verschuldigd voor de faciliteiten die ik op het fort tot mijn beschikking had. Dankzij zijn inzet en die van Mark Dekkers, is de outillage van het chemisch lab op het fort aanzienlijk verbeterd, wat de uitvoering van mijn onderzoek ten goede kwam. Tenslotte wil ik je ook bedanken, Cor, voor de discussies en reviews van mijn proefschrift. Jouw niet-chemische achtergrond gaf mij de mogelijkheid de formulering van mijn teksten te toetsen en heeft positief bijgedragen aan dit werk.

I would like to thank the people who joined me on the field trip to Moravia: Neli Jordanova, Adry van Velzen, Pavel Havlíček and Eduard Petrovský. I really enjoyed working (and wine tasting) with you all. Without your help, parts of this thesis could never have been written. Furthermore, I am pleased to have received the honorary citizenship of the free federal republic of Kraví Hora for my expertise of the wines of that district.

The third part of this thesis would never have seen the light of day, without the help of several people. I thank Eduard Petrovský for introducing me to Tomáš Grygar, and I thank Tomáš for showing me the magical world of electrochemistry, and for helping me explore the exciting possibilities of VMP. The help of Hilde Passier, and of Pieter Kleingeld and Ralf Haese of the geochemistry group in Utrecht, as well as the help (and great food and beer) of the people in the lab at the Institute of Inorganic Chemistry in Řež was greatly appreciated. I thank them for their patience and all the fruitful discussions about electrochemistry. Furthermore, I want to thank Tomáš and Edita Grygar for the pleasant talks, strolls and visits we had during our co-operation.

Gregg McIntosh and Pauline Kruiver kindly provided me with the samples necessary for my research. I greatly appreciated the fruitful discussions we had about my work. Judith Beks heeft met haar labwerk bijgedragen aan de totstandkoming van hoofdstuk 5.

Alle medewerkers op het fort hebben, op hun eigen manier, mijn tijd op het fort verrijkt. Daarvoor mijn dank. Ik heb mijn promotie-periode als zeer prettig ervaren en er zijn een aantal collega's die ik daarvoor in het bijzonder wil bedanken. Dit zijn op de eerste plaats mijn kamergenoten; Sebastien Bailly, Cor de Boer,

Jaume Dinares, Hilde Passier, Geert Strik, en Michael Urvat. We hebben door de jaren heen veel samen gelachen en geborreld, en zij waren ook op de moeilijke momenten altijd weer in staat mij op te vrolijken. Charon Duermeijer, David Heslop, Wout Krijgsman, Pauline Kruiver, en Piet-Jan en Conny Verplak wil ik bedanken voor de gezelligheid die ze mij (ook buiten kantooruren) brachten. Willy van Beek ben ik tenslotte zeer dankbaar voor alle kopieën, tickets en andere beslommeringen die ze in de afgelopen jaren voor mij geregeld heeft.

Alle vrienden en familie wil ik bedanken voor hun steun en gezelligheid tijdens deze promotieperiode. Zij gaven mij steeds een welkome afleiding naar het leven buiten de wetenschappelijke wereld. De reünies en uitstapjes met de ‘geologen club’ waren en zijn altijd weer gezellig, en ik bedank Karine, Doorke, Edwin, Willem-Maarten, Liesbeth, Sander, Lennard en Frouke voor al die leuke bijeenkomsten. Hetzelfde geldt voor mijn allereerste huisgenoten Janneke en Mirèse, en voor Jolina en Mirjam, onze vriendschap heeft gelukkig ook op afstand en tijdens mijn drukke schrijfperiode de tand des tijds doorstaan. Gedurende mijn tijd bij de Chemiewinkel, maar ook daarna, heb ik het leuke contact met alle vrijwilligers zeer gewaardeerd. Met name mijn wandelmaatjes, Marjan, Monique, Ivo, Marc, en Nico wil ik bedanken, zij waren gedurende vele kilometers, spelletjesavonden en cafébezoekjes altijd weer bereid naar mijn gezeur te luisteren. En dan doel ik met name op mijn paranimf, Marjan. Je gaf me steeds weer nieuwe moed of nieuwe inzichten.

Mijn zus en paranimf, Astrid, ben ik dankbaar. Jouw persoonlijke kracht en je passie voor de wetenschap waren een groot voorbeeld voor mij. Dit proefschrift is opgedragen aan mijn ouders, Arnold en Dorien van Oorschot. Het vertrouwen, de liefde, hulp en vrijheid (en niet te vergeten de eigenwijsheid) die jullie mij hebben geschonken gaven mij het doorzettingsvermogen dat nodig was voor de afronding van dit proefschrift.

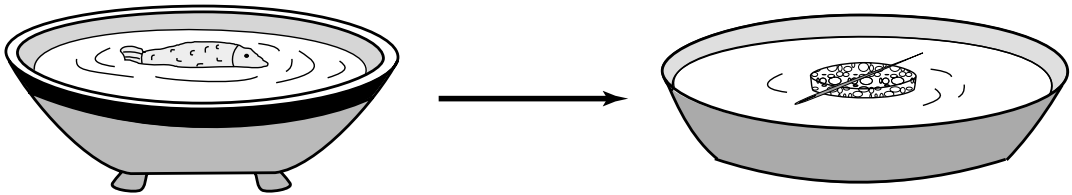
Ingeborg,
juni 2001

Create Your Own Compass

If you don't have a compass, you can create your own in much the same way people did hundreds of years ago (like the Chinese 'floating fish'). To create your own compass you will need the following materials:

- A needle or some other wire-like piece of steel (a straightened paper clip, for example).
- Something small that floats. A piece of cork, the bottom of a Styrofoam coffee cup, a piece of plastic, etc. will do.
- A dish, or preferably a pie plate 9 to 12 inches in diameter, with about an inch of water in it.

The first step is to turn the needle into a magnet. The easiest way to do this is with another magnet - stroke the magnet along the needle 10 or 20 times (always in the same direction). Place your float in the middle of your dish of water as shown in the picture. Centre your magnetic needle on the float. It very slowly will point toward north. You have created a compass!



Maak zelf een kompas

Als je geen kompas hebt, kun je er altijd zelf een maken op dezelfde manier dat mensen dat honderden jaren geleden ook deden (denk maar aan het Chinese 'vis-kompas'). Om zelf een kompas te maken heb je het volgende nodig:

- Een naald of iets anders draadvormig van metaal (een rechtgebogen paperclip bijvoorbeeld).
- Iets kleins dat kan drijven. Een stukje kurk, piepschuim of plastic voldoet prima.
- Een schaal, liefst een van zo'n 23 tot 31 cm in doorsnede, gevuld met ongeveer 2,5 centimeter water.

Allereerst moet je de naald magnetisch maken. Dit gaat het makkelijkst met een magneet: wrijf de magneet zo'n 10 tot 20 keer langs de lengte van de naald (altijd in dezelfde richting). Plaats nu je drijver in het midden van de schaal met water (zoals in de figuur). Leg dan je gemagnetiseerde naald op de drijver, hij zal nu langzaam naar het noorden gaan draaien. Je hebt een kompas gemaakt!

Curriculum Vitae

Ingeborg van Oorschoot werd op 18 mei 1973 in Heesch geboren. In 1985 begon zij haar middelbare schoolopleiding aan de Katholiek Scholengemeenschap Etten-Leur e.o. Na het behalen van haar VWO diploma in 1991, begon ze datzelfde jaar met de opleiding geologie aan de Universiteit Utrecht. In 1992 behaalde ze haar propaedeuse diploma en begon met de vervolgopleiding geochemie aan dezelfde universiteit. Het doctoraal examen (Exogene Milieugeochemie) behaalde ze in 1996. Vervolgens werkte ze van september tot en met december 1996 als junior onderzoeker bij de Chemiewinkel (Universiteit Utrecht). Van januari 1997 tot en met juni 2001 werkte zij als Onderzoeker in Opleiding in dienst van NWO (Nederlandse Organisatie voor Wetenschappelijk Onderzoek) en later van de Universiteit Utrecht op het palaeomagnetisch laboratorium 'Fort Hoofddijk' van de faculteit Aardwetenschappen, Universiteit Utrecht. Vanaf 1 juli 2001 werkt ze als projectmedewerker Soil & Spatial Development, bij de divisie Milieu van Haskoning in Nijmegen.

Publications

I.H.M. van Oorschot and M.J. Dekkers (1999). Dissolution behaviour of fine-grained magnetite and maghemite in the citrate-bicarbonate-dithionite extraction method. *Earth and Planetary Science Letters* 167, 283-295. (part of Chapter 2) reprinted with permission of Elsevier Science

I.H.M. van Oorschot and M.J. Dekkers (2001). Selective dissolution of magnetic iron oxides in the acid-ammonium-oxalate/ferrous-iron extraction method; I. Synthetic samples. *Geophysical Journal International* 145(3), 740-748. (Chapter 3) reprinted with permission of Blackwell Science Ltd.

I.H.M. van Oorschot and M.J. Dekkers. Dissolution of iron oxides from a loess-palaeosol sequence with the citrate-bicarbonate-dithionite extraction method. *to be submitted shortly* (Chapter 5).

I.H.M. van Oorschot, M.J. Dekkers and P. Havlíček. Selective dissolution of iron oxides with the acid-ammonium-oxalate/ferrous-iron extraction technique; II. Natural loess and palaeosol samples. *submitted to Geophysical Journal International*. (Chapter 6)

I.H.M. van Oorschot, T. Grygar and M.J. Dekkers. Detection of low concentrations of fine-grained iron oxides by voltammetry of microparticles. *submitted to Earth and Planetary Science Letters*. (Chapter 8)

T. Grygar and I.H.M. van Oorschot. Voltammetric identification of pedogenic iron oxides in palaeosol and loess. *Electroanalysis, in press*. (Chapter 9) reprinted with permission of Wiley-VCH Verlag GmbH

No man steps in the same river twice, for it is not the same river, and he is not the same man.

Heraclites, Greek philosopher (535-475 B.C.)

So take this world and shake it ... go carpe diem baby!

Metallica (Carpe Diem baby)